

Development of hydrological equations from modern
rivers on convergent margins and applications to fluvial
successions in rock records

January 2022

Shibata Kenichiro

Graduate School of
Science and Engineering
CHIBA UNIVERSITY

(千葉大学審査学位論文)

Development of hydrological equations from modern
rivers on convergent margins and applications to fluvial
successions in rock records

January 2022

Shibata Kenichiro

Graduate School of
Science and Engineering
CHIBA UNIVERSITY

Contents

Abstract	1
General introduction	2
Part 1. Relationships between cross-sectional dimensions and hydrological parameters of fluvial channels in the Japanese Archipelago	9
1-1. Introduction	9
1-2. Tectonic and climatic settings of modern fluvial channels	10
1-3. Human impacts on modern fluvial channels.....	13
1-4. Datasets and methods.....	14
1-4-1. Relationships between W_b , Q , and A_d	15
1-4-2. Relationship between A_d and L_d	17
1-4-3. Relationships between d , d_m , and W_b	18
1-5. Results.....	20
1-5-1. Relationships between W_b , Q , and A_d	20
1-5-2. Relationship between A_d and L_d	21
1-5-3. Relationships between d , d_m , and W_b	21
1-6. Discussion.....	22
1-6-1. Regional variations in the relationships between W_b , Q , and A_d	22
1-6-2. Comparison of empirical relationships with those from continental areas and other convergent margins.....	24
1-7. Conclusions.....	31
Part 2. Fluvial response to relative sea-level change: The Paleogene fluvial successions developed in a temperate forearc-basin setting.....	34

2-1. Introduction	34
2-2. Geological setting	35
2-3. Datasets and methods.....	37
2-4. Bounding surfaces.....	38
2-5. Architectural elements	39
2-6. Spatial variation in channel complexes	39
2-7. paleohydrology	40
2-8. Discussion.....	43
2-8-1. Fluvial evolution.....	43
2-8-2. Paleohydrological parameters and provenance	46
2-8-3. Sequence-stratigraphic implications.....	50
2-9. Conclusions.....	53

Part 3. Fluvial response to tectonic cycles: The Paleogene tropical fluvial deposits

developed in a forearc-basin setting	55
3-1. Introduction	55
3-2. Geological setting	56
3-3. Datasets and methods.....	58
3-4. Temporal variations in the fluvial deposits.....	59
3-5. Paleohydrology	61
3-6. Discussion.....	62
3-6-1. Relationship between paleohydrological features and stacking pattern	62
3-6-2. Sediment provenance.....	63
3-7. Conclusions.....	64

Part 4. Fluvial response to climatic drying: The Upper Triassic fluvial successions

developed in a continental backarc-basin setting	66
4-1. Introduction	66
4-2. Geological setting	67
4-2-1. Tectonic setting and provenance.....	67
4-2-2. Lithostratigraphy and age	68
4-2-3. Paleoclimates	70
4-3. Datasets and methods.....	71
4-3-1. Fluvial architecture	71
4-3-2. Paleohydrology	72
4-3-3. Detrital composition	72
4-4. Fluvial architecture	74
4-4-1. Lithofacies	74
4-4-2. Architectural elements	74
4-4-3. Bounding-surface (BS) types and architectural hierarchy.....	79
4-4-4. Stratigraphic change	80
4-5. Paleohydrology	82
4-6. Detrital composition	86
4-6-1. Clast composition of conglomerates.....	87
4-6-2. Sandstone framework composition.....	87
4-6-3. Clay minerals	88
4-7. Discussion.....	89
4-7-1. Fluvial styles	89
4-7-2. Paleohydrological features.....	92
4-7-3. Detrital composition	94

4-7-4. Climatic shift	98
4-7-5. Basin evolution	99
4-8. Conclusions.....	103
Part 5. Recommendations for applications of the empirical equations to ancient successions.....	105
5-1. Equations between W_b and Q	105
5-2. Equations between d_m and W_b	106
5-3. Equations between Q_b , A_d , and L_d	107
5-4. Uncertainties of the paleohydrological estimations.....	109
General conclusions.....	111
Acknowledgments	113
References	115
Figures and Tables	148

Abstract

The present study developed empirical relationships between the channel cross-sectional dimensions, discharges, and areas and length of drainage basin using datasets mainly from modern rivers in the Japanese Archipelago with supplementary datasets from the rivers in the Indonesian Archipelago and the contiguous United States. The relationship between the bankfull channel width and the bankfull discharge of Japanese rivers is similar to that described from fluvial systems in other geographical regions. In contrast, some of the relationships are different from those proposed from rivers in other regions. The discrepancies are considered to reflect variations in tectonic and climatic settings of each fluvial system.

The empirical equations were applied to bar deposits and cross-set thicknesses of fluvial successions in rock records. The major outcomes are as follows: (1) Million-year-scale temporal changes in bankfull channel cross-sectional dimensions in transgressive fluvial deposits from the Paleogene Iwaki Formation of Northeast Japan are not distinctly documented and this implies that a rise in relative sea level did not affect the channel dimension; (2) Million-year-scale temporal variations in the channel dimensions from the Paleogene Bayah Formation of West Java are interpreted to have been caused primarily by changes in a rate of basin subsidence; (3) A 10 million-year scale upward decrease in the channel dimensions from the Upper Triassic Chinle Formation of Southwest Utah is interpreted to have been caused mainly by climatic drying, and document the stacking pattern similar to some standard nonmarine transgressive sequence-stratigraphic models; (4) The estimated drainage basin lengths of fluvial systems from both the Iwaki and Bayah formations restricted their source areas of detrital fragments more precisely than those that have previously been inferred on the basis mainly of petrographic features of sediment particles.

General introduction

Quantitative reconstructions of geomorphological and hydrological features of fluvial channels and drainage basins from stratigraphic successions are one of the useful techniques to understand past terrestrial environments, climates, and fluvial architectural features. The reconstructed terrestrial environments and climates are crucial to understand terrestrial paleoecosystems, which is an interaction between terrestrial and aquatic organisms and non-animate environments. Vertebrate fossil tracks are common in the fluvial deposits, and the detailed analyses of fluvial paleohydrological features can also be useful for a better understanding of individual and social behaviors, ecology, and evolution of ancient animals including dinosaurs and extinct mammals (Lockley, 1991; Lockley and Hunt, 1995; Matsukawa et al., 2005; Matsukawa and Shibata, 2015). In contrast, the fluvial architecture, stacking patterns, and quantitative channel cross-sectional dimensions enable us to understand allogenic controls on fluvial sedimentation such as response to relative sea-level cycles, tectonic movements, and climatic changes, and to predict subsurface distribution and continuity of channel sandstone bodies as hydrocarbon reservoirs (Miall, 1996; Bridge and Tye, 2000; Trendell et al., 2012).

The reconstruction method for the fluvial paleohydrological features was initially developed by Allen (1970) and Leeder (1973). An essential and important concept for the reconstruction is that the thickness of the untruncated bar deposits with fining-upward trends are approximately equal to the bankfull channel depth (Allen, 1970; Leeder, 1973; Lunt et al., 2004; Bridge, 2003; Xu et al., 2017) (Fig. 1A). In addition, mean height of bedform (e.g. ripples and dunes) is approximately three times

the mean cross-set thicknesses (Leclair and Bridge, 2001), and the formative depth of the bedform is approximately six times the height of the bedform (Allen, 1982; Bridge, 2003) (Fig. 1B). Other geomorphological and hydrological parameters, such as the mean bankfull channel depth, bankfull channel width, mean and bankfull discharges, and the drainage basin area, can also be estimated using empirical equations between bankfull channel depth and other parameters, which were developed from datasets of modern fluvial systems (e.g. Williams, 1986; Osterkamp and Hedman, 1982; Bridge and Mackey, 1993; Davidson and North, 2009; Blum et al., 2013) (Fig. 1).

Hydrological features of fluvial systems are considered to be sensitive to allogenic controls, such as tectonic and climatic settings (Kuenzi et al., 1979; Knox, 1983; Leeder and Gawthorpe, 1987; Miall, 1996, 2014; Blum et al., 2000; Blum and Törnqvist, 2000; Straffin et al., 2000; Gawthorpe and Leeder, 2000). For instance, precipitation, valley slope, and rate of uplift control spatial and temporal variations in hydrological features in fluvial systems, such as water and sediment discharge, and denudation rates (Ohmori, 1983a, b; Blum and Törnqvist, 2000). These hydrological features also affect bed material size, proportion of bedload relative to suspended load, and channel form (Leopold et al., 1964; Carson, 1984; Schumm, 1985; Orton and Reading, 1993). The empirical equations between geomorphological and hydrological features, such as the bankfull channel depth, bankfull channel width, mean and bankfull discharges, and drainage basin area of modern fluvial systems in various tectonic and climatic settings, have been established in terms of regional hydraulic geometry (Jowett, 1998; Castro and Jackson, 2001; Montgomery and Gran, 2001; Moody et al., 2003; Chaplin, 2005; Modrick and Georgakakos, 2014). However, empirical equations developed from datasets of fluvial systems in the convergent margin settings have not yet been

sufficiently studied. For instance, the empirical equations between geomorphological and hydrological features of a fluvial system that is developed in a temperate arc–trench system, like the Japanese Archipelago, have not yet been developed. One of the exceptions is a fluvial system of a tropic arc–trench system. Adhiperdana et al. (2018) determined the empirical relationships between the channel cross-sectional dimensions and discharge characteristics on the basis of the modern fluvial systems in the Indonesian Archipelago.

On the other hand, geomorphological and hydrological features of ancient fluvial systems should be reconstructed on the basis of empirical equations derived from modern fluvial systems, which have similar channel form and are developed under equivalent tectonic and climatic settings, as pointed out by Williams (1984b) and Davidson and North (2009). However, in the studies on ancient fluvial systems, empirical relationships that were derived from datasets obtained mainly from meandering rivers in a passive continental margin and continental interior settings or those from different river types worldwide (Leopold and Maddock, 1953; Leeder, 1973; Ethridge and Schumm, 1978; Williams, 1984a, 1986; Bridge and Mackey, 1993; Blum et al., 2013) have been commonly used to estimate the geomorphological and hydrological features of ancient fluvial systems (Makino et al., 1981; Lorenz et al., 1985; Khan et al., 1997; Bridge and Tye, 2000; Bridge et al., 2000; Adams and Bhattacharya, 2005; McLaurin and Steel, 2007; Hampson et al., 2013; Xu et al., 2017; Milliken et al., 2018; Liu et al., 2019; Paredes et al., 2018; Phillips et al., 2021), regardless of the tectonic and climatic settings.

Temporal variations in fluvial architecture and stacking patterns are affected by external forces, such as relative sea-level cycles, tectonic movements, and climatic

changes (Shanley and McCabe, 1994; Blum and Törnqvist, 2000, Holbrook et al., 2006). In terms of the nonmarine sequence stratigraphy, some standard models demonstrate that interconnectedness of fluvial channel sandstone bodies as well as the widths and thicknesses of channel deposits decrease in response to a rise in relative sea level on the basis of fluvial rock records from passive margin basins and foreland basins (Wright and Marriott, 1993; Shanley and McCabe, 1994; Catuneanu et al., 2009; Blum et al., 2013) (Fig. 2). However, few case studies have examined temporal variations in quantitative hydrological features of fluvial systems such as bankfull channel depth, bankfull channel width, and discharges in response to a change in relative sea level (Adams and Bhattacharya, 2005; McLaurin and Steel, 2007; Hampson et al., 2013). In addition, an interaction between fluvial architecture, paleohydrological features, and a change in relative sea level has not yet been sufficiently studied in fluvial systems that developed in convergent margin basins, such as forearc and backarc basins.

Basin subsidence and uplift of source mountains control regional valley slope, a rate of accommodation creation, and spatial and temporal variations in stacking patterns of fluvial deposits (Bridge and Leeder, 1979; Blakey and Gubitosa, 1984; Blair and Bilodeau, 1988; Shanley and McCabe, 1994; Martinsen et al., 1999; Jo, 2003; Scherer et al., 2015). However, temporal variations in paleochannel cross-sectional dimensions and hydrological features of the fluvial systems in response to tectonic cycles have not yet been examined quantitatively.

The quantitative reconstructions of the channel cross-sectional dimensions and discharges for paleochannels should also be useful for a better understanding of paleoclimates because these parameters of the paleochannels reflect flood magnitudes and precipitation at the source areas (Knox, 1985; Carson et al., 2007; Colombera et al.,

2017; Chen et al., 2018) (Fig. 1C). For example, Carson et al. (2007) reconstructed the bankfull discharges from bankfull cross-sections of Holocene abandoned channels in the northern Uinta Mountains, Utah, and showed that the systematic variations of the bankfull floods responded to the Holocene climate change. Colombera et al. (2017) and Chen et al. (2018) also reported that channel deposit thicknesses and widths increased during an early phase of the Paleocene–Eocene Thermal Maximum in Spain. On the other hand, an interaction between climatic changes and variations in fluvial architecture, stacking patterns, and channel cross-sectional dimensions has not yet been well understood (Blum and Törnqvist, 2000). The detailed analyses of fluvial architecture and hydrological features, together with paleoclimatic analyses such as detrital compositions that document temporal variation in relative intensity of physical and chemical weathering, are required for a better understanding of the climatic controls on the fluvial sedimentation and architecture.

Quantitative analyses of drainage basin characteristics of the ancient fluvial systems could provide information about the paleogeography and sediment provenance, which are an independent technique of other provenance analyses using detrital zircon U-Pb ages and petrographic features of detrital sediments (Davidson and North, 2009; Xu et al., 2017; Milliken et al., 2018; Liu et al., 2019). In addition to estimation of drainage basin areas, previous studies mainly focused on estimation of stream length (Paredes et al., 2018) or longest river length (Xu et al., 2017; Liu et al., 2019). However, channel courses of upstream areas have hardly been preserved. Thus, a linear distance between an investigated area of the rock record and a point most distant from the investigated area in the drainage basin (i.e., drainage basin length) is considered to be useful, although a relationship between the drainage basin length and other parameters

has not yet been well studied. In terms of the provenance analysis, the reconstruction of drainage basin lengths has a potential to restrict the source rocks which have multiple and separate distributions, but have similar detrital zircon ages and petrographic features (Fig. 1C).

On the basis of the above research background, the major purposes of the present study are (1) to reconstruct empirical equations using datasets from modern fluvial systems on convergent margin settings (Part 1), and (2) to apply the newly determined equations to ancient fluvial deposits that developed in convergent margin settings, such as temperate forearc-basin, tropical forearc-basin, and tropical continental backarc-basin settings to elucidate allogenic controls on both fluvial architecture and sediment provenances (Part 2 to 4). In part 1, the main subject is to establish empirical equations between geomorphological and hydrological parameters of fluvial systems that are developed in an arc–trench system, and to compare the empirical equations with those derived from fluvial systems in different tectonic and climatic settings. The present study focuses mainly on the modern fluvial system of the Japanese Archipelago, and also supplementally examines rivers in the Indonesian Archipelago and the contiguous United States for comparison. Part 2 examines transgressive fluvial deposits of the Paleogene Iwaki Formation, Northeast Japan. An interaction between a rise in relative sea level and temporal variations in fluvial architecture and paleohydrological features are mainly discussed as an example of a fluvial system developed in a temperate forearc-basin setting. Part 3 examines temporal variations in hydrological features of a fluvial system of the Paleogene Bayah Formation in West Java, as an example of an ancient fluvial system formed in an actively subsided forearc-basin setting under a tropical climatic condition. The fluvial response to tectonic cycles is

mainly examined in this part. Part 4 focuses on the Upper Triassic Chinle Formation of Southwest Utah, U.S.A., which was developed in a continental backarc region of western Pangaea, to elucidate a relationship between climatic drying and stacking pattern of the fluvial deposits. Stratigraphic changes in detrital compositions of sandstone framework grains and clay minerals are also examined to reveal a Late Triassic climatic change in Southwest Utah. Finally, some recommendations for applications of the empirical equations from the modern fluvial systems to rock records are summarized on the basis of outcomes of the present study in Part 5.

Part 1. Relationships between cross-sectional dimensions and hydrological parameters of fluvial channels in the Japanese Archipelago

1-1. Introduction

Empirical relationships between geomorphic attributes of modern fluvial systems and the water conveyed through them, including the relationships between the bankfull channel depth, bankfull channel width, annual mean and bankfull water discharge, drainage basin area, and between variations in paleocurrent directions and sinuosity, have been used to estimate the geomorphological and hydrological features of ancient fluvial systems (Lorenz et al., 1985; Khan et al., 1997; Bridge and Tye, 2000; Bridge et al., 2000; Adams and Bhattacharya, 2005; McLaurin and Steel, 2007; Hampson et al., 2013; Xu et al., 2017). These studies used empirical equations that were derived from datasets obtained mainly from meandering rivers in both passive continental margin and continental interior settings (Leopold and Maddock, 1953; Leeder, 1973; Ethridge and Schumm, 1978; Williams, 1984a, 1986; Blum et al., 2013). In contrast to fluvial systems in these settings, those on convergent margins such as in Japan, are typically characterized by shorter longitudinal profiles, steeper gradients, higher erosion rates, and higher sediment yields (Takahashi and Sakaguchi, 1976; Ohmori, 1983a, b; Sakaguchi et al., 1986; Milliman and Syvitski, 1992). In addition, climatic conditions such as precipitation, vegetation, and rate of evaporation control hydrological features in fluvial systems, such as water and sediment discharge, and denudation rates (Ohmori, 1983a, b; Blum and Törnqvist, 2000; Gran and Paola, 2001; Tal and Paola, 2010). Thus, some revision of existing hydrological equations is required

for the reconstruction of paleohydrological and geomorphological features of fluvial systems in convergent margin settings according to climatic conditions.

The major purposes of this part are to (1) construct empirical equations between the bankfull channel width, mean, bankfull, and maximum discharges, drainage basin areas, and drainage basin length from data of modern Japanese rivers, (2) construct empirical equations that describe the relationships between bankfull channel depths, mean bankfull channel depths, and bankfull channel widths, based on the geomorphological datasets of the modern fluvial channels of the Kanto region, Japan, and (3) compare the empirical equations derived from the present study with those derived from fluvial systems in different tectonic and climatic settings, such as the modern fluvial systems in the Indonesian Archipelago and the contiguous United States.

1-2. Tectonic and climatic settings of modern fluvial channels

The Japanese Archipelago is characterized by an arc–trench system which was formed as a result of subduction of the Pacific and Philippine Sea plates beneath the Amur and Okhotsk plates (Taira et al., 2016) (Fig. 3). The subduction of the oceanic plates, in general, causes violent crustal uplifts and sustaining steep slopes and undulations of mountains, and resultant higher denudation rates (Ohmori, 1983a, b; Sakaguchi et al., 1986). In general, the temperate climatic condition in the Japanese Archipelago is characterized by four distinct seasons and humid conditions with plentiful precipitation of about 900 mm to 3,800 mm per year in average recorded from 1981 to 2010 (The National Astronomical Observatory of Japan, 2016), which were measured by the Japan Meteorological Agency. In contrast, Hokkaido (Fig. 4) has a colder climate than the other regions of Japan, and generally lacks the rainy season in

early summer and is affected by fewer typhoons (Nakamura et al., 1986). The rivers in Hokkaido are also characterized by annual snowmelt-related floods, although such floods also occur locally in the Tohoku and Hokuriku regions, but on a smaller scale (Sakaguchi et al., 1986). Northeast Japan has larger rivers in terms of their length and the size of their drainage basins, such as the Tone and Shinano Rivers, and broad alluvial plains are developed in their lower reaches (Fig. 5). Some rivers in the Chubu region are characterized by steeper valley slopes, higher erosion rates, and higher sediment yields than rivers in the other regions (Takahashi and Sakaguchi, 1976; Ohmori, 1983; Sakaguchi et al., 1986). These rivers flow directly into deep sea (e.g. Suruga and Toyama Bays) and lack the alluvial plains to form fan deltas in their lower reaches (Sakaguchi et al., 1986) (Fig. 6). Rivers in Southwest Japan are characterized by shorter longitudinal profiles, smaller sizes of drainage basins, and relatively gentle slopes than rivers in the other regions (Fig. 6). Therefore, few alluvial fans have developed in Southwest Japan (Saito, 1988, 1999). Southwest Japan is also affected more frequently by heavy typhoon-related storms during the summer and early autumn seasons, and by seasonal rain fronts in early summer, compared with the other regions (Nakamura et al., 1986). These geographic and climatic variations have led to the development of different hydrological conditions in the various fluvial systems in the Japanese Archipelago.

The Kanto Plain is located in a forearc region of the Honshu Arc in the central part of the Japanese Archipelago, and has been formed in response to the subduction of the Pacific and Philippine Sea plates beneath the Okhotsk plate (Taira et al. 2016) (Fig. 3). In addition to the plate subduction, the collision of the Izu–Ogasawara (Bonin) Arc with the Honshu Arc has caused uplift of the mountains around the Kanto Plain in

association with the development of active volcanoes in these mountains (Fig. 7). The Kanto region experiences heavy rainfall in summer and early autumn in association with seasonal rain fronts and typhoons, although sunny weather is common even during the winter season. In addition, the mountain areas in the northern Kanto region also experience sudden thunderstorm-related showers in summer seasons (Nakamura et al., 1986). The annual mean precipitation and annual mean air temperature of Maebashi, Gunma Prefecture, located in the upstream area of the Tone River (Fig. 7), are 1248.5 mm and 14.6 °C (both averages from 1981 to 2010), respectively (The National Astronomical Observatory of Japan, 2016).

In general, fluvial lowlands in the Japanese Archipelago are divided into alluvial fan, natural levee and back marsh, and delta regions in the downstream directions (Yoshikawa et al., 1973). Ikeda (1975) classified the configuration of alluvial channels in the four regions into four types in the downstream direction as follows: (1) sandy and gravelly multiple bars, (2) sandy and gravelly alternate bars with sharp crest lines, (3) sandy alternate bars with obscure crest lines, and (4) absence of bars. For the relationships between channel cross-sectional dimensions, the present study examined gravelly fluvial channels in the Kanto region (Fig. 7), which have developed mainly in a levee and back marsh region and also partly in a distal part of alluvial fan region. The gravelly fluvial channels are commonly characterized by multiple-thread channels that are associated with point bars, mid-channel bars, and braid bars, and are equivalent to ‘sandy and gravelly multiple bars’, and ‘sandy and gravelly alternate bars with sharp crest line’ types that were defined by Ikeda (1975), although these two types of bed configurations gradually change in the downstream directions in each river. The studied gravelly fluvial channels are also considered to be classified as ‘braided, point bar’ type

as defined by Ethridge (2011). The slope and hydrological parameters, such as the specific mean annual discharge and denudation rate of the Tone River, which is the longest river in the Kanto region, are larger than those of continental area rivers, although these values are relatively small in rivers of the Japanese Archipelago (Ohmori, 1983a, b; Sakaguchi et al., 1986). In addition, the Tone and some other rivers in the Kanto region have also received regular inputs of volcanoclastic material from active volcanoes in their hinterlands (Sakaguchi et al., 1986; Nakayama, 1997).

1-3. Human impacts on modern fluvial channels

Most modern river channels in the Japanese Archipelago have been subjected to engineering work, so they have not necessarily retained their natural geomorphological and hydrological features. The human impacts on the geomorphological and hydrological features of modern river channels were reviewed by Takahashi (1971, 1990) and Yamamoto (2004). For example, banks have been constructed on the natural levees on both sides of river channels to prevent floodwater discharge into floodplains and residential areas. The Tone River, which is the longest river in the Kanto region and the river with the largest drainage basin in the Japanese Archipelago, was excavated between 1594 and 1654, and the channel course was redirected (Ohkawara et al., 1992; Nakayama, 1997; Sawaguchi, 2000). The data of these artificially excavated channels were excluded from the present analyses as much as possible. River channels in Japan usually consist of low- and high-water channels. The high-water channels, which are present between the artificial banks on both sides, are locally vegetated, and include a part of the floodplain of the low-water channels. On the other hand, the filled condition of the low-water channel is considered to be the

bankfull condition (Suetsugu, 2005; Fukuoka, 2010). The high-water channels were locally expanded and flattened artificially for decreasing flow velocity near the artificial banks to prevent damage to the banks at flood stages, and for increasing the utility of a part of the high-water channels at ordinary water-stages. The widening of high-water channels causes concentration of water flow on the low-water channels and scouring of riverbeds (Fukuoka, 2008, 2010). Locally, some low-water channels have also been widened to increase its flow capacity to prevent flooding (Yamamoto, 2004). The construction of reservoirs in the upper reaches of rivers since the 1950s, together with the construction of artificial banks and water abstraction from the rivers, have resulted in change in flood and/or ordinary discharges (Takahashi, 1971; Yamamoto, 2004). Although engineering work of fluvial channels was commonly conducted in the Japanese rivers, artificially modified channels have returned to the original conditions by bar depositions and/or bank erosion (Yamamoto, 2004; Suetsugu, 2005; Moro et al., 2011). In addition, the heights of riverbeds at some study sites have been relatively stable since the 1980s (website of the Ministry of Land, Infrastructure, Transport and Tourism, http://www.mlit.go.jp/river/basic_info/jigyo_keikaku/gaiyou/seibi/). Thus, the measured cross-sectional parameters including bankfull channel depth and width in the present study seem to represent the channel features under the conditions of present day water discharge and sediment supply.

1-4. Datasets and methods

Alluvial channel patterns are commonly subdivided into four end-member types: straight, meandering, braided, and anastomosed rivers (Schumm, 1985; Miall, 1996; Bridge, 2003). However, the channel patterns are highly variable, and transitional

channel forms between the end-member types are common (Schumm, 2005; Ethridge, 2011). The fluvial system in the Japanese Archipelago also represents a gradual downstream variation in plan view channel patterns (Ikeda, 1975). Therefore, the present study focuses to examine the channel cross-sectional dimensions and hydrological parameters regardless of channel forms.

1-4-1. Relationships between W_b , Q , and A_d

Water-discharge data from 368 sites are available for modern rivers in the Japanese Archipelago and were used in the present study (Figs. 4–6; Table 1). From these datasets, the present study used mainly mean (Q_{mean}) and maximum (Q_{max}) discharge data published by the River Bureau, Ministry of Land, Infrastructure and Transport in 2009. Q_{mean} is the average of the mean annual discharge recorded in defined periods. Here, the mean annual discharge is the summation of averaged daily discharges divided by the number of days of the concerned year. Q_{max} is the maximum flood peak discharge recorded in the defined period, and the Q_{max} values reflect episodic flood conditions. The observation periods for these data vary from 5 to 66 years, and the latest observations were conducted in 2004 at each site (The River Bureau, Ministry of Land, Infrastructure and Transport, 2009). The present study also used data on the bankfull discharge (Q_b) of the rivers. Generally, Q_b is considered to be the channel-forming discharge, and the mean annual flood discharge is commonly interpreted to be equivalent to Q_b (Dury, 1976; Bridge, 2003, Yamamoto, 2004). The recurrence interval of the mean annual flood discharge for the Japanese rivers is interpreted to be about 2.3 years (Yamamoto, 2004). In the present study, the data of the annual flood discharge (maximum daily discharge in a concerned year) in 2001, 2002, and 2003, respectively,

were obtained from the datasets provided by the Japan River Association (2007), and the mean annual flood discharge for the period of 2001–2003 was mainly estimated. During this period, the Japanese Archipelago did not experience extraordinary heavy rain or drought, although a large amount of precipitation has been recorded in some sites in Southwest Japan (Japan River Association, 2007). Therefore, the mean annual flood discharge can be considered to correspond to Q_b .

The bankfull channel width (W_b) at the 368 sites was measured using aerial photographs from Google map (<https://www.google.co.jp/maps/>). W_b is well defined, and was measured following methodologies in the previous studies (e.g., Williams, 1986; Atha, 2014). Distances between the present-day levees in both sides of fluvial channels, which locally have sandy bars without dense vegetation in the satellite images, were measured along three cross-sections at each gauging station (observation site), and the average value was estimated as W_b (Fig. 8).

The drainage basin area (A_d) at the 368 sites is available from a dataset published by the River Bureau, Ministry of Land, Infrastructure and Transport (2009). Here, A_d means the area size that includes a gauging station and an area which gathers precipitation water and directs it to the gauging station.

W_b has been found to be most closely correlated with discharge (e.g. Osterkamp and Hedman, 1982; Williams, 1984a). In addition, A_d has been considered to be closely correlated with d_m , W_b , and Q_b (Dunne and Leopold, 1978; Sakaguchi et al., 1986; Blum et al., 2013; Modrick and Georgakakos, 2014). In the present study, the relationships between W_b and various measures of discharges (Q_{mean} , Q_b , and Q_{max}), and between A_d and Q_b are analyzed in the Japanese rivers and a simple power function was developed:

$$Q = \alpha W_b^\beta$$

$$A_d = \gamma Q_b^\delta$$

where Q is discharge ($\text{m}^3 \text{s}^{-1}$), α and γ are coefficients, and β and δ are exponents. The statistical parameters describing the relationship between $\log Q$ and $\log W_b$, and between $\log A_d$ and $\log Q_b$, such as the correlation coefficient (r), the coefficient of determination (R^2), and the level of significance from the F -ratio for the width (p), were also calculated. The correlation coefficient is an indicator of data scatter relative to the range of the data. The coefficient of determination indicates the fitting quality of the data to the regression line. The F -ratio is the ratio of the explained to unexplained variance in the dependent variable. The level of significance can be determined from the F -ratio and the numbers of cases and variables. If probability (p -value) was less than the level of significance (0.05), the estimated equation was judged to be meaningful. The symbols used in the present study are listed in Table 2.

In the present analysis, the datasets from the 368 sites were tentatively classified into four groups on the basis of the geographic and climatic settings at each site:

Group 1: rivers in Hokkaido;

Group 2: rivers in Northeast Japan;

Group 3: rivers flowing from the mountains in the Chubu region (including the Japanese Alps); and

Group 4: rivers in Southwest Japan.

1-4-2. Relationship between A_d and L_d

The present study also examined the drainage basin area (A_d) and the drainage basin length (L_d) at 106 gauging stations of the modern Japanese rivers (Table 1). In the present study, L_d was defined as a linear distance between the gauging station and the point most distant from the station in the drainage basin. The data of A_d values were taken from the River Bureau, Ministry of Land, Infrastructure and Transport (2009), and L_d values were measured using Google map (<https://www.google.co.jp/maps>) and the drainage basin maps by the River Bureau, Ministry of Land, Infrastructure and Transport (2009).

L_d was considered to be closely correlated with the bankfull channel depth (Xu et al., 2017; Liu et al., 2019). Because the bankfull channel depth has been found to be closely correlated with mean bankfull channel depth (d_m), W_b , Q_b , and A_d as discussed later, the relationships between A_d and L_d is analyzed and a simple power function was developed:

$$L_d = \varepsilon A_d^\zeta$$

where ε is coefficients, and ζ is exponents. The statistical parameters describing the relationship between $\log A_d$ and $\log L_d$, were also calculated.

1-4-3. Relationships between d , d_m , and W_b

Cross-sectional data of gravelly fluvial channels from 24 sites in the Kanto region of central Japan are used in the present study (Fig. 7, Table 3). The data were measured in 2013 or 2014 and provided by the Ministry of Land, Infrastructure, Transport and Tourism of the Kanto Regional Development Bureau. Although

identification of bankfull condition in multiple-thread braided rivers is sometimes difficult (Xia et al., 2010), banks are easily defined by the ‘bankfull edge’ that is located at the edge of flat high water channels in the case of fluvial channels in the Kanto region (Fig. 9). The bankfull edges can be defined in cross sections on the basis of abrupt change in slope, and the distance between the bankfull edges is measured as W_b (Fig. 9A, C). Using both cross sections and satellite images from Google map (<https://www.google.co.jp/maps>), the W_b was measured. Densely vegetated areas were excluded from the W_b measurements. The difference in the elevation between the thalweg and the water level at bankfull condition, as assessed from the cross-sectional data, was used to represent the bankfull channel depth (d). The cross-sectional area (C) and the wetted perimeter (S) at the bankfull condition were measured by counting the number of pixels in a cross-sectional view raster file of each cross section using ‘Image J’ software (<http://imagej.nih.gov/ij/>), and the hydraulic radius at a bankfull water stage (i.e., mean bankfull channel depth: d_m) was calculated by dividing C by S (Fig. 9). In addition, Bridge and Mackey (1993) and Moody et al. (2003) proposed an empirical equation between d_m and d . In the present study, the relationships between d , d_m , and W_b were determined as follows:

$$d_m = \theta d$$

$$W_b = \iota d_m^\kappa$$

where, θ and ι are coefficients, and κ is an exponent. The statistical parameters describing the relationship between d and d_m , and between $\log d_m$ and $\log W_b$ were also calculated.

1-5. Results

1-5-1. Relationships between W_b , Q , and A_d

The present study examined all data from the 368 sites in Japanese rivers, and also the data from each group; i.e. from the 46 sites in Hokkaido, 125 sites in Northeast Japan, 28 sites in the Chubu region, and 169 sites in Southwest Japan (Table 1). The present analysis showed that the bankfull channel width (W_b) from 368 sites ranges from 13.7 to 541.4 m, the mean discharge (Q_{mean}) from 367 sites (data from one site is missing) from 1.3 to 503 $\text{m}^3 \text{s}^{-1}$, the maximum discharge (Q_{max}) from 368 sites from 92 to 18,000 $\text{m}^3 \text{s}^{-1}$, and the bankfull discharge (Q_b) from the 356 sites (data from 11 sites are missing) 28.4 to 5438.9 $\text{m}^3 \text{s}^{-1}$. Furthermore, drainage basin area (A_d) from the 368 sites ranges from 0.0 to 12,697 m^2 (Table 1).

On the basis of data analysis for the four regions defined above, regional variations in Q_{mean} , Q_b , and Q_{max} discharges relative to W_b are summarized in Figs. 10–12, and Table 4. The absolute values of r range from 0.58 to 0.79 for each region. Values of R^2 are in the range of 0.33–0.63, and this indicates that 33% to 63% of the factors, which control logarithmic discharge characteristics, are explained by $\log W_b$. Because values of p are much less than 0.05, these equations are considered to be statistically significant.

Similarly, regional variations in A_d relative to Q_b are shown in Fig. 13 and Table 4. In the present study, data of artificially excavated or replaced channels which show quite smaller drainage basin area were excluded from the analysis (e.g. 0.0 km^2 for Kyuyoshinogawa in Table 1). Thus, data from 350 sites were analyzed. Values of R^2 are in the range of 0.54–0.83, and this indicates that 54% to 83% of the factors, which

control $\log A_d$, are explained by $\log Q_b$.

On the basis of the regression curves for the relationships between Q_b and Q_{\max} discharges and W_b , these hydrological parameters do not show any distinct variations between the fluvial systems in the four regions (Figs. 11 and 12), although the regression equations are represented by coefficients and exponents that differ slightly between the regions (Table 4). In contrast, Q_{mean} for a given W_b shows regional variations larger than those for Q_b and Q_{\max} . In particular, Q_{mean} of the rivers in Hokkaido and Northeast Japan have smaller values, although Q_{mean} of the rivers in the Chubu region and Southwest Japan have larger values for a given W_b (Fig. 10). The regression curves for the relationships between Q_b and A_d show slight regional variations. A_d values of the rivers in Hokkaido and Northeast Japan have larger values than those of the Chubu region and Southwest Japan for a given Q_b (Fig. 13).

1-5-2. Relationship between A_d and L_d

Among the examined data, the drainage basin area (A_d) ranges from 167.3 to 12,697 km², and the drainage basin length (L_d) from 19.5 to 169.4 km (Table 1). Scatter diagrams and the relationship between logarithmic L_d and logarithmic A_d are shown in Figure 14 and Table 4. The absolute value of r is 0.89, the values of R^2 are 0.79, and the values of p is less than 0.05. These statistical parameters indicate that $\log L_d$ and $\log A_d$ are well correlated, and the present study can use the equation in Figure 14.

1-5-3. Relationships between d , d_m , and W_b

Cross-sectional data of fluvial channels from the 24 sites in the Kanto region were examined (Table 3). The bankfull channel depth (d) ranges from 2.3 to 9.4 m, the

bankfull channel width (W_b) from 31.0 to 485.0 m, the bankfull cross-sectional area (C) is from 33.3 to 2384.7 m², and the bankfull wetted perimeter (S) is from 32.6 to 499.8 m. The calculated hydraulic radius at bankfull conditions (i.e., the mean bankfull channel depth: d_m) ranges from 1.0 to 6.7 m.

Scatter diagrams and relationships between d_m and d , and between W_b and d_m are summarized in Figures 15, and Table 5. The absolute values of r in Table 5 are 0.87 and 0.47. On the other hand, the values of R^2 are 0.76 and 0.22. The values of r and R^2 in the relationship between $\log W_b$ and $\log d_m$ (0.47 and 0.22) are relatively lower. However, the values of p in all equations in Table 5 are less than 0.05. This indicates that these two equations are statistically significant, and we can use these equations.

1-6. Discussion

1-6-1. Regional variations in the relationships between W_b , Q , and A_d

Because the bankfull (Q_b) or maximum (Q_{max}) discharges relative to the bankfull channel width (W_b) do not show any distinct regional variations, the channel geometry of the rivers in the Japanese Archipelago seems to have adjusted to the flows under the bankfull and/or the episodic flood-induced hydrodynamic conditions, and the ordinary water discharge hydrodynamic conditions may not have played an important role in the development of channel geometry. Consequently, the equations that express the relationship between Q_b or Q_{max} discharges and W_b (Table 4) can be used to estimate one of these parameters (provided the other is known) in both modern and ancient fluvial systems formed in convergent margin under mid-latitude and temperate-climatic conditions.

Although Q_b and Q_{max} relative to the bankfull channel width (W_b) do not show

any distinct regional variations across the Japanese Archipelago (Figs. 11 and 12), the mean discharges (Q_{mean}) show distinct regional variations (Fig. 10). The lower values of Q_{mean} relative to W_b were recorded from the rivers in the Chubu region and Southwest Japan. In other words, the rivers in the Chubu region and Southwest Japan are characterized by larger values of W_b relative to Q_{mean} . These hydrological and geomorphological features are thought to reflect the specific climatic and geomorphic conditions of these regions. The rivers in Southwest Japan are characterized by a higher episodic flood-induced discharge, and this is interpreted to be the result of appreciable precipitation during the typhoon and rainy seasons from early summer to mid-autumn (Nakamura et al., 1986). The rivers in the Chubu region also record a higher episodic flood-induced discharge in association with steeper valley slopes, higher denudation rates, and appreciable precipitation (Ohmori, 1983a, b; Sakaguchi et al., 1986). These climatic and geomorphological features of the Chubu region and Southwest Japan are also represented by higher values of flood specific discharge that is defined by flood discharge divided by area size of the drainage basin at a gauging station (Takahashi and Sakaguchi, 1976). Therefore, these higher episodic flood-induced discharges seem to result in the formation of wider W_b relative to Q_{mean} in rivers in the Chubu region and Southwest Japan.

The rivers in the Chubu region and Southwest Japan are also characterized by smaller values of the drainage basin area (A_d) relative to Q_b than those in Hokkaido and Northeast Japan (Fig. 13). In other words, this means the bankfull specific discharges for the Chubu region and Southwest Japan, which are defined by bankfull discharges divided by area sizes of the drainage basin at gauging stations, are larger than those of Hokkaido and Northeast Japan. These variations of the bankfull specific discharges are

also interpreted to reflect higher values of the bankfull discharges, which are caused by steeper valley slopes, higher denudation rates, and appreciable precipitation for the Chubu region (Ohmori, 1983a, b; Sakaguchi et al., 1986), and appreciable precipitation during the typhoon and rainy seasons from early summer to mid-autumn for Southwest Japan, respectively (Nakamura et al., 1986). Furthermore, relatively larger drainage basin areas with longer longitudinal profiles of rivers in Hokkaido and Northeast Japan (Sakaguchi et al., 1986) are also interpreted to give rise to smaller values of the bankfull specific discharge in these regions.

1-6-2. Comparison of empirical relationships with those from continental areas and other convergent margins

1-6-2-1. Relationships between Q , W_b , and A_d

Empirical relationships between discharges (Q_{mean} and Q_b) and W_b have been proposed from some case studies of modern fluvial systems in passive continental margins, continental interior basins, and convergent margin settings (e.g. Carlston, 1965; Dury, 1976; Osterkamp and Hedman, 1982; Williams, 1984a; Mackey, 1993; Adhiperdana et al., 2018). Fig. 16 and Table 6 summarize these relationships, together with those from the present study, although the methods used to measure discharges and channel width differed among the case studies.

The relationship between W_b and Q_{mean} varies among the previous case studies, regardless of the tectonic and climatic conditions of examined fluvial systems (Fig. 16A). Although fluvial systems are generally influenced by monthly variations in discharges in each year (e.g. Schumm, 1977), regardless of their tectonic and climatic settings, the magnitude of the monthly variations in discharge in each case-study area

varies in response to specific climatic conditions, and the relationship between W_b and Q_{mean} is considered to be variable in time and space. In contrast, the relationship between W_b and Q_b from the present study yields an empirical equation similar to that from Swedish and Indonesian rivers (Williams, 1984a; Adhiperdana et al., 2018); and Dury (1976) and Mackey (1993) presented similar empirical equations, although the regression coefficient from their datasets is larger than for the other fluvial systems (Fig. 16B). The higher value of the regression coefficient of Dury (1976) seems to reflect the combined datasets from different continents, which have been influenced by different types of tectonic and climatic conditions (Table 6). The relationship between W_b and the 2-year flood discharge (Q_2) of the Missouri River also has an empirical equation similar to that of the present study, although Q_2 was obtained from a dataset different from that of Q_b (Osterkamp and Hedman, 1982; Table 6) and has a somewhat larger value than Q_b of rivers in the Japanese Archipelago for a given W_b (Fig. 16B). The similar nature of the empirical equations that describe the relationship between the W_b and Q_b supports the interpretation that the bankfull discharge controls fluvial form as it is the channel forming discharge (e.g. Dury, 1976; Bridge, 2003; Yamamoto, 2004).

Consequently, the empirical equations in Table 4, in particular the relationships between W_b and Q_b , can be interpreted as representing a specific hydrological characteristic of modern Japanese rivers, and may also be more widely applicable to other fluvial systems in arc–trench systems with a temperate climate. Because the equation relating W_b to Q_b for the Japanese rivers is similar to that from the other continents, this equation may have even wider applicability for the estimation of hydrological features of ancient fluvial systems in passive continental margins and continental interior basins.

A few examples of the relationships between Q_b and the drainage basin (A_d) have been investigated in the continental areas. The present study compared the relationships of rivers worldwide (Blum et al., 2013) and of Indonesian rivers with those of the Japanese Archipelago (Fig. 17). In Figure 17, data of Q_b and A_d of the Indonesian rivers (Java, Sumatra, and Kalimantan) were taken from Adhiperdana et al. (2018) and the Center for Water Resources Development and Research (2011) (Table 7). The relationship between Q_b and A_d of the Japanese rivers is similar to that of the Indonesian rivers. Although the Japanese and Indonesian fluvial systems developed in the temperate and tropic climatic conditions, respectively, both fluvial systems are affected by heavy rains that result in extensive floods (Nakamura et al., 1986; the Asian Disaster Preparedness Center, 2000). Furthermore, both of the Japanese and Indonesian Archipelagos were developed in the convergent margin settings of the arc–trench systems, which have been formed as a result of the subduction of oceanic plates, and their fluvial systems are represented by smaller drainage basins on narrow arc systems, although Kalimantan, Indonesia, is a part of the Sundaland continental mass. Thus, the similarity between the A_d – Q_b relationships for the Japanese and Indonesian fluvial systems are interpreted to be caused by their climatic and tectonic settings, which are characterized by extensive floods and smaller drainage basin areas. In contrast, the relationship between Q_b and A_d of rivers worldwide (Blum et al., 2013) represents much larger A_d for a given value of Q_b than that for rivers in the Japanese and Indonesian Archipelagos, and the difference is more than an order of magnitude (Fig. 17). The majority of data of the rivers worldwide by Blum et al. (2013) seems to be derived from fluvial systems in passive continental margin and continental interior basin settings, which are characterized by larger drainage basins than those in active margin settings

(Sakaguchi et al., 1986; Syvitski and Milliman, 2007). Furthermore, in response to the increase in the drainage basin areas, the smaller flood and bankfull discharges seem to be recorded, because flood discharge is determined by precipitation of heavy rain at a part of the drainage basin (Sakaguchi et al., 1986). Therefore, the variations in the $A_d - Q_b$ relationships are interpreted to be caused mainly by differences in the drainage basin areas between convergent margin basins and passive continental margin and continental interior basins. Therefore, the equations derived from the modern Japanese rivers can be applied directly to drainage basins of modern and ancient fluvial systems in the convergent margin settings, in particular those that are characterized by the arc–trench systems.

1-6-2-2. Relationships between A_d and L_d

In order to compare the relationship between A_d and the drainage basin length (L_d) derived from the modern Japanese fluvial system with that from the fluvial systems of the other convergent margins and of continental areas, the present study also examined the $L_d - A_d$ relationships from the modern fluvial system of the Indonesian Archipelago and of the contiguous United States. The A_d data of the modern fluvial systems of the Indonesian Archipelago and the contiguous United States were taken from datasets of the Center for Water Resources Development and Research (2011) for Indonesia, and of Takahashi (2013) for the United States (Table 8). The L_d values were measured using google map (<https://www.google.co.jp/maps>). These data were plotted in a log-log graph, and the regression curves were also determined (Fig. 18A).

The comparison indicates that the $L_d - A_d$ relationship of the Japanese fluvial system is similar to that of the Indonesian fluvial system, although the Japanese

regression curve estimates slightly larger values of L_d for a given value of A_d . In contrast, the L_d – A_d relationship of the drainage basins of the contiguous United States estimates large values of L_d for a given value of A_d than that of the Japanese and Indonesian fluvial systems. This means that shapes of the drainage basins of the contiguous United States are narrow. In general, the rivers of the contiguous United States run through vast plains such as the Great Plains, Central Lowlands, and Atlantic and Gulf Coastal plains, and large and small rivers tend to flow in parallel towards coastlines. In contrast, river courses in the Japanese and Indonesian Archipelagos seem to curve in response to the locations of hills and mountains, which reflect complicated geology that was caused by active crustal deformations. These geomorphologic and geological features may cause the difference between shapes of the drainage basins in arc–trench systems and the contiguous United States (Fig. 18B and C).

1-6-2-3. Relationships between channel cross-sectional dimensions

The empirical relationships between bankfull channel depth (d) or mean bankfull channel depth (d_m) and W_b have been developed from compiled datasets of modern fluvial systems in various climatic and tectonic settings (Leeder, 1973; Williams, 1986; Bridge and Mackey, 1993). Xu (2004) also proposed empirical equations between W_b , d_m , and Q_b of sand- and gravel-bed rivers of varying channel patterns using datasets from modern rivers around the world. Analyses of regional hydraulic geometry have also been conducted using data from modern fluvial systems, particularly in the U.S.A. (Castro and Jackson, 2001; McCandless and Everett, 2002; Moody et al. 2003; Chaplin, 2005; Modrick and Georgakakos, 2014). Their empirical equations between d_m , W_b , Q_b , and A_d can be combined into the W_b – d_m relationships, although direct calculations of

regressions of W_b on d_m using their original datasets result in different exponents and coefficients (Williams, 1986). Bridge and Mackey (1993), Moody et al. (2003), and Adhiperdana et al. (2018) proposed the relationships between d and d_m . Although the procedures of data sampling differed among the above studies, and some of the studies combined different equations, the empirical equations (i.e., regression lines or curves) between d_m and d , and between W_b and d_m are summarized and compared with those developed in the present study (Fig. 19, and Table 9).

The d_m estimated from d_m-d relationship by Bridge and Mackey (1993) and Moody et al. (2003) (Table 9) is slightly less than that estimated from the equation developed by the present study for a given value of d . In addition, the half value of d has also been used as d_m (Bridge and Tye, 2000; McLaurin and Steel, 2007). Thus, the d_m-d equation derived from the present study estimates d_m as slightly deeper than that from the previously proposed equations. The slightly deeper d_m is considered to indicate relatively flatter riverbeds and lack of deeper thalweg in association with the development of braided bars in the Kanto region. This possibly reflects steeper valley slopes and higher values of mean annual and bankfull specific discharge of river water in the Kanto region (Fig. 17) (Ohmori, 1983a, b). The d_m-d relationship by Adhiperdana et al. (2018), which was determined from the Indonesian rivers, estimates d_m as slightly deeper than that by the present study (Table 9). These deeper channels in the Indonesian rivers are also interpreted to reflect higher mean and bankfull specific discharges during wet seasons (Adhiperdana et al., 2018), because steeper valley slopes and the higher discharge and stream power promote degradation of alluvial channels (Blum and Törnqvist, 2000).

With respect to d_m-W_b relationships, the regression curves from each study

show variation in slope and intercept in a logarithmic graph (Fig. 19). The regression exponent value (slope in the log-log plot) for the modern rivers in the Kanto region (Table 5) is found to be small, and as large as that of sand meandering rivers (Xu, 2004). In contrast, the coefficient value (intercept in the log-log plot) for the rivers in the Kanto region is larger than other meandering rivers. Consequently, the W_b-d_m equation for the rivers in the Kanto region estimates W_b to be larger than that calculated by the equation for meandering rivers, and smaller than that for the equation for braided rivers for a relatively small value of d_m ($d_m < 3$ m). In contrast, almost the same values of W_b are obtained by the equations of both the rivers in the Kanto region and meandering rivers for a relatively large value of d_m ($d_m > 3$ m). The gravelly rivers in the Kanto region have an intermediate geomorphological relationship between braided and meandering rivers around the world in terms of the W_b-d_m relationship (Fig. 19). As the river channels in the Kanto region are classified as ‘braided, point bar’ type of Ethridge (2011), a geomorphological feature may be intermediate between that of braided and meandering rivers. The large W_b/d_m ratios for the equations of braided rivers by Xu (2004) seem to be caused by data from braided rivers on fluvio-glacial fans, such as the Rakaia and Waimakiriri rivers in New Zealand (Wilson, 1985), which have been collected by van den Berg (1995). Therefore, the W_b-d_m equations for the gravelly rivers in the Kanto region can be applied to gravelly rivers with multiple and alternate bars, in particular to those developed in a convergent-margin setting under a temperate climatic condition, but cannot be applicable directly to braided rivers on alluvial fans and fan deltas. In contrast, the regression curve of d_m-W_b relationship from the Indonesian rivers (Adhiperdana et al., 2018) has similar exponent and coefficient values to that from the rivers of the Kanto region, which has smaller exponent and larger

coefficient values (slope and intercept in log-log plot) (Fig. 19). Adhiperdana et al. (2018) interpreted that these features of the regression curve reflect higher flood discharge during wet seasons in Indonesia and resultant downward erosion of riverbeds by floodwaters. In addition, the growth of thick vegetation covers on overbanks and floodplains in tropical rivers is interpreted to strengthen riverbanks, increase their resistance to bank erosion, and prevent river channels from widening (Gran and Paola, 2001; Tal and Paola, 2010; Adhiperdana, 2018), although vegetation may decrease slope stability due to the occurrence of cracks and increase in water permeability (Greenway, 1987). Although the Indonesian and Japanese Archipelagos are characterized by tropic and temperate climatic conditions, respectively, the higher flood discharge and thick vegetation are common features for the fluvial systems in both regions. Therefore, the empirical equations between d_m and d , and between W_b and d_m (Table 5) can be interpreted to also be widely applicable to fluvial systems developed in arc-trench systems under temperate and tropic climatic settings.

1-7. Conclusions

The relationships between the bankfull channel depth (d), mean bankfull channel depth (d_m), bankfull channel width (W_b), the mean (Q_{mean}), bankfull (Q_b), and maximum (Q_{max}) discharges, the drainage basin area (A_d) and the drainage basin length (L_d) of the rivers in the Japanese Archipelago were investigated using hydrological and geomorphological data in the modern fluvial system. The major conclusions of the study in this chapter are outlined below.

- (1) Although Q_b and Q_{max} relative to W_b do not show any distinct regional variations across the Japanese Archipelago, Q_{mean} shows distinct regional variations. In

particular, fluvial systems in the Chubu region and Southwest Japan have lower Q_{mean} relative to W_b than those in Hokkaido and Northeast Japan, and this variation is interpreted to reflect spatial variations in climatic conditions, such as the effects of the rainy season and the magnitudes and frequency of typhoon-related floods.

- (2) The relationship between W_b and Q_b from the Japanese rivers can be expressed by an empirical equation quite similar to equations obtained from fluvial systems in Europe, America, and the Indonesian Archipelago. Because Q_b is believed to control fluvial styles as the channel-forming discharge, the equation that describes this relationship is likely to have wider applicability for the estimation of hydrological parameters for modern and ancient fluvial systems with various tectonic and climatic settings, in particular arc–trench systems influenced by mid-latitude temperate climates.
- (3) The A_d – Q_b regression curves from data of the modern Japanese and Indonesian rivers estimate quite smaller A_d values than those of rivers worldwide for a given value of Q_b . These regional variations are interpreted to be caused by heavy rains that result in extensive floods, and smaller drainage basins for the fluvial systems in Japan and Indonesia. The empirical equation relating Q_b and A_d derived from the modern Japanese fluvial system can be applied to the modern and ancient fluvial systems developed in the convergent margins that are characterized mainly by the arc–trench systems.
- (4) The L_d – A_d relationships from data of the modern Japanese and Indonesian rivers are characterized by smaller L_d relative to A_d than those of the contiguous United States. These variations are interpreted to be caused by the drainage basins with hills and mountains in the Japanese and Indonesian fluvial systems. The empirical equations

derived from data from the Japanese drainage basins can be well applied to those formed in a convergent margin setting that are characterized mainly by the arc-trench systems.

- (5) Although the W_b-d_m relationship shows variations between datasets used by the present study and previous studies, the regression curves developed from Japanese and Indonesian rivers have similar exponent and coefficient values in log-log plot. The similarity in the regression curves are interpreted to reflect higher flood discharges, downward erosions of riverbeds by floodwaters, and the growth of thick vegetation covers on floodplains which prevent river channels from widening for the rivers in Japan and Indonesia. The empirical equations developed in the present study can be applied to both modern and ancient fluvial systems formed in the arc-trench systems under temperate and trophic climatic conditions.

Part 2. Fluvial response to relative sea-level change: The Paleogene fluvial successions developed in a temperate forearc-basin setting

2-1. Introduction

Fluvial systems are very sensitive to external forces, such as changes in climates, relative sea level, and tectonics (e.g. Blair and Bilodeau, 1988; Blum and Törnqvist, 2000). The interaction between these variables controls spatial and temporal variations in channel patterns and the geometry of a fluvial system (e.g. Summerfield, 1985; Posamentier and Allen, 1993; Schumm, 1993; Shanley and McCabe, 1994; Paola, 2000). In terms of sequence stratigraphy, stacking patterns and sinuosity of fluvial channels have been interpreted to vary in response to a relative sea-level cycle (Wright and Marriott, 1993; Shanley and McCabe, 1994). However, the geometry of fluvial systems is also controlled by hydraulic variables, such as water discharge, grain-size distribution, channel slope, and sediment-transport rate (e.g. Ikeda, 1975; Ferguson, 1987; Blum and Törnqvist, 2000; Bridge, 2003). These hydraulic variables are interpreted to modify the sequence-stratigraphic response of a fluvial system (e.g. Wescott, 1993; Schumm, 1993; Adams and Bhattacharya, 2005). Although variations in the fluvial sequence-stratigraphic models have been discussed elsewhere, sequence-stratigraphic responses of gravelly fluvial systems have not yet been thoroughly investigated compared with those of sandy fluvial systems. Furthermore, a temporal variation in channel cross-sectional dimensions and hydrological features of the paleoriver systems in response to a relative sea-level cycle has not yet been sufficiently examined.

Part 2 investigates temporal variations in geometry and internal organization of a gravelly fluvial system of the Iwaki Formation in Northeast Japan. The formation is

interpreted to have developed in an Eocene to Oligocene forearc basin as a response to an overall rise in relative sea level. This part intends to clarify three-dimensional variations in architecture and component lithofacies assemblages of the gravelly fluvial deposits in terms of the combination of forearc-basin setting and relative sea-level change using well-exposed three-dimensional outcrops. The empirical equations derived from the modern Japanese rivers are also applied to the fluvial deposits of the Iwaki Formation to examine a relationship between fluvial architecture, channel cross-sectional dimensions, water discharges, and a rise in relative sea level. In addition, the present study also discusses a sediment provenance of the Iwaki Formation fluvial deposits on the basis of the estimated drainage basin characteristics.

2-2. Geological Setting

The Iwaki Formation is distributed along the eastern rim of the Abukuma Highlands on the Pacific coast of Northeast Japan (Fig. 20). This area is called the Joban Coalfield, because coal beds in the Paleogene successions were formerly mined in this area. The Iwaki Formation represents the basal unit of the Paleogene Shiramizu Group. The group developed in a forearc-basin setting called the Joban subbasin, which is a part of the Cretaceous to Paleogene Yezo forearc basin (e.g. Ando, 2003). The Shiramizu Group consists of the Iwaki, Asagai, and Shirasaka formations in ascending order, and these formations are characterized by fluvial, shallow-marine, and deep-marine deposits, respectively (Fig. 21) (Sugai et al., 1957; Okami, 1973; Kubo et al., 2002; Komatsubara, 2004; Suto et al., 2005). A part of the Iwaki Formation in the southern Joban Coalfield is also locally characterized by an estuarine deposit (Ueda et al., 2003). The age of the Iwaki Formation is Late Eocene to early Early Oligocene on

the basis of mammalian tooth and pollen assemblages (Tomida, 1986; Sato, 1989).

Kubo et al. (2002) and Suto et al. (2005) inferred that the upper part of the Iwaki Formation contains the Eocene–Oligocene boundary. This interpretation is based on floral and faunal changes of pollen (Sato, 1989) and molluscan (Nemoto and O’Hara, 2001) fossils that indicate a distinct climatic cooling (e.g. Lear et al., 2008).

This study focused on the Iwaki Formation in the northern part of the Joban Coalfield where the formation unconformably overlies the Upper Cretaceous Futaba Group. The Iwaki Formation in the study area (Fig. 20B) is about 190 m in thickness, and is represented mainly by a gravelly fluvial succession (about 75 % in total stratigraphic thickness of the formation) except for the uppermost part, which is represented by an overall coarsening-upward succession from shelf to delta deposits (Fig. 21), and the base of the shelf deposits is defined by a ravinement surface (RS1 in Fig. 21). Therefore, the Shiramizu Group in the study area is interpreted to represent an overall transgressive succession (Komatsubara, 2004; Suto et al., 2005). Although the radioisotopic age of the Iwaki Formation has not yet been obtained, depositional rate of the formation is about 10 cm/1,000 years on the basis of the total stratigraphic thickness of the formation, biostratigraphic datum defined by pollens, diatoms, silicoflagellates, and dinoflagellates of the Shiramizu Group, and an age framework based on regional stratigraphic correlation of the Shiramizu Group and its age-equivalent stratigraphic successions in the Ishikari Coalfield of Hokkaido (Kubo et al., 2002; Suto et al., 2005).

The clast composition of the Iwaki Formation is represented by chert fragments (approximately up to 55%), together with fragments of granitic and porphyritic rock, green schist, basic intrusive rock, slate, and sandstone (Okami, 1973). These clasts are considered to have been derived mainly from metamorphic rocks, granitic rocks,

non-metamorphic Paleozoic rocks, and intrusive rocks in the Abukuma Highlands (Fig. 20). Some chert clasts, which include Triassic conodonts, have also been interpreted to be derived from Jurassic accretionary deposits in the Yamizo and Ashio Mountains (Okami et al., 1978). Only the basal part of the formation shows spatial variation in the clast composition of conglomerates (Okami, 1973).

2-3. Datasets and methods

Three-dimensional lithofacies and architectural analyses of the gravelly fluvial deposits were conducted using large outcrops in a major quarry and a roadside cliff. Photographic mosaics from these outcrops and additional measured sections from several other quarries and riverside cliffs were used for the present analyses. The present study employed the basic concept of the hierarchical bounding-surface and architectural element analyses of Miall (1985, 1988, 1996) for the definition of lithofacies assemblages and fluvial forms in the outcrops.

The data of paleocurrent directions were measured mainly from dip directions of the axial part of trough or planar cross-bedded surfaces. Mean clast-size of conglomerates was measured at the basal part of each channel deposit (5th-order depositional unit discussed below) using grids laid over the surface of vertical exposures. One hundred of the clasts were taken at grid intersections, and the long axis of the selected clasts was measured. Subsequently, the mean clast-size was calculated. The relative thickness between gravelly, sandy, and muddy components of each channel deposits was calculated on the basis of measured sections. Thickness of bar deposits (thickness of 4th-order depositional unit discussed below) was measured using outcrops and outcrop photographs. In this paper, 'bar deposits' were defined as deposits that are

equivalent to the compound bar (Bridge, 2003) deposits or the macroform element (Miall, 1996). The bankfull depth, mean bankfull channel depth, bankfull channel width, mean discharge, bankfull discharge, drainage basin area, and drainage basin length are also estimated using measured thickness of bar deposits and the empirical equations of modern Japanese rivers that were determined in part 1. Furthermore, channel slopes and backwater length can be estimated from median grain size and bankfull channel depth using equations by Paola and Mohrig (1996) and Blum et al. (2013).

2-4. Bounding surfaces

In this study, six major bounding-surface (BS) types (1st- to 6th-order in increasing scale order) were discriminated in the Iwaki Formation. The hierarchical classification of the bounding-surface types was defined by lateral continuity, geometry, lithofacies features, and paleocurrent directions of the encased fluvial deposits (Table 10). Each bounding-surface type defines a depositional-unit (DU) type (1st- to 6th-order DU types in increasing scale order) (Fig. 22).

In the Iwaki Formation fluvial deposits, multi-stacking of the bar deposits (4th-order DU) constitutes a channel deposit (5th-order DU: CH) of up to 24 m thick (Figs. 23–25). Everywhere, sandy and/or muddy deposits of up to 3 m thick characterize the uppermost parts of each channel deposit. These finer-grained deposits, which extend laterally up to hundreds of meters, are truncated by the overlying channel deposits.

Sets of 2 to 4 stories of stacked channel deposits are bounded by the 6th-order BS in the base and top, and constitute a channel complex of up to 60 m thick (6th-order DU: CHC). Three major channel complexes are identified in the Iwaki Formation. Thicker floodplain muddy deposits as much as 3 m thick, in local association with coal

beds of up to 3 m thick, characterize the uppermost part of each channel complex. Overall, gravelly fluvial deposits of the Iwaki Formation are subdivided into three major channel complexes (CHC-I to CHC-III) and ten component channel deposits (CH-A to CH-J) (Figs. 23–25), which onlap onto the basal unconformity in the north (Fig. 26). The stratigraphic cross-section in Figure 26 indicates that the along-strike distribution of the channel complexes extended sequentially to the north in response to the northward migration of depocenters. The basal unconformity of the formation corresponds to a sequence boundary (SB1 in Figs. 23, 24, 26), and the upper surface of the uppermost channel complex is a ravinement surface (RS 1 in Figs. 21, 25, 26) on which shelf deposits of the uppermost Iwaki Formation were formed.

2-5. Architectural elements

Eight architectural element types are discriminated in the Iwaki Formation (Fig. 27). Gravel-bar (GB) deposits laterally change to downstream-accreting (DA) deposits (Fig. 28A). The combination of these two elements represents about 60% of the Iwaki Formation in the sections. Gravel-bar deposits are also locally associated with lateral-accreting (LA) deposits, which are a minor element in the Iwaki Formation. Small-scale channel-fill (SCH) deposits (Fig. 28B) rest commonly on gravel-bar and sandy-bar (SD) deposits. Everywhere, sandy-bar and floodplain muddy (FF) deposits (Fig. 28C) characterize the uppermost parts of each channel (CH) and channel complex (CHC) deposit.

2-6. Spatial variation in channel complexes

Figure 29 summarizes vertical changes in paleocurrent directions, mean clast-size,

and thickness ratio of gravelly, sandy, and muddy components through the channel deposits of the Iwaki Formation (Investigated Routes 7a and 7b in Fig. 20B and Section 7 in Fig. 26). In general, paleocurrents are directed to the east and northeast, and do not show any distinct spatial and temporal variations (Figs. 26, 29). The mean clast-size decreases upsection in each channel complex (CHC), except for a minor increase from CH-E to CH-F of CHC-II (Fig. 29). The mean clast-size also exhibits an overall decrease from CHC-I to CHC-III. Thickness ratios of muddy and sandy components relative to a gravelly component also show vertical changes from CHC-I to CHC-III, similar to those of the mean clast size. In CHC-I and CHC-II, the uppermost channel deposits (CH-D and CH-H) contain thicker muddy deposits (i.e. FF element) than the underlying channel deposits. Although CHC-III does not exhibit a distinct upward increase in the thickness ratio of muddy and sandy components relative to a gravelly component in the channel deposits, the upper part (CH-J) is also characterized more by deposition of thick floodplain muddy deposits in association with coal beds, than the lower part.

2-7. Paleohydrology

Bankfull channel depth (d) is roughly equivalent to the stratigraphic thickness of a fully preserved bar deposit (h) (Allen, 1970; Leeder, 1973; Elliott, 1976; Bridge and Diemer, 1983; Lorenz et al., 1985). Although this model is more appropriate for untruncated point bar deposits near bend apices of meandering channels (Bridge and Mackey, 1993), a model of gravelly braided rivers by Lunt et al. (2004) also indicates that the thickness of compound braid bar is largely equal to d . This model is also supported by a cross-section of the Tone River at Yattajima (Site 7 in Fig. 7 and Table 3;

Fig. 9C), where the thickness of a compound bar is almost the same as d . The thickness of bar accretionary units, barforms, and channel stories of multiple-thread, braided paleochannel deposits have also been used for the depth estimations (Adams and Bhattacharya, 2005; McLaurin and Steel, 2007; Hampson et al., 2013). In the present study, thicknesses of 3 to 16 bar deposits (h) of each channel deposit (CH-A to CH-J) in the Iwaki Formation fluvial deposits were measured at a major quarry and a roadside cliff (Investigated routes 7a and 7b in Fig. 20) using photographic mosaics of outcrops and measured sections (Figs. 23–26, 30). The measured data of bar deposit thickness range from 2.2 to 6.6 m with an average of 3.9 m. Practical thicknesses of bar deposits are interpreted to be slightly less (90%) than the maximum bankfull depth (Bridge and Diemer, 1983; Bridge and Mackey 1993). Because stratigraphic thickness of bar deposits has been affected by compaction, the reduction in thickness for coarse-grained sediments (sands, gravels, and grainstones) is up to 40–60 % (Stow, 2005). Ethridge and Schumm (1978) and Lorenz et al. (1985) suggested that a 10 % compaction factor is reasonable for the estimation of sandy paleochannel depths. The present study also tentatively adopted the 10% compaction factor. Thus, the corrected h is used for the calculation of d (i.e., $d = h \times 10/9 \times 10/9$). Therefore, d is estimated at 2.7 to 8.1 m with an average of 4.8 m. Using the empirical relationship between d and d_m from the rivers of the Kanto region ($d_m = 0.62d$) (Table 5), d_m is estimated at 1.7 to 5.1 m with an average of 3.0 m. On the other hand, the relationship between d_m and W_b from the rivers of the Kanto region ($W_b = 49.16 d_m^{0.66}$) (Table 5) estimates W_b at 69.3 to 143.2 m with an average of 100.9 m. Using the empirical relationships between W_b and the mean discharge (Q_{mean}) and bankfull discharge (Q_b) of Japanese rivers ($Q_{\text{mean}} = 0.17 W_b^{1.21}$, $Q_b = 2.78 W_b^{1.17}$) (Table 4), Q_{mean} is calculated at 28.7 to 69.0 m^3s^{-1} with an average of

45.4 m³s⁻¹, and Q_b at 396.3 to 925.6 m³s⁻¹ with an average of 616.6 m³s⁻¹. Finally, the equation of the relationship between Q_b and drainage basin area (A_d) ($A_d = 3.41 Q_b^{0.89}$) and between A_d and drainage basin length (L_d) ($L_d = 1.73 A_d^{0.47}$) from the modern Japanese rivers (Table 4) estimate the A_d and L_d values of the Iwaki Formation fluvial system at 699.8 to 1,489.0 km² with an average of 1,035.3 km², and 37.6 to 53.6 km with an average of 45.0 km, respectively. These estimated parameters for each channel deposit (CH-A to CH-J) do not show any distinct vertical changes through the entire fluvial succession (Fig. 31; Table 11).

Channel slope (S) for coarse-grained braided channel deposits can be estimated by using an equation proposed by Paola and Mohrig (1996):

$$S = 0.094 D_{50}/d$$

where D_{50} and d are median grain size and bankfull channel depth, respectively. D_{50} for each channel deposit (CH-A to CH-J) ranges from 6.5 to 34.0 mm with an average of 18.3 mm, and channel slopes were estimated at 1/10,911 to 1/2,549 with an average of 1/4,278. Backwater length (L_b), which defines the inland distance over which there is a clear morphodynamic link with sea level, is calculated by an equation that was proposed by Paola and Mohrig (1996) (Blum et al., 2013):

$$L_b = d / S$$

where d and S are bankfull channel depth and channel slope, respectively. This equation estimated the backwater length for each channel deposit at 15.1 to 72.7 km with an

average of 27.2 km. The values of S decrease upsection in each channel complex (CHC), and they also exhibit an overall decrease from CHC-I to CHC-III (Table 11).

2-8. Discussion

2-8-1. Fluvial evolution

Downstream-fining of bed-load clast-size in gravelly fluvial systems is controlled by selective transport or abrasion, but the relative importance of these processes still remains controversial in relation to different hydraulic settings (e.g. Werritty, 1992; Kodama, 1994; Gasparini, et al. 1999; Hoey and Bluck, 1999; Rice, 1999). Under turbulent flow conditions, longitudinal clast-size sorting is the result of bar–pool system migration in fluvial channels, and this type of local-scale sorting is interpreted to contribute substantially to longer-scale downstream-fining along a river system (Clifford et al., 1993). Except for the CH-A deposit, clast composition of fluvial-channel deposits does not show any distinct sequential change (Okami, 1973). Therefore, the overall fining-upward patterns in both the entire fluvial succession of the Iwaki Formation and the component channel complexes (CHC-I to CHC-III) are interpreted to document downstream-fining of clast-sizes (Fig. 29) as a result of selective sorting (e.g. Hoey and Bluck, 1999; Gasparini et al., 1999).

On the other hand, maximum clast-sizes of gravelly fluvial deposits reflect flow competence (bed shear stress) and are controlled by flow depth, flow velocities, slopes, and flow discharges even within deposits of mixed sizes (Wilcock, 1992; Komar, 1996). During the deposition of the Iwaki Formation fluvial deposits, there is no positive evidence of climatic changes (Sato, 1989; Kubo et al., 2002; Suto et al., 2005). Furthermore, the estimated bankfull channel width and bankfull discharge vary from

100 to 140 m and from 600 to 925 m³/s, respectively (Table 11), and do not show any distinct million-year-scale temporal variations through the entire fluvial succession (Fig. 31). These geomorphological and hydrological features imply that the precipitation of the Iwaki Formation drainage basin has been constant during the deposition of the Iwaki Formation fluvial deposits. Thus, the two-fold fining-upward patterns in each channel complex (CHC) and in the entire fluvial succession of the Iwaki Formation are interpreted to have been caused by the reduction in slopes (Table 11), which appears to have responded to relative rise in sea level.

Although amalgamated channel and bar deposits characterize the channel complexes, the uppermost part of each channel complex is represented by thicker sandy and muddy deposits in association with laterally extensive coal deposits. Furthermore, the Iwaki Formation represents progressive onlapping of the fluvial deposits over the basement rocks upsection (Fig. 26). These vertical changes in lithofacies features and stacking patterns appear to have responded to the increase in nonmarine accommodation during the rise in relative sea level and also to the resultant rise in the water table as pointed out by Wright and Marriott (1993) and Shanley and McCabe (1994).

Although there is no independent outcrop evidence of relative rise in sea level from coeval coastal and shallow-marine successions in the study area, an Oligocene transgressive succession from coastal- and shallow-marine sandstones to deeper marine mudstones was identified in a site about 50 km offshore to the east of the study area in the Joban subbasin (Iwata et al., 2002) (Iwaki-oki Gas Field) (Fig. 3). The succession in the offshore site is considered to represent a lower reach of the Iwaki Formation fluvial system on the basis of the age framework (Iwata et al., 2002) and paleocurrents of the formation (Figs. 26, 29). Thus, the Iwaki Formation fluvial system appears to have been

sensitive to the relative change in sea level at the age-equivalent coastal environments. Furthermore, the Iwaki Formation fluvial system changes locally into sandy fluvial and estuarine deposits that show two transgressive-regressive cycles in the southern Joban subbasin (Ueda et al., 2003). This spatial variation in the coeval depositional environments indicates that a part of the Iwaki Formation developed in response to a transgression, although the Iwaki Formation fluvial system does not document any tidal signature, which is one of the important diagnostic features of a transgressive fluvial system (Shanley and McCabe, 1994). On the basis of this interpretation, a Paleogene coastline of the Joban Coalfield area can be considered to be within 30 km east of the investigated area, because the backwater lengths of the Iwaki Formation fluvial system were estimated at 15.1 to 72.7 km with an average of 27.2 km (Table 11).

Modern gravelly river systems in the forearc-basin setting such as the Naka and Kinu Rivers and some other rivers near the study area have longitudinal downstream length of less than 150 km, and the transition areas between gravelly and sandy deposits are located at a 10–50 km upper reach from the river mouths (Yatsu, 1951; 1957) (Fig. 7). Because the Iwaki Formation fluvial system is considered to have developed in an area of about 30 km upstream from the coastline as described above, sandy fluvial deposits seem to have been formed in the lower reach of the Iwaki Formation fluvial system in an area farther east of the study area. Thus, the fining-upward patterns in each channel complex of the Iwaki Formation fluvial deposits are interpreted to reflect upslope migration of the gravel/sand transition area. Although lateral migration and abandonment of a gravelly fluvial system as a result of autogenic processes are also alternative possible processes for developing fining-upward patterns in each channel complex, the fining-upward cycles in the channel complex-scale fluvial deposits (up to

60 m thick) are commonly interpreted to have formed as a response to allogenic processes (Godin, 1991).

An alluvial-fan system is also characterized by gravelly fluvial deposits and can develop fining-upward patterns as a response to lateral migration of the depocenters, in particular along basin-margin faults (e.g. Steel, 1988; Miall, 1996; Gawthorpe and Leeder, 2000). In the Iwaki Formation fluvial system, the along-strike distribution of gravelly deposits is not laterally limited and the basin margins are not represented by faults (Fig. 20B). Furthermore, the unidirectional paleocurrent data of the formation does not indicate a cone-shaped fluvial form (Figs. 26, 29). Thus, this gravelly fluvial system is interpreted to have developed as a gravelly braided plain rather than a gravelly alluvial fan.

In general, the uppermost deposits of each channel complex are not deeply incised by the base of the overlying channel complex (Fig. 26). This relationship suggests that vertical stacking of the three channel complexes was not accompanied by an appreciable fall in relative sea level. Thus, the development of vertically stacked fluvial deposits of the Iwaki Formation appears to have been controlled by the active creation of nonmarine accommodation in association with relative rise in sea level. Therefore, the overall rise in relative sea level for the entire gravelly fluvial succession is interpreted to have consisted of three superimposed shorter-term rises, each of which was followed by a stillstand and/or minor fall in relative sea level (Fig. 32).

2-8-2. Paleohydrological parameters and provenance

Although the results of paleochannel reconstruction from the Iwaki Formation have wide ranges (Fig. 31), these variations are derived from incomplete preservation of

original thicknesses of bar deposits as a result of subsequent erosion of the overlying channel deposits. Some well-preserved bar deposits, which are overlain by floodplain muddy deposits, were also used in the present study. Thus, the present study interpreted that the thickest values of bar deposits and the resultant maximum geomorphological and hydrological parameters in each channel deposit (CH-A to CH-J) are more plausible than average values for representing bar thickness, channel sizes, drainage basin areas, and discharges of the Iwaki Formation fluvial system. With respect to these maximum values for each channel deposit (CH-A to CH-J), the bankfull channel depth (d) is determined from 4.7 to 8.1 m, mean bankfull channel depth (d_m) from 2.9 to 5.1 m, bankfull channel width (W_b) from 99.5 to 143.2 m, mean discharge (Q_{mean}) from 44.4 to 69.0 m^3s^{-1} , and bankfull discharge (Q_b) from 604.4 to 925.6 m^3s^{-1} , drainage basin area (A_d) from 1018.8 to 1498.0 km^2 , and drainage basin length (L_d) from 44.9 to 53.6 km. Figure 33A illustrates the reconstructed Iwaki Formation fluvial system with the estimated maximum values using the data of CH-A. These values indicate that the fluvial deposits of the Iwaki Formation are interpreted to have formed by a fluvial system, which had geometric and hydrological characteristics almost equal to, or bigger than modern gravelly rivers flowing in the Kanto region. In particular, the estimated values of the Iwaki Formation fluvial system are represented by geomorphological and hydrological parameters that are approximately equivalent to those obtained from the gauging stations between the middle (Yamagata: $d = 2.9$ m, $d_m = 1.6$ m, $W_b = 98.0$ m, $A_d = 897.8$ km^2 , $Q_m = 25.7$ m^3s^{-1} , $Q_b = 431.6$ m^3s^{-1}) and lower (Sakakibashi: $d = 7.2$ m, $d_m = 2.8$ m, $W_b = 360.0$ m, $A_d = 1422.0$ km^2 , $Q_m = 15.6$ m^3s^{-1} , $Q_b = 666.2$ m^3s^{-1}) reaches of the modern Kuji River in the northern Kanto region (Fig. 7) (Japan River Association, 2007; The River Bureau, Ministry of Land, Infrastructure and Transport ed., 2009). In

contrast, an average of channel slopes for each channel deposit ($S = 1/4,278$) is equivalent to the slope of the lower reaches of the modern Naka River ($S = 1/7,000$ to $1/4,000$) in the northern Kanto region (Fig. 7) (Takahashi, 2013). A transition area between gravelly and sandy river bed is located in the lower reaches of the Kuji and Naka rivers (Yatsu, 1951; Fig. 7). Three cycles of fining-upward trend in each channel complex (CHC) of the Iwaki Formation fluvial deposits are also interpreted to reflect upslope migration of the gravel to sand transition area, as a response to rises in relative sea level as discussed above. Therefore, the Iwaki Formation fluvial system is interpreted to have formed in geomorphological and hydrological settings equivalent to those observed in the middle to lower reaches of the modern Kuji River and the lower reaches of the Naka River.

The sediment source area cannot be determined directly from the calculated A_d values. Davidson and North (2009) assumed a range of plausible valley widths for the estimated drainage basin areas for some ancient fluvial systems, and discussed possible drainage basin lengths. In contrast, Xu et al. (2017) established an equation for the relationship between the stream length and the channel-belt thickness (i.e. bar deposit thickness) on the basis of data from the five Miocene fluvial systems in the Gulf of Mexico basin, and Liu et al. (2019) also applied the equation to the Middle Jurassic fluvial deposits, in the northern Qaidam Basin, NW China. The present study used the empirical equation between the drainage basin length (L_d) and drainage basin area (A_d) derived from the modern Japanese rivers, and estimated L_d values of the Iwaki Formation drainage basin for each channel deposits (CH A to J) at 44.9 to 53.6 km with an average of 49.3 km. Because the paleocurrent directions of the Iwaki Formation fluvial system were towards the east and northeast, the source area and the headwater

are expected to have been to the west or southwest of the investigated area. However, their exact locations cannot be directly determined, because the paleoriver courses have not been preserved. This study reconstructed a possible spatial range of the most distant headwaters for the Iwaki Formation fluvial system using the estimated L_d values on a Paleogene paleogeographic map (Fig. 33B). In Figure 33B, possible headwaters are mainly located at the present Abukuma Highlands, which have been interpreted to be a main source area of the clastic sediments of the Iwaki Formation based on petrographic characteristics of conglomerates and sandstones (Okami, 1973). In addition, the most distant possible headwaters from the study area may reach the Yamizo Mountains, which are located about 50–70 km west-southwest of the study area. This possible hinterland is beyond the Tanakura Tectonic Line, which is a NNW–SSE trending major fault that divides pre-Neogene basement rocks into Northeast and Southwest Japan (Awaji et al., 2006; Yanai et al., 2010). The Tanakura Tectonic Line is interpreted to have been active up to at least the Miocene time (Awaji et al., 2006; Yanai et al., 2010). The fault displacement is interpreted to be less than 100 km after Miocene (Takahashi and Ando, 2016) because the lower to middle Miocene successions are distributed successively on both sides of the tectonic line (Amano, 2018). Furthermore, relative locations between the investigated area and the Yamizo and Ashio Mountains are considered not to have been significantly changed after Cretaceous (Ando and Takahashi, 2017). This tectonic setting indicates that some clastic sediments of the Iwaki Formation may have been derived from the basement rocks of the Yamizo Mountains. The sediment supply from the Yamizo Mountains to the Iwaki Formation has also been assumed on the basis of the common occurrences of the Triassic conodonts from some chert clasts of the formation and from the Jurassic accretionary

deposits in the Yamizo and Ashio Mountains (Okami et al., 1978). On the other hand, the sediment supply from the Ashio Mountains to the Iwaki Formation fluvial system is improbable, because the Ashio Mountains are located more than 120 km southwest of the study area, and the distance is quite far from the estimated location of possible headwaters of the Iwaki Formation fluvial system (Fig. 33B). Consequently, on the basis of the estimation of A_d and L_d values, the possible sediment provenance of the Iwaki Formation fluvial deposits can be narrowed down to having been the Abukuma Highlands and Yamizo Mountains, which have not yet been determined from the analyses of the petrographic features of the Iwaki Formation detrital fragments.

2-8-3. Sequence-stratigraphic implications

The standard sequence-stratigraphic models predict that, in response to a rise in relative sea level, the connectivity of fluvial channels and channel deposit dimensions decrease and the sedimentation rate in the floodplain increases to the point where isolated single story channels develop (Wright and Marriott, 1993; Shanley and McCabe, 1994; Catuneanu et al., 2009, Blum et al., 2013). However, the gravelly fluvial successions of the Iwaki Formation neither exhibit distinct temporal change in major architectural elements and channel cross-sectional dimensions nor include the point-bar and isolated channel deposits encased in floodplain muddy deposits. Such architectural features of the Iwaki Formation fluvial system alternatively suggest that fluvial styles did not change in response to the relative rise in sea level.

In general, fluvial systems in the Japanese Archipelago are characterized by several geomorphologic and hydrologic features, which reflect temperate climatic conditions influenced by monsoons and active tectonic movement as a convergent plate

margin (e.g. Takahashi and Sakaguchi, 1976; Sakaguchi et al., 1986). That is, modern rivers of Japan are characterized by shorter length and higher gradient than those in continental areas. Higher values of mean annual and bankfull specific discharge (in $\text{m}^3\text{s}^{-1}\text{km}^{-2}$) and of the coefficient of river regime also characterize the modern rivers of Japan in association with higher denudation rates in the drainage basins compared with modern rivers in continental areas (Ohmori, 1983a, b). These distinctive features of the modern rivers of Japan suggest a potential for having developed thick successions of coarse-grained fluvial deposits in ancient forearc basins in response to the creation of nonmarine accommodation, although the modern rivers of Japan have been formed mainly during late highstand- or earliest falling-stages in relative sea level (e.g. Oya, 1993).

Although a strong monsoonal circulation is interpreted to have developed since 8 Ma (e.g. Nishi and Takashima, 2005), the Iwaki Formation fluvial system seems to have developed under a paleohydrologic condition similar to that for modern rivers in the forearc-basin setting in Japan because of the following two reasons. First, downstream variation in mean clast-size of the gravely deposits documented in the Iwaki Formation fluvial system (Fig. 29) is similar to that of modern Japanese rivers (Yatsu, 1951; Fig. 7). Second, the channel dimensions of the Iwaki Formation fluvial system were as large as that of modern rivers around the study area, such as Kuji River, central Japan. Third, the Iwaki Formation fluvial deposits contain some pollen floras that characterize a temperate climate similar to modern Kanto region, such as *Quercus*, temperate tricolpate pollen, *Liquidambar*, *Rhus* or *Nyssa*, *Ilex*, and *Carya* (Sato, 1989). Therefore, the monsoon climates are not necessarily prerequisite for the paleohydrologic similarity between the Iwaki Formation fluvial system and modern

fluvial systems in Japan, but the similarities seems to have been controlled by the temperate climates as suggested by the pollen floras.

In terms of channel cross-sectional dimensions, Adams and Bhattacharya (2005) reported an example of slight change in fluvial channel dimensions across a sequence boundary. In contrast, Hampson et al. (2013) reconstructed broader multiple-thread channels with higher discharges in the upper parts, and narrower single-thread channels with lower discharges in the lower parts of sandbodies within a regressive fluvial-to-deltaic succession. They suggested that if these temporal variations in channel size and discharge had been caused by shifts of channel position relative to the shoreline, multiple-thread channels with higher discharge branched downstream to form distributary channels with lower discharge on the delta plain. In the case of the Iwaki Formation fluvial system, the estimated bankfull channel dimensions and hydrological parameters do not show any distinct vertical changes within the fluvial succession, except for the reconstructed parameters in CH-C that are smaller than the other deposits (Fig. 31). Because the bar deposits of CH-C are not covered by muddy floodplain deposits and the upper parts of the bar deposits were commonly subjected to distinct erosion by younger bar deposits, the preserved stratigraphic thickness of the bar deposits of CH-C results in smaller estimation of hydrological parameters. Consequently, the channel cross-sectional dimensions (d , d_m , and W_b), and discharge parameters (Q_m and Q_b) of the Iwaki Formation fluvial system are considered to have been affected neither by both an overall rise and superimposed shorter-term rises in relative sea level nor the resultant changes in the distance from the coeval shoreline. In addition, because there is no evidence of climatic change during the deposition of the fluvial successions of the Iwaki Formation, the geomorphological and hydrological

parameters of the Iwaki Formation fluvial system appear to have been affected by fixed water discharge and sediment supply derived from hinterland.

On the basis of the paleohydrologic similarity between the Paleogene and modern fluvial systems in the forearc-basin setting in Japan, the higher denudation rates in the drainage basin and higher values of mean annual and bankfull specific discharge seem to have also played an important role for developing amalgamated channel deposits with minor variations in the bankfull channel cross-sectional dimensions in the Iwaki Formation fluvial system. Therefore, the present example from the Iwaki Formation indicates that a gravelly fluvial channel and floodplain muddy deposits do not have to exhibit any distinct temporal change in geometry, stacking patterns, and channel dimensions, but rather can be characterized by an overall fining of mean clast-sizes in response to an overall rise in relative sea level. This type of sequence-stratigraphic fluvial signature is likely representative of active-margin-basin settings in temperate climates, where fluvial systems have steeper valley slopes and active shedding of coarse-grained sediments along with high annual discharges.

2-9. Conclusions

- (1) Architectural element analyses of the Paleogene Iwaki Formation, Northeast Japan, revealed that the fluvial succession was represented by couplets of amalgamated bar and channel deposits and minor floodplain muddy deposits, which constitute three major channel complexes.
- (2) The succession is interpreted to have been deposited during transgressive stages in response to relative rise in sea level on the basis of stacking patterns and lithofacies features of the fluvial deposits and of correlation with a coeval marine succession in

the offshore area. Channel complexes are defined by regionally mappable bounding surfaces. These surfaces do not exhibit distinct erosion except for the basal unconformity of the formation, which is characterized by a stepped erosional surface, and considered to have developed during the preceding fall in relative sea level.

- (3) The empirical equations, which were developed by the present study, were applied to a transgressive gravelly fluvial succession of the formation. The result indicates that geomorphological and hydrological conditions of the Iwaki Formation fluvial system were equivalent to those of the middle to lower reaches of the modern Kuji and Naka rivers in the northern Kanto region of central Japan.
- (4) The estimated drainage basin dimensions indicate that the sediment provenance of the Iwaki Formation fluvial deposits is interpreted to have been the Abukuma Highlands and Yamizo Mountains.
- (5) Major fluvial styles, stacking patterns, and channel cross-sectional dimensions do not show any distinct changes throughout the entire fluvial succession. The present example is from a forearc-basin setting, and this type of basin is characterized by steeper valley slopes, active shedding of coarse-grained sediments from the nearby hinterlands, and shorter longitudinal profiles to the river mouth. This geologic framework is responsible for the diversion away from the standard fluvial sequence-stratigraphic models. Thus, the present example represents one type of the variation in the standard fluvial sequence-stratigraphic models.

Part 3. Fluvial response to tectonic cycles: The Paleogene tropical fluvial deposits developed in a forearc-basin setting

3-1. Introduction

Fluvial systems developed in inland basins are affected by tectonic cycles and climatic fluctuations (Blair and Bilodeau, 1988; Shanley and McCabe, 1994; Blum and Törnqvist, 2000; Bridge, 2003; Holbrook et al., 2006; Miall, 2014). Basin subsidence and the uplift of provenance control regional valley slope, the relief in the source area, and a rate of accommodation creation (Blair and Bilodeau, 1988; Shanley and McCabe, 1994; Miall, 2014). In contrast, precipitation and evaporation, which are characterized by specific climatic conditions, control hydrological features of fluvial systems, such as water and sediment discharges and vegetation cover (Knox, 1983; Ohmori, 1983a, b). These geomorphological and hydrological features have also been considered to control spatial and temporal variations in stacking patterns of fluvial deposits and cross-sectional dimensions of ancient fluvial channels (Martinsen et al., 1999; Jo, 2003; Paredes et al., 2007, 2018; Hillier et al., 2007; Colombera et al., 2017). Therefore, some case studies of paleohydrological reconstruction are required for fluvial deposits that developed under various tectonic and climatic conditions for a better understanding of the allogenic controls on the fluvial architectural features. In particular, the application of empirical equations has not yet been tested in an ancient fluvial system that developed under a tropic climatic condition in the convergent-margin setting.

Part 3 examines temporal variations in stacking patterns, channel cross-sectional dimensions, discharges, and drainage basin characteristics of a fluvial system of the Eocene–Oligocene Bayah Formation in West Java, as an example of an ancient fluvial

system formed in a forearc-basin setting under a tropical climatic condition. The present study applies the empirical equations of the modern Indonesian fluvial system to the Paleogene fluvial deposits in order to discuss a fluvial response to tectonic cycles in terms of paleohydrological features and stacking patterns. In addition, a sandstone provenance of the Bayah Formation is examined with comparison between the results from the application of the empirical equations and the previously published data of detrital zircon U-Pb ages.

3-2. Geological setting

The present study focused on the Paleogene Bayah Formation, which is characterized by fluvial and lacustrine-delta successions about 900 m in thickness, and is exposed in the Sukabumi high, at the southwestern part of Java. During the Paleogene, western Java was situated at the southern edge of the Sundaland continent, which was a part of the SE Asian continent (Fig. 34). In Early Eocene, a sedimentary basin of the Bayah Formation is interpreted to have developed in a forearc region of the Sunda–Java volcanic arc (Adhiperdana, 2018), although the volcanic arc shifted to the southern part of the basin in Late Oligocene or Miocene (Soeria-Atmadja and Noeradi, 2005). A Paleogene coastline was located tens of kilometers south of the present coastline (Hall, 2012), and the distance between the Paleogene coastline and the Bayah Formation depositional basin in the Sukabumi high is interpreted to have been more than 80 km. The major direction of sediment delivery system in western Java is considered to have been south or southwest during Eocene (Clements and Hall, 2011; Adhiperdana, 2018). The major sediment provenance of the Bayah Formation in the Sukabumi high is interpreted to have been derived from the Paleozoic–Mesozoic basement rocks of the

Sundaland continental margin located to the north of the Bayah Formation depositional basin (Hamilton, 1979; Hall, 2012). On the basis of sandstone framework composition of the Bayah Formation (Adhiperdana, 2018), the provenance of the Bayah Formation is suggested to have been derived from the basement rock terrain that consists primarily of granitoid, metasedimentary, and low-grade metamorphic rocks (Hamilton, 1979). In contrast, on the basis of detrital zircon U-Pb ages, Clements and Hall (2011) demonstrated that the detrital fragments of the Bayah Formation were derived from the Cretaceous granites that are distributed in the present Sunda Shelf (Williams et al., 1988) and the Schwaner Mountains of SW Kalimantan (van Hattum et al., 2006), and from the Permian and Triassic granites distributed in the Indonesian Tin Islands (Cobbing et al., 1992) (Fig. 34).

The basal contact of the Bayah Formation with the basement rocks is not exposed in the Sukabumi high. In contrast, the formation is unconformably overlain by marine limestones of the Rajamandala Formation and marine shales of the Batuasih Formation. Based on spores and pollen found from the upper part of the Bayah Formation, the age of the formation was assigned to be Early Oligocene (Martodjojo, 1984). In contrast, the palynological records from the formation indicate the age of the formation as Late Eocene (Morley, 2012) or Early to Late Eocene (Adhiperdana, personal communication 2021). Calcareous nanno plankton and planktonic foraminifera samples from marine deposits of the Batuasih Formation that conformably overlies the Bayah Formation represent Early–Late Oligocene (Morgenroth et al., 2011; Hendrizan et al., 2012). Although the detailed radioisotopic age of the Bayah Formation has not yet been determined, depositional rate of the formation is up to 14 cm/1,000 year on the basis of the total stratigraphic thickness of the formation, and the ages of some datum

that were defined by pollen and spore biostratigraphy (Martodjojo, 1984; Morley, 2012; Adhiperdana, 2018).

During the Eocene, equatorial paleoclimate in the Sundaland region, including Java, is interpreted to have been a subhumid ever-wet to seasonal, which was suggested by the common occurrence of coals (Morley, 2012). In addition, the widespread occurrence of the low-pollen vegetation from Sumatra to West Java suggests that the Oligocene climates in some parts of Sumatra and Java Sea were from subhumid seasonal to ever-wet conditions (Morley, 2012; Morley and Morley, 2013). Palynological evidence also suggests that the islands of Sumatra and Kalimantan maintained an equatorial position, and the position of Java was situated slightly south of the equator (Boucot et al., 2013). In contrast, the detrital composition of sandstone framework grains and clay minerals in the Bayah Formation fluvial deposits do not indicate distinct climatic change (Adhiperdana, 2018). Consequently, the Bayah Formation represents a fluvial succession deposited under a stable climate of tropical, subhumid seasonal and/or ever-wet conditions.

3-3. Data and methods

The channel cross-sectional dimensions, such as bankfull channel depth (d), mean bankfull channel depth (d_m), bankfull channel width (W_b), and mean (Q_{mean}) and bankfull (Q_b) discharges of the Bayah Formation fluvial channel-fill deposits are available from datasets by Adhiperdana (2018) (Fig. 35; Table 12). Because the modern fluvial systems of the Indonesian Archipelago are considered to be consistent with the regional setting for the Bayah Formation fluvial system that were situated in an active margin of the Sundaland under the tropical-climate condition in equatorial zone, the

application of the empirical equations developed from the modern Indonesian rivers to the Bayah Formation fluvial system is reasonable. The present study established the relationships between Q_b , the drainage basin area (A_d), and the length (L_d) of the modern Indonesian rivers on the basis of datasets by Adhiperdana et al. (2018) and the Center for Water Resources Development and Research (2011) (see Part 1) (Fig. 17 and 18), and applied them to the Bayah Formation fluvial successions.

3-4. Temporal variation in the fluvial deposits

Packages of sandstone–conglomerate fluvial bodies in the Bayah Formation were subdivided into three major types (Adhiperdana, 2018) on the basis of internal lithofacies organizations and geometry of the deposits. The conglomerate-dominated packages (Type 1) mainly consist of vertically stacked conglomerates with crudely horizontal and trough cross-stratification. Inclined foreset bedding indicating downstream accretion of bar deposits is also locally observed. The type 1 packages do not show distinct upward-fining trend. The individual beds are of more than 8 m in thickness, and can be traced more than 250 m laterally. This package type is interpreted to represent a bedload-dominated sedimentation in gravelly braided rivers (Adhiperdana, 2018). The conglomeratic sandstone packages (Type 2) are characterized by crudely horizontal and trough-cross stratified conglomeratic sandstone, and gently inclined foreset which indicates downstream-accreted bar deposits. The individual beds are more than 3 m in thickness, and are more than 100 m in the lateral extent. The type 2 packages were interpreted to represent longitudinal and transverse bars that developed in a transitional area between braided and sinuous rivers by Adhiperdana (2018). However, the lack of point bar deposits that are characterized by lateral accretion

surfaces in type 2 packages may indicate gravelly and sandy braided rivers with longitudinal and transverse bars. The lenticular and tabular sandstone-dominated packages (Type 3) are characterized by pebbly sandstones at the basal parts, which incised into the underlain muddy deposits and have either concave-upward or planar-shaped basal surfaces. This package type shows distinct upward-fining trends, and passes upward into the interbedded thin sandstone and mudstone deposits with lateral accretion surfaces, and is finally covered with thick carbonaceous mudstone deposits. The thickest deposits can be laterally traced for more than 200 m. This package type is interpreted to represent mixed-load sedimentation in meandering rivers (Adhiperdana, 2018).

The fluvial and lacustrine-delta successions of the formation can be divided into seven intervals (IV1–IV7 in ascending order) by six distinct erosional surfaces (ES1–ES6 in ascending order) (Adhiperdana, 2018) (Fig. 35). These erosional surfaces are defined in the base of channel-fill deposits or mouth-bar deposits, which are coarser than those developed beneath each erosional surface. Thicknesses of these intervals range from about 36 to 370 m. Within each interval (IV1–IV7), coarser-grained channel-fill deposits developed on the basal erosional surfaces and commonly pass upward into sandstone-dominated channel-fill deposits in association with the increase in floodplain muddy deposits. Lacustrine muddy deposits and delta-mouth bar deposits are mainly developed only in the intervals IV4–IV6 of the western part of the Sukabumi high. The conglomerate-dominated packages (Type 1) are commonly observed in IV3, and the lower parts of IV4 and IV6. The conglomeratic sandstone packages (Type 2) are common in the lower part of IV2 and IV4, and the sandstone-dominated packages (Type 3) are commonly observed in IV1, in the upper part of IV2, IV5, and IV7 (Fig. 35). The

fluvial deposits in IV1 and IV7 contain thicker floodplain muddy deposits and isolated channel-fill deposits. In contrast, fluvial deposits in IV3 and IV4 are characterized by thinner floodplain muddy deposits and amalgamated channel-fill deposits. Those in IV2, IV5, and IV6 indicate moderate interconnectedness of the channel-fill deposits between the above mentioned two contrast horizons. Overall, the Bayah Formation fluvial deposits represent one cycle of upward increase and decrease in the interconnectedness of the channel-fill deposits (Fig. 36).

3-5. Paleohydrology

Adhiperdana (2018) estimated the Q_b values of the Bayah Formation fluvial system in each interval at 337 to 3,615 m^3s^{-1} . As discussed in the paleohydrological reconstruction of the Iwaki Formation, incomplete preservation of original thicknesses of bar deposits caused by subsequent erosion of the overlying channel deposits may result in underestimation of the geomorphological and hydrological parameters. Thus, the thickest values of bar deposits and the resultant maximum parameters in each interval (IV 1–IV 7) were adopted here. In this method, Q_b values of the Bayah Formation fluvial systems range from 2,273 m^3s^{-1} (IV 7) to 3,615 m^3s^{-1} (IV 4). Using the equation of the relationship between Q_b and A_d for the modern Indonesian rivers ($A_d = 2.36 Q_b^{0.98}$), which were developed in the present study (Fig. 17), the A_d values were estimated at 4,596.0 to 7,242.0 km^2 (Fig. 37A). In order to estimate the L_d values of the Bayah Formation fluvial system, the empirical equation between L_d and A_d ($L_d = 1.01 A_d^{0.53}$) from the Indonesian fluvial system (Fig. 18A) was also applied. As a result, L_d values of the Bayah Formation drainage basin for channel deposits in each intervals (IV 1–IV 7) were estimated at 88.2 to 112.2 km (Fig. 37A; Table 12). These estimated

parameters for channel-fill deposits in each interval (IV 1–IV 7) show slight vertical changes through the entire fluvial succession (Fig. 37A; Table 12).

3-6. Discussion

3-6-1. Relationship between paleohydrological features and stacking pattern

The detrital composition of sandstone framework grains and clay minerals in the Bayah Formation fluvial deposits do not indicate distinct temporal changes in intensity of chemical weathering and climatic condition (Adhiperdana, 2018). In addition, the Paleogene coastline was about 80 km south of the study area (Hall, 2012). Although the upstream limits of sea-level influence varies significantly between river systems, the backwater length is up to tens of kilometers for smaller and steeper river systems, such as the Eel River, California (orders of 10^4 km²) (Blum et al., 2013). Thus, the effect of sea-level may not have been a primary controlling factor for the Bayah Formation fluvial system, and tectonic cycles may have controlled the stacking pattern of the fluvial system. In general, an increase in the rate of basin subsidence and a high rate of accommodation creation are interpreted to have resulted in a higher potential for development of thick floodplain deposits and a reduction in slope, and to have caused the successive decrease in the interconnectedness of channel deposits in response to an overall upward-fining pattern (Bridge and Leeder, 1979; Wright and Marriott, 1993). In contrast, during a tectonically quiescent phase, progradation of proximal systems and a resultant increase in slope are expected, and coarse-grained and amalgamated channel deposits with higher interconnectedness likely developed (Bridge and Leeder, 1979; Blair and Bilodeau, 1988). On the basis of the so-called ‘LAB models’ (Bryant et al., 1995), the IV1 and IV7 in the Bayah Formation, which are mainly characterized by

floodplain muddy deposits and sandstone-dominated channel-fill deposits (Type 3 package) with lower interconnectedness (Figs. 35 and 36), possibly represent deposition under a phase of active basin subsidence. In contrast, the IV3 and lower part of IV4 are characterized by amalgamated conglomerate-dominated channel-fill deposits (Type 1) (Figs. 35 and 36), and are interpreted to represent proximal fluvial facies under a tectonically quiescent phase. The IV2, IV5, and IV6 with moderately amalgamated channel-fill deposits are also interpreted to have been caused by intermediate rate of basin subsidence between tectonically active and quiescent phases. The temporal change in the interconnectedness is in harmony with the change of channel cross-sectional dimensions (i.e., bankfull channel depth and width). The changes in the channel cross-sectional dimensions are interpreted to have been caused by fluctuation of bankfull discharge, which was also controlled by change in slope. This temporal variation in the stacking pattern of the Bayah Formation fluvial deposits is similar to that of the nonmarine sequence stratigraphic models (Wright and Marriott, 1993; Shanley and McCabe, 1994; Blum et al., 2013). Consequently, the origin of the stacking pattern is alternatively interpreted to have been developed by temporal change in the rate of tectonic basin subsidence rather than only by relative change in sea level.

3-6-2. Sediment provenance

The source area of the detrital fragments is expected to have been to the north or northeast of the Sukabumi high on the basis of paleocurrent directions (Adhiperdana, 2018). A possible spatial range of the most distant headwaters for the Bayah Formation fluvial system based on the estimated L_d values and the paleocurrent directions, is mainly in the present Northwest Java (Fig. 37B). This prediction of the headwaters does

not contradict with a location of the Eocene–Oligocene magmatic arc, which was extended west and east in northern Java (Soeria-Atmadja and Noeradi, 2005). In addition, both in the onshore and offshore of the West Java area, the Cretaceous granitoid rocks, various kinds of metamorphic rocks, especially the low-grade metamorphic envelopes, such as phyllite, schist, argillite, and other types of Mesozoic metasedimentary rocks have evidently been found in well drillings (Hamilton, 1979) (Fig. 37B). The isotopic ages of these basement rocks also can be seen in the Isotopic Ages Database by the Southeast Asia Research Group, Royal Holloway University of London (<http://searg.rhul.ac.uk/current-research/isotopic-ages/>). From the Bayah Formation sandstone samples, Cretaceous and Permian–Triassic detrital zircons were also reported by Clements and Hall (2011). Therefore, the contribution of detrital fragments from the Cretaceous granitoid rocks and other Mesozoic metasedimentary rocks in Northwest Java to the Bayah Formation depositional basin is reasonable. In contrast, the contributions from the Cretaceous granites of the Schwaner Mountains in SW Kalimantan and from the Permian–Triassic granites of the Indonesian Tin Islands, which were suggested by Clements and Hall (2011), are improbable, because these granites are located more than 900 km northeast and more than 600 km north-northwest from the study area, respectively (Fig. 34). These distances are quite far from the Bayah Formation depositional basin from the view point of cross-sectional dimensions and discharges of the Bayah Formation fluvial channels.

3-7. Conclusions

- (1) The empirical equations developed from the modern Indonesian fluvial system were applied to the Bayah Formation fluvial deposits, West Java. On the basis of the

thickness of bar deposits, maximum value of the bankfull channel depth, mean bankfull channel depth, bankfull channel width, mean and bankfull discharges, drainage basin area, and drainage basin length are estimated.

- (2) The Bayah Formation fluvial deposits represent an overall upward increase and decrease in both interconnectedness of the channel-fill deposits and channel cross-sectional dimensions. These variations are interpreted to have been controlled by variation in a rate of basin subsidence.
- (3) The estimated drainage basin area and drainage basin length, which was estimated up to 112 km, indicate that the detrital fragments of the Bayah Formation fluvial deposits were derived mainly from the Mesozoic granitoid and metasedimentary rocks distributed in the subsurface of Northwest Java.

Part 4. Fluvial response to climatic drying: The Upper Triassic fluvial successions developed in a continental backarc-basin setting

4-1. Introduction

Although the interaction between climatic and tectonic fluctuations has been considered to be responsible for spatial and temporal variations in fluvial systems developed in continental interior basins, relative contribution of these allogenic controls still remains controversial (Dickinson et al., 1994; Cleveland et al., 2007; Varban and Plint, 2008; Antia and Fielding, 2011; Dubiel and Hasiotis, 2011; Trendell et al., 2012; Miall, 2014). In addition, fluvial architectural and paleohydrological variations linked to climatic changes have not yet been sufficiently understood (Blum and Törnqvist, 2000).

During the Late Triassic, the Pangaeian monsoonal circulation is considered to have been at maximum strength, and western Pangaea began to shift from wet to wet-dry seasonal climatic conditions (Parrish, 1993). This climatic change, together with the development of a volcanic arc system along the western margin of the Pangaea, is interpreted to have been documented in fluvial and lacustrine systems formed in the present western U.S.A. (Stewart et al., 1972; Blakey and Gubitosa, 1984; Dubiel and Hasiotis, 2011; Nordt et al., 2015). These Late Triassic terrestrial depositional systems are widely distributed around the Colorado Plateau. (Fig. 38). However, detailed analyses of fluvial architecture, paleoclimates, and geologic ages of the fluvial systems and related depositional systems have mainly been conducted in the Upper Triassic successions that are developed in the Four Corners region (a junction area of Arizona, Utah, Colorado, and New Mexico that includes Petrified Forest National Park in northern Arizona) (Blakey and Gubitosa, 1984; Kraus and Middleton, 1987; Dubiel,

1991; Riggs et al., 2003; Dubiel and Hasiotis, 2011; Trendell et al., 2012, 2013; Atchley et al., 2013; Howell and Blakey, 2013; Nordt et al., 2015; Jin et al., 2018; Rasmussen et al., 2020). In contrast, the Upper Triassic successions in Southwest Utah have not yet been focused upon in terms of climatic and tectonic changes in western Pangaea (Martz et al., 2017), although geologic studies in southwestern Utah should have a potential to fill a niche for a better understanding of climatic and tectonic fluctuations in the western Pangaea during the Late Triassic. One of the potential stratigraphic successions for these studies in Southwest Utah is the Upper Triassic Chinle Formation.

Part 4 focuses on the Chinle Formation that is distributed in and around Zion National Park on the western margin of the Colorado Plateau of Southwest Utah (Fig. 39). The main purpose of this part is to analyze spatial and temporal variations in fluvial architecture, stacking patterns, and paleohydrological features including drainage basin dimensions of the Chinle Formation to clarify an interaction between stacking patterns of fluvial deposits and climatic and/or tectonic fluctuations. In order to reconstruct the Late Triassic climatic change in Southwest Utah, vertical changes in detrital compositions of sandstone framework grains and clay minerals were also analyzed. In addition, paleogeography and sediment provenance of Upper Triassic sedimentary basins that formed in the western Pangaea is also examined by estimating drainage basin characteristics of the Chinle Formation.

4-2. Geological setting

4-2-1. Tectonic setting and provenance

The Chinle Formation and its age-equivalent strata are widely distributed in the Colorado Plateau and adjacent areas (Fig. 38). The formation is characterized by fluvial

and lacustrine deposits, and is interpreted to have developed in a continental backarc region in western Pangaea (Blakey and Gubitosa, 1984; Dubiel et al., 1991; Tanner, 2000; Trendell et al., 2012; Martz et al., 2017). The Chinle Formation developed in sedimentary basins that were surrounded by Cordilleran volcanic arc in California, the Ancestral Uncompahgre and Front Range uplifts in Colorado, the Mogollon Slope in Arizona, Amarillo–Wichita Uplift in northwestern Texas, and Ouachita–Marathon Orogenic Belt in Texas (Dickinson and Gehrels, 2008) (Fig. 38). The major sediment transport direction in the Colorado Plateau region is interpreted to have been northwest during the Late Triassic (Stewart et al., 1972; Dubiel et al., 1991; Blakey and Ranney, 2008; Dubiel and Hasiotis, 2011; Martz et al., 2017), and the major provenance of the detrital fragments of the Chinle Formation in Southwest Utah is interpreted to have been from the Mogollon Slope in southern Arizona (Stewart et al., 1972; Bilodeau, 1986; Dubiel, 1992; Dickinson and Gehrels, 2008; Martz et al., 2017). The Mogollon Slope consists of Proterozoic sedimentary, volcanic, granitic, and metamorphic rocks, and Paleozoic sedimentary rocks, such as conglomerates, sandstones, siltstones, shale, limestone, dolostone, and chert (Stewart et al., 1972; Parker et al., 2005). In addition, the Late Triassic Cordilleran volcanic arc is also considered to have supplied some volcanic detritus to the Chinle Formation sedimentary basins (Riggs et al., 2003, 2013, 2016; Dickinson and Gehrels, 2008). The lower part of the Chinle Formation in Southwest Utah is interpreted to have deposited within the Vermillion Cliffs paleovalley (Dickinson and Gehrels, 2008; Martz et al., 2017).

4-2-2. Lithostratigraphy and age

The Chinle Formation in southern Utah is subdivided into the Shinarump,

Monitor Butte/Cameron, Moss Back, Petrified Forest, Owl Rock (partially the Kane Springs Beds), and Church Rock members in ascending order (Martz et al., 2017) (Fig. 40A). In the study area, the Chinle Formation overlies the lower Middle Triassic coastal plain deposits of the Upper Red Member of the Moenkopi Formation. The uppermost part of the Moenkopi Formation locally includes paleosol mottling with reddish brown and light greenish gray colors, which was informally called ‘mottled strata’, and was included in the basal part of the Chinle Formation (Stewart et al., 1972). The Chinle Formation is subdivided, in ascending order, into the Shinarump (~40 m thick) and Cameron (~95 m thick) members, and the “purple pedogenic beds” (~25 m thick) (Martz et al., 2017). Although the upper part of the formation (i.e., the Cameron Member and “purple pedogenic beds”) was previously correlated to the Petrified Forest Member (Stewart et al., 1972; Hintze, 1997), recent studies of vertebrate biostratigraphy indicate that the upper part correlates to the Cameron Member rather than to the Petrified Forest Member on the basis of the occurrences of a unique phytosaur skull in the lower part of the Cameron Member, which is likely a basal member of the clade Leptosuchomorpha (Martz et al., 2017). It should be noted however, that the mapping division of the Utah Geological Survey still refer to the Cameron Member and “purple pedogenic beds” as the Petrified Forest Member (e.g., Biek et al., 2010). The Chinle Formation is unconformably overlain by the Upper Triassic–Lower Jurassic Moenave Formation (Kirkland and Milner, 2006; Lucas and Tanner, 2007; Kirkland et al., 2014) (Fig. 40B). The unconformity at the Chinle–Moenave contact (or J-0 unconformity of previous authors) is overlain regionally by an approximately one meter thick poorly cemented chert and anhydrite pebble conglomerate (Kirkland and Milner, 2006; Kirkland et al., 2014; Martz et al., 2017).

The radioisotopic ages of the Chinle Formation have been investigated using samples mainly from the Petrified Forest National Park in northern Arizona (Riggs et al., 2003; Ramezani et al., 2011; Atchley et al., 2013; Nordt et al., 2015; Rasmussen et al., 2020). The Chinle Formation in northern Arizona is subdivided into the Shinarump, Mesa Redondo, Blue Mesa, Sonsela, Petrified Forest, and Owl Rock members in ascending order (Trendell et al., 2013; Nordt et al., 2015), and the radioisotopic dating indicates that the Mesa Redondo, Blue Mesa, Sonsela, and Petrified Forest members are correlative to the Norian, while the Owl Rock Member is Rhaetian in age (Fig. 40A). Although the radioisotopic age of the Chinle Formation in Southwest Utah has not yet been conducted, the Shinarump Member is correlative to the Shinarump and Mesa Redondo members in northern Arizona, and the Cameron Member and “purple pedogenic beds” are considered to be correlative to the Monitor Butte Member in southeastern Utah and the Blue Mesa Member in northern Arizona (Martz et al., 2017, p. 148) (Fig. 40). Consequently, the age of the Chinle Formation in the study area is interpreted mainly to be Norian and might include the latest Carnian at the basal part (Fig. 40B). Approximate depositional rate of the formation is estimated at 1.2 cm/1,000 years on the basis of the total stratigraphic thickness of the formation and an age framework on the basis of regional stratigraphic correlation of the Chinle Formation and its age-equivalent stratigraphic successions (Fig. 40).

4-2-3. Paleoclimates

Fluctuations in paleoclimates during the deposition of the Chinle Formation have been studied on the basis of sedimentological and paleontological evidence (Dubiel et al., 1991), fossil plant assemblages (Lindström et al., 2016; Baranyi et al.,

2018), paleosol types (Dubiel and Hasiotis, 2011; Lucas and Tanner, 2018), geochemical features of paleosol (Prochnow et al., 2006; Atchley et al., 2013; Nordt et al., 2015), and petrographic features (Jin et al., 2018) of the formation. These studies indicate that the lower part of the Chinle Formation was deposited under unusually humid climatic condition with seasonality that may have been caused by ‘megamonsoon’ circulation (Dubiel et al., 1991; Dubiel and Hasiotis, 2011; Lucas and Tanner, 2018). In addition, the climates are considered to have shifted to more arid conditions after 215 Ma (Atchley et al., 2013; Nordt et al., 2015; Baranyi et al., 2018; Jin et al., 2018). This climatic change is interpreted to have been caused by the northward drift of the Chinle Formation sedimentary basins (Dubiel and Hasiotis, 2011) or the development of a rain shadow in response to the development of the Cordilleran volcanic arc in the western margin of the Pangaea (Atchley et al., 2013; Nordt et al., 2015).

4-3. Datasets and methods

4-3-1. Fluvial architecture

Three-dimensional analyses of lithofacies organization and architecture of the Chinle Formation fluvial deposits were conducted using large outcrops in seven major locations (Fig. 39). This study mainly used photographic mosaics and measured sections for the present analyses. The basic concept of the hierarchical bounding-surface and architectural element analyses (Miall, 1985, 1988; 1996; Holbrook, 2001; Ford and Pyles, 2014) was employed for the definition of fluvial forms in the outcrops.

Paleocurrent directions were measured from dip directions of the axial part of trough or planar cross-bedding.

4-3-2. Paleohydrology

Bankfull channel depths have been estimated on the thickness of bar deposits (Leeder, 1973; Bridge and Diemer, 1983; Alexander et al., 2020). The present study measured thickness of well-preserved bar deposits from the photographic mosaics and stratigraphic sections. Bankfull channel depth has also been estimated using cross-set thickness in the bar deposits using empirical equations by Leclair and Bridge (2001) and Bridge (2003). Mean bankfull channel depth (= hydraulic radius at a bankfull water stage), bankfull channel width, mean and bankfull water discharges, drainage basin area, and drainage basin length were also calculated using empirical equations that were established from modern fluvial channels (e.g., Williams, 1984a, b; Bridge and Mackey, 1993; Blum et al., 2013; Adhiperdana et al., 2018).

4-3-3. Detrital composition

Pebble samples were collected from conglomerates and pebbly sandstones of the Shinarump and Cameron members at six sites for each member (Routes 2, 4, and 5 for the Shinarump Member, and Routes 3, 4, and 6 for the Cameron Member in Fig. 39). The numbers of pebble samples from each site are 110–122 for the Shinarump Member, and 122–135 for the Cameron Member. Thin sections of 22 selected samples were observed using a polarizing microscope to identify rock types of the pebbles and the other samples were visually examined to identify their rock types.

For identifying framework composition of the sandstones, a total of 28 and 25 medium- to very coarse-grained sandstone samples were collected from the Shinarump and Cameron members, respectively. Samples were collected mainly from Routes 3, 4, and 6 in Figure 39. The framework composition was determined by point counting more

than 500 sand-sized grains in a thin section using the Gazzi-Dickinson method (Ingersoll et al., 1984). Framework grains were classified following the grain categories of Winkler (1984). The thin sections were stained to facilitate the identification of K-feldspar using a method of Bailey and Stevens (1960).

A total of 74 samples from mudstones and 52 samples from sandstones were also taken from the Shinarump and Cameron members and “purple pedogenic beds” for X-ray diffraction (XRD) analysis. These samples were collected mainly from Routes 3, 4, and 6 in Figure 39. About 3 g mudstone fragments and 15 g sandstone fragments of each sample were grinded using a mortar. Clay-size fractions less than 2 μm were separated from the grinded samples using motionless gravity settling of suspension (Stokes’ law). Clay suspension was dropped on slide glasses and was dried at 60 °C in an oven to prepare oriented clay slides. Ethylene glycol was added to the dried oriented clay slides for the identification of smectite. The XRD analysis was conducted using RIGAKU RAD-X System in the Department of Earth Sciences, Chiba University. This X-ray unit uses Ni-filtered Cu-radiation (Cu $K\alpha$) target setting of 40 kV and 20 mA. The relative composition of major clay minerals is estimated semi-quantitatively, following the peak area method (Biscaye, 1965). The relative proportions of chlorite and kaolinite were calculated from the ratio of peak heights (3.53 and 3.58 Å, respectively). If this ratio is 1, the amount of chlorite is assumed to be twice that of kaolinite (Suresh et al., 2004). A total of four samples of mudstone and two samples of sandstone were also observed by a scanning electron microscope (SEM) using HITACHI S-2400 in the Department of Earth Sciences, Chiba University to distinguish detrital and authigenic grains.

4-4. Fluvial architecture

The present study identified twelve lithofacies types, nine architectural element types, and six major bounding-surface (BS) types (1st- to 6th-order in increasing scale order) in the Chinle Formation fluvial deposits. Lithofacies types were identified only by the combination of lithologic types and physical and biological sedimentary structures (Ford and Pyles, 2014). In contrast, architectural element types were mainly classified in terms of external forms. The hierarchical classification of the bounding-surface types was defined by cross-cutting relationships of the surface types, in association with the combination between lateral continuity, geometry, lithofacies features, and paleocurrent directions of the encased fluvial deposits.

4-4-1. Lithofacies

The Chinle Formation consists of very coarse- to fine-grained, dull yellow orange-colored pebbly sandstones (Lithofacies St/Sp, Sh, Sc, and Sg/Sig), with local associations of pebble-sized conglomerates (Lithofacies Gc, and Gt/Gp), and multi-colored (e.g., gray, yellowish gray, brownish gray, reddish gray, grayish red, and reddish brown) mudstones (Lithofacies Fm, Pm, Fr, and Fl). Minor massive limestone (Lithofacies Lm) is also locally intercalated in the formation (Fig. 41). Descriptions and interpretations of lithofacies types are summarized in Table 13.

4-4-2. Architectural elements

Descriptions and interpretations of architectural element types are summarized in Table 14 and their schematic illustrations are given in Figure 42.

4-4-2-1. Channel deposits

Description. Distinct erosional surfaces in the base of sandstones are locally overlain by thin and discontinuous, pebble-sized, clast-supported conglomerates (Lithofacies Gc, Gt/Gp, and Element SG, Fig. 43A). The erosional surfaces and the basal conglomerates are overlain by moderately sorted, very coarse- to fine-grained pebbly sandstones with trough or planar (Lithofacies St/Sp) cross-stratification, in association with minor horizontal planar stratification (Lithofacies Sh). Scattered pebble-sized gravel is also locally present along the stratification. Some cross-set boundaries indicate minor truncation of underlying sandy deposits. These cross-set boundaries dip towards downstream directions (Element DA, Figs. 43B and C), and are also locally incline orthogonal to the downstream direction (Element LA, Fig. 43A). The distinction between Elements DA and LA was made using an angle of 60° between channel flow directions and orientations of the inclined boundaries, following Miall (1996). The cross-set boundaries are also locally horizontal (Element SD, Fig. 43C). Sets of cross-stratified sandstones commonly represent upward-fining trends, and often include fossil plants. Locally, moderately sorted, medium- to fine-grained, trough cross-stratified pebbly sandstones (Lithofacies St) with lenticular geometry and erosional basal surfaces (Element SCF, Fig. 44A), which are up to 1.0 m thick and 5.2 m wide, occurs on the cross-stratified sandstones with upward-fining trends. Large-scale lenticular element (~8 m thick and 40 m wide) is locally filled with alternating beds of mudstones (Lithofacies Fm, Fl, and Fr) and sandstones, which consist of the cross-stratified or horizontally stratified sandstones (Lithofacies St/Sp, Sh) that are covered by current-ripple cross-laminated sandstones with local development of convolute laminations (Lithofacies Sr and Sc), and show upward-fining trends (Element

LCF) (Fig. 44B). The stacked elements of DA, LA, SD, SCF, and LCF are locally overlain by inclined alternating beds of sandstones (Lithofacies St/Sp, Sh, Sr) and mudstones (Lithofacies Fm, Fr, and Fl) (Element UB, Fig. 44C).

Interpretation. The sandstones with erosional basal surfaces are considered to represent deposits in fluvial channels (Miall, 1988; Hampson et al., 2013; Ford and Pyles, 2014). Discontinuous pebble-sized, clast-supported conglomerates (Element SG) are interpreted as lag deposits on the erosional surfaces in the base of channels (Jo, 2003; Hampson et al., 2013). Trough or planar cross-stratified, very coarse- to fine-grained sandstones (Lithofacies St/Sp) and pebble-sized conglomerates (Lithofacies Gt/Gp) indicate deposition from straight- or sinuous-crested dunes that migrated in the downstream direction (Allen, 1982; Miall, 1996; Hampson et al., 2013). The inclined stratification in conglomerates and sandstones (Lithofacies Gt/Gp, St/Sp, Sh, and Sr), which shows inclined direction similar to paleocurrents and is represented by boundaries with minor erosional surfaces, indicates downstream accretion (Element DA) of braid bar deposits (Thomas et al., 1987; Miall, 1988; Lunt et al., 2004; Ford and Pyles, 2014). In contrast, the inclined stratification in conglomerates and sandstones (Lithofacies Gt/Gp, St /Sp, Sh, and Sr), which shows inclined directions orthogonal to paleocurrents, is considered to indicate lateral accretion (Element LA) of braid bar and point bar deposits (Thomas et al., 1987; Miall, 1988; Ford and Pyles, 2014). In addition, sandstones with horizontal cross-set boundaries (Element SD) are interpreted to represent aggradation of dunes on low-relief bars (Miall, 1985). The upward-fining successions of stacked sandstones (Elements DA, LA, SD) indicate the reduction of bed shear stress from the base to the top of the channel or bar (Allen, 1970), and the successions are interpreted to be channel and component bar deposits (Allen, 1970;

Leeder, 1973; Lorenz et al., 1985; Lunt et al., 2004; Adams and Bhattacharya, 2005).

Inclined alternating beds of sandstones and mudstones that developed over stacked sandstones (Element UB) indicate upper bar deposits (Bridge et al., 2000; Bridge, 2003; Xu et al., 2017). Small-scale lenticular sandstones (Lithofacies St and Element SCF) developed on the top of upward-fining successions (Elements DA, LA, SD) as well as alternating beds of mudstones and sandstones (Lithofacies Fm, Fl, Fr, St, Sp, Sh, and Sr) with large-scale erosional base (Element LCF) are interpreted as infills of small channels on bars (Allen, 1983; Jo, 2003) and abandoned channels (Miall, 1985, 1996; Bridge, 1993; Ford and Pyles, 2014), respectively. Alternating beds of mudstones and sandstones in Element LCF indicate repetitive depositions from suspension and traction loads, respectively. The cross-stratified or horizontally stratified sandstones (Lithofacies St/Sp, Sh), which are overlain by current-ripple cross-laminated sandstones (Lithofacies Sr) with upward-fining trends are considered to document deposition during a waning flow stage in flood events (Ray, 1976).

4-4-2-2. Floodplain deposits

Description: The couplets of sandstones with basal erosional surfaces are encased in, or overlain by multi-colored sets of massive, thick mudstone (~25 m thick) (Lithofacies Pm) or gray-colored interbeds of mudstones and very fine-grained sandstone (Lithofacies Fl, Fr, and Fm) (Element FF, Fig. 44D) with local association of climbing ripple cross-laminations (Lithofacies Fr) (Fig. 41D). Multi-colored mudstones (Lithofacies Pm) locally show distinct slickenside and cross-cutting structure. Massive limestone (Lithofacies Lm), which lacks body fossils, locally occurs in association with the multi-colored mudstones (Lithofacies Pm). The thick mudstones contain moderately

sorted, very fine- to medium-grained sandstones (~2.6 m thick) (Element FS, Fig. 44D). These sandstones typically contain inverse grading (Lithofacies Sig), planar parallel- or cross-stratification (Lithofacies Sh, St, and Sr), and/or normal grading (Lithofacies Sg), from the base to top of a bed. Sandstones of Element FS typically show upward-fining trends, and do not have distinct erosional surfaces and are represented mainly by basal flat surfaces. They also show laterally thinning trends, and locally pass into mudstones or very fine-grained muddy sandstones (Lithofacies Fm, Pm, Fr, Fl, Element FF).

Interpretation: Massive (Lithofacies Fm) and laminated (Lithofacies Fr, Fl) mudstones represent accumulation from suspension and traction loads, respectively. Development of climbing ripple cross-laminations in the intercalated very fine-grained sandstone beds (Lithofacies Fr) indicates dominance of suspension loads relative to traction loads in association with very high deposition rate (Allen, 1982). Multi-colored mudstones with distinct slickenside and cross-cutting structures (Lithofacies Pm) are interpreted as pedogenetic modification of muddy deposits that were accumulated from suspended loads (Cleveland et al., 2007; Dubiel and Hasiotis, 2011; Trendell et al., 2013). Massive limestone (Lithofacies Lm) indicates chemical precipitation of inorganic calcareous deposits, and is interpreted to have formed in small carbonate lakes or ponds (Tanner, 2000). These mudstones (Element FF) are interpreted as floodplain muddy deposits accumulated mainly by suspended loads with local association with tractional structures (Miall, 1985, 1988; Ford and Pyles, 2004).

Normally or inversely graded sandstones (Lithofacies Sg/Sig) and planar parallel- or cross-stratified sandstones (Lithofacies Sh, St, and Sr) represent depositions from suspension and traction loads, respectively. The inversely graded sandy deposits have been described from modern flood-induced deposits in an overbank environment,

and are interpreted to represent temporal increase in discharge and sediment concentration in flood water (Iseya, 1989). Planar parallel- or cross-stratified sandstones (Lithofacies Sh, St, and Sr) and normally graded sandstones (Lithofacies Sg) that show overall upward-fining trends suggest the deposition from waning flow during flood events (Ray, 1976). A depositional model of crevasse-splay deposits by Burns et al. (2017) suggests that their average thicknesses in proximal, medial, and distal parts are 2.1 m, 1.5 m, and 0.8 m, respectively. The lateral variation in thickness of Element FS of the present study exhibits a pattern similar to that in the model. Therefore, the sandstones of Element FS are interpreted to be overbank sandy deposit generated by flood events.

4-4-3. Bounding-surface (BS) types and architectural hierarchy

Descriptions and interpretations of bounding-surface (BS) types are summarized in Table 15. An erosional surface type, which is commonly overlain by laterally discontinuous pebble-sized conglomerates (Element SG), corresponds to a channel base (4th-order BS), and a set of Element SG and overlying sandstones (Element SG, DA, LA, SD, and UB) indicates sandy channel deposits ranging from 3 m to 13 m in thickness (Figs. 43C and 45). A basal surface of abandoned channel deposits (Element LCF) is also represented by this order surface type (Fig. 44B). Top surfaces of the channel deposits that are overlain by thick mudstones (Element FF) represent bar-top surfaces (3rd-order BS) (Fig. 45A). The boundaries of bar deposits within channel deposits (Fig. 43B), basal surface of the small-scale channel-fill deposits (SCF) (Fig. 44A), and the basal-and top-surfaces of the floodplain sandy deposits (Element FS) encased in the floodplain muddy deposits (Element FF) (Fig. 44D) are also equivalent

to this order surface (3rd-order BS). Within the channel and bar deposits, gently inclined stratification that is bounded by minor erosional surfaces (Elements DA and LA) and horizontal stratification (Element SD) records accretion and vertical aggradation of bars (2nd-order BS) (Figs. 43 and 44), respectively. In addition, the constituent cross-set boundaries (1st-order BS) represent migration of dunes and ripples.

Vertically and laterally stacked sets of channel deposits are bounded by higher-scale, compound basal erosional surfaces (5th-order BS) (Fig. 45A). A set of channelized deposits that is bounded by this bounding-surface type is termed, herein, as a channel complex (up to 25 m thick). A compound basal erosional surface (5th-order BS) commonly incises into underlying finer-grained deposits (Elements UB and FF) (Fig. 45A). In addition, a basal surface of the stacked channel complexes corresponds to a sequence boundary (6th-order BS) (Fig. 45, see Discussion).

4-4-4. Stratigraphic change

4-4-4-1. Shinarump Member

In the Shinarump Member, cross-stratified sandstones with inclined accretion surfaces (Elements DA, LA, and UB) together with horizontal stratification (Element SD) constitute 74–99 % of the total thickness, with a small proportion of conglomerates of Element SG (<5%) (Figs. 45A and 47), and the component cross-sets are up to 135 cm thick. Cross-stratified sandstones with downstream-directed accretion (Element DA) are dominant throughout the member (Fig. 44B), although laterally accreting, cross-stratified sandstones (Element LA) also locally occur in the upper part of the member (Fig. 43A). These sandstones and conglomerates are mainly channel deposits, which are bounded by erosional basal surfaces of channel deposits (4th-order BS) or

channel complexes (5th-order BS) (Fig. 45A). The upper part of an upward-fining trend in channel deposits is characterized locally by inclined alternating beds of sandstones and mudstones (Element UB) (Fig. 44C). A channel complex is overlain locally by alternating beds of mudstones and very fine-grained sandstones (Element FF), which are truncated by distinct erosional surfaces (5th-order BS) and are overlain by a younger channel complex (Fig. 45A). These mudstones and very fine-grained sandstones constitute a small proportion (1–10 %) of the total thickness of the member. Overall, the Shinarump Member consists of two or three vertically stacked cycles of channel complexes, which contain 1–4 cycles of channel deposits (Fig. 47). Trough cross-stratification and current-ripple cross-laminations in sandstones (Elements DA, LA, and SD) are characterized by unidirectional paleocurrents that show a dominant flow direction toward the north, northwest, and/or west (Figs. 43–45, and 47). An exceptional flow direction is in the south-southeast (Route 5 in Figs. 39 and 47), which are observed in some laterally accreting deposits (Element LA) (Figs. 43A).

4-4-4-2. Cameron Member and “purple pedogenic beds”

The stacked channelized sandstones of the Shinarump Member are abruptly replaced by multi-colored and massive mudstones of the Cameron Member and “purple pedogenic bed” (Element FF), which were formed mainly in floodplains and comprise 72–95 % of the total thickness (Fig. 47). Thick multi-colored mudstones contain channel deposits and channel complexes with distinct erosional basal surfaces (4th- and 5th-order BS) (Figs. 46 and 47) in the Cameron Member. Cross-stratified conglomerates and sandstones of the channel deposits are minor components of the Cameron Member and “purple pedogenic beds” in total thickness (<2 % and 6–20 %, respectively).

Cross-sets in the channel deposits are up to 90 cm in thickness, and the cross-set boundaries are commonly horizontal (Element SD), and locally dip obliquely to paleocurrent directions (Element DA) (Fig. 43C). The channel deposits lack alternating beds of sandstones and mudstones (Element UB) in their uppermost part and are covered only by muddy deposits (Element FF). Isolated channel complexes consist of 1–3 cycles of the channel deposits and are encased in multi-colored floodplain muddy deposits. The largest channel complex in the Cameron Member (Fig. 46) is about 20 m in thickness and about 450 m in width in an outcrop that trends nearly orthogonal to a mean paleocurrent direction (Fig. 47) with a width/thickness ratio of 22.5. Sandstone interbeds of floodplain sandy deposits (Elements FS) (~2.6 m thick) are also intercalated in the thick multi-colored mudstones (Fig. 44D) and are also minor components (0–7 % of the total thickness). Paleocurrent data of the channel deposits and the floodplain sandy deposits show flow directions mainly towards the north and northwest (Fig. 47).

4-5. Paleohydrology

Stratigraphic thicknesses of bar deposits (h) are interpreted to be slightly less (90%) than bankfull channel depth (d) (Bridge and Diemer, 1983; Bridge and Mackey 1993), and Ethridge and Schumm (1978) and Lorenz et al. (1985) used a 10 % compaction factor to correct stratigraphic thickness for the estimation of paleochannel depths from sandy bar deposits. The present study also adopted the 10% compaction factor, and we used corrected h for the calculation of d as follows:

$$d = h \times 10/9 \times 10/9$$

The present study also calculated the mean cross-set thickness (S_{mean}) and standard deviation (S_{sd}), and estimated the mean dune height (H_{mean}), using the following equations (Leclair and Bridge, 2001; Bridge, 2003):

$$H_{mean} = 5.3\beta$$

$$\beta \approx S_{sd}/1.8$$

In this method, S_{sd}/S_{mean} should be approximately equal to 0.88 (± 0.3). Mean dune height increases with the increase in flow depth, and the flow depth is interpreted to be approximately six times that of the mean height of river dunes (Allen, 1982; Bridge, 2003).

For the reconstruction of paleohydrological features of the Chinle Formation, the present study used outcrop data from eight well-exposed channel complexes of the Shinarump and Cameron members (CHC I–VIII in Fig. 47). Although some bar deposits are truncated by overlying younger bar or channel-fill deposits, the thickest values of bar deposits were used to estimate the maximum geomorphological and hydrological parameters in each channel complex. Thickness of the thickest bar deposits with upward-fining trend (h), which are defined by the 4th- (basal surface of channel deposits) and 3rd- (basal and top surfaces of bar deposits) order bounding surfaces, range from 7.2 to 9.9 m in the Shinarump Member (CHC I–V). On the basis of the empirical equation between h and d , the d value can be estimated at 8.9–12.2 m. Following the similar procedures, the h and d values of the fluvial channels of the Cameron Member (CHC VI–VIII) can be estimated at 4.6–5.4 m and 5.7–6.7 m,

respectively.

The S_{mean} values of the channel complexes in the Shinarump and Cameron members are 42.1–58.2 cm and 30.9–38.6 cm, respectively, and the H_{mean} values in the members were estimated at 124.1–171.3 cm and 90.9–113.7 cm, respectively, with the values of S_{sd}/S_{mean} ranging from 0.58 to 0.84. These results indicate that the d value of the paleochannels was estimated at 7.4–10.3 m for the Shinarump Member, and 5.5–6.9 m for the Cameron Member, respectively.

The Chinle Formation is interpreted to have developed in a convergent margin continental backarc region that is influenced by a low-latitude monsoonal climate. Thus, the present study applied the empirical equations to the Chinle Formation fluvial deposits in two different ways for the estimation of mean channel depth (d_m), bankfull channel depth (W_b), mean and bankfull discharges (Q_{mean} , Q_b), drainage basin area (A_d), and drainage basin length (L_d). First, the equations from the modern Indonesian fluvial system between d , d_m , W_b , Q_{mean} , and Q_b (Adhiperdana et al., 2018), and those between Q_b , A_d , and L_d developed by the present study (Figs. 17A and 18A) were used as follows:

$$d_m = 0.65 d$$

$$W_b = 52.88 d_m^{0.7}$$

$$Q_{\text{mean}} = 0.06 W_b^{1.645}$$

$$Q_b = 1.098 W_b^{1.42}$$

$$A_d = 2.36 Q_b^{0.98}$$

$$L_d = 1.01 A_d^{0.53}$$

Second, the equations from modern rivers of the contiguous United States between d_m and d (Moody et al., 2003), between W_b and d_m (Leopold and Maddock, 1953; Adhiperdana et al., 2018), between Q_{mean} , a flood discharge with a 2-year recurrence interval (almost equivalent to Q_b), and W_b (Osterkamp and Hedman, 1982), and between L_d and A_d developed by the present study (Fig. 18A), together with the equations of global rivers between d and A_d (Xu et al., 2017) were used as follows:

$$d_m = 0.58 d$$

$$W_b = 47.00 d_m^{0.98}$$

$$Q_{\text{mean}} = 0.027 W_b^{1.17}$$

$$Q_b = 1.9 W_b^{1.22}$$

$$A_d = 277.29 d^{2.3761}$$

$$L_d = 2.78 A_d^{0.47}$$

These calculation methods are hereafter called an Indonesian scaling method and a continental scaling method, respectively.

Using the Indonesian scaling method, W_b values were estimated at 159.5–225.6 m for channel complexes of the Shinarump Member, and 128.3–150.0 m for those of the Cameron Member. Similarly, the Q_b values can be estimated, respectively, at 1,473.7–2,411.8 m^3s^{-1} and 1,081.9–1,351.1 m^3s^{-1} for the channel complexes of the Shinarump and Cameron members. Finally, the A_d and L_d values for channel complexes of the Shinarump Member were estimated at 3,005.8–4,870.8 km^2 and 70.4–90.9 km, and those for the Cameron Member were at 2,220.4–2760.5 km^2 and 60.0–67.3 km, respectively.

Using the continental scaling method, W_b values were estimated at 157.9–320.4 m for channel complexes of the Shinarump Member, and 145.4–234.5 m for those of the Cameron Member. Similarly, the Q_b values can be estimated, respectively, at 913.9–2166.0 m^3s^{-1} and 825.9–1,480.2 m^3s^{-1} for the channel complexes of the Shinarump and Cameron members. Finally, the A_d and L_d values for channel complexes of the Shinarump Member were estimated at 32,714.1–106,196.9 km^2 and 368.1–640.2 km, and those for the Cameron Member were at 15,628.3–49,830.0 km^2 and 260.1–448.6 km, respectively. These estimated values are summarized in Figure 48 and Table 16.

The estimated values indicate that paleochannels of the Shinarump Member were generally larger than those of the Cameron Member. The d values estimated from the measurements of bar deposit and cross-set thicknesses resulted in equivalent values for the Shinarump and Cameron member paleochannels. Although the continental scaling method estimated somewhat larger values of W_b than the Indonesian scaling method, both methods also estimated nearly equivalent values of Q_b . The significant differences in the estimated values were A_d and L_d , and the continental scaling method estimated their values to be much larger than those by the Indonesian scaling method. The W_b and Q_b values of the Shinarump Member fluvial channels are almost equal to or slightly larger than those of the modern Yellowstone River near Miles City, Montana. In contrast, the estimated values of the Cameron Member fluvial channels are approximately equivalent to or slightly larger than those obtained from the modern Green River near Green River, Utah and from the modern Colorado River near Hite, Utah (Table 17).

4-6. Detrital composition

4-6-1. Clast composition of conglomerates

Chert and quartzite are dominant clast types of conglomerates in both the Shinarump and Cameron members, although quartzite and chert clasts are the most common clast types in the Shinarump and Cameron members, respectively (Figs. 49A, B, and 50). Quartz fragments are also common in the Shinarump Member, while mudstone and sandstone clasts are minor components in both members (Figs. 49C, D and 50). Mudstone pebbles are represented commonly by black hard mudstone, while a brownish laminated mudstone pebble was identified only in the Cameron Member. Furthermore, three types of pebble-sized volcanic rock fragments were identified. The first type is acidic (rhyolitic) volcanic rock fragments with felsitic texture, which includes partially devitrified volcanic glass and embayed monocrystalline quartz (Fig. 49E). Only one clast of this type is identified in the Cameron Member. The second type is almost fully devitrified acidic tuff including clots of quartz and/or feldspar with a dull appearance (Fig. 49F), and was identified in both the Shinarump and Cameron members. The third type is partially devitrified tuff, which is characterized by fine-grained groundmass and embayed monocrystalline quartz. This type was found only in the Cameron Member.

4-6-2. Sandstone framework composition

Framework composition of the Chinle Formation sandstones is generally represented by quartzose grains in association with minor feldspar grains and lithic fragments (Figs. 51, 52 and Table 18). The Shinarump Member is characterized by more contents of quartzose grains than the Cameron Member, which has more feldspar grains and lithic fragments than the Shinarump Member (Figs. 51, 52 and Table 18).

Monocrystalline quartz grains show straight or undulose extinction (Fig. 51A and B), and some of them indicate embayed shape with rounded corner (Fig. 51C). Overall, monocrystalline quartz grains are dominant throughout the formation, and the other quartz grains, such as the polycrystalline quartz, quartz-tectonite, and chert (Fig. 51D), are minor components. K-feldspar grains with cross-hatched twinning (Fig. 51A), pericline twinning, and perthite twinning were commonly altered and replaced by clay minerals and calcite (Fig. 51E). Plagioclase feldspar is also represented by polysynthetic twinning and commonly sericitized (Fig. 51F). K-feldspar is more abundant than plagioclase feldspar in the two members. Volcanic lithic fragments are acidic and are classified into two types. One is intersertal (felted) volcanic lithic fragments, which show completely devitrified volcanic glass with a dull appearance (Fig. 51G), and the other type shows felsitic texture (Fig. 51H). These volcanic lithic fragments do not show evidence of intense surface weathering such as replacement and grain coating. Small amounts of sedimentary lithic fragment (Fig. 51A) and quartz-mica tectonite grains (Fig. 51I) also occur in some samples of the Shinarump and Cameron members.

4-6-3. Clay minerals

Clay mineral composition of the rock samples from the Shinarump Member, Cameron Member, and “purple pedogenic beds” that was analyzed by XRD is summarized in Figures 53–57 and Table 19. Sandstone samples from the Shinarump Member contain abundant kaolinite followed by illite, smectite and chlorite (Figs. 54–56), although chlorite was identified only in six sandstone samples. In contrast, mudstone samples of the Shinarump Member are represented by nearly equal amounts of illite and kaolinite, and less amounts of chlorite (Figs. 54–56). Mudstone samples

from the Shinarump Member do not have smectite at all. SEM images of both sandstone and mudstone samples from the Shinarump Member do not show authigenic features such as booklet structure and fan-like morphology, which are interpreted to characterize authigenic kaolinite (Do Campo et al., 2010; Huyghe et al., 2011) (Fig. 58A).

Sandstone samples from the Cameron Member also have abundant kaolinite, followed by minor illite and smectite in association with non-clay feldspar, although chlorite was identified only in one sandstone sample (Figs. 53, 54, 56 and 57). In contrast, mudstone samples of the Cameron Member and “purple pedogenic beds” are characterized by the dominance of kaolinite and smectite, and by minor illite and chlorite (Figs. 54, 56, and 57). The amounts of kaolinite are inversely proportional to those of smectite, and their relative abundance shows temporal variations with three cycles of zigzag pattern. Smectite in some mudstone samples are randomly interstratified with illite (Fig. 53A). Either kaolinite with booklet structure and fan-like morphology, or smectite with honeycomb structure and rose-like texture, which are common structures of authigenic clays (Do Campo et al., 2010; Huyghe et al., 2011), were not observed in the samples from the Cameron Member and “purple pedogenic beds” using SEM images (Fig. 58B–C).

4-7. Discussion

4-7-1. Fluvial styles

Recent studies on modern fluvial systems indicate that plan view channel forms are highly variable, and transitional channel forms between end-member types, such as braided, meandering, and straight, are often observed (Schumm, 2005; Ethridge, 2011). In addition, some modern rivers develop channel belts that include braided, meandering,

and anastomosing segments within a same valley reach (Lunt et al., 2004; Schumm, 2005). Thus, Ethridge (2011) criticized the prediction and classification of ancient channel planform types in terms of straight, meandering, anastomosed, and braided channels, on the basis only of facies and architectural analyses of stratigraphic successions. Nevertheless, the Chinle Formation fluvial deposits document temporal changes in architectural element types from Element DA dominant stacked channel complexes (Fig. 45A) to isolated channel complexes with Element SD and DA that are encased in floodplain muddy deposits (Element FF) (Fig. 46). This suggests that a distinct change in fluvial styles occurred from the Shinarump Member to the Cameron Member and “purple pedogenic beds”.

The fluvial style of the Shinarump Member is interpreted to have been low sinuous and braided types (Fig. 59). In general, downstream-accreting bar deposits (Element DA) have been interpreted to be a characteristic component of downstream parts of braid bar deposits (Miall, 1985; Lunt et al., 2004; Adams and Bhattacharya, 2005; Ford and Pyles, 2014). Small-scale channel fills (Element SCF) are indicative of cross-bar channels, and suggest the channel pattern was multi-threaded. Fine-grained fills with erosional bases, which are equivalent to large-scale channel fills (Element LCF) of the present study, have also been documented from ancient braided channel deposits (Ford and Pyles, 2014). Paleocurrent data, which show flow directions toward the north, northwest, or west (Fig. 47), also suggest the existence of low sinuous fluvial channels, although a channel complex (CHC-IV in Fig. 47) is locally composed of laterally accreting, cross-stratified sandstone (Element LA) that exhibits the southeastward-directed paleocurrents (Fig.43A). This channel complex possibly indicates a local development of a point bar in response to bending of paleochannels.

The channel complexes of the Cameron Member are generally isolated within floodplain muddy deposits of the Cameron Member and “purple pedogenic beds” and do not show lateral continuity between the studied sections (width/thickness ratio ≤ 30). In addition, they consist mainly of horizontally stratified sandstones (Element SD) in association with minor downstream-accreting, cross-stratified sandstones (Element DA) (Figs. 43C and 46). These lithofacies and architectural features are interpreted that the fluvial system of the Cameron Member and “purple pedogenic beds” was formed mainly by vertical aggradation in a stable and fixed channel (Nadon, 1994). Although the Elements SD and DA generally represents upward-fining trends, the channel deposits of the Cameron Member lack upper bar deposits (Element UB), which are represented by alternating beds of sandstone and mudstone on Elements SD and DA, and are abruptly covered by floodplain muddy deposits (Element FF). These architectural features are consistent with a facies model of anastomosed river by Nadon (1994). Although anastomosed fluvial deposits are interpreted to typically contain coal (Flores and Pillmore, 1987), some modern anastomosed river systems even in tropical climatic settings do not develop peat (Smith, 1986). Makaske (2001) defined that anastomosed rivers are composed of two or more interconnected channels that enclose flood basins. However, the Cameron Member channel complexes do not document two or more interconnected channels, which are represented by sparsely distributed channel complexes in a stratigraphic cross-section (Fig. 47). Because paleocurrent data show the northward-, northwestward-, and/or westward-directed flows (Fig. 47), the Cameron Member fluvial system may document relatively low sinuous rivers. Consequently, the fluvial system of the Cameron Member and “purple pedogenic beds” is interpreted to have deposited as single thread, stable, and fixed channels and wide floodplains (Fig.

59).

4-7-2. Paleohydrological features

The size of channel cross-sectional area and bankfull discharge (Q_b) are controlled by flood magnitudes that are associated with large rainfalls, except for snowmelt runoff (Knox, 1985; Carson et al., 2007; Colombera et al., 2017). The main source area of the Chinle Formation was not changed during deposition, so that the temporal variation in the area size of the Chinle Formation drainage basin is also interpreted to have been insignificant. In addition, the effect of a snowmelt runoff in the Chinle Formation drainage basin can be ignored because of its low latitude climatic condition. Therefore, the upward decrease in the estimated Q_b values for the Chinle Formation fluvial channels (Fig. 48) possibly indicates temporal decrease in both flood magnitude and precipitation in the Chinle Formation depositional basin as well as in its upper reaches.

In previously published paleogeographic maps of the Chinle Formation drainage basin in Southwest Utah, the headwaters of the basin were considered to have been located along the Cordilleran Volcanic arc (Blakey and Ranney, 2008; Dubiel and Hasiotis, 2011; Bhattacharya et al., 2016; Riggs et al., 2016) (Fig. 60). The Indonesian scaling method estimated quite smaller values of the drainage basin area (A_d) and the length (L_d) compared with the headwaters of the paleogeographic maps. The estimated values of L_d ranges from 60.0 to 99.9 km, and the distance is almost equivalent to a drainage basin length of the modern Virgin River at St. George, Utah, that flows near the study area (Fig. 39) ($L_d = 79$ km). Thus, the estimated values of A_d and L_d using the Indonesian scaling method indicate that the drainage basin area of the Chinle Formation

in Southwest Utah may have been smaller than those which were previously assumed.

In contrast, the continental scaling method estimated values of L_d ranging from 260.1 to 640.2 km, and values of A_d ranging from 15,682 to 106,197 km². Although these values of the drainage basin vary widely, the estimated values of the Chinle Formation drainage basin area can be compared to that of the modern Colorado River tributaries, such as the Green River at the confluence of the Green and Colorado rivers ($A_d = 116,200$ km²), and the San Juan River at the confluence of the San Juan and Colorado rivers ($A_d = 64,000$ km²) (Table 8) (Takahashi, 2013). The range of the predicted headwaters of the Chinle Formation drainage basin reaches the Cordilleran Volcanic arc and covers the Mogollon Slope (Fig. 60). Dickinson and Gehrels (2008) determined some U-Pb age peaks of zircon grains in the range of 262–236Ma, 1,470–1,450 Ma, and 1,770–1,640 Ma from sandstone samples of the Shinarump Member, Southwest Utah. Among them, the age peaks of 1,470–1,450 Ma and 1,770–1,640 Ma were interpreted to have derived from the Yavapai–Mazatzal basement (= Mogollon Slope) (Dickinson and Gehrels, 2008). Although they interpreted that the age peaks of 262–236 Ma indicate the contribution of the Permian–Triassic East Mexico magmatic arc, some parts of the Cordilleran Volcanic arc were active during this period (Riggs et al., 2013, 2016). Thus, the sandstone samples of the Shinarump Member by Dickinson and Gehrels (2008) may have been derived from the Mogollon Slope and/or Cordilleran Volcanic arc, and this interpretation is consistent with the prediction of the range of the headwaters of the Chinle Formation drainage basin by the present study (Fig. 60). In addition, the drainage basin area of the Vermillion Cliffs paleovalley fluvial system drawn by Bhattacharya et al. (2016) is calculated at about 100,000 km², which is almost equivalent to the estimated drainage basin area in the present study. Therefore, the

continental scaling method seems to be more appropriate for the estimations of A_d and L_d values in the Chinle Formation drainage basin, although the formation developed in a backarc setting under low-latitude monsoonal climatic condition.

4-7-3. Detrital composition

Clast compositions show a distinct change from the Shinarump to Cameron members, which is characterized by upward decrease in the relative amounts of quartzite and quartz, and by upward increase in those of chert and acidic volcanic rock fragments (Fig. 50). The stratigraphic change in the clast composition is interpreted to reflect a temporal change in the source areas, and/or a successive removal of quartzite and parent rocks of quartz by denudation, which may have resulted in an expansion of the exposure of chert and acidic volcanic rocks in the source areas. Three clast types of volcanic rock fragments imply that they were derived from different volcanic terranes in terms of locations and/or ages.

Some embayed monocrystalline quartz grains of the Cameron Member (Fig. 51C) imply the supply of volcanoclastic fragments in response to active volcanism during the sedimentation of the member, and is interpreted to have been formed in acid volcanic and/or sub-volcanic rocks (Donaldson and Henderson, 1988). Partially dissolved feldspars, which are surrounded and/or replaced by authigenic clay minerals (Fig. 51E) suggest that these grains were affected by chemical weathering after the deposition. The volcanic lithic fragments without features of intense surface weathering suggest that they were also derived from active volcanism during the deposition of the Chinle Formation.

The stratigraphic variations in the framework compositions of sandstones (Fig.

52) are also interpreted to document spatial and/or temporal changes in major rock types in the source areas. Alternatively, they are also considered to have been controlled by a change in the intensity of chemical weathering in the provenance terranes (Suttner and Dutta, 1986; Garzanti et al., 2013). For example, an intense chemical weathering condition under hot and humid climates may have produced quartzose sands in the provenance (Garzanti et al., 2013). A temporal change in the intensity of volcanic activity in the hinterlands is also a possible explanation for the upward increase in feldspars and volcanic lithic fragments in association with the occurrences of embayed monocrystalline quartz grains and volcanic lithic fragments. However, relative abundances of volcanic lithic fragments are limited as a framework composition in sandstones of both the Shinarump and Cameron members (Table 18), and the effect of the temporal change in volcanic activity in the source terranes can be excluded as a major cause in the vertical change in the sandstone framework composition. Consequently, the present study interprets that the temporal variation in the sandstone framework composition was controlled by the changes in the basement rock types in the source mountains and/or the temporal changes in the intensity of chemical weathering of the source rocks.

Although smectite in some mudstone samples are randomly interstratified with illite (Fig. 53A), high percentages of smectite and kaolinite in some sandstone and mudstone samples indicate that the Chinle Formation fluvial deposits have been subjected only to the effect of an early stage in diagenesis. SEM images, which do not show authigenic structures (Fig. 58), also suggest that diagenetic modification of minerals after the deposition were insignificant. Thus, clay minerals from Chinle Formation fluvial deposit samples are mainly interpreted to be detrital in origin,

although some diagenetic modification of detrital minerals are observed in partially dissolved K-feldspar that is surrounded and replaced by clay minerals (Fig. 51E). Detrital illite and chlorite, therefore, are considered to have been mechanically ground clay minerals (Singer, 1984; Do Campo et al., 2010; Huyghe et al., 2011; Ghosh et al., 2019). Illite is interpreted to have been derived primarily from granitic, metamorphic, and/or sedimentary rocks in the source areas. Chlorite may have been derived from the igneous and/or sedimentary rocks in the source areas, or from mafic volcanic input as suggested by Jin et al. (2018), who analyzed sandstone samples from the Chinle Formation in the Petrified Forest National Park, Arizona. Because illite and chlorite are unstable under warm and humid climatic conditions (Singer, 1984, Clift et al., 2014; Ghosh et al., 2019), some of these clay minerals found in the Chinle Formation are considered to have been derived from bedrocks distributed near its depositional basin. For example, the underlying Moenkopi Formation in Southwest Utah includes abundant illite and chlorite (Schultz, 1963), and it may have been a source of illite and chlorite during the Chinle Formation fluvial depositions. Relative abundance of detrital kaolinite and smectite in the mudstone samples from the Cameron Member and “purple pedogenic beds” shows vertical variation with three cycles of zigzag pattern (Figs. 56 and 57), which is interpreted to have been caused mainly by temporal fluctuation in the intensity of chemical weathering of the basement rocks in the source areas, rather than by the change in rock types of the basement rocks. The occurrence of smectite may also indicate an effect of the input of volcaniclastic sediments from the source terraces (Singer, 1984; Do Campo et al., 2010). However, the effect of the input of volcaniclastic sediments is interpreted to have been excluded for the supply of detrital smectite to the Chinle Formation, because of a relatively small proportion of volcanic rock fragments

as sandstone framework grains (Table 18).

The channel sandstones and floodplain mudstones show very high contrast between clay mineral compositions in each member (Figs. 54–57). The differences in the clay mineral compositions between channel sandstones and floodplain mudstones may have been caused by segregation of clay particles during the transportation and deposition in the fluvial systems (Gibbs, 1977). Larger clay particles (i.e., kaolinite) seem to have selectively deposited in fluvial channels, while smaller clay particles, such as smectite, illite, and chlorite, may have been concentrated in suspended load from which floodplain muddy deposits formed. In contrast, clay mineral composition of mudstone samples from the Cameron Member and “purple pedogenic beds” document distinct vertical variation in the relative abundance of kaolinite and smectite. This vertical variation is considered to have been caused by fluctuation in the intensity of chemical weathering in the source areas in response to temporal variation in climatic conditions. The occurrence of abundant kaolinite is generally linked to a humid climate, and the increase in the relative abundance of smectite is interpreted as a signal of a climate with contrasting seasonality that may have been associated with a pronounced dry season in a continental setting (Singer, 1984; Chamley, 1989; Thiry, 2000; Net et al., 2002; Do Campo et al., 2007, Huyghe et al., 2011; Wan et al., 2007; Clift et al., 2014). Smectite and kaolinite in the mudstone samples of the Cameron Member and “purple pedogenic beds”, whose relative abundances show inversely proportional zigzag patterns (Figs. 56 and 57), are interpreted to reflect periodic changes of humid and wet-dry seasonal conditions in the source areas. The development of Vertisol (Martz et al., 2017) also suggests wet-dry seasonal conditions during the deposition of the Cameron Member. The mudstone samples of the Shinarump Member include kaolinite,

yet do not contain smectite (Figs. 54–56). These clay mineral compositions imply that wet-dry seasonal condition had not developed, and the climate was probably humid during the deposition of the Shinarump Member.

4-7-4. Climatic shift

The paleohydrological data of the Chinle Formation indicate a temporal decrease in bankfull discharge (Fig. 48). In addition, detrital compositions of sandstone framework grains (Fig. 52) and clay minerals (Figs. 54–57) also suggest a temporal reduction in the intensity of chemical weathering. These data imply that climatic conditions for the development of the Chinle Formation may have shifted from humid to wet-dry seasonal conditions within the 10 million-year scale. The stable and fixed channels of the Cameron Member (Fig. 59) also suggest a seasonal change in discharge, because the stable and fixed anastomosed fluvial systems have commonly been documented from modern fluvial systems, which have a seasonal peak in the annual hydrograph that is caused by meltwater from snow and glacier during spring and summer or by seasonal intensification of rainfall in adjacent mountains (Nadon, 1994). In addition, relative abundance in smectite and kaolinite in the mudstone samples of the upper part of the formation, which show three cycles of inversely proportional zigzag pattern (Figs. 56 and 57), is interpreted to reflect short-term fluctuations of climate.

The overall climatic shift from humid to wet-dry seasonal conditions is consistent with the interpretations of previous paleoclimatic studies of the Chinle Formation based on data from the Four Corners region (Dubiel et al., 1991; Dubiel and Hasiotis, 2011; Atchley et al., 2013; Nordt et al., 2015; Baranyi et al., 2018; Jin et al., 2018; Lucas and Tanner, 2018). In addition, the interpretation of short-term fluctuations

of climate, which were revealed by clay mineral composition from mudstone samples of the Cameron Member and “purple pedogenic beds”, may be compared to minor aggradation-and-degradation cycles by Dubiel and Hasiotis (2011). They depicted three minor cycles in the Monitor Butte Member in the Four Corners region, which is correlative to the Cameron Member and “purple pedogenic beds” in Southwest Utah. In contrast, the paleoclimate during the deposition of the lowermost Chinle Formation, such as the Shinarump Member and its age-equivalent strata, is interpreted to have been extremely humid on the basis of humid paleosol types, such as Gleysols and Oxisols (Dubiel and Hasiotis, 2011), and gleyed Spodosols (Lucas and Tanner, 2018). However, the modern tropical soils, such as Oxisols and Ultisols, which are distributed in Brazil and central Africa, contain a small amount of illite and chlorite (Ito and Wagai, 2017), because illite and chlorite are unstable under warm and humid climatic conditions (Singer, 1984, Clift et al., 2014; Ghosh et al., 2019). Moderate amounts of illite and chlorite in mudstone samples of the Shinarump Member in the study area likely indicate that the intensity of chemical weathering during the deposition of the Shinarump Member in Southwest Utah was weaker than that of the present low-latitude tropical regions, and that the lowermost part of the Chinle Formation was deposited under drier climatic condition than that was previously interpreted.

4-7-5. Basin evolution

Several sequence boundaries have been defined in the Chinle Formation on the basis of identification of distinct erosional surfaces that are interpreted to have formed in response to the development of fluvial paleovalleys and interfluvial paleosols (Dubiel, 1991; Demko et al., 1998; Cleveland et al., 2007; Dubiel and Hasiotis, 2011). Mottled

mudstones of the uppermost part of the Moenkopi Formation, which was formerly included in the basal part of the Shinarump Member by Stewart et al. (1972), is interpreted as pedogenically modified deposits (Fig. 45C) that document long term subaerial exposure of sediments and basement rocks. These pedogenically modified deposits have been interpreted to be accompanied by valley incision during degradation periods (Wright and Marriott, 1993; Shanley and McCabe, 1994). Because the basal surface of a channel complex of the Shinarump Member is a composite erosional surface of channel deposits and channel complexes (Fig. 47), the composite basal erosional surface is interpreted to have formed in response to alternation of incision and deposition, and is equivalent to regional composite scour surfaces of Holbrook and Bhattacharya (2012). Regional composite scour surfaces in fluvial successions are not consistent with the concept of the traditional sequence boundary, which is interpreted to represent a single falling stage topographic surface of erosion (i.e., unconformity) (Posamentier et al., 1988; Van Wagoner et al., 1988). Holbrook and Bhattacharya (2012) proposed an extension of the conceptual definition of the sequence boundary to include traits of regional composite scour surfaces. Following this extended definition of sequence boundary, the basal composite scour surfaces of the channel complexes of the Shinarump Member is interpreted to be a sequence boundary (6th-order BS, Figs. 45A and 47).

A factor that controlled architecture and stacking pattern of the Chinle Formation fluvial system remains controversial. Dubiel and Hasiotis (2011) and Miall (2014) interpreted that aggradation-and-degradation cycles of the Chinle Formation may have been controlled primarily by climatic fluctuation, while Blakey and Gubitosa (1984), Cleveland et al. (2007), and Trendell et al. (2012) emphasized that tectonism was the

prime controlling factor for the development of the formation. The Chinle Formation depositional basin is interpreted to have developed in a backarc region of the Cordilleran volcanic arc, and also to have been surrounded by the Cordilleran volcanic arc to the west, highlands of the Ancestral Rocky Mountains to the east, and a broad and gently sloping elevated area that is called the Mogollon Slope to the south (Fig. 38). Therefore, the basin is considered to have been affected by differential subsidence (Kraus and Middleton, 1987; Dickinson and Gehrels, 2008). However, in Southwest Utah, stratigraphic thicknesses of the Chinle Formation fluvial deposits do not exhibit distinct spatial variation, and the paleocurrent directions also do not show distinct spatial and temporal variations (Fig. 47). Furthermore, the effects of faulting and folding within the basin are not recognized during the deposition of the Chinle Formation. Consequently, the tectonic movements are not interpreted to have influenced the architecture and stacking patterns of the Chinle Formation fluvial system in Southwest Utah. Alternatively, the reduction of water discharge and sediment load is interpreted to cause an upstream shift of a distal, fine-grained fluvial facies belt in association with development of isolated channels, regardless of low rate of basin subsidence (Strong et al., 2005). Geomorphological and paleohydrological analyses of the Chinle Formation fluvial channels indicate upward decreases in the sizes of paleochannels and bankfull discharges (Fig. 48). Sediment load discharged by a fluvial system under a wet-dry seasonal climate is generally greater than those observed under a more humid monsoonal climate as a response to restriction of vegetation under a wet-dry seasonal climate (Cecil, 1990). The locally abundant occurrence of fossil plants including a variety of ferns, conifers, horsetails, and bennettitaleans from the channel deposits of both Shinarump and Cameron members (A.R.C. Milner, unpublished data),

implies that the uplands of the Chinle Formation depositional basin were well forested. In addition, the studies of fossil plant assemblages of the Chinle Formation in the Four Corners region and the adjacent areas suggest that the uplands, lowlands, and floodplains of the Chinle Formation depositional basin may have been well vegetated and forested during the Norian time (Litwin et al., 1991; Lindström et al., 2016; Baranyi et al., 2018). Consequently, sediment loads in the Chinle Formation fluvial system is considered not to have increased as a result of thick vegetation cover under the wet-dry seasonal climate. The upward decrease in channel density in the Chinle Formation, therefore, is interpreted to have responded to the upward decrease in bankfull discharge (Fig. 48) in harmony with the climatic shift within the 10 million-year scale (Figs. 52, 54–57). Therefore, the stacking patterns of the Chinle Formation channel deposits in Southwest Utah is interpreted to have been controlled mainly by the shift from humid to wet-dry seasonal climatic condition. The stacking pattern of the Chinle Formation fluvial deposits that are characterized by the upward decrease in interconnectedness of channel complexes and channel dimensions (Figs. 47, 48, 59A) is similar to that of the standard nonmarine transgressive sequence stratigraphic models (Wright and Marriott, 1993; Shanley and McCabe, 1994; Catuneanu et al., 2009; Blum et al., 2013) (Fig. 2). The backwater effect of the Colorado River-scale drainage basins (orders of 10^5 km²), which are correlative to the Chinle Formation fluvial system, is up to 100 km (Blum et al., 2013). In addition, the study area of the Chinle Formation in Southwest Utah located more than 300 km southeast from the Late Triassic coastline (Fig. 38). Thus, an effect of sea-level change can be ignored in the Chinle Formation fluvial system as an allogenic control factor. Consequently, the stacking patterns of the nonmarine transgressive sequence stratigraphic models are interpreted to develop by the discrete allogenic

factors of a rise in relative sea level and climatic drying.

4-8. Conclusions

This study investigated spatial and temporal variations in fluvial architecture, stacking patterns, paleohydrological features, and detrital composition of the Upper Triassic Chinle Formation, which consists of the Shinarump Member, Cameron Member, and “purple pedogenic beds” in ascending order in Southwest Utah, for elucidating the relationships between fluvial sedimentation and climatic fluctuation in a sedimentary basin that was formed in western Pangaea. The main conclusions of the study are as follows:

(1) The Shinarump Member consists of amalgamated channel complexes, which represent multiple-thread, braided fluvial style. In contrast, the overlying Cameron Member and “purple pedogenic beds” is represented by isolated channel complexes and component single thread, stable, and fixed channel deposits, which were encased in floodplain muddy deposits.

(2) Geomorphological and paleohydrological analyses of the channel deposits represent upward decrease in channel cross-sectional sizes and bankfull discharges of the Chinle Formation fluvial system, which indicate temporal decrease in both flood magnitude and precipitation in the depositional basin. The equations of the modern Indonesian fluvial system estimated the drainage basin area of the Chinle Formation to be smaller than that which was previously assumed. In contrast, the equations from modern rivers of the contiguous United States and global rivers scaled the Chinle Formation drainage basin area which reaches the Cordilleran Volcanic arcs and includes the Mogollon Slope.

(3) Sandstone samples from the Shinarump Member are represented by more quartzose framework composition than those from the Cameron Member. Mudstone samples from the Cameron Member and “purple pedogenic beds” are characterized by abundant contents of kaolinite and smectite, while those from the Shinarump Member lack smectite. These stratigraphical changes in detrital compositions suggest that the intensity in chemical weathering of source rocks in the provenance terranes temporally decreased.

(4) The temporal variations in the paleohydrological features and detrital compositions documented in the Chinle Formation are interpreted to have been in harmony with a temporal shift from humid to wet-dry seasonal climatic conditions in Southwest Utah during the Norian time. In contrast, the moderate amounts of illite and chlorite from the Shinarump Member mudstone samples suggest that the intensity of chemical weathering during the deposition of the Shinarump Member in Southwest Utah was weaker than that of present low-latitude tropical regions.

(5) The stratigraphical change in the fluvial architecture from the amalgamated channel complexes of multiple-thread, braided fluvial system to the isolated channel complexes of stable and fixed channels and thick floodplain muddy deposits of the Chinle Formation is interpreted to have been controlled primarily by the shift from humid to wet-dry seasonal climatic conditions rather than by tectonic movements in the sedimentary basin and its hinterland. The stacking pattern of the Chinle Formation is similar to that of the standard nonmarine transgressive sequence stratigraphic models. The fluvial architectural features of the model are interpreted to be formed by both a rise in relative sea level and climatic drying.

Part 5. Recommendations for applications of the empirical equations to ancient successions

Although empirical equations derived from a modern fluvial system developed in a specific climatic and tectonic setting should be applied to ancient fluvial successions which have similar channel form and are developed under equivalent tectonic and climatic setting (Williams, 1984b; Davidson and North, 2009; Adhiperdana et al., 2018), some recommendations for the applications are given here on the basis of the outcomes of the present study.

5-1. Equations between W_b and Q

The relationship between bankfull channel width (W_b) and bankfull discharge (Q_b) from the present study and the previous studies represent similar regression curves in log-log graph regardless of their tectonic and climatic settings (Fig. 16B). This relationship between the W_b and Q_b indicates that the bankfull discharge controls the bankfull channel width as channel forming discharge (e.g. Dury, 1976; Bridge, 2003; Yamamoto, 2004). Therefore, the empirical equation between W_b and Q_b established by the present study can be widely applied to the rock records regardless of the climatic and tectonic settings. The estimated Q_b values of the Iwaki, Bayah, and Chinle formation fluvial channels increase approximately linearly with W_b in a log-log graph (Fig. 61A). In contrast, the relationship between W_b and mean discharge (Q_{mean}) varies between the previous case studies (Fig. 16A), and these variations are interpreted to reflect annual precipitation together with magnitude of the seasonal variations in precipitation in each case-study area under specific climatic conditions. For example,

the empirical equation from the modern Indonesian rivers estimate the Q_{mean} value larger than that from the modern Japanese rivers for a given W_b although both fluvial systems developed in arc–trench systems, and the large values of Q_{mean} in the Indonesian rivers are interpreted to be caused by higher annual precipitation under subhumid ever-wet to seasonal conditions than that of the Japanese Archipelago under temperate climatic conditions. Therefore, the $Q_{\text{mean}}-W_b$ relationships should be applied to the stratigraphic records depending on, in particular, the paleoclimates in addition to tectonic settings. For example, the Q_{mean} values for the Chinle Formation fluvial system using the Indonesian and continental scaling methods are quite different (Fig. 61B). The Q_{mean} values calculated using the Indonesian scaling method are interpreted to be more valid because the formation is characterized by the low-latitude monsoonal climatic condition, which is similar to the modern Indonesian climate. In contrast, Q_b values can be estimated regardless of the paleoclimatic condition for a given W_b , and a temporal variation in Q_b values might reflect a temporal change in flood magnitude, flood-related precipitation, and evaporation of the drainage basin, as discussed in the Chinle Formation fluvial system (Fig. 48). Therefore, the estimated Q_b values are interpreted to be more useful for the discussion about climatic change in various time scales in an ancient terrestrial environment than Q_{mean} .

5-2. Equations between d_m and W_b

The relationships between mean bankfull channel depth (d_m) and W_b developed from the present study and the previous studies also represent distinct variations in the log-log graph (Fig. 19). These variations are interpreted to have been caused by the specific tectonic and climatic conditions that control geomorphological and

hydrological features such as valley slope, water and sediment discharges, denudation rates, and vegetation. Thus, the W_b values of the Chinle Formation fluvial channels represent variation between those estimated using the Indonesian and continental scaling methods (Figs. 61C). In addition, the W_b-d_m equations developed from the modern fluvial systems in the Japanese and Indonesian Archipelagos estimate narrower W_b relative to d_m for relatively large fluvial channels (Figs. 19, 62). This is interpreted to reflect higher flood discharge and resultant downward erosion of riverbeds by floodwaters, and growth of thick vegetation covers on overbanks preventing river channels from lateral erosion and widening (Gran and Paola, 2001; Tal and Paola, 2010; Adhiperdana, 2018). Furthermore, the depth to width ratio of meandering rivers is, in general, larger than that of braided rivers (Parker, 1976; Bridge, 2003; Xu, 2004) (Fig. 19). These variations indicate that the W_b-d_m equations should be used for ancient fluvial deposits depending on channel forms, and tectonic and climatic settings.

5-3. Equations between Q_b , A_d , and L_d

The empirical equations between Q_b , drainage basin area (A_d), and drainage basin length (L_d) represent distinct variation between the equations from fluvial systems developed in arc-trench systems (Japanese and Indonesian Archipelagos) and those from global and continental rivers (including the contiguous United States) (Figs. 17A and 18A). The clarification of the existence of variations is one of the most important outcomes of the present study, and suitable selection of the empirical equations is crucial for the estimations of paleohydrological features in different types of ancient fluvial systems (Figs. 61D, 61E, and 62). In general, the accuracies of values of d_m , W_b , Q_{mean} , and Q_b of the ancient fluvial systems, which are estimated from the stratigraphic

thicknesses, are difficult to judge, although the values of d_m and W_b may be checked by observations of fluvial deposits using large outcrops, which should be orthogonal to paleocurrent directions (Donselaar and Schmidt, 2005; Jensen and Pedersen, 2010). In contrast, the estimated values of A_d and L_d can be checked by comparisons with paleogeography and source areas of detrital fragments that were reconstructed from other analytical methods, such as the clast and sandstone framework grain compositions and detrital zircon U-Pb ages (Xu et al., 2017). The estimated values of A_d and L_d for the fluvial systems of the Paleogene Iwaki Formation of Northeast Japan and the Paleogene Bayah Formation of western Java, which developed in forearc-basin settings, are consistent with the source areas that were estimated from petrographic features of gravels of the Iwaki Formation, and detrital zircon U-Pb ages of the Bayah Formation, respectively (Figs. 33 and 37). These outcomes of the present case studies suggest that the proposed approach is appropriate, and the empirical equations between Q_b , A_d , and L_d , which were derived from the modern Japanese and Indonesian fluvial systems, can be applied to rock records that mainly developed in convergent margin settings, in particular in forearc-basin settings. On the other hand, the values of A_d and L_d for the Late Triassic Chinle Formation fluvial system, which developed in the continental backarc-basin region, were calculated in harmony with the previously reconstructed paleogeography on the basis of detrital zircon U-Pb age analysis using the continental scaling method (Fig. 60). This result implies that the equations derived from continental rivers are useful for the reconstruction of the drainage basin parameters of fluvial systems developed in the continental backarc basin-setting at least in some cases (Fig. 61D, E). The A_d and L_d that were estimated by using the relationships of continental rivers are represented by larger values with wider data ranges than those of rivers

developed in arc–trench systems. In addition, the range of the estimated A_d and L_d values become increasingly larger for fluvial systems in rock records that were affected by changes in flood magnitude and precipitation at the source areas, as represented by the Chinle Formation fluvial system (Fig. 60). In other words, the fluvial systems developed in forearc-basin settings, which are characterized by smaller drainage basin areas (Fig. 61E), may more accurately estimate the dimension of drainage basin, especially in the fluvial system that was not affected by changes in precipitation, evaporation, and flood magnitude, as documented in the Iwaki Formation fluvial system. Furthermore, in the Iwaki Formation example, the estimations of A_d and L_d can evaluate the possible basement source rocks, which have not yet been determined from the petrographic features (Figs. 33 and 37). Therefore, the reconstruction of drainage basin characteristics using the newly developed method should be an effective tool for an additional provenance analysis and reconstruction of paleogeography in a fluvial successions developed in forearc-basin settings (Fig. 62).

5-4. Uncertainties of the paleohydrological estimations

In the reconstructions of paleohydrological features of ancient fluvial systems, several uncertainties are arisen even if appropriate empirical equations are applied to rock records that document their own specific climatic and tectonic histories. This section briefly summarized some statistical uncertainties arisen by applying the empirical equations to rock records. Measurements of bar deposit and cross-set thickness commonly include some uncertainties. In general, distinction between upper bar deposits of alternating beds of sandy and muddy deposits and floodplain muddy deposits is difficult (Bridge and Tye, 2000; Bridge, 2003; Colombera et al., 2017; Xu et

al., 2017). Although sandy lower bar deposits are generally easy to identify in rock records, the discrimination of upper bar deposits from floodplain muddy deposits still have some uncertainties. This introduces under or over estimations of the bankfull channel depth (Bridge and Tye, 2000). In the present study, gently inclined alternating beds of sandy and muddy deposits were interpreted to be the upper bar deposits (Fig. 44C), and the total thickness of the lower and upper bar deposits were used. In addition, downward erosion of bar deposits by overlying channel and/or bar deposits also causes underestimations of the bankfull channel depth (Colombera et al., 2017; Alexander, 2020). To prevent the underestimation, the present study adopted the maximum thickness values of the bar deposit for the reconstruction of the bankfull channel depth. In contrast, locally developed scour fill deposits under bar deposits introduce overestimation of the bar deposits to estimate the bankfull channel depth. Finally, although the degree of the effect of the burial compaction is difficult to correct the original thickness of the total bar deposits, the present study used a 10 % compaction factor to correct stratigraphic thickness (Ethridge and Schumm, 1978; Lorenz et al., 1985).

General conclusions

This study examined the relationships between the bankfull channel depth (d), mean bankfull channel depth (d_m), bankfull channel width (W_b), mean (Q_{mean}), bankfull (Q_b), and maximum (Q_{max}) discharges, drainage basin area (A_d), and drainage basin length (L_d) using datasets from the modern rivers mainly in the Japanese Archipelago. Supplemental datasets from the rivers in the Indonesian Archipelago and the contiguous United States were also examined. The established equations were applied to three fluvial successions in rock records using their bar deposit and cross-set thicknesses. The general conclusions of the present study are as follows:

- (1) The empirical equations between W_b and Q_b from the Japanese rivers can be expressed by coefficients and exponents quite similar to those of the equations from other regions, and is likely to have wider applicability for modern and ancient fluvial systems. In contrast, the d_m - W_b , W_b - d_m , Q_{mean} - W_b , A_d - Q_b , and L_d - A_d relationships derived from rivers in the Japanese Archipelago and other regions represent variations in their coefficients and exponents. These differences are interpreted to be caused by variations in climatic and tectonic settings of each fluvial system.
- (2) The A_d and L_d values of the Paleogene Iwaki Formation fluvial system, Northeast Japan indicate that the detrital fragments of the formation were derived mainly from the Abukuma Highlands, and possibly from the Yamizo Mountains. The d and W_b values represent no distinct million-year-scale temporal variations in response to a rise in relative sea level within a sequence stratigraphic framework. This type of sequence-stratigraphic fluvial signature is likely representative of active-margin

basins in temperate climatic settings.

- (3) The estimated A_d and L_d values of the Paleogene Bayah Formation fluvial system, West Java, revealed that detrital fragments of the fluvial deposits were derived from basement rocks in Northwest Java. The stacking pattern of the Bayah Formation fluvial deposits represent an overall upward increase and decrease in interconnectedness of the channel-fill deposits and in channel cross-sectional dimensions, which is similar to that of the nonmarine sequence stratigraphic models. The stacking pattern is interpreted to have been controlled by million-year-scale variation in the rate of tectonic basin subsidence.
- (4) The detrital composition of the Late Triassic Chinle Formation in Southwest Utah indicates upward decrease in the intensity of chemical weathering, which reflects climatic drying. The upward decrease in channel cross-sectional dimensions and interconnectedness of channel complexes is interpreted to have developed in response to the climatic drying. The stacking pattern is similar to that of the transgressive nonmarine sequence stratigraphic models. This architectural feature is interpreted to be formed by climatic drying in addition to a rise in relative sea level and increase in a rate of basin subsidence.
- (5) The Q_b values of an ancient fluvial system are more useful for discussion about paleoclimatic change than Q_{mean} values. The estimation method of drainage basin characteristics using empirical equations from the modern fluvial systems in arc-trench systems is interpreted to be a useful tool for the reconstructions of paleogeography and sediment provenance in fluvial deposits developed in forearc-basin settings.

Acknowledgments

I'm deeply grateful to Professor Makoto Ito (Chiba University) for supervising my research. His instructions in the field considerably improved my observation skills in sedimentary structures, fluvial facies, and architecture. Fieldworks conducted with him in the Joban Coalfield and Southwest Utah are highlights of this research. The early version of this dissertation was improved drastically by his useful and critical discussions and kind reviewing.

I would also like to thank Professor Emeritus Sakae O'Hara (Chiba University) and Nagayuki Nemoto for their kind help in the field at the Joban Coalfield, Fukushima Prefecture. I'm indebted to Dr. Billy G. Adhiperdana (Padjadjaran University) for his kind support and suggestions about paleohydrological features of the Bayah Formation fluvial deposits, western Java, and petrographic analyses of sandstone samples of the Chinle Formation. I would also like to acknowledge Andrew R.C. Milner (St. George Dinosaur Discovery Site at Johnson Farm), Professor Emeritus Martin G. Lockley (Colorado University, Denver), and Professor Jerry D. Harris (Dixie State University) for suggestions and valuable discussions about stratigraphic, sedimentological, and paleontological features of the Chinle Formation, Southwest Utah. I'd like to thank Professor Emeritus Atsushi Inoue and Dr. Noboru Furukawa (Chiba University) for their technical assistance with XRD and for useful discussions about clay mineral compositions. I'd like to thank Professor Emeritus Masaki Matsukawa (Tokyo Gakugei University), Professor Keiichi Hayashi (Konan University), Dr. Katsuyoshi Baba, Dr. Kazuto Koarai (Keio Yokohama Elementary School) and Dr. Naohisa Nishida (Tokyo Gakugei University) for valuable discussions.

The Ministry of Land, Infrastructure, Transport and Tourism, Kanto Regional Development Bureau provided cross-sectional data of modern river channels. The quarry companies at the Joban Coalfield of Fukushima Prefecture provided access to their quarries during my fieldworks. Fieldworks in Utah, U.S.A. were conducted under a permit issued by the United States Department of the Interior National Park Service (Permit numbers: ZION-2005-SCI-0022, ZION-2006-SCI-0019, and ZION-2013-SCI-0015) and the Bureau of Land Management (BLM) in Utah (Tracking/Agreement number: 5-17). The dissertation has been supported in part by the Japan Society for the Promotion of Science KAKENHI Grant Number JP17K12968, and JP 21K01010. I would also like to thank these companies and organizations.

Finally, I'd like to thank my family for kindly allowing me to be away from home at times for fieldworks and to continue my research.

References

- Adams, M. M., Bhattacharya, J. P., 2005, No change in fluvial style across a sequence boundary, Cretaceous Blackhawk and Castlegate Formations of central Utah, U.S.A. *Journal of Sedimentary Research*, **75**, 1038–1051.
- Adhiperdana, B. G., 2018, *Sedimentological study of a fluvial succession of the Eocene–Oligocene Bayah Formation, West Java: Reconstruction of paleohydrological features of an ancient fluvial system using empirical equations developed from modern fluvial systems in the Indonesia islands*. PhD thesis, Division of Geosystem and Biological Sciences, Department of Earth Sciences, Chiba University Graduate School of Science, 217p.
- Adhiperdana, B. G., Hendarmawan, Shibata, K. and Ito, M., 2018, Relationships between discharge parameters and cross-sectional channel dimensions of rivers in an active margin influenced by tropical climate: The case of modern fluvial systems in the Indonesian islands. *Catena*, **171**, 645–680.
- Alexander, J. S., McElroy, B. J., Huzurbazar, S., Murr, M. L., 2020, Elevation gaps in fluvial sandbar deposition and their implications for paleodepth estimation. *Geology*, **48**, 718–722.
- Allen, J. R. L., 1970, Studies in fluvial sedimentation: a comparison of fining-upwards cyclothems, with special reference to coarse member composition and interpretation. *Journal of Sedimentary Petrology*, **40**, 298–323.
- Allen, J. R. L., 1982, *Sedimentary structures: Their character and physical basis Volume I. Developments in Sedimentology 30A*. Elsevier, Amsterdam, 593p.
- Allen J. R. L., 1983, Studies in fluvial sedimentation: bars, bar complexes and sandstone sheets (low-sinuosity braided streams) in the Brownstones (L.

- Devonian), Welsh Borders. *Sedimentary Geology*, **33**, 237–293.
- Amano, K., 1991, 3.4.3 Tanagura area. In Geological Society of Japan ed., *Regional geology of Japan 3 Kanto region*, 206–214. Asakura Shoten, Tokyo.
- Ando, H., 2003, Stratigraphic correlation of Upper Cretaceous to Paleocene forearc basin sediments in Northeast Japan: cyclic sedimentation and basin evolution. *Journal of Asian Earth Sciences*, **21**, 921–935.
- Ando, H., Seishi, M., Oshima, M. and Matsumaru, T., 1995, Fluvial–shallow marine depositional systems of the Futaba Group (Upper Cretaceous) –Depositional facies and sequences–. *Journal of Geography*, **104**, 284–303 (in Japanese with English abstract).
- Ando, H. and Takahashi, M., 2017, Reconstruction of the Cretaceous Paleo-Japan continental arc-trench system reconsidered from Cretaceous geologic record in the Japanese Islands. *Fossils (Kaseki)*, (102), 43–62.
- Antia, J. and Fielding, C. R., 2011, Sequence stratigraphy of a condensed low-accommodation succession: lower upper Cretaceous Dakota Sandstone, Henry Mountains, southeastern Utah. *The American Association of Petroleum Geologists Bulletin*, **95**, 413–447.
- Asian Disaster Preparedness Center, 2000, Indonesia country study. In Kishore, K., Subbiah, A. R., Sribimawati, T., Diharto, S., Alimoeso, S., Rogers, P., Setiana, A. eds., *Asian Disaster Preparedness Center (ADPC) Report*, 68. Pathumthani.
- Atchley, S. C., Nordt, L. C., Dworkin, S. I., Ramezani, J., Parker, W. G., Ash, S. R. and Bowring, S. A., 2013, A linkage among Pangean tectonism, cyclic alluviation, climate change, and biologic turnover in the Late Triassic: the record from the Chinle Formation, southwestern United States. *Journal of Sedimentary Research*,

84, 1147–1161.

Atha, J. B., 2014, Identification of fluvial wood using Google Earth. *River Research and Applications*, **30**, 857–864.

Awaji, D., Yamamoto, D. and Takagi, H., 2006, Kinematic history of the Tanakura Shear Zone at brittle regime. *Journal of Geological Society of Japan*, **112**, 222–240 (in Japanese with English abstract).

Bailey, E. H. and Stevens, R. E., 1960, Selective staining of K-feldspar and plagioclase on rock slabs and thin sections. *The American Mineralogist*, **45**, 1020–1025.

Baranyi, V., Reichgelt, T., Olsen, P. E., Parker, W. G. and Kürschner, W. M., 2018, Norian vegetation history and related environmental changes: New data from the Chinle Formation, Petrified Forest National Park (Arizona, SW USA). *Geological Society of America Bulletin*, **130**, 775–795.

Berwick, V. K., 1962, *Floods in Utah, Magnitude and Frequency*. Geological Survey Circular 457. U.S. Geological Survey, 24p.

Bhattacharya, J. P., Copeland, P., Lawton, T. F. and Holbrook, J., 2016, Estimation of source area, river paleo-discharge, paleoslope, and sediment budgets of linked deep-time depositional systems and implications for hydrocarbon potential. *Earth-Science Reviews*, **153**, 77–110.

Biek, R. F., Willis, G. C., Hylland, M. D., Doelling, H. H., 2010, Geology of Zion National Park, Utah. In Sprinkel, D. A., Chidsey T. C. Jr. and Anderson, P. B., eds., *Geology of Utah's Parks and Monuments*, Utah Geological Association Publication, no. 28, 107–141.

Bilodeau, W. L., 1986, The Mesozoic Mogollon Highlands, an Early Cretaceous rift shoulder. *Journal of Geology*, **94**, 724–735.

- Biscaye, P. E., 1965, Mineralogy and Sedimentation of recent deep-sea clay in the Atlantic Ocean and adjacent seas and oceans. *Geological Society of America Bulletin*, **76**, 803–832.
- Blair, T. C. and Bilodeau, W. L., 1988, Development of tectonic cyclothems in rift, pull-apart, and foreland basins: sedimentary response to episodic tectonism. *Geology*, **16**, 517–520.
- Blakey, R. C. and Gubitosa, R., 1984, Controls of sandstone body geometry and architecture in the Chinle Formation (Upper Triassic), Colorado Plateau. *Sedimentary Geology*, **38**, 51–86.
- Blakey, R. C. and Ranney, W., 2008, *Ancient landscapes of the Colorado Plateau*. Grand Canyon Association, 156p.
- Blum, M. D., Guccione, M. J., Wysocki, D. A. and Robnett, P. C., 2000, Late Pleistocene evolution of the Central Mississippi Valley, Southern Missouri to Arkansas. *Geological Society of America Bulletin*, **112**, 221–235.
- Blum, M. D., Martin, J., Milliken, K., Garvin, M., 2013, Paleovalley systems: Insights from Quaternary analogs and experiments. *Earth-Science Reviews*, **116**, 128–169.
- Blum, M. D. and Törnqvist, T. E., 2000, Fluvial responses to climate and sea-level change: a review and look forward. *Sedimentology*, **47** (Suppl. 1), 2–48.
- Boucot, A. J., Xu, C., Scotese, C. R. and Morley, R. J., 2013, Phanerozoic Paleoclimate: An atlas of lithologic indicators of climate. *SEPM Concepts in Sedimentology and Paleontology*, **11**, doi:10.2110/sepmcsp.11.
- Bridge, J. S., 1993, Description and interpretation of fluvial deposits: a critical perspective. *Sedimentology*, **40**, 801–810.

- Bridge, J. S., 2003, *Rivers and floodplains: forms, processes, and sedimentary record*. Blackwell publishing, Malden, 491p.
- Bridge, J. S., Diemer J. A., 1983, Quantitative interpretation of an evolving ancient river system. *Sedimentology*, **30**, 599–623.
- Bridge, J. S., Jalfin, G. A. and Georgieff, S. M., 2000, Geometry, lithofacies, and spatial distribution of cretaceous fluvial sandstone bodies, San Jorge basin, Argentina: outcrop analog for the hydrocarbon-bearing Chubut Group. *Journal of Sedimentary Research*, **70**, 341–359.
- Bridge, J. S. and Leeder, M. R., 1979, A simulation model of alluvial stratigraphy. *Sedimentology*, **26**, 617–644.
- Bridge, J. S., Mackey, S. D., 1993, A theoretical study of fluvial sandstone body dimensions. In Flint, S. S. and Bryant, I. D., eds., *Geological Modeling of Hydrocarbon Reservoirs, International Association of Sedimentologists, Special Publication*, no. 15, 213–236.
- Bridge, J. S. and Tye, R. S., 2000, Interpreting the dimensions of ancient fluvial channel bars, channels, and channel belts from wireline-logs and cores. *The American Association of Petroleum Geologists Bulletin*, **84**, 1205–1228.
- Bryant, M., Falk, P. and Paola, C., 1995, Experimental study of avulsion frequency and rate of deposition. *Geology*, **23**, 365–368.
- Burns, C. E., Mountney, N. P., Hodgson, D. M. and Colombera, L., 2017, Anatomy and dimensions of fluvial crevasse-splay deposits: Examples from the Cretaceous Castlegate Sandstone and Neslen Formation, Utah, U.S.A. *Sedimentary Geology*, **351**, 21–35.
- Carlston, C. W., 1965, The relation of free meander geometry to stream discharge and

- its geomorphic implications. *American Journal of Science*, **263**, 864–885.
- Carson, E. C., Knox, J. C. and Mickelson, D. M., 2007, Response of bankfull flood magnitudes to Holocene climate change, Uinta Mountains, northeastern Utah. *Geological Society of America Bulletin*, **119**, 1066–1078.
- Carson, M. A., 1984, The meandering-braided river threshold: a reappraisal. *Journal of Hydrology*, **73**, 315–334.
- Castro, J. M. and Jackson, P. L., 2001, Bankfull discharge recurrence intervals and regional hydraulic geometry relationships: patterns in the Pacific northwest, USA. *Journal of the American Water Resources Association*, **37**, 1249–1262.
- Catuneanu, O., Abreu, V., Bhattacharya, J. P., Blum, M. D., Dalrymple, R. W., Eriksson, P. G., Fielding, C. R., Fisher, W. L., Galloway, W. E., Gibling, M. R., Giles, K. A., Holbrook, J. M., Jordan, R., Kendall, C. G. St. C., Macurda, B., Martinsen, O. J., Miall, A. D., Neal, J. E., Nummedal, D., Pomar, L., Posamentier, H.W., Pratt, B. R., Sarg, J. F., Shanley, K. W., Steel, R. J., Strasser, A., Tucker, M. E., and Winker, C., 2009, Towards the standardization of sequence stratigraphy. *Earth-Science Reviews*, **92**, 1–33.
- Cecil, C. B., 1990, Paleoclimate controls on stratigraphic repetition of chemical and siliciclastic rocks. *Geology*, **18**, 533–536.
- Center for Water Resources Development and Research, 2011, *Hydrology Year Book: Annual River Discharge of Sumatra, Java and Kalimantan, Year 1968–2011*. Digital copy. Ministry of Public Works and Housing, Republic of Indonesia, Bandung (in Indonesian).
- Chamley, H., 1989, *Clay Sedimentology*. Springer-Verlag, New York, 623p.
- Chaplin, J. J., 2005, *Development of regional curves relating bankfull-channel geometry*

- and discharge to drainage area for streams in Pennsylvania and select areas of Maryland. Scientific Investigations Report 2005–5147. U.S. Geological Survey, Reston, 34p.*
- Chen, C., Guerit, L., Foreman, B. Z., Hassenruck-Gudipati, H. J., Adatte, T., Honegger, L., Perret, M., Sluijs, A. and Castellort, S., 2018, Estimating regional flood discharge during Paleocene–Eocene global warming. *Scientific Reports*, **8**, DOI : 10.1038/s41598-018-31076-3.
- Clements, B. and Hall, B., 2011, A record of continental collision and regional sediment flux for the Cretaceous and Paleogene core of SE Asia: implications for early Cenozoic palaeogeography. *Journal of the Geological Society, London*, **168**, 1187–1200.
- Cleveland, D. M., Atchley, S. C. and Nordt, L. C., 2007, Continental sequence stratigraphy of the Upper Triassic (Norian-Rhaetian) Chinle strata, northern New Mexico, U.S.A.: allocyclic and autocyclic origins of paleosol-bearing alluvial successions. *Journal of Sedimentary Research*, **77**, 909–924.
- Clifford, N. J., Hardisty, J., French, J. R. and Hart, S., 1993, Downstream variation in bed material characteristics: a turbulence-controlled form-process feedback mechanism. In Best J. L. and Bristow C. S., eds., *Braided Rivers, Geological Society, London, Special Publication*, no. 75, 89–104.
- Clift, P. D., Wan, S. and Blusztajn, J., 2014, Reconstructing chemical weathering, physical erosion and monsoon intensity since 25 Ma in the northern South China Sea: A review of competing proxies. *Earth-Science Reviews*, **130**, 86–102.
- Cobbing, E. J., Pitfield, P. E. J., Darbyshire, D. P. F. and Mallick, D. I. J., 1992, *The granites of the South-East Asian Tin Belt. British Geological Survey, Overseas*

Memoir, 10. 369p.

- Colombera, L., Arévalo, O. J. and Mountney, N. P., 2017, Fluvial-system response to climate change: The Paleocene-Eocene Tresp Group, Pyrenees, Spain. *Global and Planetary Change*, **157**, 1–17.
- Davidson, S. K. and North, C. P., 2009, Geomorphological regional curves for prediction of drainage area and screening modern analogues for rivers in the rock record. *Journal of Sedimentary Research*, **79**, 773–792.
- Demko, T. M., Dubiel, R. F. and Parrish, J. T., 1998, Plant taphonomy in incised valleys: Implications for interpreting paleoclimate from fossil plants. *Geology*, **26**, 1119–1122.
- Dickinson, W. R. and Gehrels, G. E., 2008, U-Pb ages of detrital zircons in relation to paleogeography: Triassic paleodrainage networks and sediment dispersal across southwest Laurentia. *Journal of Sedimentary Research*, **78**, 745–764.
- Dickinson, W. R., Soreghan, G. S., Giles, K. A., 1994, Glacio-eustatic origin of Permo-Carboniferous stratigraphic cycles: evidence from the southern Cordilleran foreland region. In Dennison, J. M. and Ettensohn, F. R., eds., *Tectonic and eustatic controls on sedimentary cycles, Concepts in Sedimentology and Paleontology*, no. 4, 25–34. SEPM.
- Do Campo, M., del Papa, C., Jiménez-Millán, J. and Nieto, F., 2007, Clay mineral assemblages and analcime formation in a Palaeogene fluvial-lacustrine sequence (Maíz Gordo Formation Palaeogen) from northwestern Argentina. *Sedimentary Geology*, **201**, 56–74.
- Do Campo, M., del Papa, C., Nieto, F., Hongn, F. and Petrinovic, I., 2010, Integrated analysis for constraining paleoclimatic and volcanic influences on clay-mineral

- assemblages in orogenic basins (Paleogene Andean foreland, Northwestern Argentina). *Sedimentary Geology*, **228**, 98–112.
- Donaldson, C. H., Henderson, C. M. B., 1988, A new interpretation of round embayments in quartz crystals. *Mineralogical Magazine*, **52**, 27–33.
- Donselaar, M. E. and Schmidt, J. M., 2005, Integration of outcrop and borehole image logs for high-resolution facies interpretation: example from a fluvial fan in the Ebro Basin, Spain. *Sedimentology*, **52**, 1021–1042.
- Dubiel, R. F., 1991, Architectural-facies analysis of nonmarine depositional systems in the Upper Triassic Chinle Formation, southeastern Utah. In Miall, A. D. and Tyler, N., eds., *The three-dimensional facies architecture of terrigenous clastic sediments and its implications for hydrocarbon discovery and recovery*, *Concepts in Sedimentology and Paleontology*, no. 3, 103–110. SEPM.
- Dubiel, R. F., 1992, Sedimentology and depositional history of the Upper Triassic Chinle Formation in the Uinta, Piceance, and Eagle basins, northwestern Colorado and northeastern Utah. *United States Geological Survey Bulletin*, **1787-W**, 1–25.
- Dubiel, R. F. and Hasiotis, S. T., 2011, Deposystems, paleosols, and climatic variability in a continental system: the Upper Triassic Chinle Formation, Colorado Plateau, U.S.A. In Davidson, S. K., Leleu, S. and North, C. P., eds., *From River to rock record: the preservation of fluvial sediments and their subsequent interpretation*, *SEPM Special Publication*, no. 97, 393–421.
- Dubiel, R. F., Parrish, J. T., Parrish, J. M. and Good, S. C., 1991, The Pangaeon Megamonsoon –Evidence from the Upper Triassic Chinle Formation, Colorado Plateau. *PALAIOS*, **6**, 347–370.

- Dunne, T. and Leopold, L., 1978, *Water in Environmental Planning*. W.H. Freeman and Co., San Francisco, 818p.
- Dury, G. H., 1976, Discharge prediction, present and former, from channel dimensions. *Journal of Hydrology*, **30**, 219–245.
- Effendi, A. C., Kusnama and Hermanto, B., 1998, Geological map of the Bogor quadrangle, Java (1:100,000). Bandung.
- Elliott, T., 1976, The morphology magnitude and regime of a Carboniferous fluvial-distributary channel. *Journal of Sedimentary Petrology*, **46**, 70–76.
- Ethridge, F. G., 2011, Interpretation of ancient fluvial channel deposits: review and recommendations. In Davidson, S. K., Leleu, S. and North, C. P., eds., *From river to rock record, SEPM Special Publication*, no. 97, 9–35.
- Ethridge, F. G. and Schumm, S. A., 1978, Reconstructing paleochannel morphologic and flow characteristics: methodology, limitations, and assessment. In Miall, A. D., ed., *Fluvial sedimentology, Canadian Society Petroleum Geologists Memoir*, no. 5, 703–721.
- Ferguson, R. I. 1987, Hydraulic and sedimentary controls of channel pattern. In Richards K. S., ed., *River channels: Environment and Process*, 125–158. Blackwell, Oxford.
- Flores, R. M. and Pillmore, C. L., 1987, Tectonic control on alluvial paleoarchitecture of the Cretaceous and Tertiary Raton Basin, Colorado and New Mexico. In Ethridge, F. G., Flores, R. M. and Harvey, M. D., eds., *Recent Development in Fluvial Sedimentology, SEPM Special Publication*, no. 39, 311–320.
- Ford, G. L. and Pyles, D. R., 2014, A hierarchical approach for evaluating fluvial systems: Architectural analysis and sequential evolution of the high net-sand

- content, middle Wasatch Formation, Uinta Basin, Utah. *The American Association of Petroleum Geologists Bulletin*, **98**, 1273–1304.
- Fukuoka, S., 2008, Flood flow and bed variation analysis considering the change in sediment environment—Practical issues and perspectives of the sediment research—. *Advances in river engineering*, **14**, 2–6. Japan Society of Civil Engineers, River Section. (in Japanese with English abstract)
- Fukuoka, S., 2010, A new perspective on river management –Lessons from natural rivers. *Kasen*, **66**, 3–9. Japan River Association. (in Japanese)
- Garzanti, E., Padoan, M., Andò, S., Resentini, A., Vezzoli, G. and Lustrino, M., 2013, Weathering and relative durability of detrital minerals in equatorial climate: sand petrology and geochemistry in the East African Rift. *The Journal of Geology*, **121**, 547–580.
- Gasparini, N. M., Tucker G. E. and Bras, R. L., 1999, Downstream fining through selective particle sorting in an equilibrium drainage network. *Geology*, **27**, 1079–1082.
- Gawthorpe, R. L. and Leeder, M. R., 2000, Tectono-sedimentary evolution of active extensional basins. *Basin Research*, **12**, 195–218.
- Ghosh, S., Mukhopadhyay, J. and Chakraborty, A., 2019, Clay mineral and geochemical proxies for intense climate change in the Permian Gondwana Rock Record from eastern India. *AAAS Research*, 2019, <https://doi.org/10.34133/2019/8974075>.
- Gibbs, R. J., 1977, Clay mineral segregation in the marine environment. *Journal of Sedimentary Petrology*, **47**, 237–243.
- Gibling, M. R., 2006, Width and thickness of fluvial channel bodies and valley fills in the geological record: a literature compilation and classification. *Journal of*

- Sedimentary Research*, **76**, 731–770.
- Godin, P.D., 1991, Fining-upward cycles in the sandy braided-river deposits of the West water Canyon Member (Upper Jurassic), Morrison Formation, New Mexico. *Sedimentary Geology*, **70**, 61–82.
- Gran, K. and Paola, C., 2001, Riparian vegetation controls on braided stream dynamics. *Water Resource Research*, **37**, 3275–3283.
- Greenway, D. R., 1987, Vegetation and slope stability. In Anderson, M. F. and Richards, K. S., eds., *Slope Stability*, 187–230. Wiley, New York.
- Hall, R., 1996, Reconstructing Cenozoic SE Asia. *Geological Society of London Special Publication*, no. 106, 153–184.
- Hall, R., 2012, Late Jurassic-Cenozoic reconstructions of the Indonesian region and the Indian Ocean. *Tectonophysics*, **570–571**, 1–41, doi:10.1016/j.tecto.2012.04.021.
- Hamilton, W., 1979, *Tectonic of the Indonesia Region*. U. S. Geological Survey Professional Paper, no. 1078, 345p.
- Hampson, G. J., Jewell, T. O., Irfan, N., Gani, M. R. and Bracken, B., 2013, Modest change in fluvial style with varying accommodation in regressive alluvial-to-coastal-plain wedge: Upper Cretaceous Blackhawk Formation, Wasatch Plateau, central Utah, U.S.A. *Journal of Sedimentary Research*, **83**, 145–169.
- Hendrizon, M., Praptisih, P. and Putra, S., 2012, Depositional environment of the Batuasih Formation on the basis of foraminifera content: A case study in Sukabumi Region, West Java Province, Indonesia. *Indonesian Journal on Geoscience*, **7**, 101–112.
- Hillier, R. D., Marriott, S. B., Williams, B. P. J. and Wright, V. P., 2007, Possible climate

- variability in the Lower Old Red Sandstone Conigar Pit Sandstone Member (early Devonian), South Wales, UK. *Sedimentary Geology*, **202**, 35–57.
- Hintze, L. F., 1997, *Geologic highway map Utah with a topographic map that shows western national parks*. Brigham Young University Geology Studies–Special Publication no. 3.
- Hoey, T. B. and Bluck, B. J., 1999, Identifying the controls over downstream fining of river gravels. *Journal of Sedimentary Research*, **69**, 40–50.
- Holbrook, J. M., 2001, Origin, genetic interrelationships, and stratigraphy over the continuum of fluvial channel-form bounding surfaces: an illustration from middle Cretaceous strata, south-eastern Colorado. *Sedimentary Geology*, **144**, 179–222.
- Holbrook, J. M. and Bhattacharya, J. P., 2012, Reappraisal of the sequence boundary in time and space: Case and considerations for an SU (subaerial unconformity) that is not a sediment bypass surface, a time barrier, or an unconformity. *Earth-Science Reviews*, **113**, 271–302.
- Holbrook, J., Scott, R. W. and Oboh-Ikuenobe, F. E., 2006, Base-level and buttresses: a model for upstream versus downstream control on fluvial geometry and architecture within sequences. *Journal of Sedimentary Research*, **76**, 162–174.
- Howell, E. R. and Blakey, R. C., 2013, Sedimentological constraints on the evolution of the Cordilleran arc: New insights from the Sonsela Member, Upper Triassic Chinle Formation, Petrified Forest National Park (Arizona, USA). *Geological Society of America Bulletin*, **125**, 1349–1368.
- Huyghe, P., Guilbaud, R., Bernet, M., Galy, A. and Gajurel, A. P., 2011, Significance of the clay mineral distribution in fluvial sediments of the Neogene to Recent

- Himalayan Foreland Basin (west-central Nepal). *Basin Research*, **23**, 332–345.
- Ikeda, H., 1975, On the bed configuration in alluvial channels; their types and condition of formation with reference to bars. *Geographical Review of Japan*, **48**, 712–730. (in Japanese with English abstract)
- Ingersoll, R. V., Bullard, T. F., Ford, R. L., Grimm, J. P., Pickle, J. D. and Sares, S. W., 1984, The effect of grain size on detrital modes: a test of the Gazzi-Dickinson point-counting method. *Journal of Sedimentary Petrology*, **54**, 103–116.
- Iseya, F., 1989, Mechanism of inverse grading of suspended load deposits. In Taira, A. and Masuda, F., eds., *Sedimentary Facies in the Active Plate Margin*, 113–129. Terra Scientific Publishing Company, Tokyo.
- Ito, A. and Wagai, R., 2017, Global distribution of clay-size minerals on land surface for biogeochemical and climatological studies. *Scientific data*, **4**, 170103, DOI: 10.1038/sdata.2017.103.
- Iwata, T., Hirai, A., Inoba, T. and Hirano, M., 2002, Petroleum system in the Offshore Joban Basin, northeast Japan. *Journal of the Japanese Association for Petroleum Technology*, **67**, 62–71. (in Japanese with English abstract)
- Japan River Association, 2007, *Database of Precipitation and River Discharges Year Book of Japan from 1938 to 2003*. DVD-ROM. (in Japanese)
- Jensen, M. A. and Pedersen, G. K., 2010, Architecture of vertically stacked fluvial deposits, Atane Formation, Cretaceous, Nuussuaq, central West Greenland. *Sedimentology*, **57**, 1280–1314.
- Jin, C., Dworkin, S., Atchley, S. and Nordt, L., 2018, Eogenetic diagenesis of Chinle sandstones, Petrified Forest National Park (Arizona, USA): A record of Late Triassic climate change. *Sedimentology*, **65**, 1277–1300.

- Jo, H. R., 2003, Depositional environments, architecture, and controls of Early Cretaceous non-marine successions in the northwestern part of Kyongsang Basin, Korea. *Sedimentary Geology*, **161**, 269–294.
- Jowett, I. G., 1998, Hydraulic geometry of New Zealand rivers and its use as a preliminary method of habitat assessment. *Regulated Rivers: Research & Management*, **14**, 451–466.
- Khan, I. A., Bridge, J. S., Kappelman, J. and Wilson, R., 1997, Evolution of Miocene fluvial environments, eastern Potwar plateau, northern Pakistan. *Sedimentology*, **44**, 221–251.
- Kirkland, J. I. and Milner, A. R. C., 2006, The Moenave Formation at the St. George Dinosaur Discovery Site at Johnson Farm, St. George, southwestern Utah. *New Mexico Museum of Natural History & Science Bulletin*, no. 37, 289–309.
- Kirkland, J. I., Milner, A. R. C., Olsen, P. E. and Hargrave, J. E., 2014, The Whitmore Point Member of the Moenave Formation in its type area in northern Arizona and its age and correlation with the section in St. George, Utah: Evidence for two major lacustrine sequences. *Utah Geological Association Publication*, no. 43, 321–355.
- Knox, J. C., 1983, Responses of river systems to Holocene climates. In Wright, H. E. and Porter, S. C., eds., *Late Quaternary Environments of the United States, Vol. 2, Holocene*, 26–41. University of Minnesota Press.
- Knox, J. C., 1985, Responses of floods to Holocene climatic change in the Upper Mississippi Valley. *Quaternary Research*, **23**, 287–300.
- Kodama, Y., 1994, Downstream changes in the lithology and grain size of fluvial gravels, the Watarase River, Japan: evidence of the role of abrasion in

- downstream fining. *Journal of Sedimentary Research*, **A64**, 68–75.
- Komar, P. D., 1996, Entrainment of sediments from deposits of mixed grain sizes and densities. In Caring P. A. and Dawson M. R., eds., *Advances in Fluvial Dynamics and Stratigraphy*, 127–181. Wiley & Sons, Chichester.
- Komatsubara, J., 2004, Fluvial architecture and sequence stratigraphy of the Eocene to Oligocene Iwaki Formation, northeast Japan: channel-fills related to the sea-level change. *Sedimentary Geology*, **168**, 109–123.
- Kraus, M. J., Middleton, L. T., 1987, Dissected paleotopography and base-level changes in a Triassic fluvial sequence. *Geology*, **15**, 18–21.
- Kubo, K., Yanagisawa, Y., Toshimitsu, S., Banno, Y., Kaneko, N., Yoshioka, T. and Takagi, T., 2002, *Geology of the Kawamae and Ide district*. Quadrangle Series, 1:50,000, 136p. Geological Survey of Japan, AIST. (in Japanese with English abstract)
- Kuenzi, W. D., Horst O. H. and McGehee, R. V., 1979, Effect of volcanic activity on fluvial-deltaic sedimentation in a modern arc–trench gap, southwestern Guatemala. *Geological Society of America Bulletin, Part I*, **90**, 827–838.
- Lear, C. H., Bailey, T. R., Pearson, P. N., Coxall, H. K. and Rosenthal, Y., 2008, Cooling and ice growth across the Eocene-Oligocene transition. *Geology*, **36**, 251–254.
- Leclair, S. F. and Bridge, J. S., 2001, Quantitative interpretation of sedimentary structures formed by river dunes. *Journal of Sedimentary Research*, **71**, 713–716.
- Leeder, M. R., 1973, Fluvial fining-upwards cycles and the magnitude of palaeochannels. *Geological Magazine*, **110**, 265–276.
- Leeder, M. R. and Gawthorpe, R. L., 1987, Sedimentary models for extensional

- tilt-block/half-graben basins. In Coward, M. P., Dewey, J. F. and Hancock, P. L., eds., *Continental extension tectonics. Geological Society of London Special Publication*, no. 28, 139–152.
- Leopold, L. B. and Maddock, T., 1953, *The hydraulic geometry of stream channels and some physiographic implications*. U.S. Geological Survey Professional Paper, no. 252, 57p.
- Leopold, L. B., Wolman, M. G. and Miller J. P., 1964, *Fluvial processes in geomorphology*. W.H. Freeman and Co., San Francisco, 522p.
- Lindström, S., Irmis, R. B., Whiteside, J. H., Smith, N. D., Nesbitt, S. J. and Turner, A. H., 2016, Palynology of the upper Chinle Formation in northern New Mexico, U.S.A.: Implications for biostratigraphy and terrestrial ecosystem change during the Late Triassic (Norian–Rhaetian). *Review of Palaeobotany and Palynology*, **225**, 106–131.
- Litwin, R. J., Traverse, A. and Ash, S. R., 1991, Preliminary palynological zonation of the Chinle Formation, southwestern U.S.A., and its correlation to the Newark Supergroup (eastern U.S.A.). *Review of Palaeobotany and Palynology*, **68**, 269–287.
- Liu, B-Q., Shao, L-Y., Wang, X-T., and Xu J., 2019, Application of channel-belt scaling relationship to Middle Jurassic source-to-sink system in the Saishiteng area of the northern Qaidam Basin, NW China. *Journal of Palaeogeography*, **8**, 16, <https://doi.org/10.1186/s42501-019-0031-9>.
- Lockley, M. G., 1991, *Tracking dinosaurs a new look at an ancient world*. Cambridge University Press, New York, 238p.
- Lockley, M. G. and Hunt, A. P., 1995, *Dinosaur tracks and other fossil footprints of the*

western United States. Columbia University Press, New York, 338p.

- Lorenz, J. C., Heinze, D. M., Clark, J. A. and Searls, C. A., 1985, Determination of widths of meander-belt sandstone reservoirs from vertical downhole data, Mesaverde Group, Piceance Creek Basin, Colorado. *The American Association of Petroleum Geologists Bulletin*, **69**, 710–721.
- Lucas, S. G. and Tanner, L. H., 2007, Tetrapod biostratigraphy and biochronology of the Triassic–Jurassic transition on the southern Colorado Plateau, USA. *Palaeogeography, Palaeoclimatology, Palaeoecology*, **244**, 247–256.
- Lucas, S. G. and Tanner, L. H., 2018, Record of the Carnian wet episode in strata of the Chinle Group, western USA. *Journal of Geological Society*, **175**, 1004–1011.
- Lunt, I. A., Bridge, J. S. and Tye, R. S., 2004, A quantitative, three dimensional depositional model of gravelly braided rivers. *Sedimentology*, **51**, 377–414.
- Mackey, S. D., 1993, *Theoretical modeling of alluvial architecture*. PhD thesis, State University of New York, Binghamton.
- Makaske, B., 2001, Anastomosing rivers: a review of their classification, origin and sedimentary products. *Earth-Science Reviews*, **53**, 149–196.
- Makino, Y., Masuda, F. and Katsura, Y., 1981, Paleochannel morphology and paleoflow characteristics: Quaternary fluvial sediments in Ibaraki Prefecture. *Bulletin of the Faculty of Education, Ibaraki University, Natural science*, no. 30, 71–86.
- Martinsen, O. J., Ryseth, A., Helland-Hansen, W., Flesche, H., Torkildsen and G. Idil, S., 1999, Stratigraphic base level and fluvial architecture: Ericson Sandstone (Campanian), Rock Springs Uplift, SW Wyoming, USA. *Sedimentology*, **46**, 235–259.
- Martodjojo, S., 1984, *Evolusi Cekungan Bogor*. Bandung Institute of Technology (ITB),

396p.

- Martz, J. W., Kirkland, J. I., Milner, A. R. C., Parker W. G., Santucci, V. L., 2017, Upper Triassic lithostratigraphy, depositional systems, and vertebrate paleontology across southern Utah. *Geology of the Intermountain West*, **4**, 99–180.
- Matsukawa, M. and Shibata, K. 2015, Review of Japanese Cenozoic (Miocene–modern) vertebrate tracks. *Ichnos*, **22**: 261–290.
- Matsukawa, M., Shibata, K., Kukihara, R., Koarai, K. and Lockley, M. G., 2005, Review of Japanese dinosaur track localities: implications for ichnotaxonomy, paleogeography and stratigraphic correlation. *Ichnos*, **12**: 201–222.
- McCandless, T. L. and Everett, R. A., 2002, *Maryland stream survey: bankfull discharge and channel characteristics of streams in the piedmont hydrologic region*. U.S. Fish & Wildlife Service, 40p.
- McLaurin, B. T. and Steel, R. J., 2006, Architecture and origin of an amalgamated fluvial sheet sand, lower Castlegate Formation, Book Cliffs, Utah. *Sedimentary Geology*, **197**, 291–311.
- Miall, A. D., 1985, Architectural-element analysis: a new method of facies analysis applied to fluvial deposits. *Earth Science Reviews*, **22**, 261–308.
- Miall, A. D., 1988, Reservoir heterogeneities in fluvial sandstones: Lessons from outcrop studies. *The American Association of Petroleum Geologists Bulletin*, **72**, 682–697.
- Miall, A. D., 1996, *The geology of fluvial deposits: sedimentary facies, basin analysis, and petroleum geology*. Springer-Verlag, Heidelberg, 582p.
- Miall, A. D., 2014, *Fluvial depositional systems*. Springer-Verlag, Berlin, 316p.
- Milliken, K. T., Blum, M. D., Snedden, J. W. and Galloway, W. E., 2018, Application of

- fluvial scaling relationships to reconstruct drainage-basin evolution and sediment routing for the Cretaceous and Paleocene of the Gulf of Mexico. *Geosphere*, **14**, 749–767.
- Milliman, J. D. and Syvitski, P. M., 1992, Geomorphic/tectonic control of sediment discharge to the ocean: the importance of small mountainous rivers. *Journal of Geology*, **100**, 525–544.
- Modrick, T. M. and Georgakakos, K. P., 2014, Regional bankfull geometry relationships for southern California mountain streams and hydrologic applications. *Geomorphology*, **221**, 242–260.
- Montgomery, D. R. and Gran, K. B., 2001, Downstream variation in the width of bedrock channels. *Water Resources Research*, **37**, 1841–1846.
- Moody, T., Wirtanen, M. and Yard, S. N., 2003, *Regional relationships for bankfull stage in natural channels of the arid southwest*. Natural Channel Design Inc., Flagstaff, 38p.
- Morgenroth, P., Rahardjo, A. T. and Maryunani, K. A., 2011, Dinoflagellate cysts from two Oligocene surface sections on Java Island, Indonesia. *Palaeontographica Abteilung B*, **284**, 125–157.
- Morley, R. J., 2012, A review of the Cenozoic palaeoclimate history of Southeast Asia. In Gower, D. J., Johnson, K., Richardson, J., Rosen, B., Rüber, L., eds., *Biotic Evolution and Environmental Change in Southeast Asia*, 79–114. Cambridge University Press.
- Morley, R. J. and Morley, H. P., 2013, Mid Cenozoic freshwater wetlands of the Sunda Region. *Journal of Limnology*, **72**, 18–35.
- Moro, Y., Kazama, S. and Fukuoka, S., 2011, Change of river improvement works of the

- lower Tone River and effectiveness of channel dredging. *Advances in river engineering, Japan Society of Civil Engineers*, **17**, 101–106. (in Japanese with English abstract)
- Nadon, G. C., 1994, The genesis and recognition of anastomosed fluvial deposits: data from the St. Mary River Formation, southwestern Alberta, Canada. *Journal of Sedimentary Research*, **B64**, 451–463.
- Nakamura, K., Kimura, R. and Uchijima, Z., 1986, *Nature in Japan Part 5: The Climate of Japan*. Iwanami Shoten, Tokyo, 237p. (in Japanese)
- Nakayama, M., 1997, Changes in topographical environment and social history in the middle reaches of the Tone River in medieval and early modern times–The relationship between a massive volcanic eruption and the course change of the Tone River–. *The Historical Geography*, **39**, 1–24. (in Japanese with English abstract)
- National Astronomical Observatory of Japan, 2016, *Rika Nenpyo (Chronological Scientific Tables 2017)*. Maruzen Publishing, Tokyo, 1104p. (in Japanese)
- Nemoto, N. and O'Hara, S. 2001, Molluscan assemblages and sedimentary environments of the Shiramizu Group in the northern area of the Joban district. *Bulletin of Taira Geological Club*, no. 23, 21–51 (in Japanese with English abstract).
- Nemoto, N., 1989, 5.1 Joban area. In Oide, K., Nakagawa, H. and Kanisawa, S., eds., *Regional Geology of Japan Part 2 TOHOKU*, 94–99. Kyoritsu Shuppan, Tokyo (in Japanese)
- Net, L. I., Alonso, M. S. and Limarino, C. O., 2002, Source rock and environmental control on clay mineral associations, Lower Section of Paganzo Group

- (Carboniferous), Northwest Argentina. *Sedimentary Geology*, **152**, 183–199.
- Nishi, H. and Takashima, R., 2005, Paleoenvironment and climate changes caused by the Himalayan Tectonics in the East Asia. *Journal of the Japanese Association for Petroleum Technology*, **70**, 6–14 (in Japanese with English abstract).
- Nordt, L., Atchley, S. and Dworkin, S., 2015, Collapse of the Late Triassic megamonsoon in western equatorial Pangea, present-day American Southwest. *Geological Society of America Bulletin*, **127**, 1798–1815.
- Ohkawara, H., Ikeda, H. and Iseya, F., 1992, Evolution of fluvial environment in the lowland of the middle part of the River Tone. *Environmental Research Center Papers, the University of Tsukuba*, no. 16, 79–91.
- Ohmori, H., 1983a, Erosion rates and their relation to vegetation from the viewpoint of world-wide distribution. *Bulletin of the Department of Geography, University of Tokyo*, no. 15, 77–91.
- Ohmori, H., 1983b, Characteristics of the erosion rate in the Japanese mountains from the viewpoint of climatic geomorphology. *Zeitschrift für Geomorphologie*, Supplementband, **46**, 1–14.
- Okami, K., 1973, Sedimentological study of the Iwaki Formation of the Joban Coal Field. *Science Report of the Tohoku University, 2nd series (Geology)*, no. 44, 1–53, pls., 1–12.
- Okami, K., Endo, S. and Murata, M., 1978, Discovery of Triassic conodonts from the chert pebbles of the Tertiary conglomerates of Joban coal-field (The conglomerate of the eastern terrain of the Abukuma plateau, part 2). *Journal of the Geological Society of Japan*, **84**, 87-90 (in Japanese).
- Orton, G. J. and Reading J. G., 1993, Variability of deltaic processes in terms of

- sediment supply, with particular emphasis on grain size. *Sedimentology*, **40**, 475–512.
- Osterkamp, W. R. and Hedman, E. R., 1982, *Perennial-streamflow characteristics related to channel geometry and sediment in Missouri River Basin*. U. S. Geological Survey Professional Paper, no. 1242, 37p.
- Oya, M., 1993, *Fluvial Geomorphology*. Kokonshoin, Tokyo, 253p. (in Japanese).
- Paola, C., 2000, Quantitative models of sedimentary basin filling. *Sedimentology*, **47** (Suppl. 1), 121–178.
- Paola, C. and Mohrig, D., 1996, Palaeohydraulics revised: paleoslope estimation in coarse-grained braided rivers. *Basin Research*, **8**, 243–254.
- Paredes, J. M., Foix, N., Allard J. O., Valle, M. N. and Giordano, S. R. 2018, Complex alluvial architecture, paleohydraulics and controls of a multichannel fluvial system: Bajo Barreal Formation (Upper Cretaceous) in the Cerro Ballena anticline, Golfo San Jorge Basin, Patagonia. *Journal of South American Earth Sciences*, **85**, 168–190.
- Paredes, J. M., Foix, N., Piñol, F. C., Nillni, A., Allard J. O. and Marquillas, R. A. 2007, Volcanic and climatic controls on fluvial style in a high-energy system: The Lower Cretaceous Matasiete Formation, Golfo San Jorge Basin, Argentina. *Sedimentary Geology*, **202**, 96–123.
- Parker, G., 1976, On the cause and the characteristic scales of meandering and braiding in rivers. *Journal of Fluid Mechanics*, **76**, 457–480.
- Parker, J. T. C., Steinkampf, W. C., Flynn, M. E., 2005, *Hydrogeology of the Mogollon Highlands, central Arizona*. U.S. Geological Survey Scientific Investigations Report 2004–5294, 87p.

- Parrish, J. T., 1993, Climate of the supercontinent Pangea. *The Journal of Geology*, **101**, 215–233.
- Phillips S. P., Howell, J. A., Hartley, A. J., Chmielewska, M. and Hudson, S. M., 2021, Evolution of foreland basin fluvial systems in the mid-Cretaceous of Utah, USA (upper Cedar Mountain and Naturita formations). *Sedimentology*, doi: 10.1111/sed.12845.
- Posamentier, H. W. and Allen, G. P. 1993, Siliciclastic sequence stratigraphic patterns in foreland ramp-type basins. *Geology*, **21**, 455–458.
- Posamentier, H. W., Jervey, M. T. and Vail, P. R., 1988, Eustatic controls on clastic deposition I—conceptual framework. In Wilgus C. K., Hastings, B. S., Kendall, C. G. St. C., Posamentier, H. W., Ross, C. A. and Van Wagoner, J. C., eds., *Sea-level research: an integrated approach*. SEPM Special Publication, no. 42, 109–124.
- Prochnow, S. J., Nordt, L. C., Atchley, S. C. and Hudec, M. R., 2006, Multi-proxy paleosol evidence for Middle and Late Triassic Climate Trends in eastern Utah. *Palaeogeography, Palaeoclimatology, Palaeoecology*, **232**, 53–72.
- Ramezani, J., Hoke, G. D., Fastovsky, D. E., Bowring, S. A., Therrien, F., Dworkin, S. I., Atchley, S. C. and Nordt, L. C., 2011, High-precision U-Pb zircon geochronology of the Late Triassic Chinle Formation, Petrified Forest National Park (Arizona, USA): Temporal constraints on the early evolution of dinosaurs. *Geological Society of America Bulletin*, **123**, 2142–2159.
- Rasmussen, C., Mundil, R., Irmis, R. B., Geisler, D., Gehrels, G. E., Olsen, P. E., Kent, D. V., Lepre, C., Kinney, S. T., Geissman, J. W. and Parker, W. G., 2020, U-Pb zircon geochronology and depositional age models for the Upper Triassic Chinle

- Formation (Petrified Forest National Park, Arizona, USA): Implications for Late Triassic paleoecological and paleoenvironmental change. *Geological Society of America Bulletin*, doi: <https://doi.org/10.1130/B35485.1>.
- Ray, P. K., 1976, Structure and sedimentological history of the overbank deposits of a Mississippi River point bar. *Journal of Sedimentary Petrology*, **46**, 788–801.
- Rice, S., 1999, The nature and controls on downstream fining within sedimentary links. *Journal of Sedimentary Research*, **69**, 32–39.
- Riggs, N. R., Ash, S. R., Barth, A. P., Gehrels, G. E. and Wooden, J. L., 2003, Isotopic age of the Black Forest bed, Petrified Forest Member, Chinle Formation, Arizona: An example of dating a continental sandstone. *Geological Society of America Bulletin*, **115**, 1315–1323.
- Riggs, N. R., Oberling, Z. A., Howell, E. R., Parker, W. G., Barth, A. P., Cecil, M. R. and Martz, J. W., 2016, Sources of volcanic detritus in the basal Chinle Formation, southwestern Laurentia, and implications for the Early Mesozoic magmatic arc. *Geosphere*, **12**, 439–463.
- Riggs, N. R., Reynolds, S. J., Lindner, P. J., Howell, E. R., Barth, A. P., Parker, W. G. and Walker, J. D., 2013, The Early Mesozoic Cordilleran arc and Late Triassic paleotopography: The detrital record in Upper Triassic sedimentary successions on and off the Colorado Plateau. *Geosphere*, **9**, 602–613.
- River Bureau, Ministry of Land, Infrastructure and Transport, 2009, *River Discharges Year Book of Japan (Year 2004, Vol. 57)*. Japan River Association, Tokyo, 464p. (in Japanese and English)
- Saito, K., 1988, *Alluvial Fans in Japan*. Kokon Shoin, Tokyo. 280p. (in Japanese)
- Saito, K., 1999, Development of mountains and alluvial fans in Japan, Taiwan, and the

- Philippines. *Geographical Review of Japan*, **72B**, 162–172.
- Sakaguchi, Y., Takahashi, Y. and Ohmori, H., 1986, *Nature in Japan Part 3: Rivers of Japan*. Iwanamishoten, Tokyo, 248p. (in Japanese).
- Sato, S., 1989, Palyno-stratigraphic study of the Tertiary in the Joban coal field, Northeast Japan. *Journal of the Geological Society of Japan*, **95**, 171–187 (in Japanese with English Abstract).
- Sawaguchi, H., 2000, *Relocating the Tone River towards east*. Jomo Shinbun, Maebashi, 213p. (in Japanese)
- Scherer, C. M. S., Goldberg, K. and Barodola, T., 2015, Facies architecture and sequence stratigraphy of an early post-rift fluvial succession, Aptian Barbalha Formation, Araripe Basin, northeastern Brazil. *Sedimentology*, **322**, 43–62.
- Schultz, L. G., 1963, *Clay minerals in Triassic rocks of the Colorado Plateau*. U.S. Geological Survey Bulletin 1147-C. United States Government Printing Office, 71p.
- Schumm, S. A., 1977, *The Fluvial System*. John Wiley and Sons, New York, 338p.
- Schumm, S. A., 1985, Patterns of alluvial rivers. *Annual Review of Earth and Planetary Sciences*, **13**, 5–27.
- Schumm, S. A., 1993, River response to baselevel change: implications for sequence stratigraphy. *Journal of Geology*, **101**, 279–294.
- Schumm, S. A., 2005, *River variability and complexity*. Cambridge University Press, 220p.
- Shanley, K.W. and McCabe, P. J., 1994, Perspectives on the sequence stratigraphy of continental strata. *The American Association of Petroleum Geologists Bulletin*, **78**, 544–568.

- Singer, A., 1984, The paleoclimatic interpretation of clay minerals in sediments—a review. *Earth-Science Reviews*, **21**, 251–293.
- Smith, D. G., 1986, Anastomosing river deposits, sedimentation rates and basin subsidence, Magdalena River, northwestern Colombia, South America. *Sedimentary Geology*, **46**, 177–196.
- Soeria-Atmadja, R. and Noeradi, D., 2005, Distribution of early tertiary volcanic rocks in south Sumatra and west Java. *The Island Arc*, **14**, 679–686.
- Steel, R. J., 1988, Coarsening-upward and skewed fan bodies: symptoms of strike-slip and transfer movement in sedimentary basins. In Nemec W. and Steel R. J., eds., *Fan Deltas: Sedimentology and Tectonic Settings*, 75–83. Blackie and Son, Glasgow.
- Stewart, J. H., Poole, F. G. and Wilson, R. F., 1972, *Stratigraphy and origin of the Chinle Formation and related Upper Triassic strata in the Colorado Plateau region*. U.S. Geological Survey Professional Paper, no. 690, 336p.
- Stow, D. A. V., 2005, *Sedimentary rocks in the field: A colour guide*. Manson Publishing, London, 320p.
- Straffin, E. C., Blum, M. D., Colls, A. and Stokes, S., 2000, Alluvial stratigraphy of the Loire and Arroux Rivers, Burgundy, France. *Quaternaire*, **10**, 271–282.
- Strong, N., Sheets, B., Hickson, T., and Paola, C. 2005, A mass-balance framework for quantifying downstream changes in fluvial architecture. In Blum M. D., Marriott S. B. and Leclair S. F. eds., *Fluvial sedimentology VII*, International Association of Sedimentologists, Special Publication, no. 35, 243–253.
- Suetsugu, T., 2005, *Science of rivers*. Natsumesha, Tokyo, 239p. (in Japanese)
- Sugai, K., Matsui, H., Sato, S., Kitagawa, Y., Sasaki, M., Miyashita, M. and Kawachi,

- H., 1957, *Geological maps of the coal fields of Japan I: explanatory text of the Joban Coal Field*. Geological Survey of Japan, 154p. (in Japanese with English abstract).
- Summerfield, M. A., 1985, Plate tectonics and landscape development on the African continent. In Morisawa, M. and Hack, J., eds., *Tectonic Geomorphology*, 27–51. Allen and Unwin, Boston.
- Suresh, N., Ghosh, S. K., Kumar, R. and Sangode, S. J., 2004, Clay-mineral distribution pattern in late Neogene fluvial sediments of the Subathu sub-basin, central sector of Himalayan foreland basin: implications for provenance and climate. *Sedimentary Geology*, **163**, 265–278.
- Suto, I., Yanagisawa, Y. and Ogasawara, K., 2005, Tertiary geology and chronostratigraphy of the Joban area and its environs, northeastern Japan. *Bulletin of the Geological Survey of Japan*, **56**, 375–409 (in Japanese with English abstract).
- Suttner, L. J. and Dutta, P. K., 1986, Alluvial sandstone composition and paleoclimate, I. Framework mineralogy. *Journal of Sedimentary Petrology*, **56**, 329–345.
- Syvitski, J. P. M. and Milliman, J. D., 2007, Geology, geography, and humans battle for dominance over the delivery of fluvial sediment to the coastal Ocean. *The Journal of Geology*, **115**, 1–19.
- Taira, A., Ohara, Y., Wallis, S. R., Ishiwatari, A. and Iryu, Y. 2016, Geological evolution of Japan: an overview. In Moreno, T., Wallis, S., Kojima, T. and Gibbons, W. eds., *The Geology of Japan*, 1–24. Geological Society, London.
- Takahashi, M. and Ando, H., 2016, Reconstruction of the Cretaceous continental arc of Japan on a viewpoint of arc-trench system. *Fossils (Kaseki)*, no. 100, 45–59.

- Takahashi, Y., 1971, *Metamorphosis of a Country and Flood Damage*. Iwanamishoten, Tokyo, 216p. (in Japanese)
- Takahashi, Y., 1990, *River Engineering*. University of Tokyo Press, Tokyo, 311p. (in Japanese)
- Takahashi, Y. (editor in chief), 2013, *Encyclopedia of rivers all over the world*. Maruzen Publishing, Tokyo, 1040p. (Witten in Japanese).
- Takahashi, Y. and Sakaguchi, Y., 1976, Characteristics of Japanese rivers. *Kagaku*, **46**, 488–499. (in Japanese)
- Tal, M. and Paola, C., 2010, Effects of vegetation on channel morphodynamics: results and insights from laboratory experiments. *Earth Surface Processes and Landforms*, **35**, 1014–1028.
- Tanner, L. H., 2000, Palustrine-lacustrine alluvial facies of the (Norian) Owl Rock Formation (Chinle Group), four corners region, southwestern U.S.A.: implications for Late Triassic paleoclimate. *Journal of Sedimentary Research*, **70**, 1280–1289.
- Thiry, M., 2000, Palaeoclimatic interpretation of clay minerals in marine deposits: an outlook from the continental origin. *Earth-Science Reviews*, **49**, 201–221.
- Thomas, R. G., Smith, D. G., Wood, J. M., Visser, J., Calverley-Range, E. A. and Koster, E. H., 1987, Inclined heterolithic stratification--Terminology, description, interpretation and significance. *Sedimentary Geology*, **53**, 123–179.
- Tomida, Y., 1986, Recognition of the Genus *Entelodon* (Artiodactyla, Mammalia) from the Joban Coalfield, Japan, and the age of the Iwaki Formation. *Bulletin of the National Science Museum, Tokyo, Series C*, **12**, 165–170.
- Trendell, A. M., Atchley, S. C. and Nordt, L. C., 2012, Depositional and diagenetic

- controls on reservoir attributes within a fluvial outcrop analog: Upper Triassic Sonsela member of the Chinle Formation, Petrified Forest National Park, Arizona. *The American Association of Petroleum Geologists Bulletin*, **96**, 679–707.
- Trendell, A. M., Atchley, S. C. and Nordt, L. C., 2013, Facies analysis of a probable large-fluvial-fan depositional system: the Upper Triassic Chinle Formation at Petrified Forest National Park, Arizona, U.S.A. *Journal of Sedimentary Research*, **83**, 873–895.
- Ueda, Y., Ando, H. and Shinozaki, M., 2003, Depositional facies and their paleogeographic implications of the Oligocene Iwaki to Asagai formations, Shiramizu Group in Northern Ibaraki Prefecture. *Bulletin of the Ibaraki Nature Museum*, no. 6, 1–17 (in Japanese with English abstract).
- van Hattum, M. W. A., Hall, R., Pickard, A. L. and Nichols, G. J., 2006, SE Asian sediments not from Asia: Provenance and geochronology of North Borneo sandstones. *Geology*, **34**, 589–592.
- van den Berg, J. H., 1995, Prediction of alluvial channel pattern of perennial rivers. *Geomorphology*, **12**, 259–279.
- Van Wagoner, J. C., Posamentier, H. W., Mitchum, R. M., Vail, P. R., Sarg, J. F., Loutit, T. S. and Hardenbol, J., 1988, An overview of the fundamentals of sequence stratigraphy and key definitions. In Wilgus C. K., Hastings, B. S., Kendall, C. G. St. C., Posamentier, H. W., Ross, C. A. and Van Wagoner, J. C., eds., *Sea-level research: an integrated approach*. SEPM Special Publication, no. 42, 39–45.
- Varban, B. L. and Plint, A. G., 2008, Sequence stacking patterns in the Western Canada foredeep: influence of tectonics, sediment loading and eustasy on deposition of

- the Upper Cretaceous Kaskapau and Cardium formations. *Sedimentology*, **55**, 395–421.
- Wan, S., Li, A., Clift, P. D. and Stuut, J.-B.W., 2007, Development of the East Asian monsoon: mineralogical and sedimentologic records in the northern South China Sea since 20 Ma. *Palaeogeography, Palaeoclimatology, Palaeoecology*, **254**, 561–582.
- Werritty, A., 1992, Downstream fining in a gravel-bed river in southern Poland: lithologic controls and the role of abrasion. In Billi, P., Hey, R. D., Thorne, C. R. and Tacconi, P., eds., *Dynamics of Gravel-bed Rivers*, 333–346. Wiley, Chichester.
- Wescott, W. A., 1993, Geomorphic thresholds and complex response of fluvial systems –some implications of sequence stratigraphy. *The American Association of Petroleum Geologists Bulletin*, **77**, 1208–1218.
- Wilcock, P. R., 1992, Experimental investigation of the effect of mixture properties on transport dynamics. In Billi, P., Hey, R. D., Thorne, C. R. and Tacconi, P., eds., *Dynamics of Gravel-bed Rivers*, 109–139. Wiley, Chichester.
- Williams, G. P., 1984a, Paleohydrological methods and some examples from Swedish fluvial environments II–River meanders. *Geografiska Annaler*, **66A**, 89–102.
- Williams, G. P., 1984b, Paleohydrologic equations for rivers. In Costa, J. E. and Fleisher, P. J., Eds., *Developments and Applications of Geomorphology*, 343–367. Springer-Verlag, Berlin.
- Williams, G. P., 1986, River meanders and channel size. *Journal of Hydrology*, **88**, 147–164.
- Williams, P. R., Johnston, C. R., Almond, R. A. and Simamora, W. H., 1988, Late

Cretaceous to Early Tertiary structural elements of West Kalimantan.

Tectonophysics, **148**, 279–298.

Wilson, D. D., 1985, Erosional and depositional trends in rivers of the Canterbury Plains, New Zealand. *Journal of Hydrology (N. Z.)*, **24**, 32–44.

Winkler, W., 1984, Paleocurrents and petrography of the Gurnigel-Schliren Flysh: A basin analysis. *Sedimentary Geology*, **40**, 169–189.

Wright, V. P. and Marriott, S. B., 1993, The sequence stratigraphy of fluvial depositional systems: the role of floodplain sediment storage. *Sedimentary Geology*, **86**, 203–210.

Xia, J., Wu, B., Wang, G. and Wang, Y., 2010, Estimation of bankfull discharge in the Lower Yellow River using different approaches. *Geomorphology*, **117**, 66–77.

Xu, J., 2004, Comparison of hydraulic geometry between sand- and gravel-bed rivers in relation to channel pattern discrimination. *Earth Surface Processes and Landforms*, **29**, 645–657.

Xu, J., Snedden, J. W., Galloway, W. E., Milliken, K. T. and Blum, M. D., 2017, Channel-belt scaling relationship and application to early Miocene source-to-sink system in the Gulf of Mexico basin. *Geosphere*, **13**, 179–200.

Yamamoto, K., 2004, *Structural Alluvial Potamology: Its Structural Characteristic and Movement*. Sankaido, Tokyo, 690p. (in Japanese)

Yanai, S., Aoki, K. and Akahori, Y., 2010, Opening of Japan Sea and major tectonic lines of Japan: MTL, TTL and Fossa Magna. *Journal of Geography (Chigaku Zasshi)*, **119**, 1079–1124. (in Japanese with English abstract)

Yatsu, E., 1951, Preliminary study on the fluvial deposits of main rivers in Kanto-plain: Report on the fluvial deposits No. 3. *Geographical Review of Japan*, **24**, 144–

147. (in Japanese)

Yatsu, E., 1957, On the discontinuity of grain size distribution of fluvial deposits and its geomorphological significance. *International Geographical Union Proceedings, Regional Conference in Japan*, 224–237.

Yoshikawa, T., Sugimura, A., Kaizuka, S., Ohta, Y. and Sakaguchi, Y., 1973, *Geomorphology of Japan*. University of Tokyo Press, Tokyo, 415pp. (in Japanese)

Figures and Tables

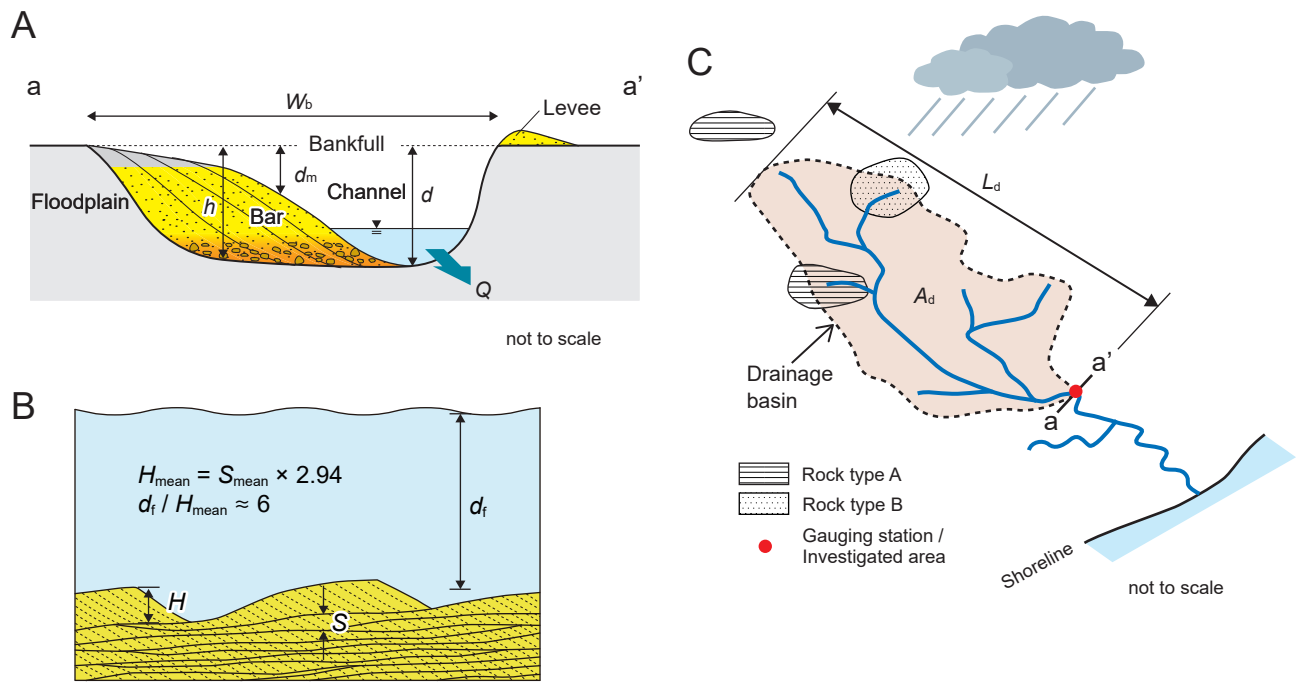


Fig. 1. A: Schematic cross section of a fluvial channel. h : Thickness of bar deposit, d : bankfull channel depth, d_m : mean bankfull channel depth (hydraulic radius), W_b : bankfull channel width, Q : discharge. Thickness of bar deposit approximately equals d . B: Estimation of mean dune height and flow depth from cross-set thicknesses. S_{mean} : Mean cross-set thickness, H_{mean} : mean bedform height, d_f : flow depth. After Leclair and Bridge (2001) and Bridge (2003). C: Schematic illustration of a drainage basin. A_d : drainage basin area, L_d : drainage basin length.

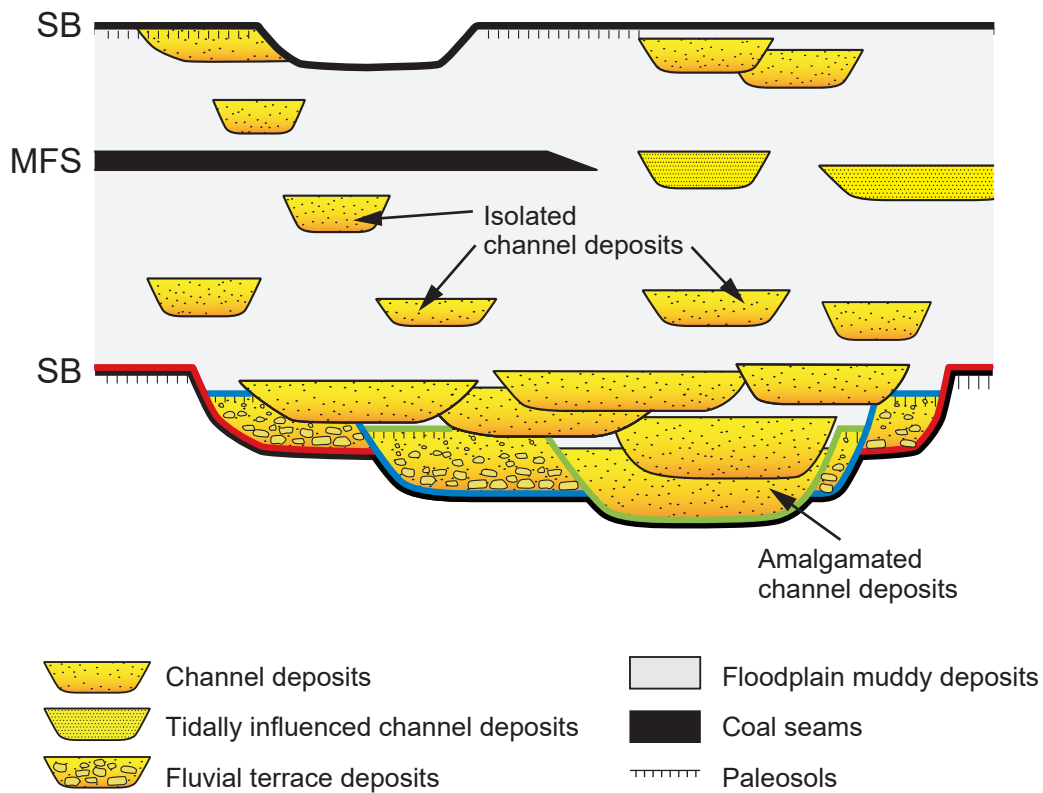


Fig. 2. Sequence stratigraphic model of fluvial deposits. SB: Sequence boundary, MFS: Maximum flooding surface. In response to a rise in relative sea level, large-scale, amalgamated channel deposits change into small-scale, isolated channel deposits that are encased in floodplain muddy deposits. Red, blue and green lines indicate basal erosional surfaces of fluvial and channel deposits and laterally traceable upper surfaces of terrace deposits that were formed different ages. These composite erosional surfaces comprise a sequence boundary (SB). Based on Wright and Marriott (1993), Shanley and McCabe (1994), Miall (1996), Holbrook and Bhattacharya (2012), and Blum et al. (2013).



Fig. 3. Map showing the five major regions used in the analysis of hydrological and geomorphological data from the Japanese fluvial systems. Location of the Paleogene Iwaki Formation is also shown. Structural boundaries are after Taira et al. (2016).

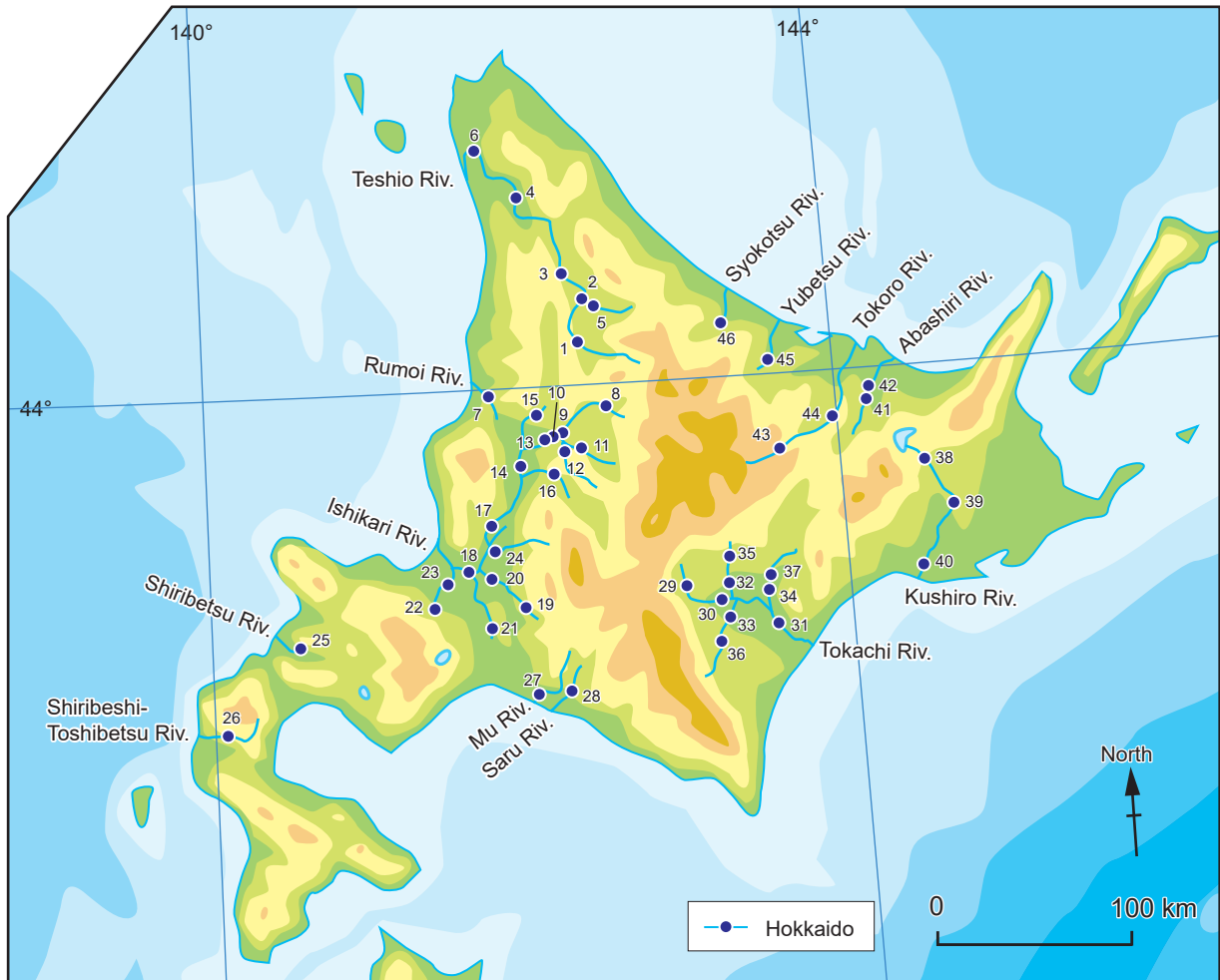


Fig. 4. Location of measurement sites in Hokkaido, Japan. Numbers indicate the sites listed in Table 1.

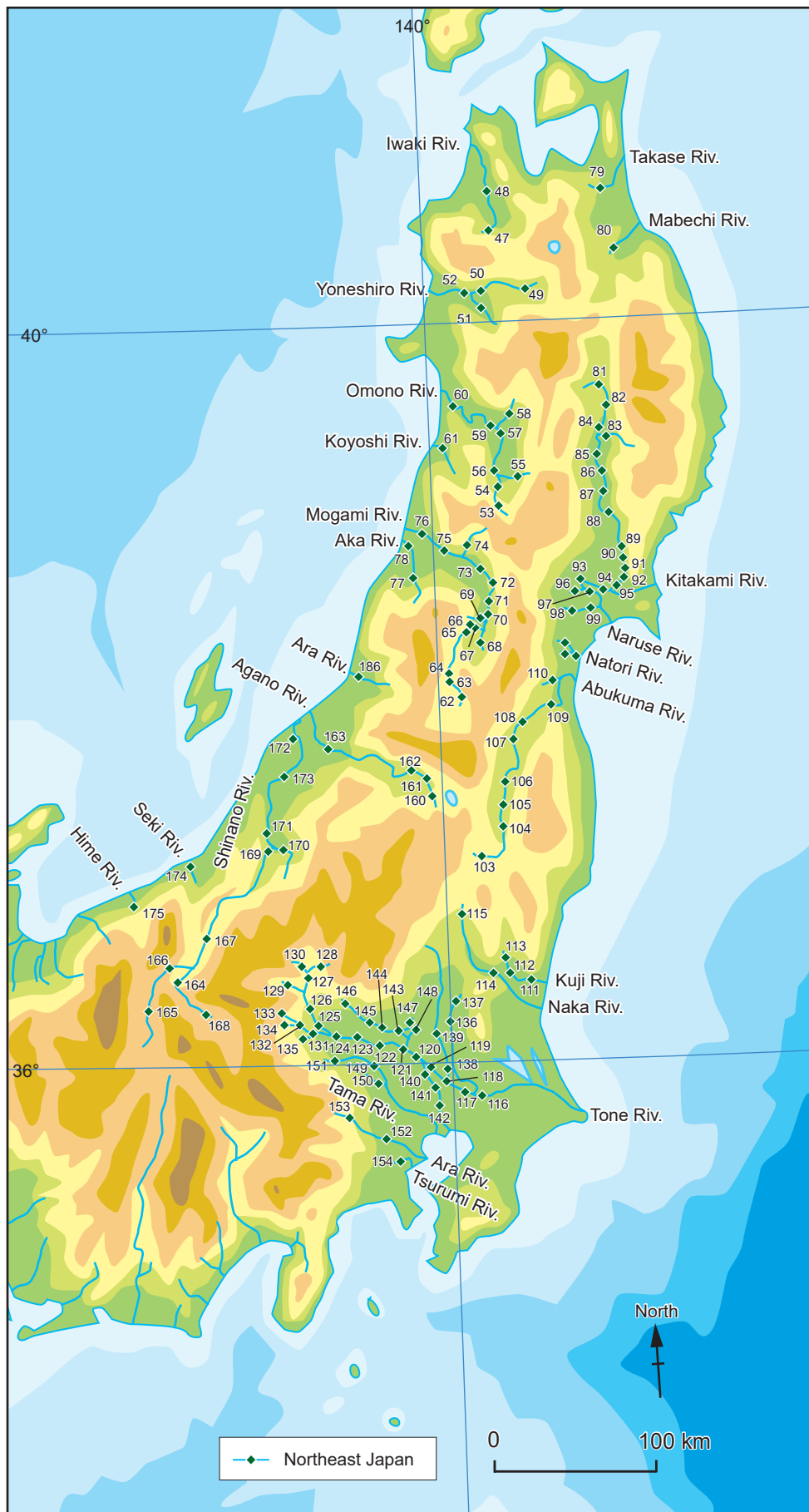


Fig. 5. Location of measurement sites in Northeast Japan. Numbers indicate the sites listed in Table 1.

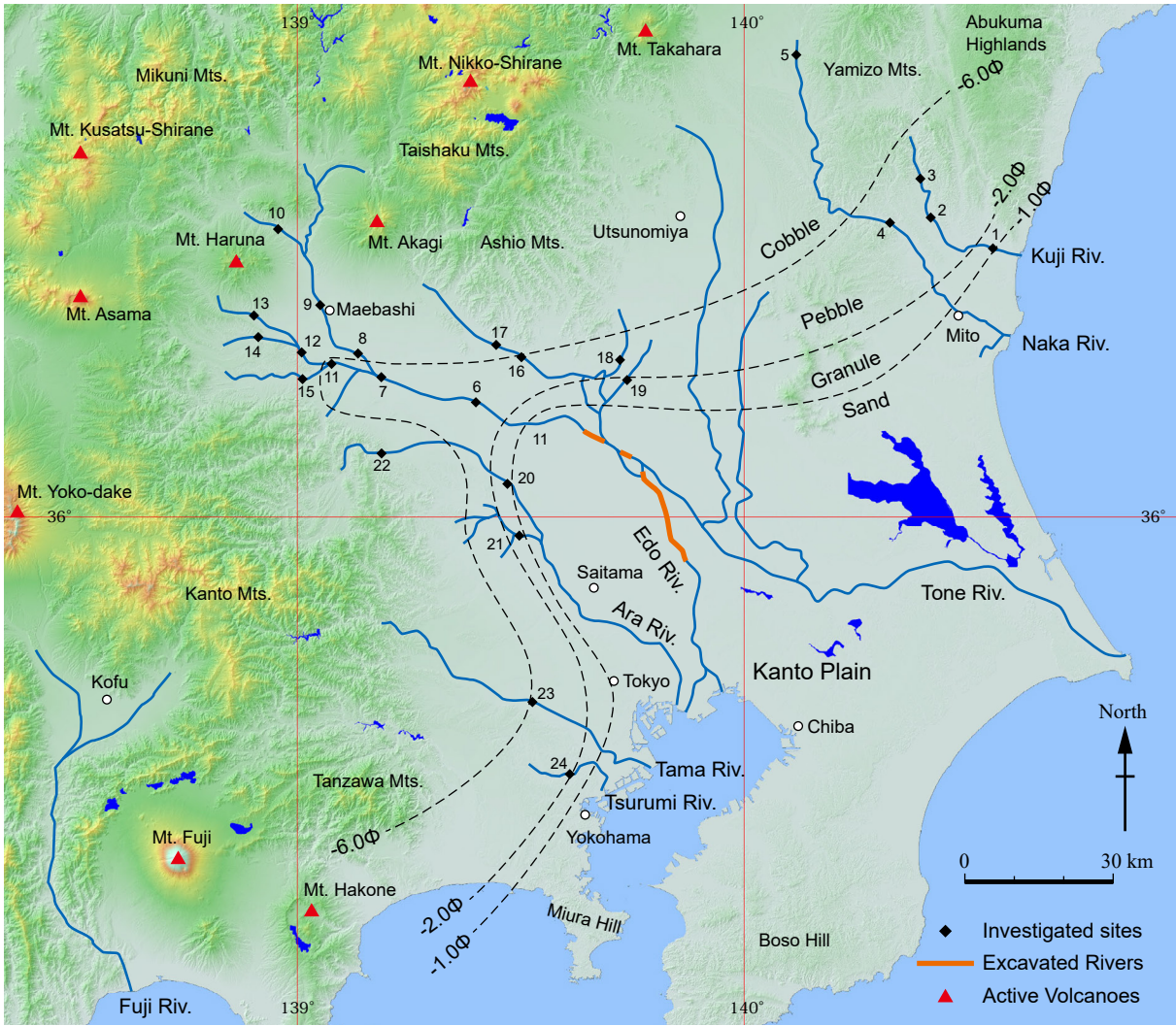


Fig. 7. Study sites in the Kanto region. Numbers indicate the sites listed in Table 3. Isopleths represent median diameters of river bed materials in phi scale. Data of median diameters of river bed materials are from Yatsu (1951). The locations of excavated river channels are on the basis of Sawaguchi (2000). The topographic map was made using basic map information by the Geospatial Information Authority of Japan, and 'KASHMIR 3d' software (<http://www.kashmir3d.com/>).



Fig. 8. Measurement of a bankfull channel width (W_b) from an aerial photograph (Google Map: <https://www.google.co.jp/maps>). The examined river is the Otofuke River near Shihoro, Hokkaido ($43^{\circ}11'11.5''N$, $143^{\circ}13'20.1''E$) (site 35 in Fig. 4 and Table 1).

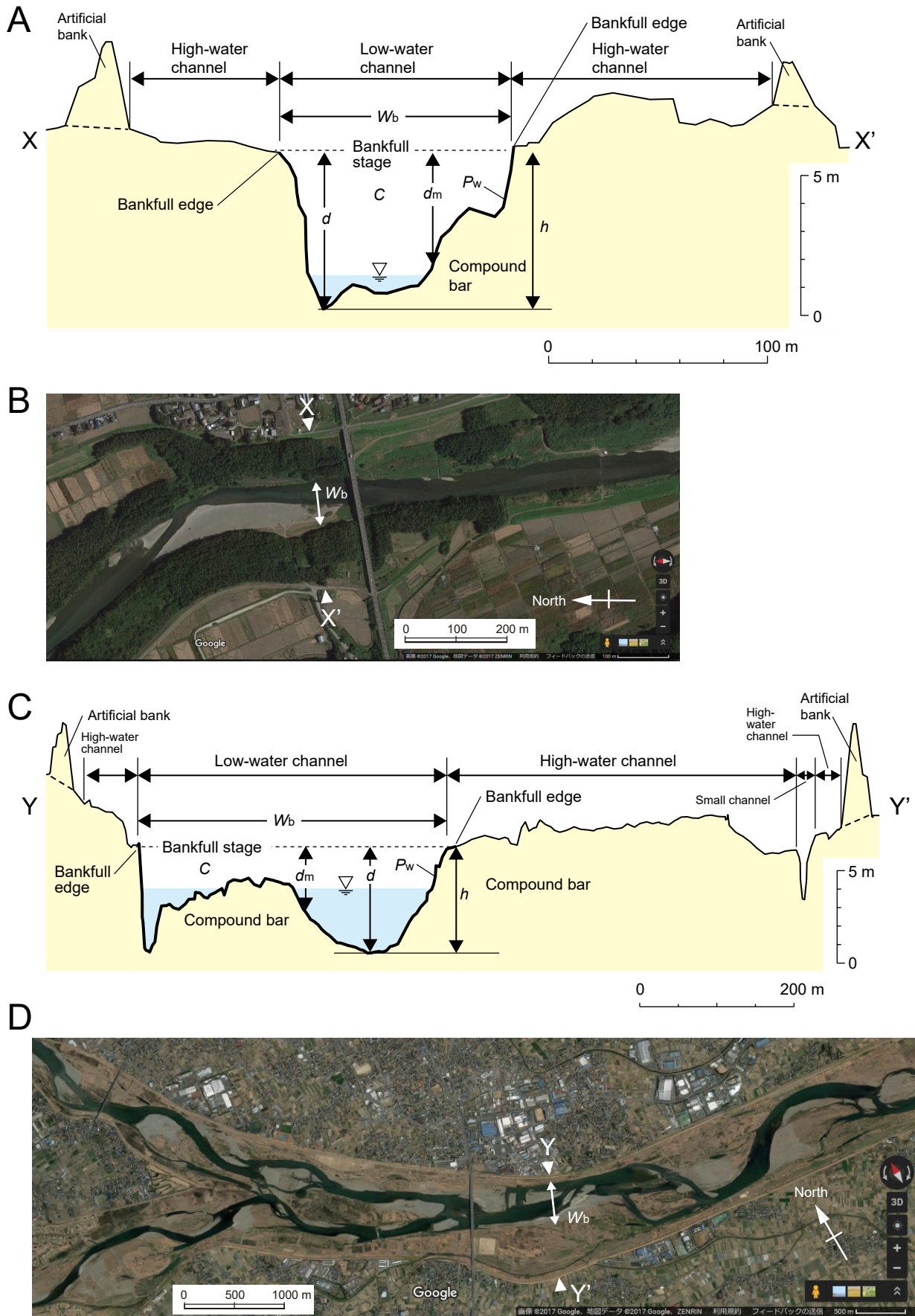


Fig. 9. Examples of cross-sectional geometry (A and C) with definitions of the cross-sectional parameters and their aerial photographs (B and D) of river channels. A and B: Tomioka, in the middle reach of the Kuji River (Site 2 in Fig. 7 and Table 3). C and D: Yattajima, in the upper reach of the Tone River (Site 7 in Fig. 7 and Table 5). Aerial photographs are from google map. See the list of symbols in Table 2. A and C were surveyed using an auto level and a total station, respectively. Data of cross-sectional geometry was provided by the Kanto Regional Development Bureau, Ministry of Land, Infrastructure, Transport and Tourism.

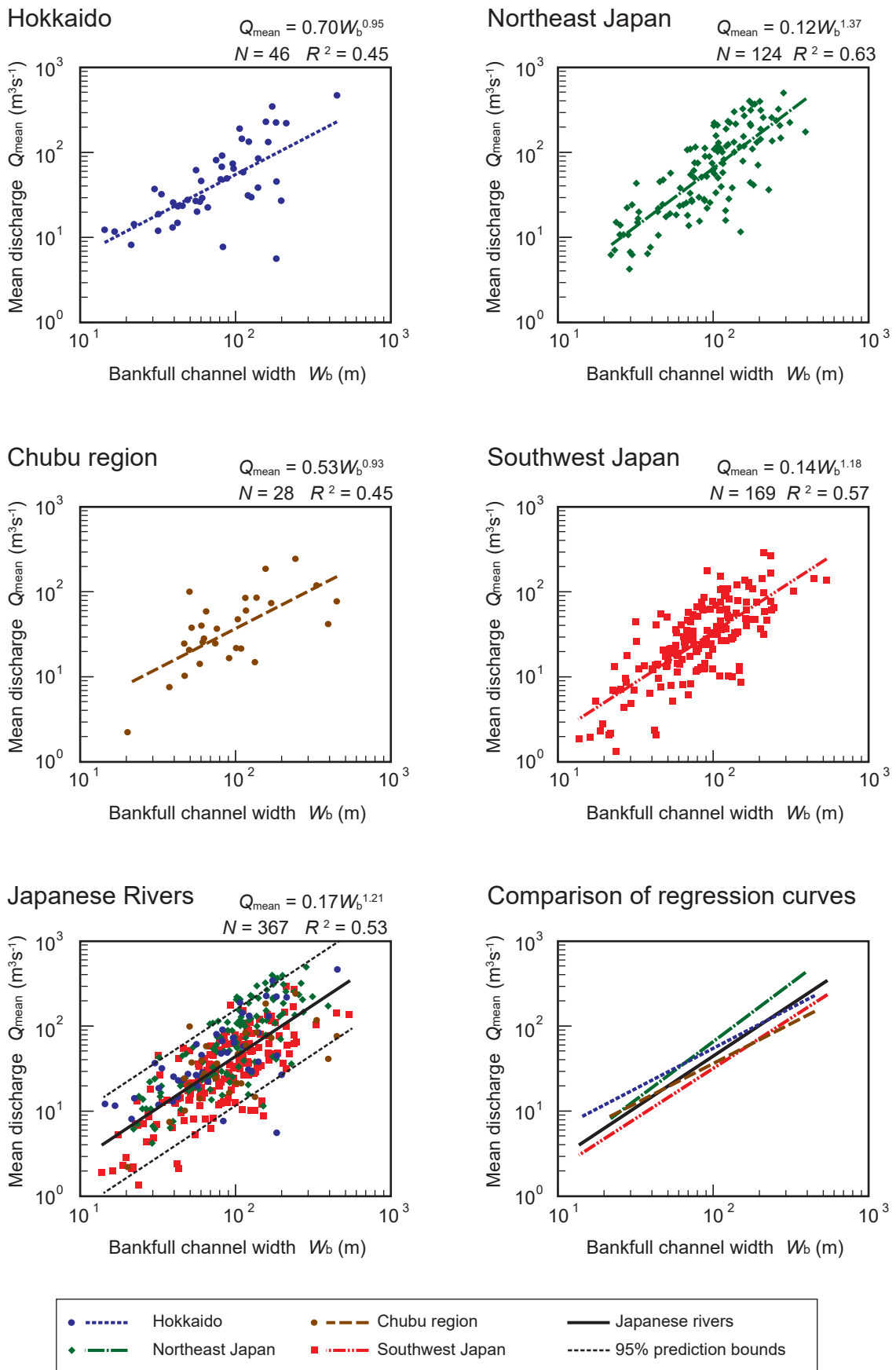


Fig. 10. Relationship between the bankfull channel width (W_b) and the mean discharge (Q_{mean}) for the four regions and the whole of Japan, and a comparison of their regression curves.

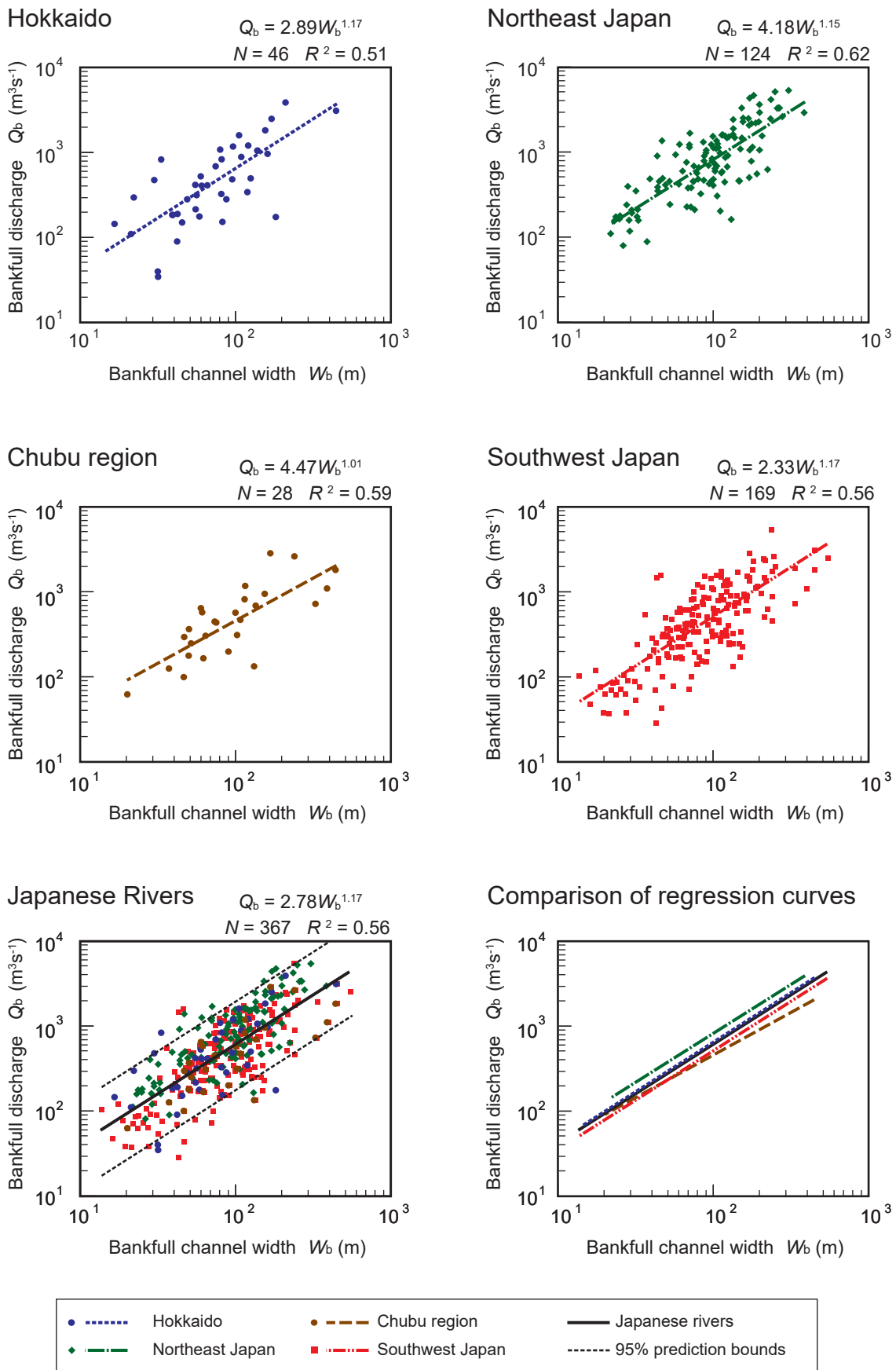


Fig. 11. Relationship between the bankfull channel width (W_b) and the bankfull discharge (Q_b) for the four regions and the whole of Japan, and a comparison of their regression curves.

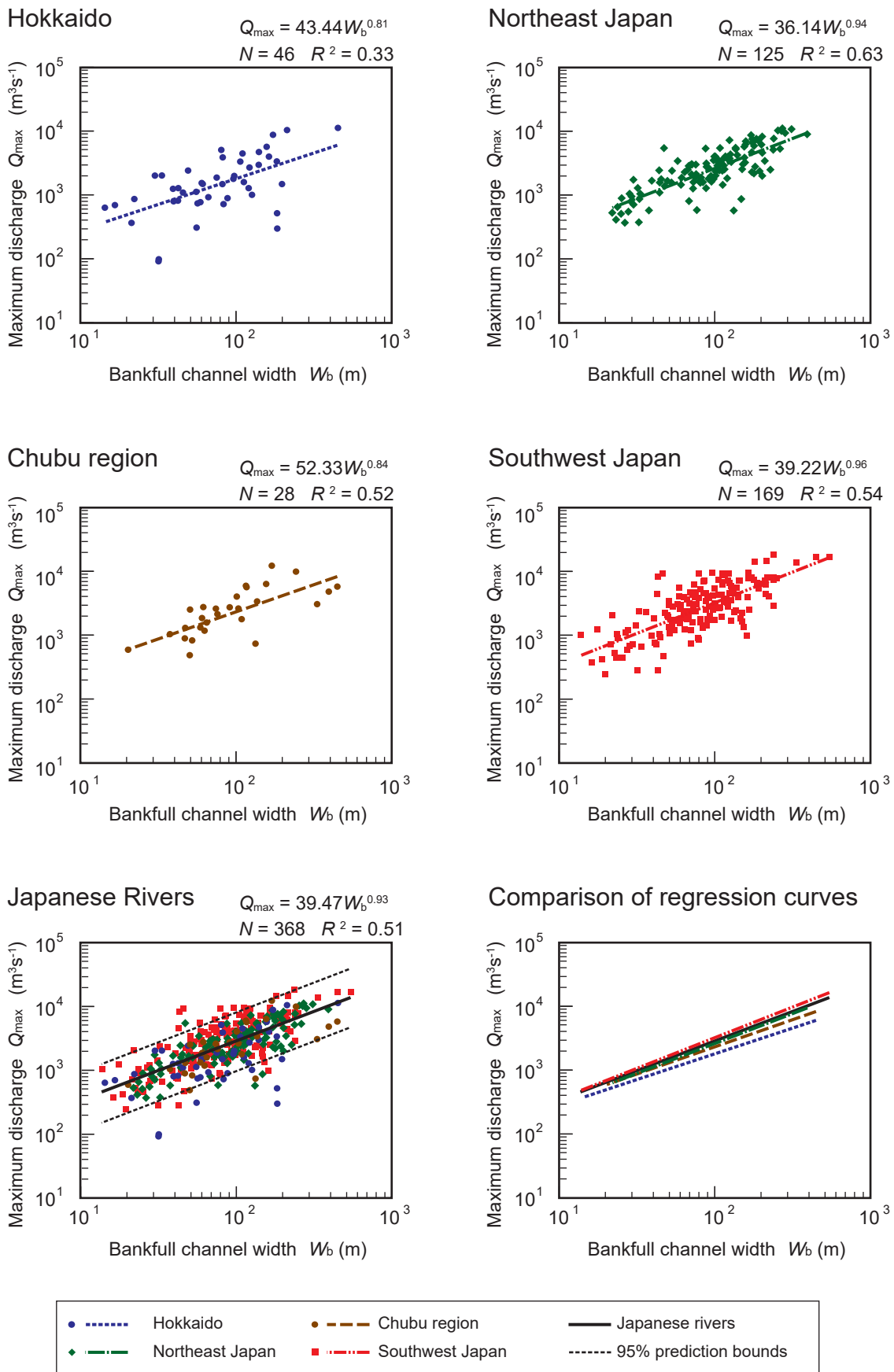


Fig. 12. Relationship between the bankfull channel width (W_b) and the maximum discharge (Q_{\max}) for the four regions and the whole of Japan, and a comparison of their regression curves.

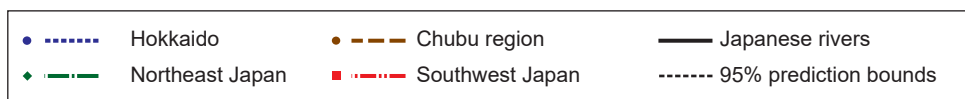
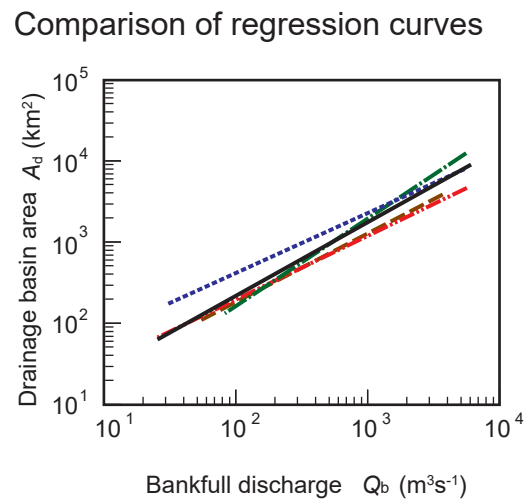
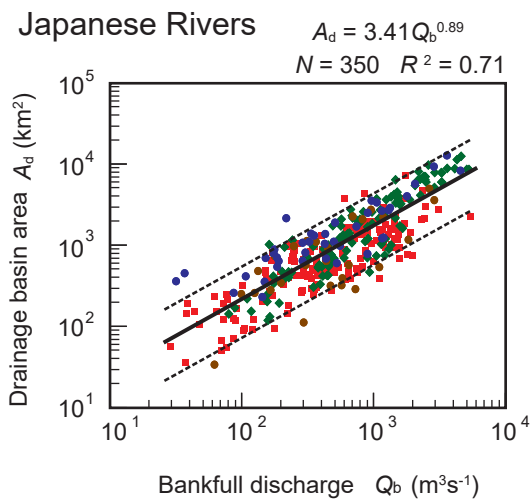
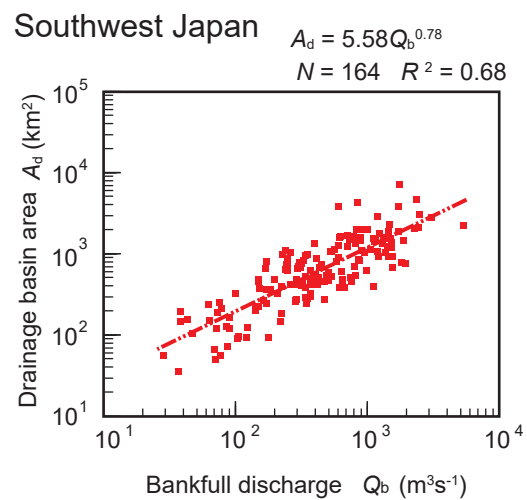
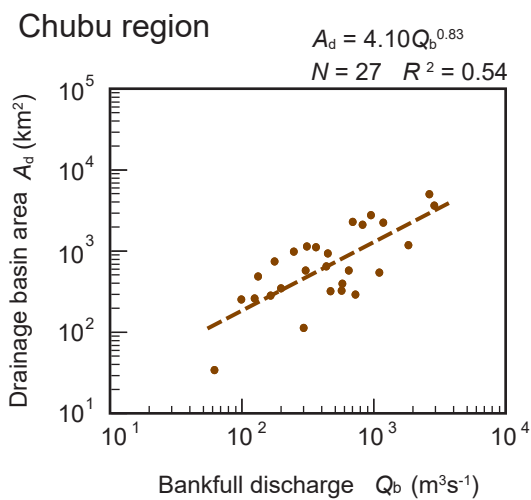
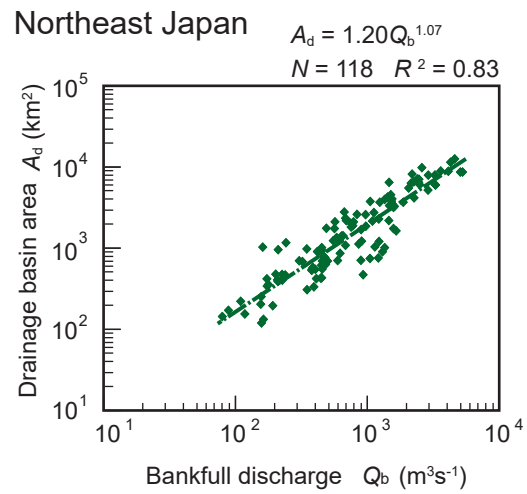
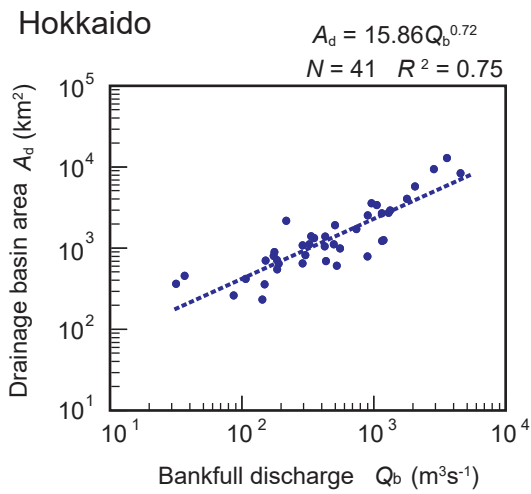


Fig. 13. Relationships between bankfull discharge (Q_b) and drainage basin area (A_d) for Japanese rivers, and a comparison of their regression curves.

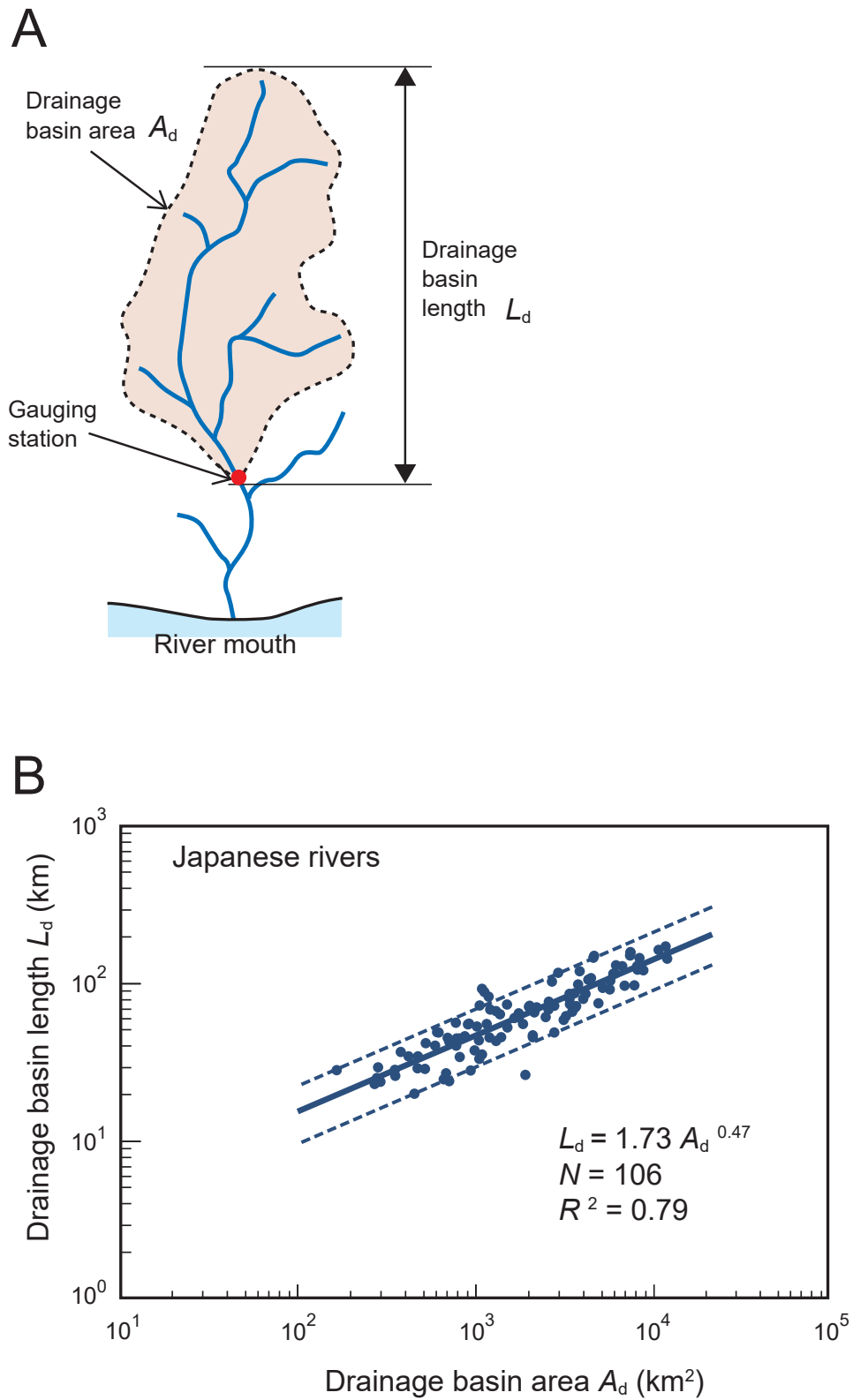


Fig. 14. A: Schematic illustration of a drainage basin with definitions of the drainage basin area (A_d) and drainage basin length (L_d). B: Relationships between A_d and L_d for Japanese rivers. Solid line: regression curve, dashed lines: 95% prediction bounds.

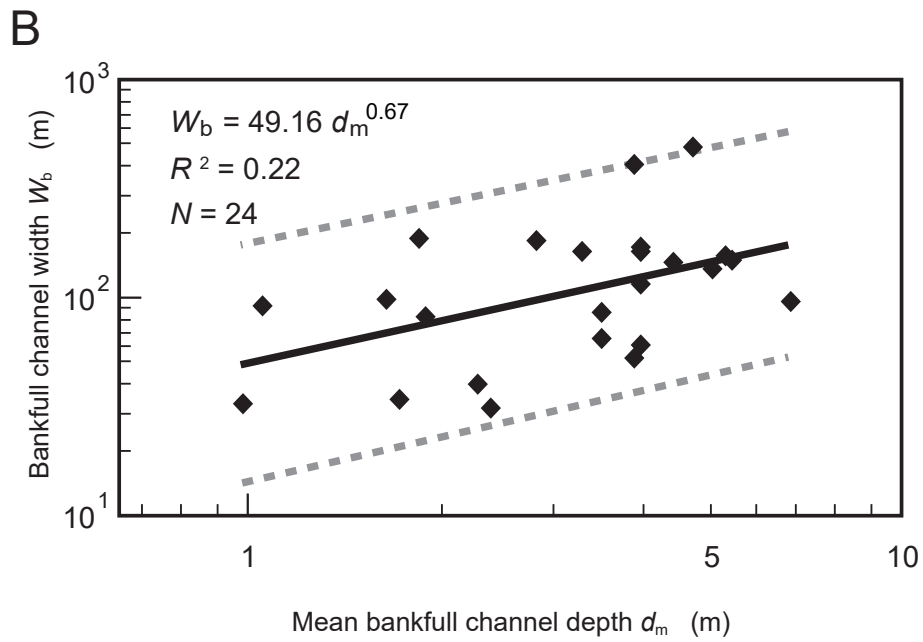
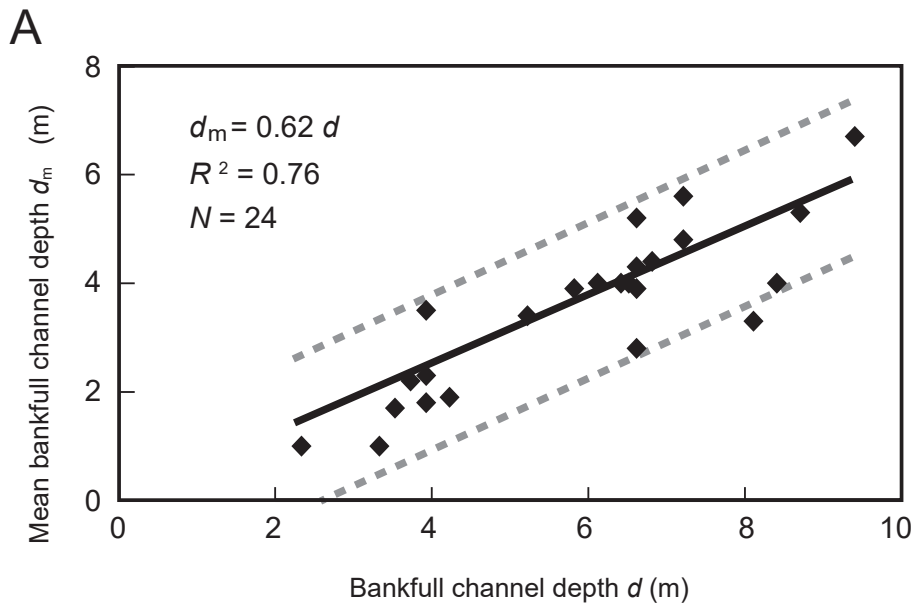


Fig. 15. Relationships between (A) bankfull channel depth (d) and mean bankfull channel depth (d_m), and (B) d_m and bankfull channel width (W_b) for rivers in the Kanto region. Solid line: regression line or curve. Dashed line: 95% prediction bounds.

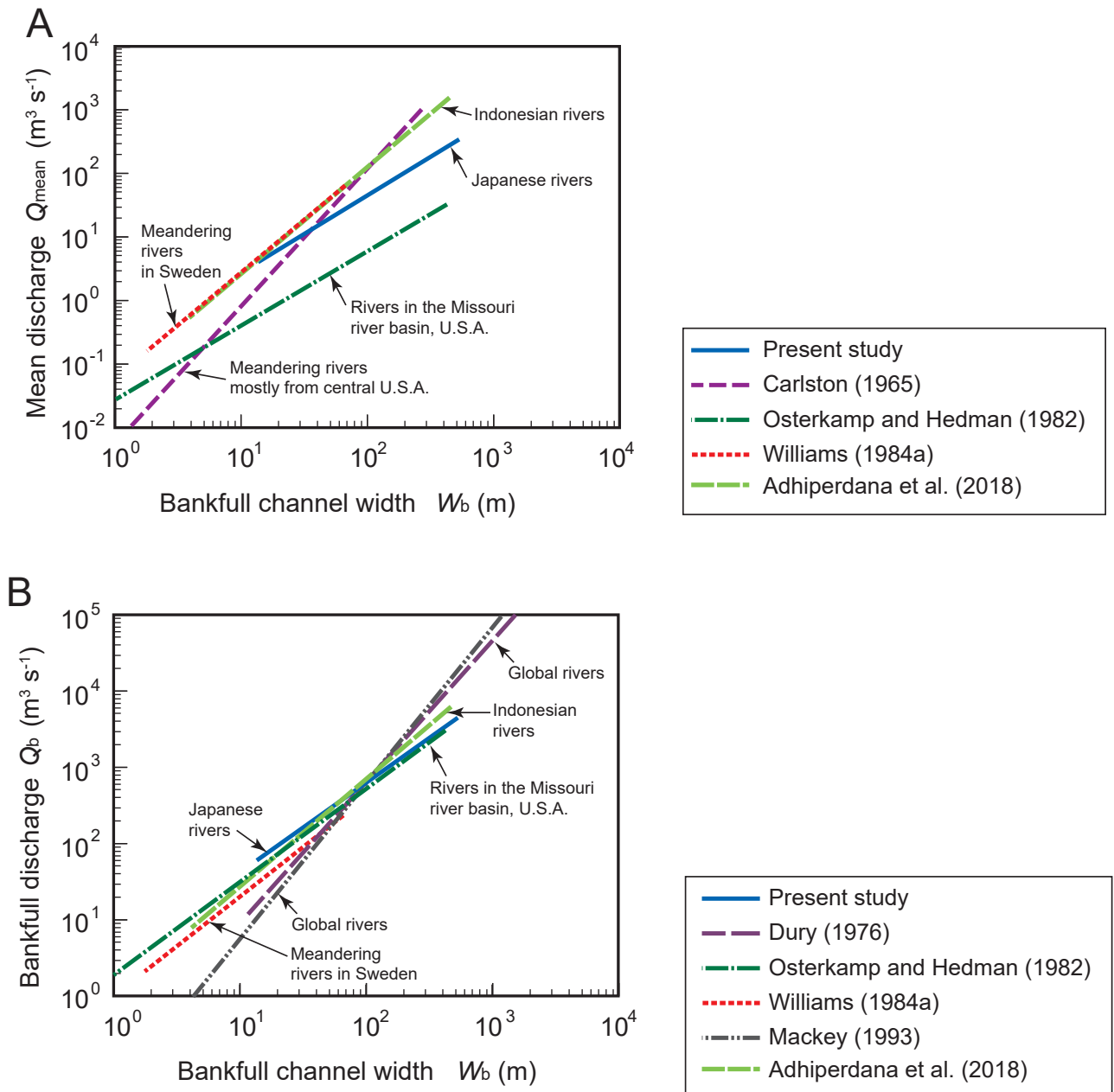


Fig. 16. Relationships between the bankfull channel width (W_b) and discharge characteristics for rivers in the Japanese Archipelago and some rivers in the Eurasian, North American, and Australian continents and Indonesian Archipelago. A: Relationships between W_b and the mean discharge (Q_{mean}). B: Relationships between W_b and the bankfull discharge (Q_b). See Table 6 for the equations of each regression curve.

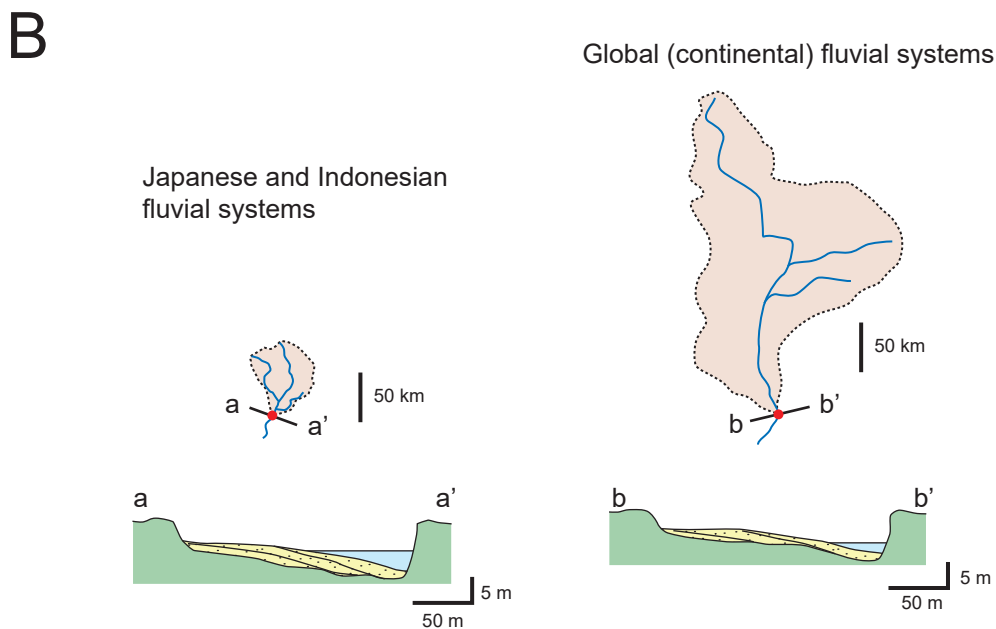
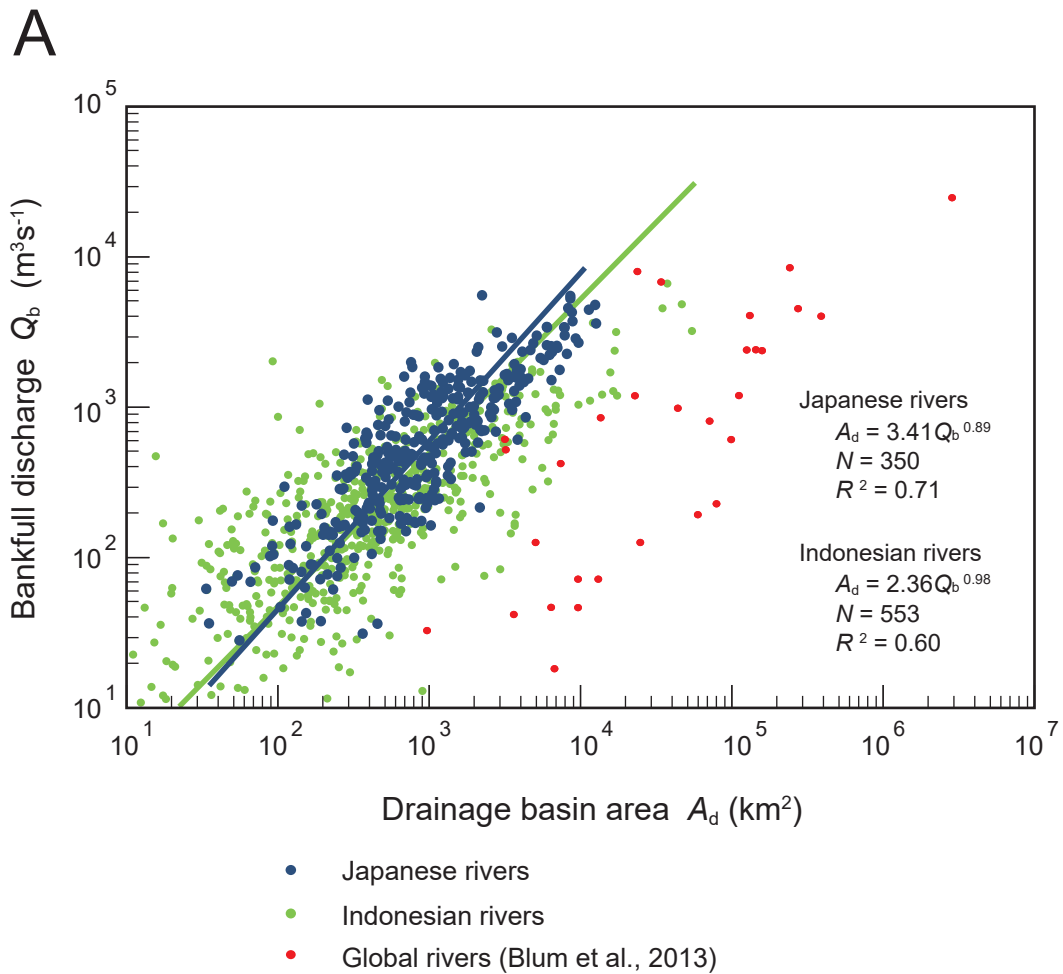


Fig. 17. A: Relationships between bankfull discharge (Q_b) and drainage basin area (A_d) for Japanese rivers, Indonesian rivers, and global rivers. Data of Indonesian rivers are from the Center for Water Resources Development and Research (2011) and Adhiperdana et al. (2018). Plots of global rivers are after Blum et al. (2013). B: Schematic illustrations of the Japanese and Indonesian, and global (continental) fluvial channels and drainage basins.

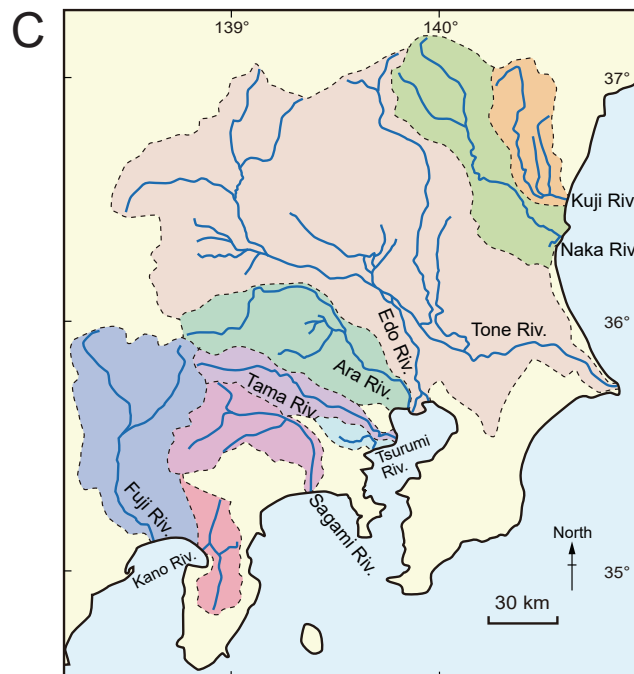
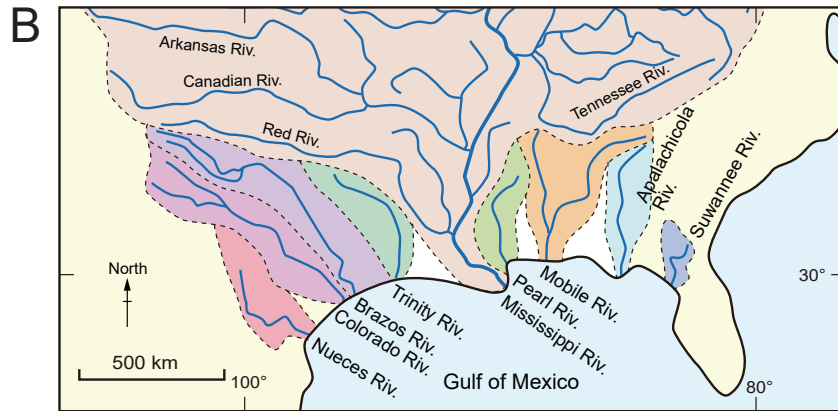
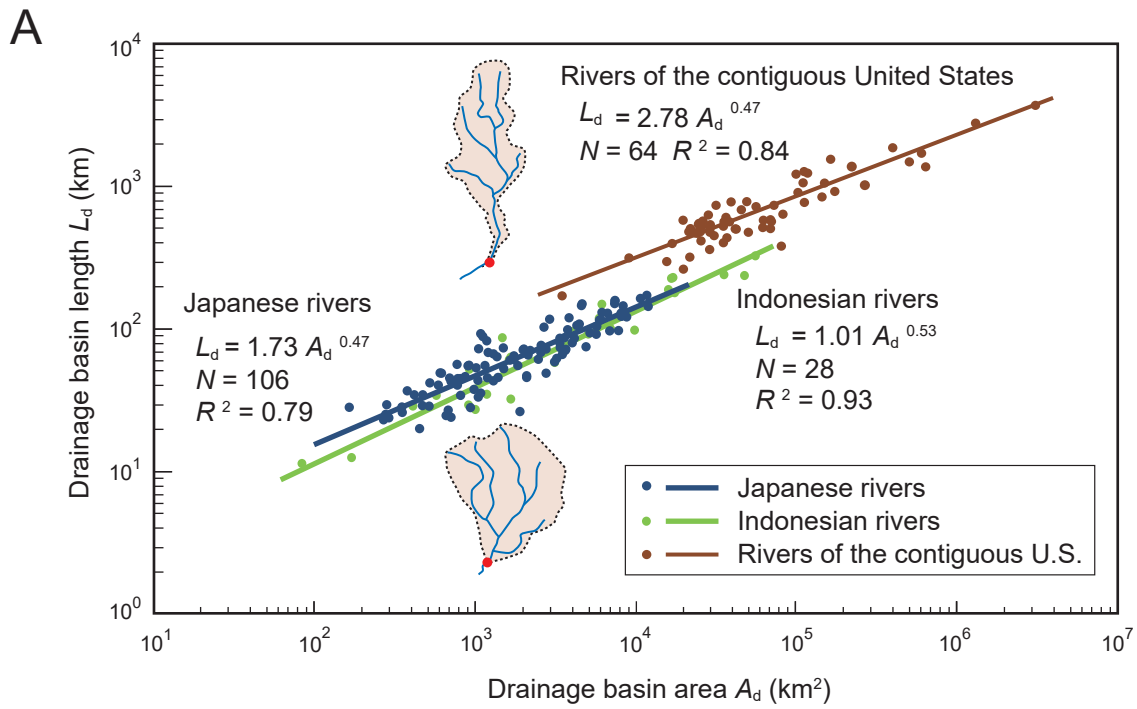
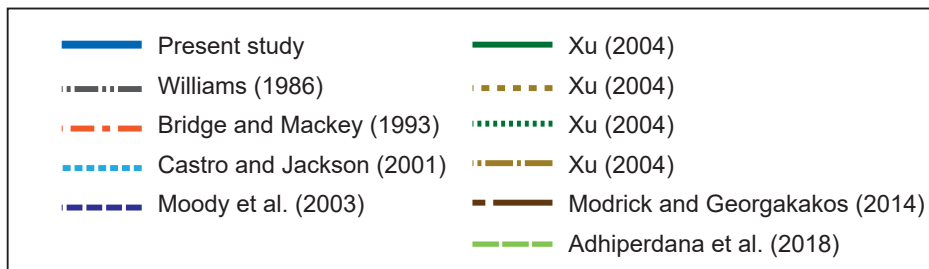
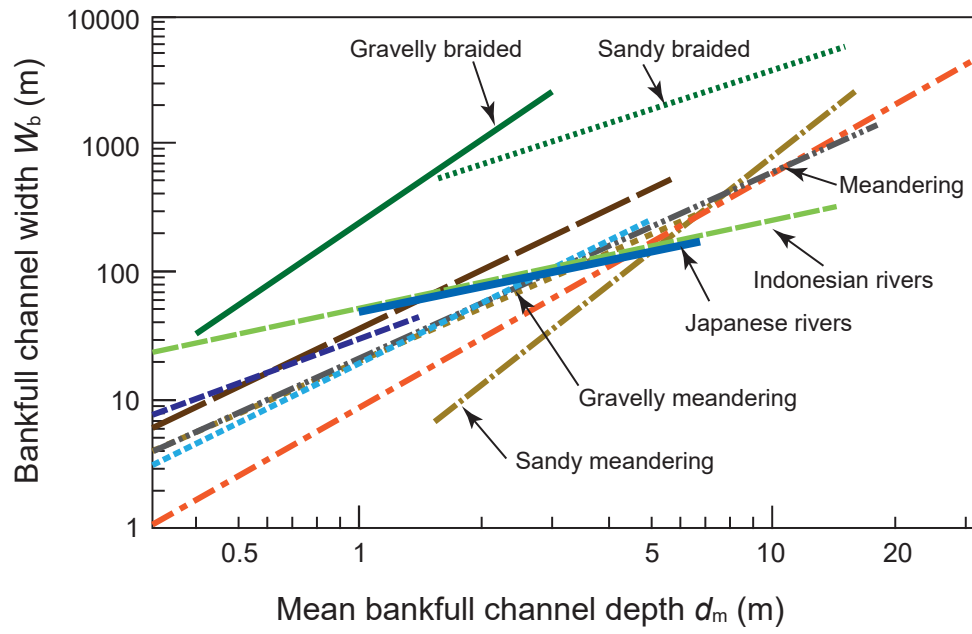


Fig. 18. A: Relationships between drainage basin area (A_d) and drainage basin length (L_d) for Japanese rivers, Indonesian rivers, and rivers of the contiguous United States. B: Schematic drainage map of the modern major fluvial systems of the Gulf of Mexico. C: Schematic drainage map of the modern fluvial systems of the Kanto region, central Japan.

A



B

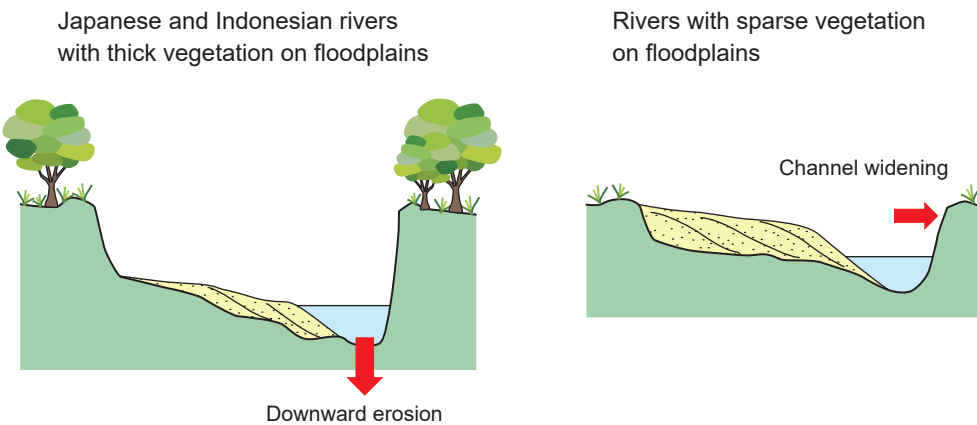


Fig. 19. A: Relationship between mean bankfull channel depth (d_m) and bankfull channel width (W_b) for rivers in Japan (the Kanto region) and that of the previous studies with channel patterns and bed material types. See Table 9 for details of the equations. B: Schematic cross-sections of Japanese and Indonesian river channel and of river channel with sparse vegetation on floodplains.

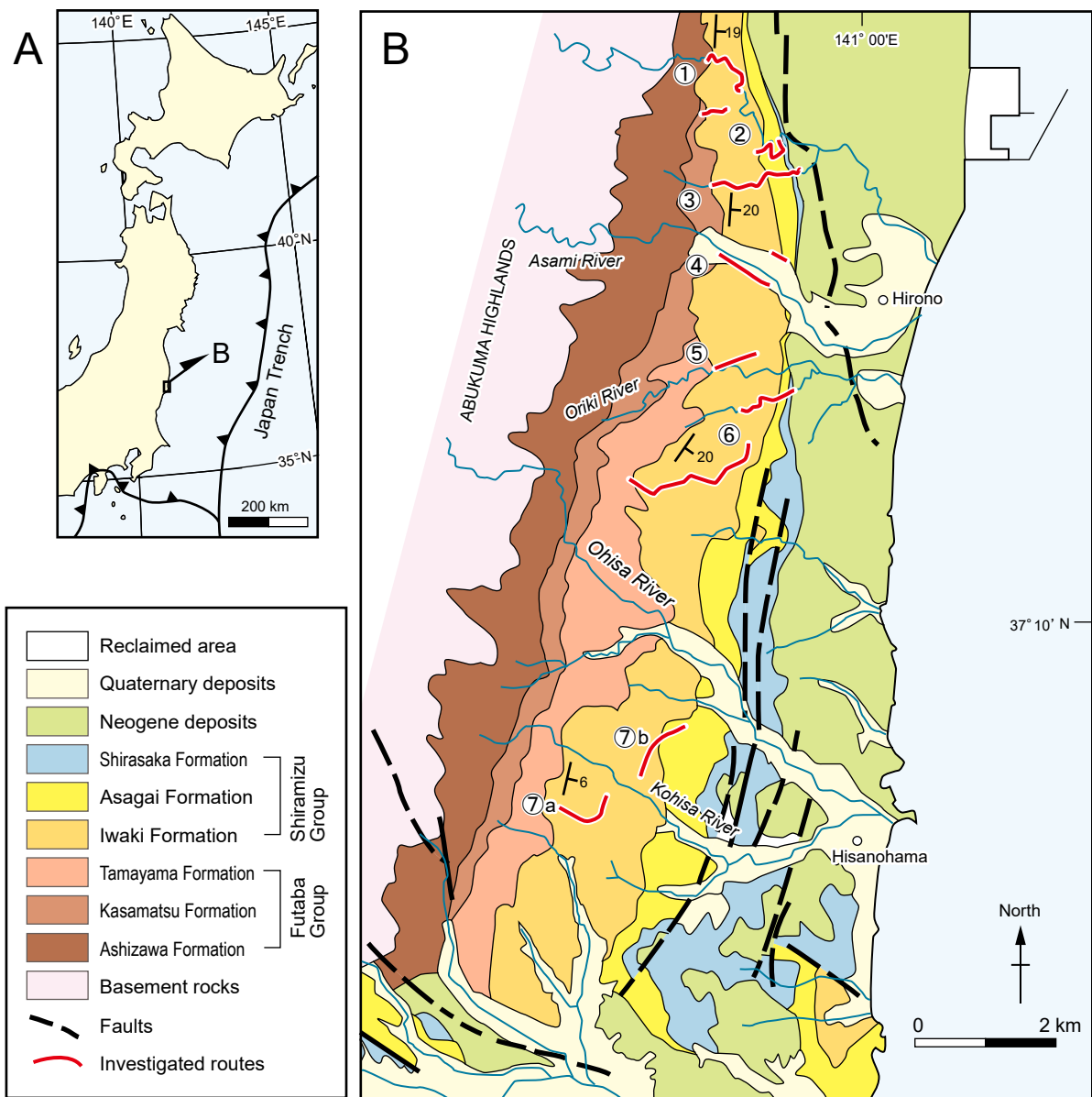


Fig. 20. A: Index map of the Joban Coalfield, Northeast Japan. B: Geologic map of the study area. Circled numbers in B indicate the investigated routes: 1) Nanamagari, 2) Nabetsuka, 3) Dokkameki, 4) Asami River, 5) Kitazawa, 6) Oriki River, and 7) Kohisa River. Geological map of B is modified after Okami (1973), Nemoto (1989), and Ando et al. (1995).

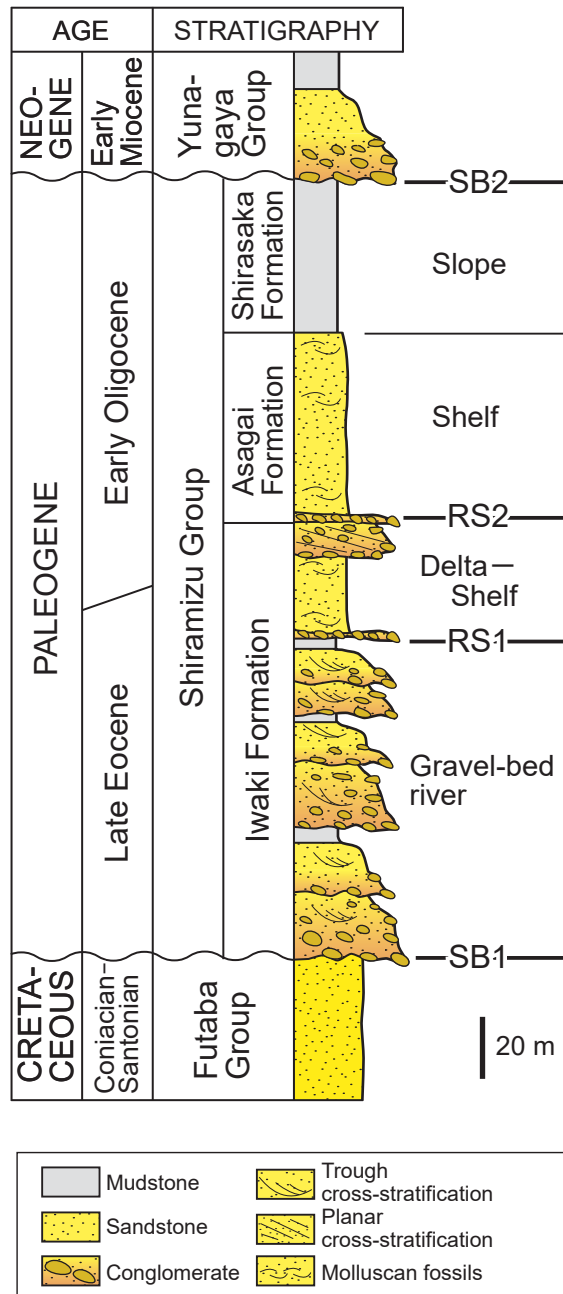


Fig. 21. Stratigraphy and sedimentary environments of the Paleogene Shiramizu Group in the study area. SB1 and SB2 = sequence boundaries, and RS1 and RS2 = ravinement surfaces. Stratigraphy is after Sugai et al. (1957), Kubo et al. (2002), and Suto et al. (2005).

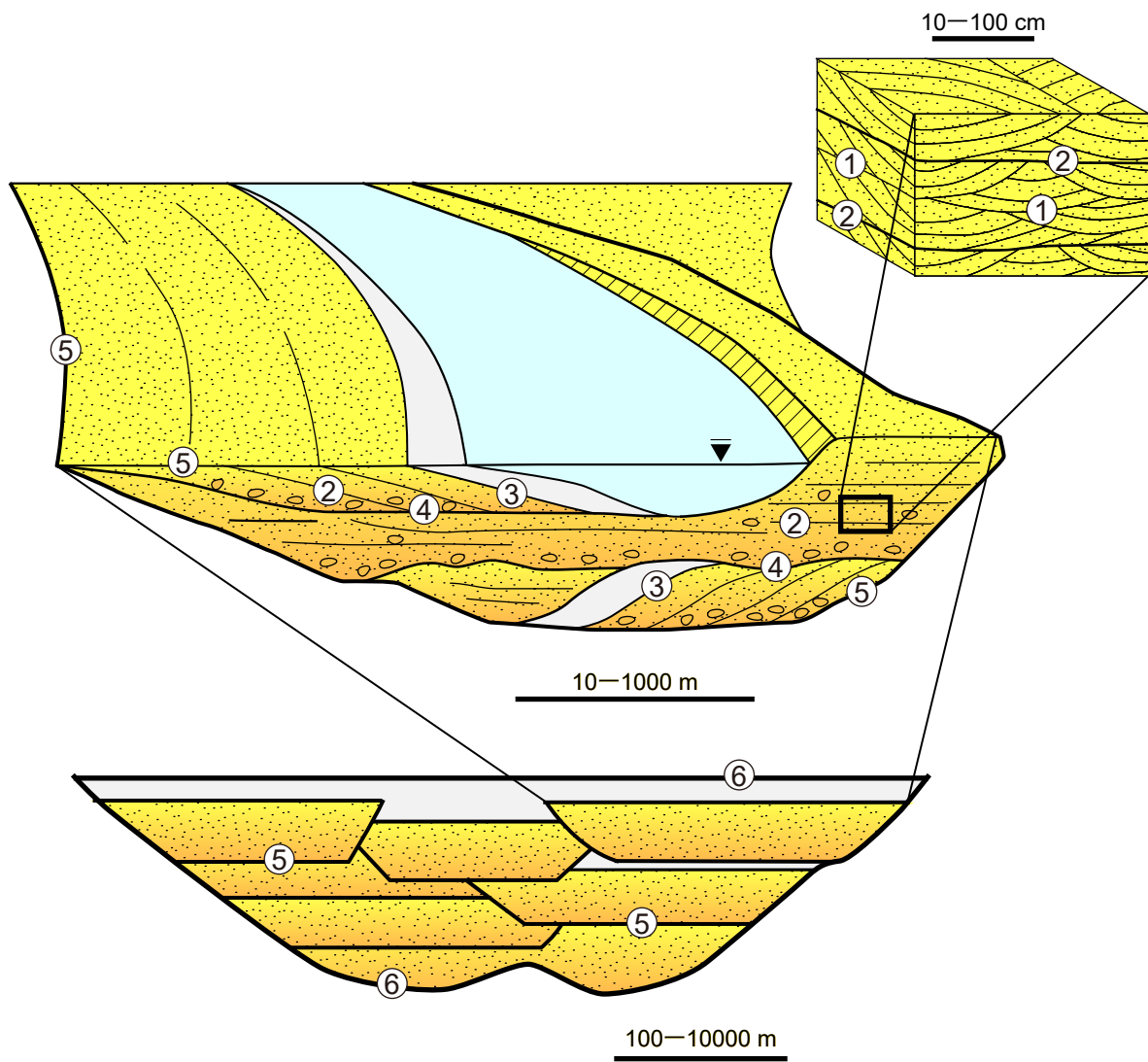


Fig. 22. Schematic illustration of hierarchical bounding-surface (BS) and depositional-unit (DU) types used in the Iwaki Formation fluvial deposits. Circled numbers indicate hierarchical classification of bounding-surface types.

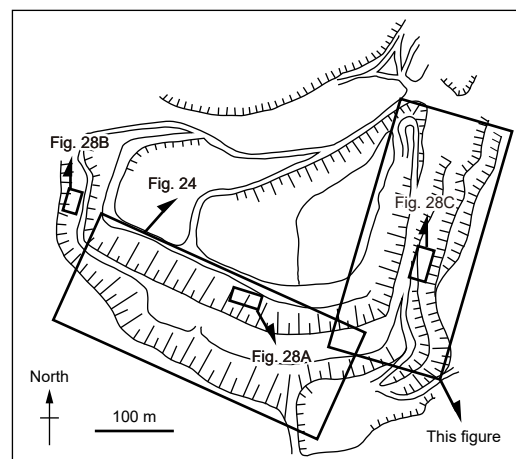
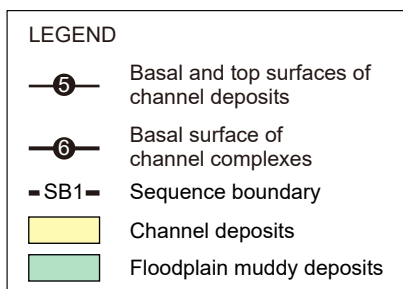
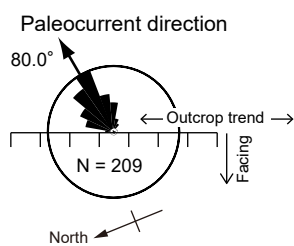
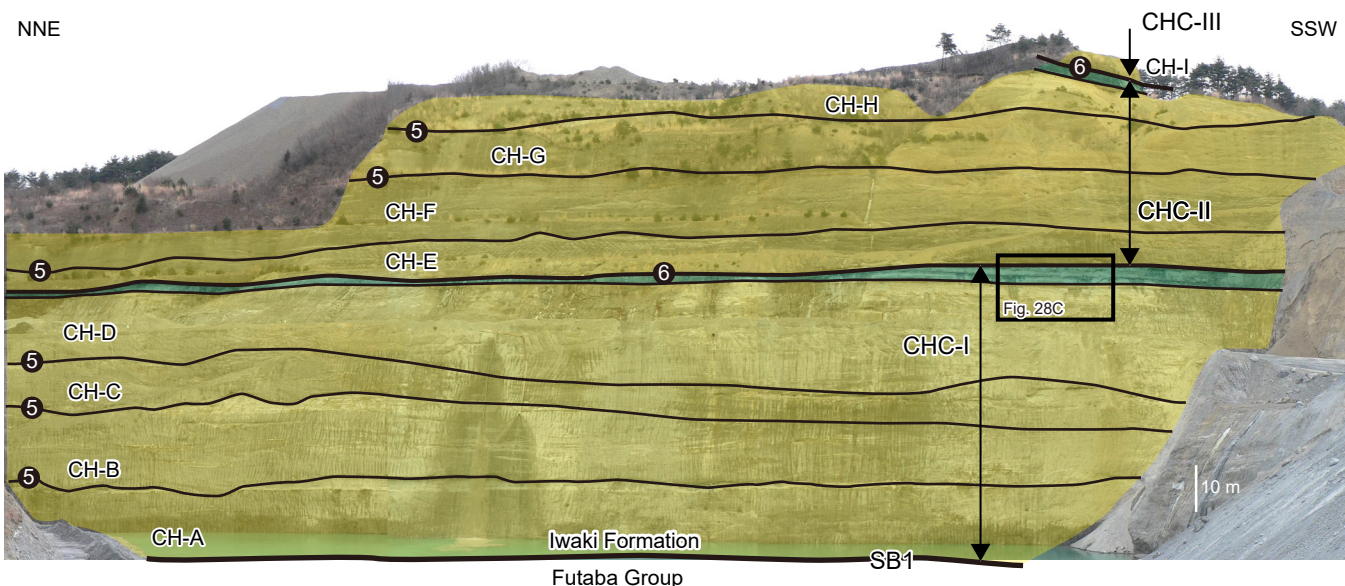
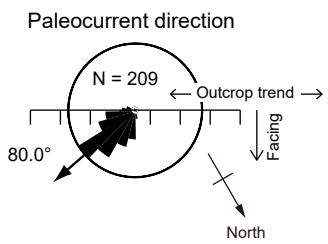
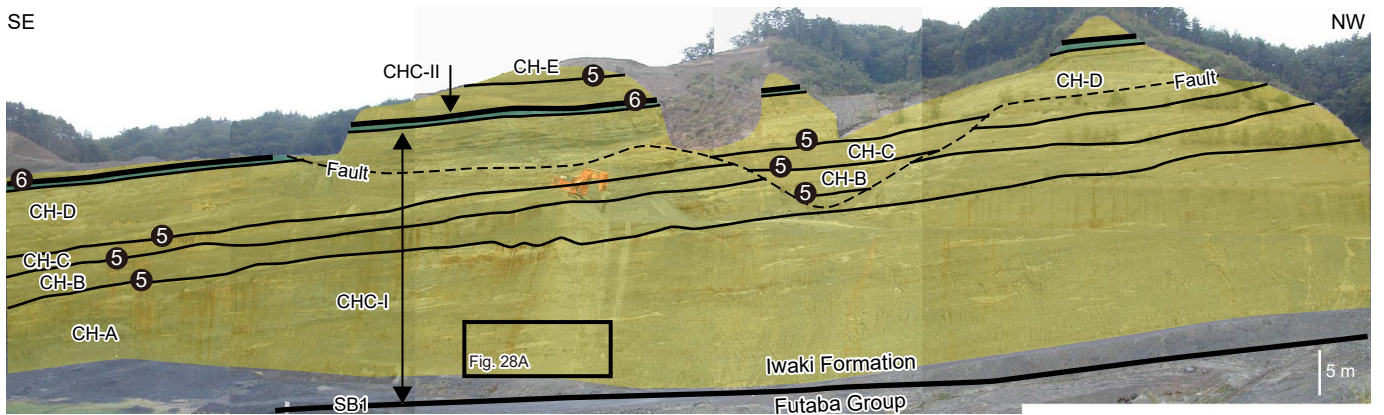


Fig. 23. Panorama photograph of an outcrop at a quarry along the Kohisa River route (Route 7a in Fig. 20B) ($37^{\circ}08'46.5''N$, $140^{\circ}57'15.3''E$), showing nine channel (CH-A to CH-I) deposits and three channel complexes (CHC-I to CHC-III). N is the number of paleocurrent measurements. Index map in the lower right indicates locations of outcrops in this quarry shown in Figs. 24 and 28.



LEGEND	
	Basal and top surfaces of channel deposits
	Basal surface of channel complexes
	Sequence boundary
	Channel deposits
	Floodplain muddy deposits

Fig. 24. Panorama photograph of an outcrop at a quarry along the Kohisa River route (Route 7a in Fig. 20B) (37°08'44.1"N, 140°57'10.2"E). N is the number of paleocurrent measurements.

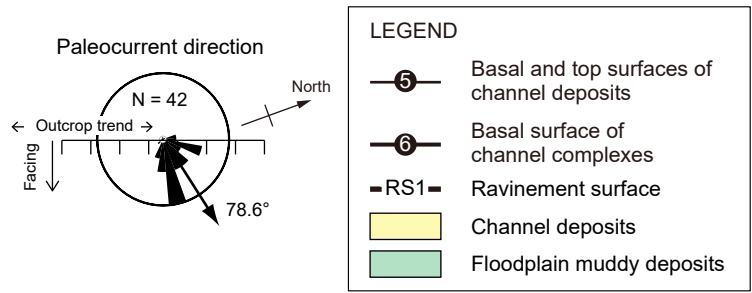
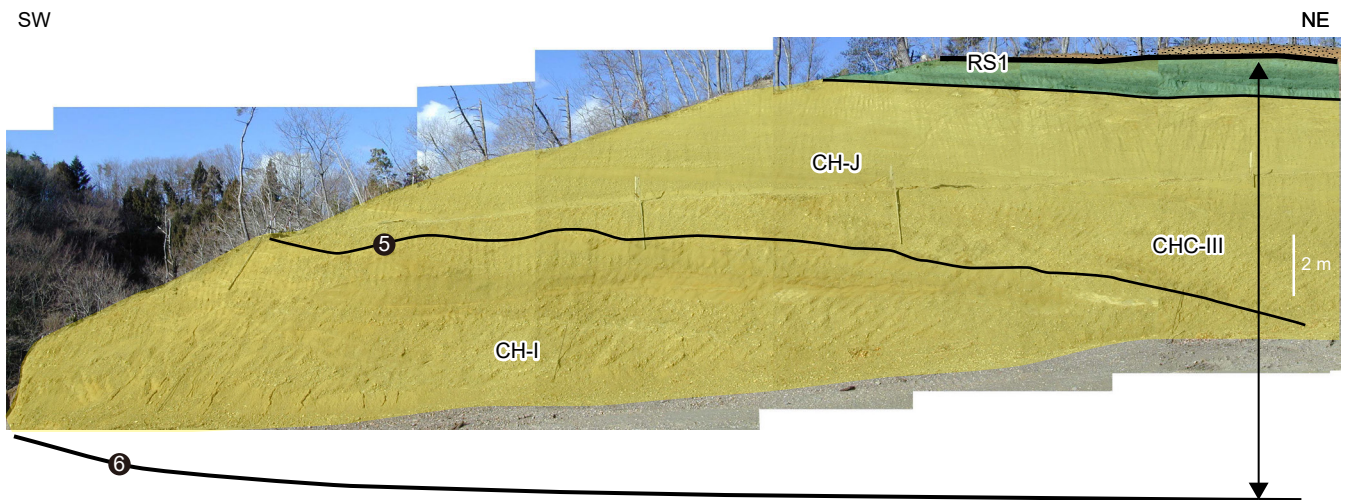
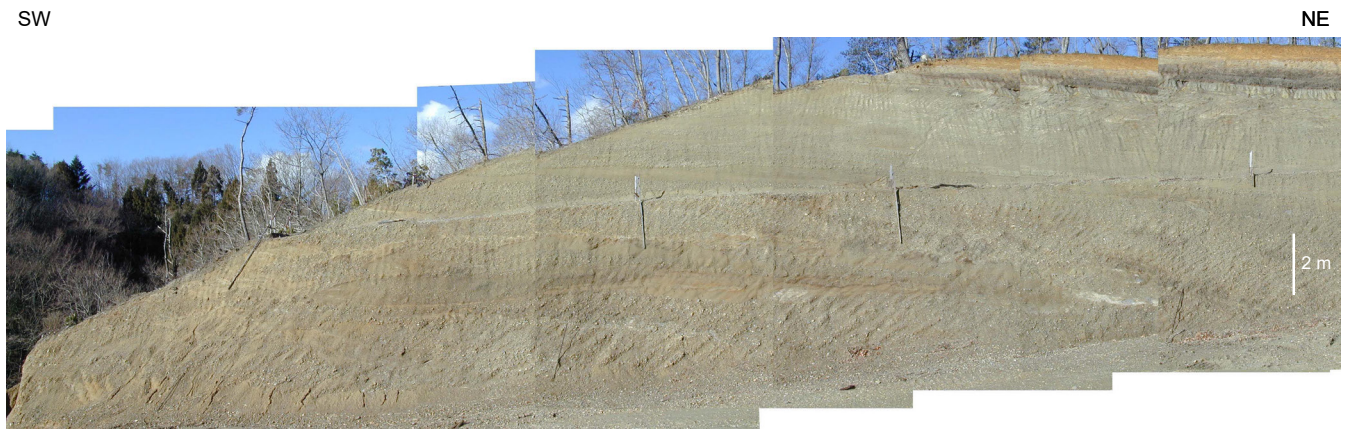


Fig. 25. A roadside outcrop along the Kohisa River route (Route 7b in Fig. 20B) ($37^{\circ}09'16.3''\text{N}$, $140^{\circ}57'47.2''\text{E}$), showing two channel (CH-I and CH-J) deposits of a channel complex (CHC-III). N is the number of paleocurrent measurements.

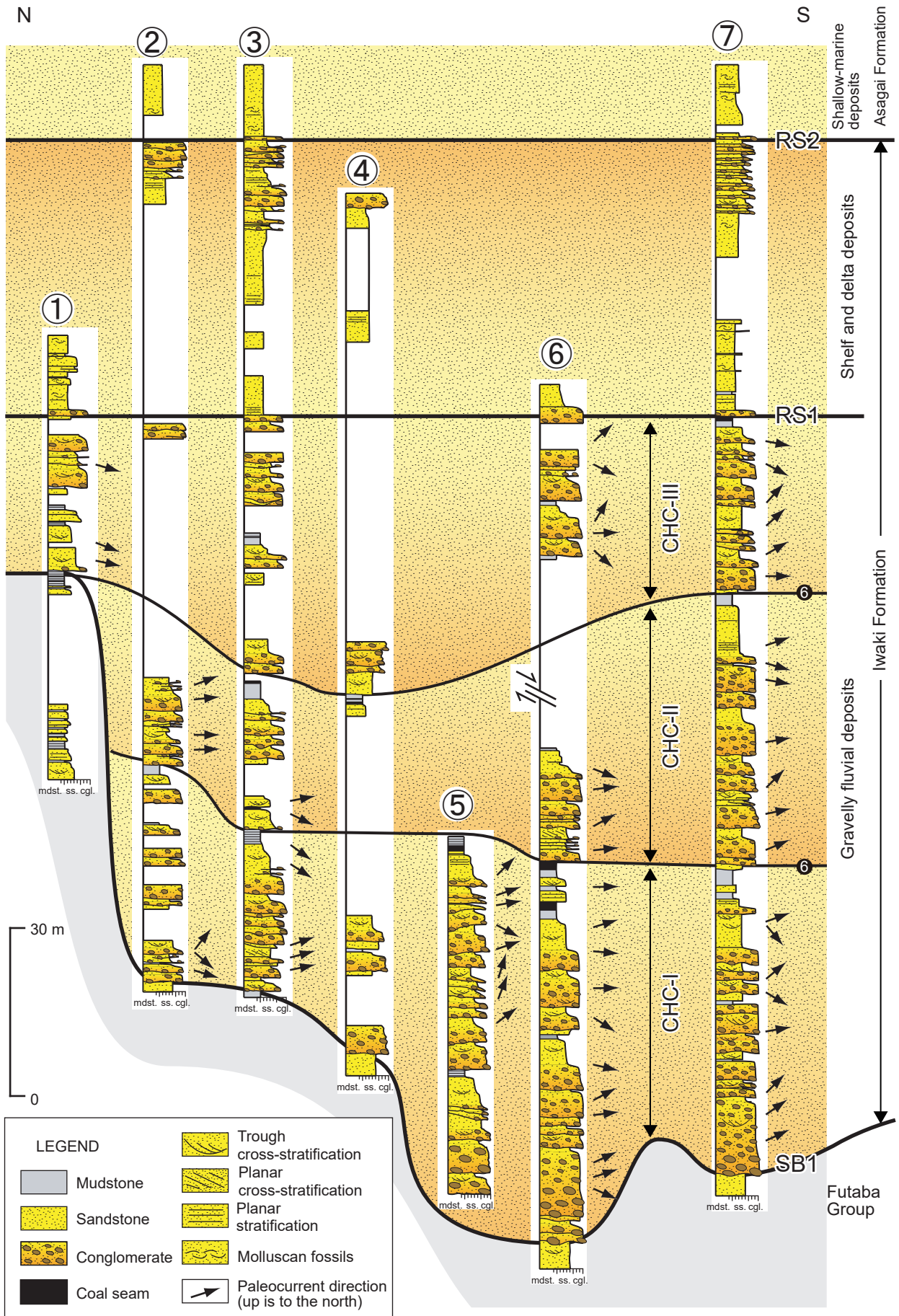


Fig. 26. Stratigraphic cross-section of the gravely fluvial deposits of the Iwaki Formation. Circled numbers indicate the investigated routes shown in Figure 20.

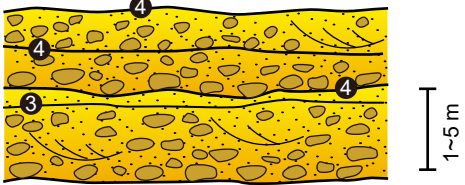
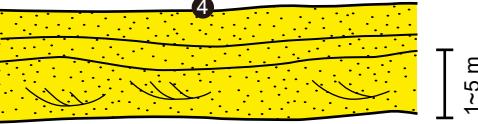
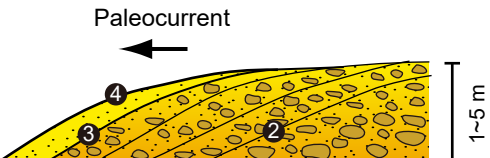
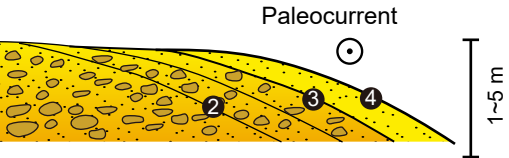



Elements	Description	Interpretation
<p>Gravel-bar (GB) deposits</p> 	<p>Tabular or sheet-like elements mainly composed of pebble- to cobble-sized, clast-supported conglomerates with medium- to coarse-grained sandstone matrix; commonly massive; occasionally showing trough or planar cross-stratification and fining-upward trends.</p>	<p>Longitudinal bar, transverse bar, gravel bedform (Miall, 1985, 1988)</p>
<p>Sandy-bar (SD) deposits</p> 	<p>Tabular or sheet-like elements composed of fine- to very coarse-grained (locally pebbly) sandstone; commonly showing trough and planar cross-stratification; occasionally massive.</p>	<p>Longitudinal bar, transverse bar, sandy bedform (Miall, 1985, 1988)</p>
<p>Downstream-accreting (DA) deposits</p> 	<p>Stacked sets of trough or planar cross-stratified, fine- to very coarse-grained (locally pebbly) sandstones and conglomerates (granule- to cobble-sized clasts) with inclined 2nd-order BS dipping in the same directions as internal stratification in the 1st-order BS (paleocurrent directions).</p>	<p>Downstream part of longitudinal or transverse bar (Allen, 1983; Miall, 1985, 1988)</p>
<p>Lateral-accreting (LA) deposits</p> 	<p>Stacked sets of trough or planar cross-stratified, fine- to very coarse-grained (locally pebbly) sandstones and conglomerates (granule- to cobble-sized clasts) with low-angled, inclined 2nd-order BS dipping perpendicular or high-angled to downstream directions.</p>	<p>Lateral part of longitudinal bar (Allen, 1983; Miall, 1985, 1988; Bridge, 1993)</p>
<p>Small-scale channel-fill (SCH) deposits</p> 	<p>Small-scale, concave-up shaped, lenticular elements with erosional base filled with cross-stratified, and/or by massive sandstone and conglomerates.</p>	<p>Filling of abandoned cross-bar channel (Miall, 1985, 1988; Bridge, 1993)</p>
<p>Floodplain muddy (FF) deposits</p> 	<p>Tabular or sheet-like elements mainly composed of very fine-grained sandstone, mudstone, and coal seams.</p>	<p>Overbank, floodplain deposit (Miall, 1985, 1988; Bridge, 1993)</p>
<p>Channel (CH) deposits</p> 	<p>Lenticular or tabular units with erosional base of the 5th-order BS; composed of any combination of lithofacies and architectural elements such as GB, SD, DA, LA, SCH, and FF deposits.</p>	<p>Channel deposit (Miall, 1985, 1988; Bridge, 1993; Gibling, 2006)</p>
<p>Channel complexes (CHC)</p>	<p>Stacked sets of channel (CH) deposits separated by 6th-order BS.</p>	<p>Channel complex (Holbrook, 2001)</p>

Fig. 27. Description and interpretation of architectural elements of the Iwaki Formation. Circled numbers in schematic illustrations of architectural elements indicate bounding-surface hierarchy.

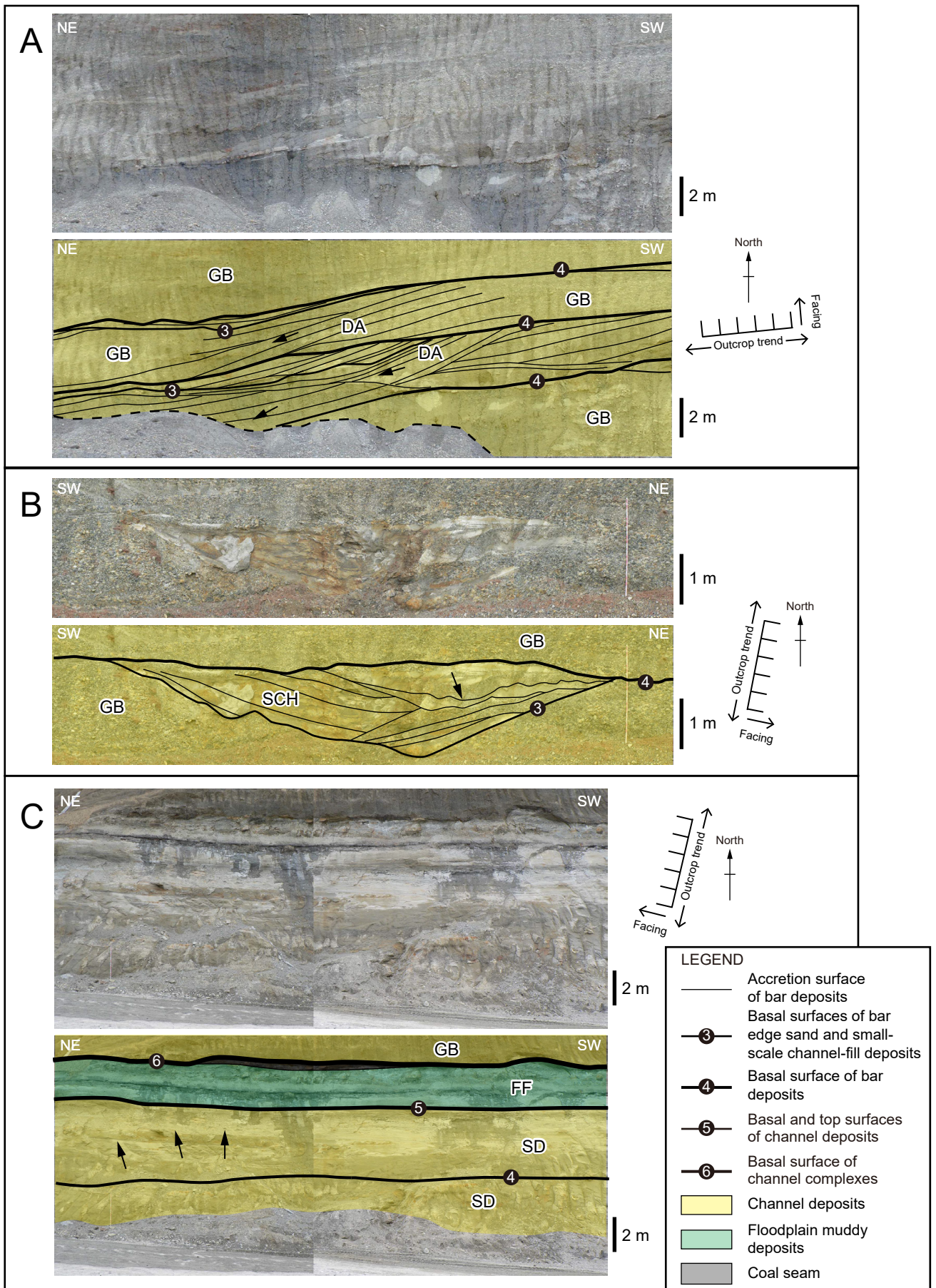


Fig. 28. A: Gravel-bar (GB) and downstream-accreting (DA) deposits, which define longitudinal-bar deposits ($37^{\circ}08'44.6''\text{N}$, $140^{\circ}57'10.2''\text{E}$). B: Small-scale channel-fill (SCH) deposit intercalated in gravel-bar (GB) deposits ($37^{\circ}08'44.9''\text{N}$, $140^{\circ}56'58.4''\text{E}$). C: Sandy-bar (SD) and floodplain muddy (FF) deposits overlain by the GB deposits ($37^{\circ}08'45.6''\text{N}$, $140^{\circ}57'14.9''\text{E}$). All outcrops are at a quarry along the Kohisa River route (Route 7a in Fig. 20B). Arrows represent paleocurrent directions relative to the outcrop (up is into the outcrop). See the index in Fig. 23 for the location of these outcrops.

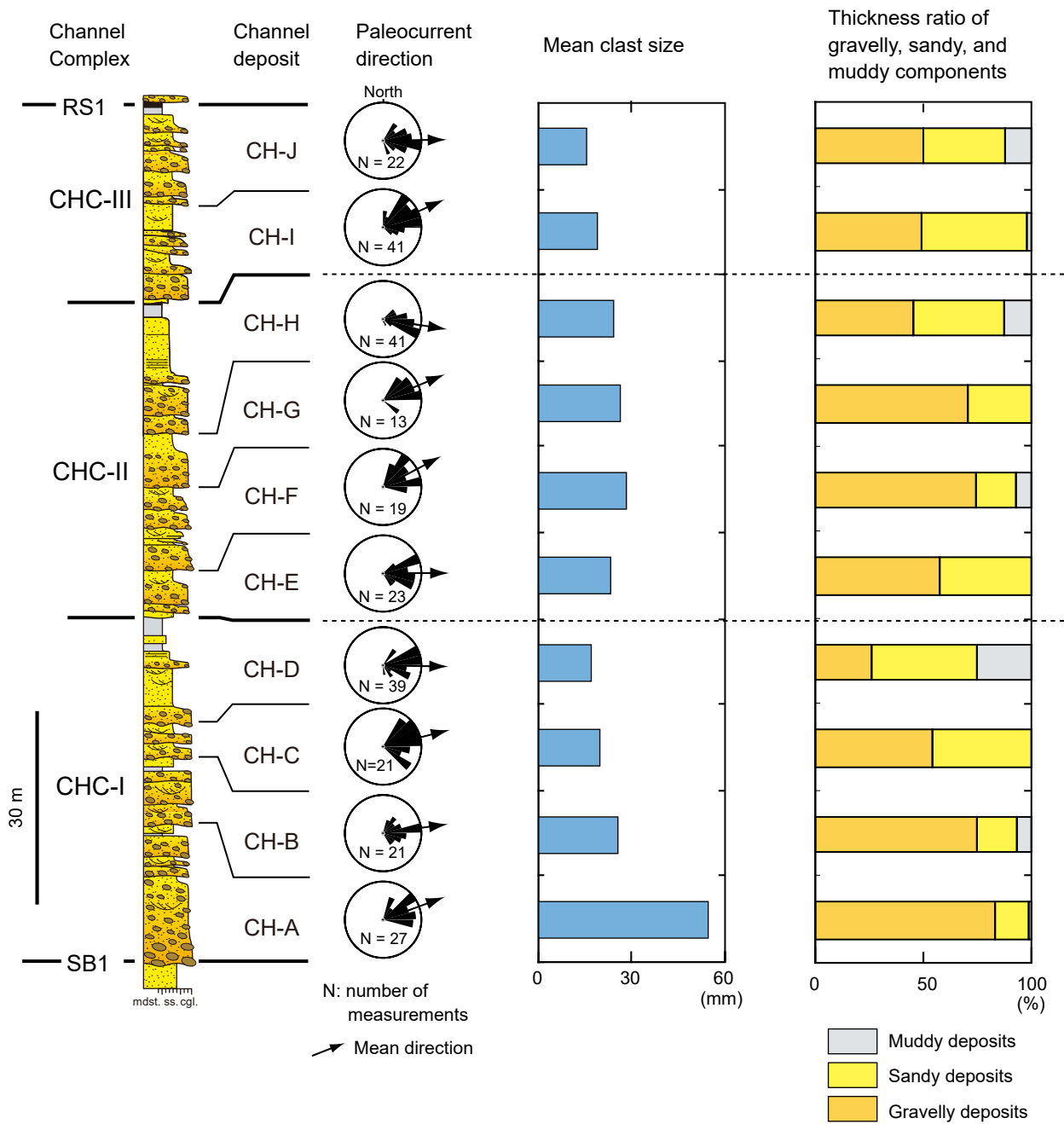


Fig. 29. Vertical changes in sedimentological features of channel deposits of the Iwaki Formation. Data is from Route 7 in Fig. 20B. SB1 = sequence boundary, and RS1 = ravinement surface.

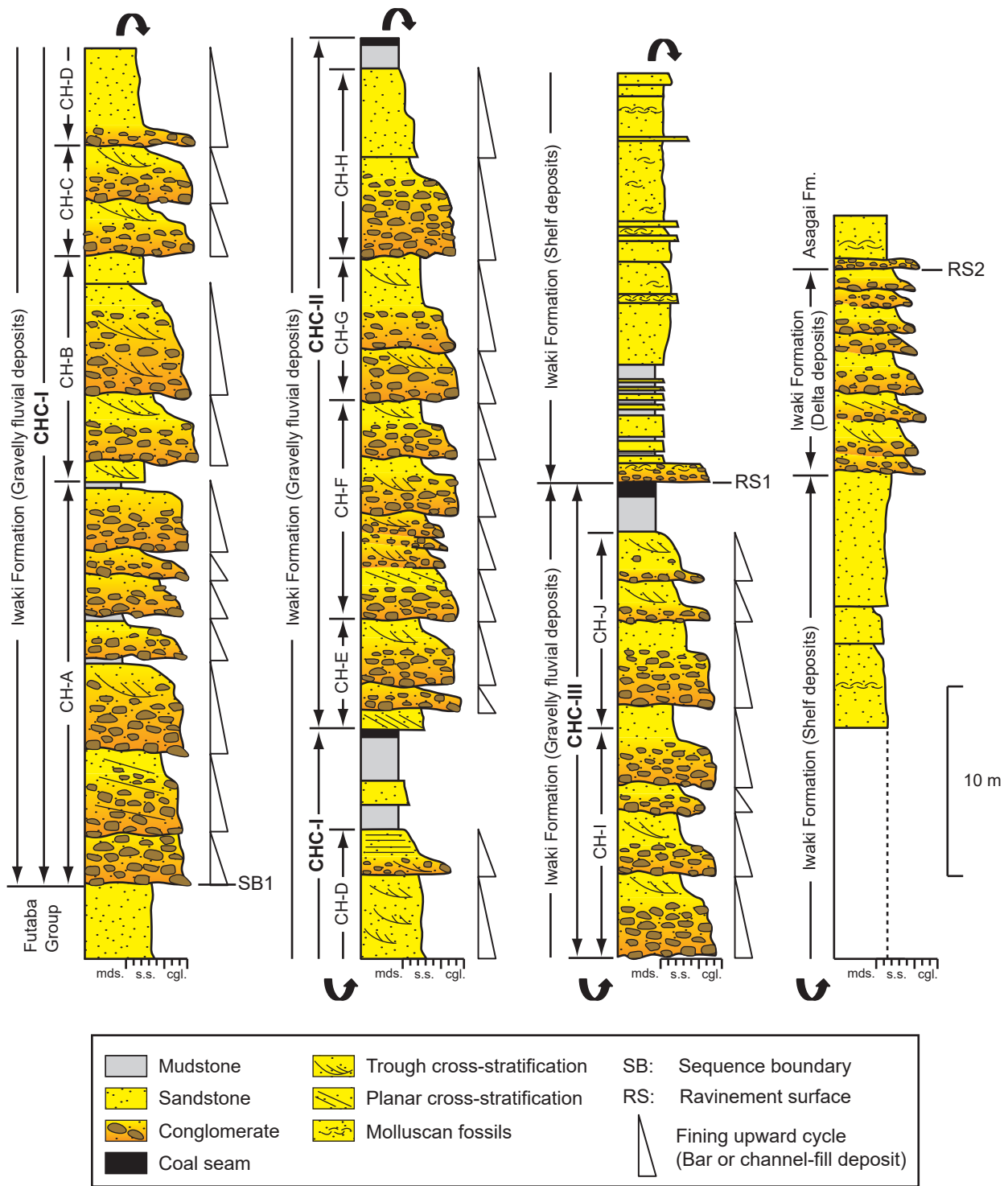


Fig. 30. Stratigraphic columnar section of the Paleogene Iwaki Formation at the investigated route 7a and 7b. See Fig. 20B for the investigated route.

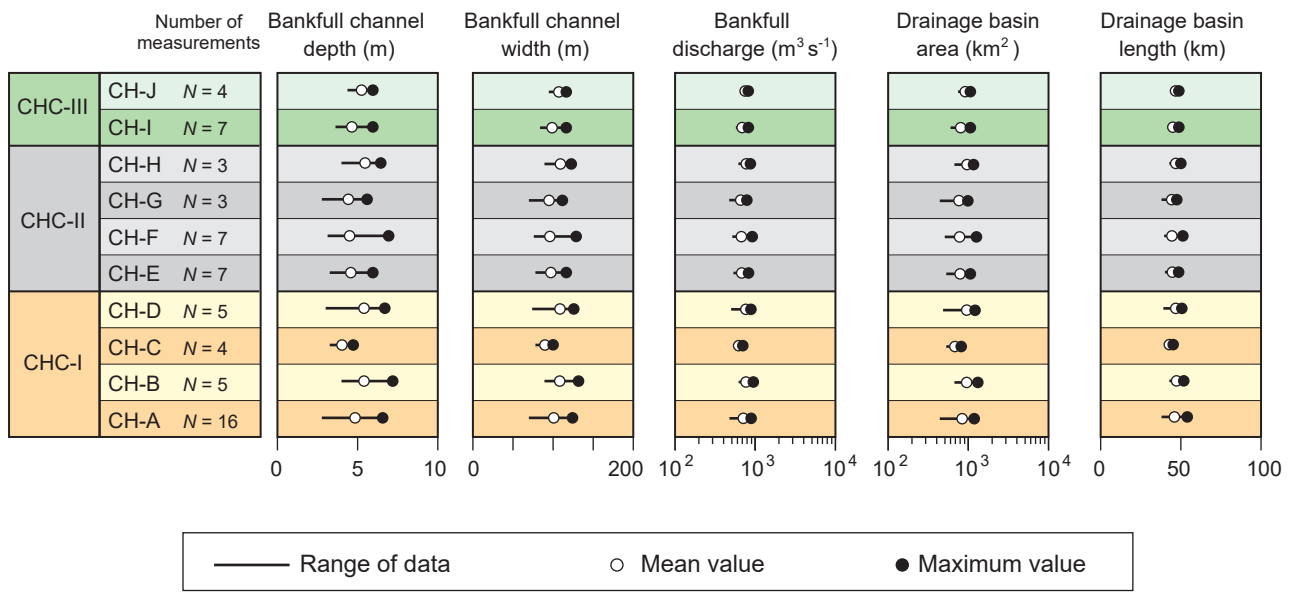


Fig. 31. Result of the paleochannel and drainage basin reconstructions using data from the gravelly fluvial deposits of the Iwaki Formation.

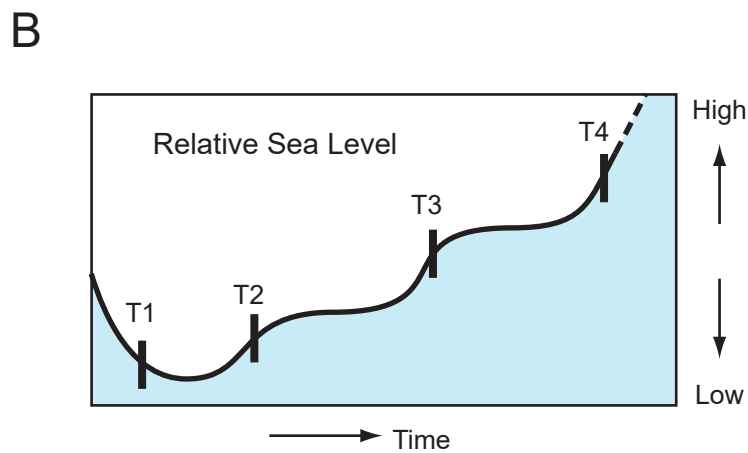
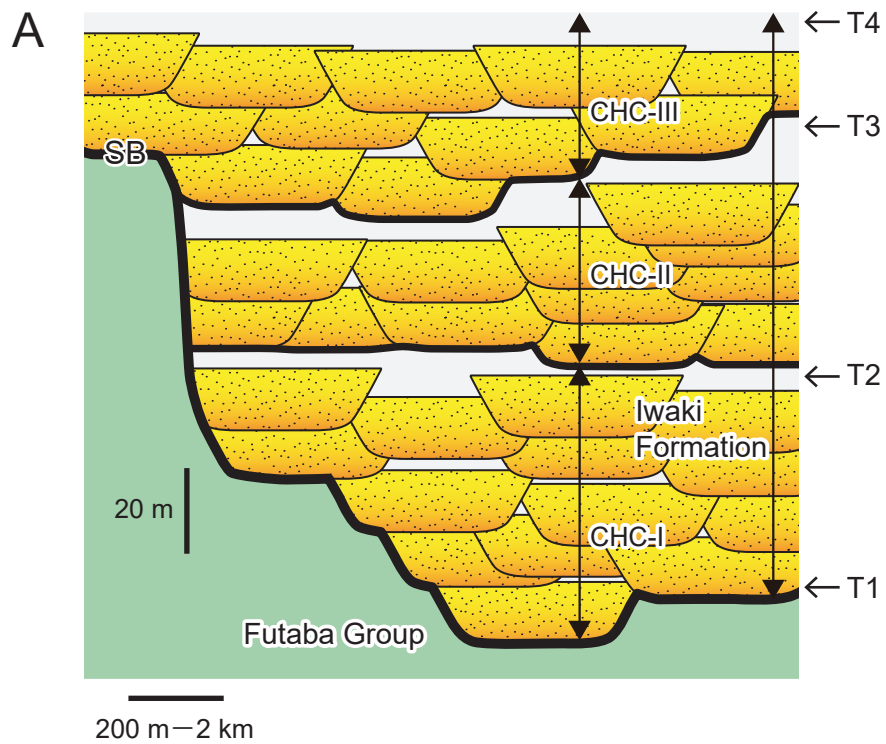


Fig. 32. A: Schematic stacking pattern of three cycles of channel complexes of the Iwaki Formation (CHC-I to CHC-III). **B:** Relative sea-level cycles predicted from the stacking pattern and architecture of the Iwaki Formation fluvial deposits.

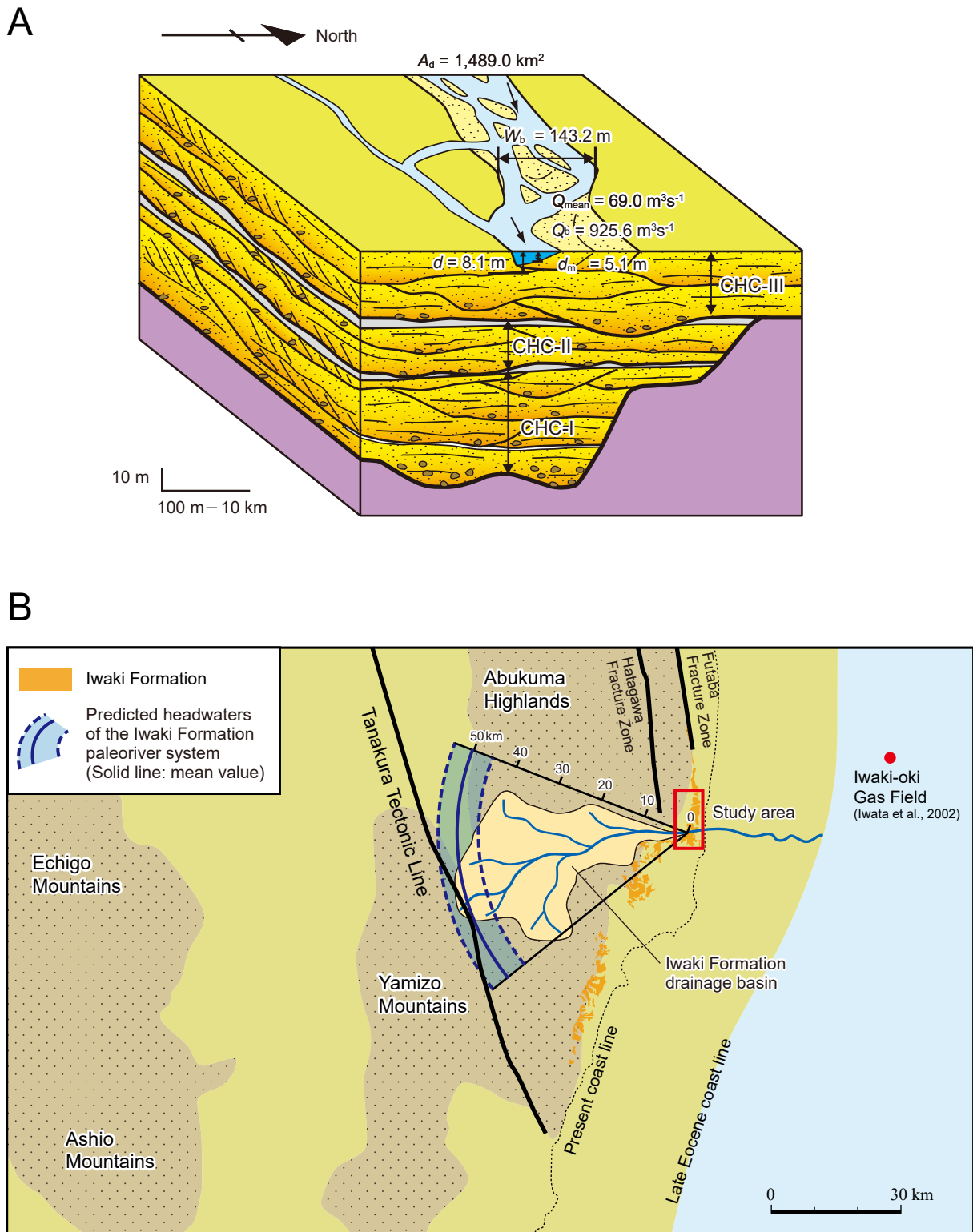


Fig. 33. A: Quantitative reconstruction of the Iwaki Formation fluvial paleochannel. Paleogeomorphological and paleohydrological parameters are maximum values estimated from the outcrop data. B: Predicted Iwaki Formation drainage basin based on the estimated values of drainage basin area and length. Location of Late Eocene coast line is on the basis of the estimated backwater length. Distribution of the Iwaki Formation is after Okami (1973).

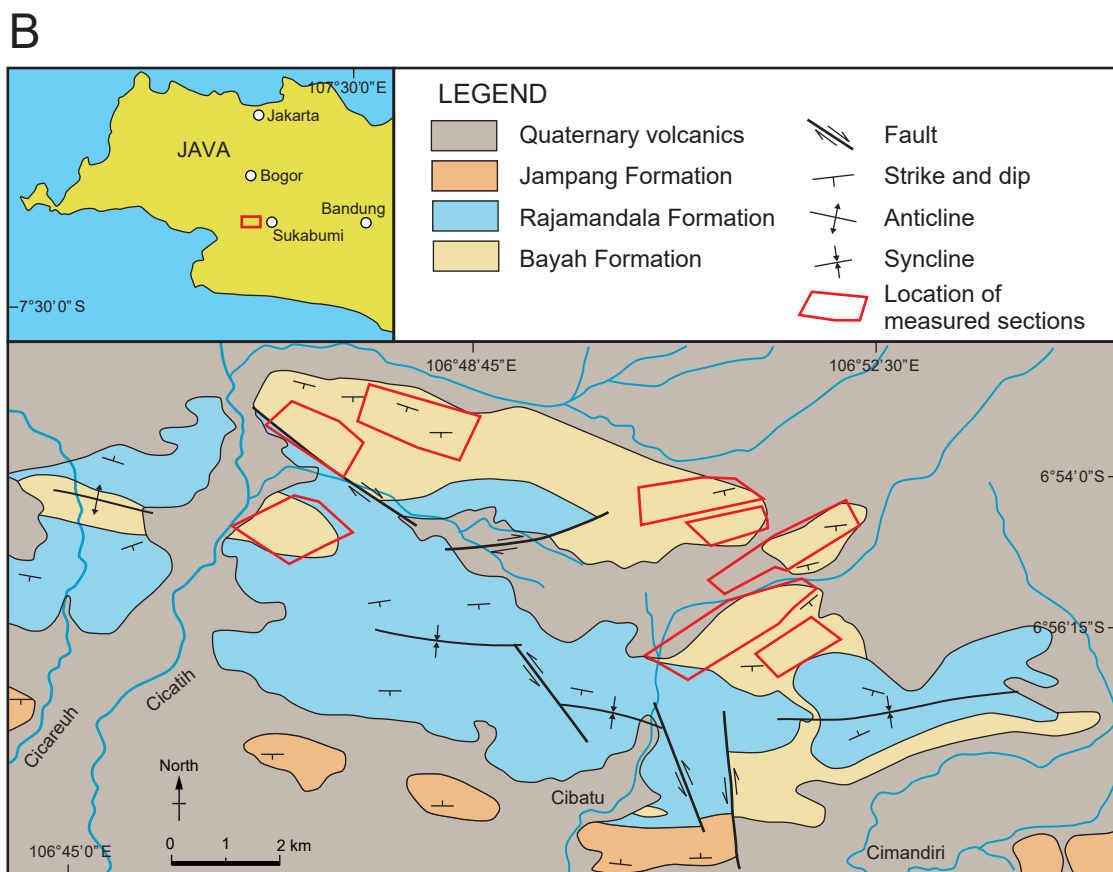
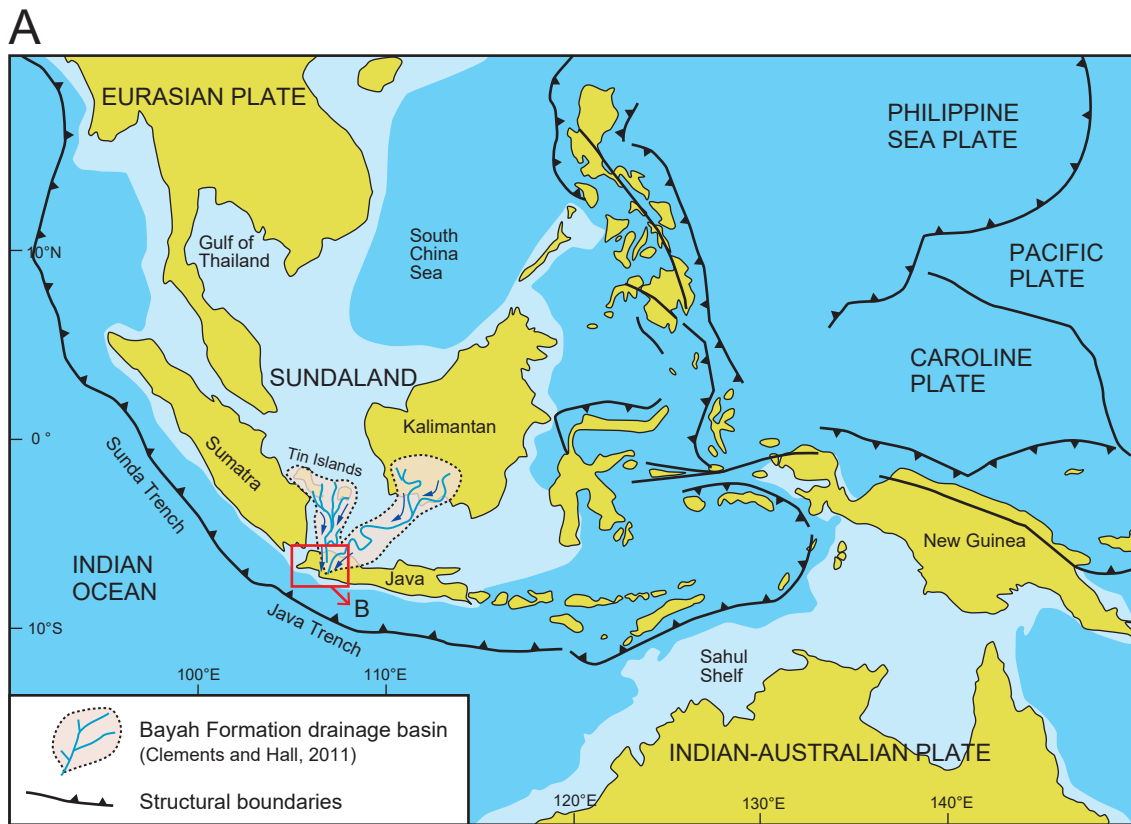


Fig. 34. A: Present day plate-tectonic setting of Indonesian Archipelago. The Paleogene Bayah Formation drainage basin reconstructed by Clements and Hall (2011) are also shown. The map was modified from Hall (1996, 2012). B: Geological map of the Sukabumi high. Modified from Effendi et al. (1989) and Adhiperdana (2018).

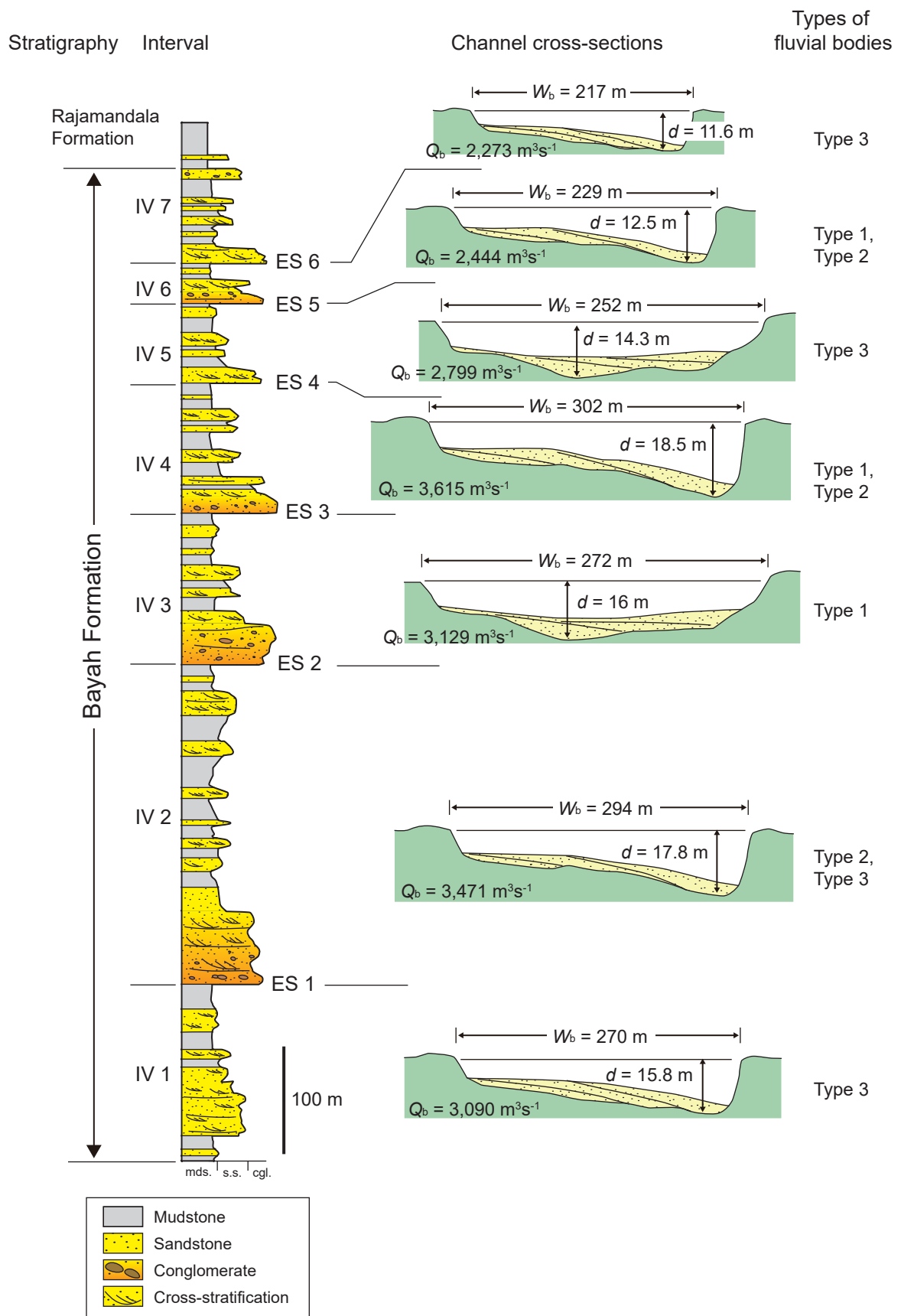


Fig. 35. Temporal variation in the bankfull channel depth (d), bankfull channel width (W_b), and bankfull discharge (Q_b) of the Bayah Formation fluvial system. Each estimated parameter represents maximum values of the intervals (IV 1–IV 7), which are divided by six distinct erosional surfaces (ES 1–ES 6). Type of fluvial bodies are Type 1: conglomerate-dominated packages, Type 2: conglomeratic sandstone packages, and Type 3: sandstone-dominated packages. Section and estimated parameters are on the basis of Adhiperdana (2018).

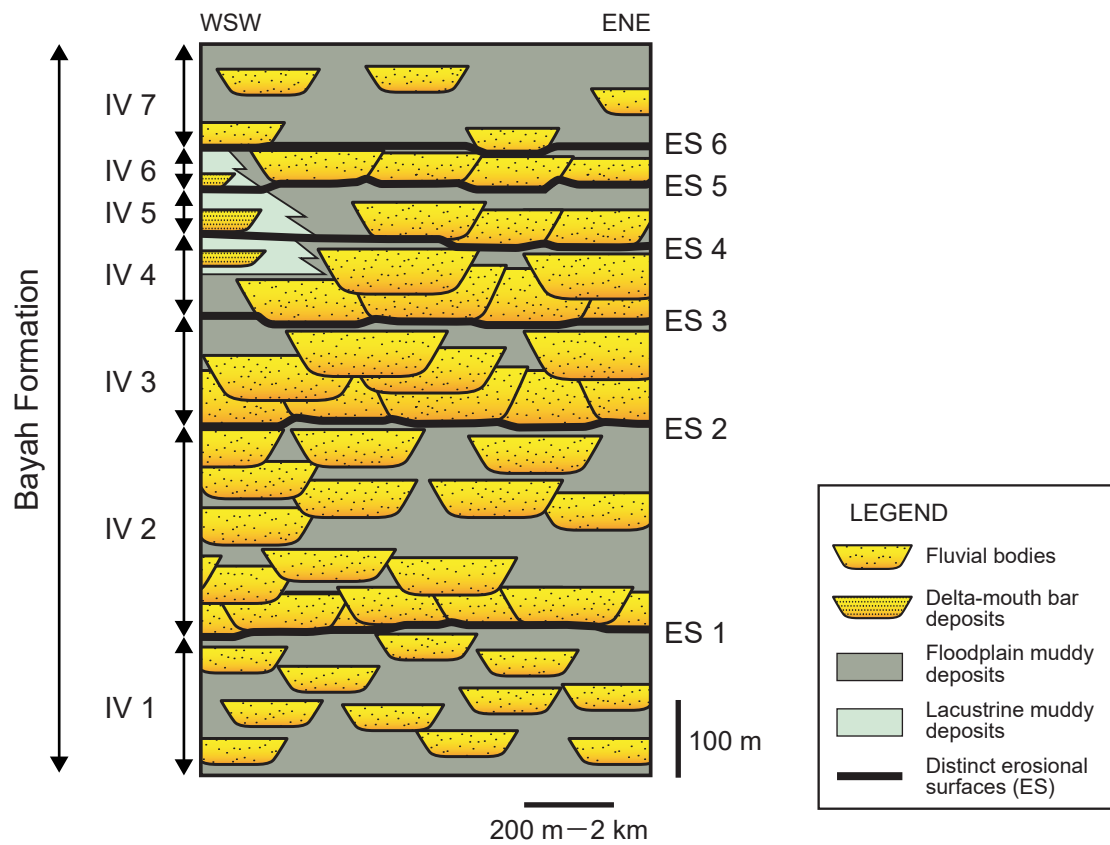
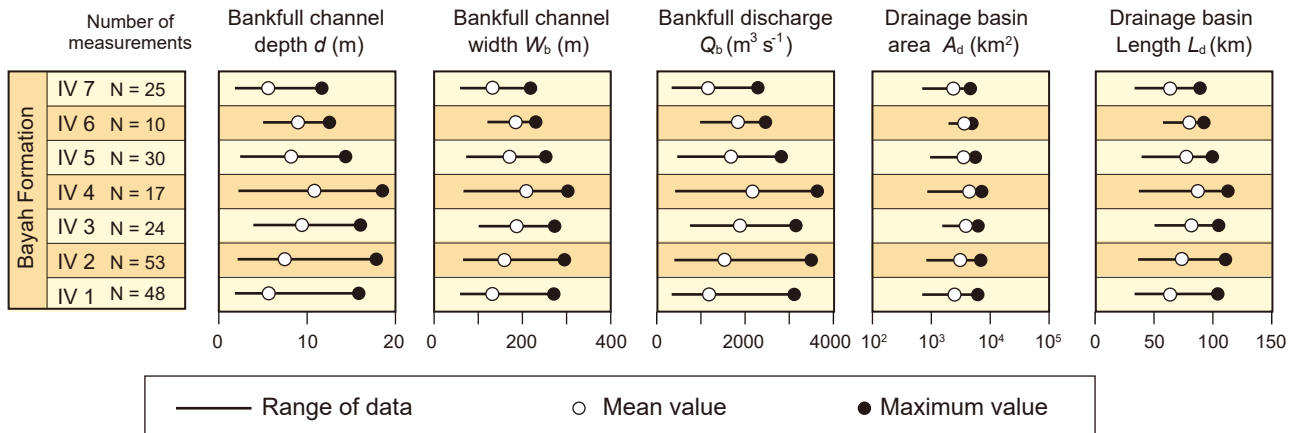


Fig. 36. Schematic illustration of the stacking pattern of the Bayah Formation fluvial bodies for each interval (IV 1 to IV 7). Stacking pattern is on the basis of Adhiperdana (2018).

A



B

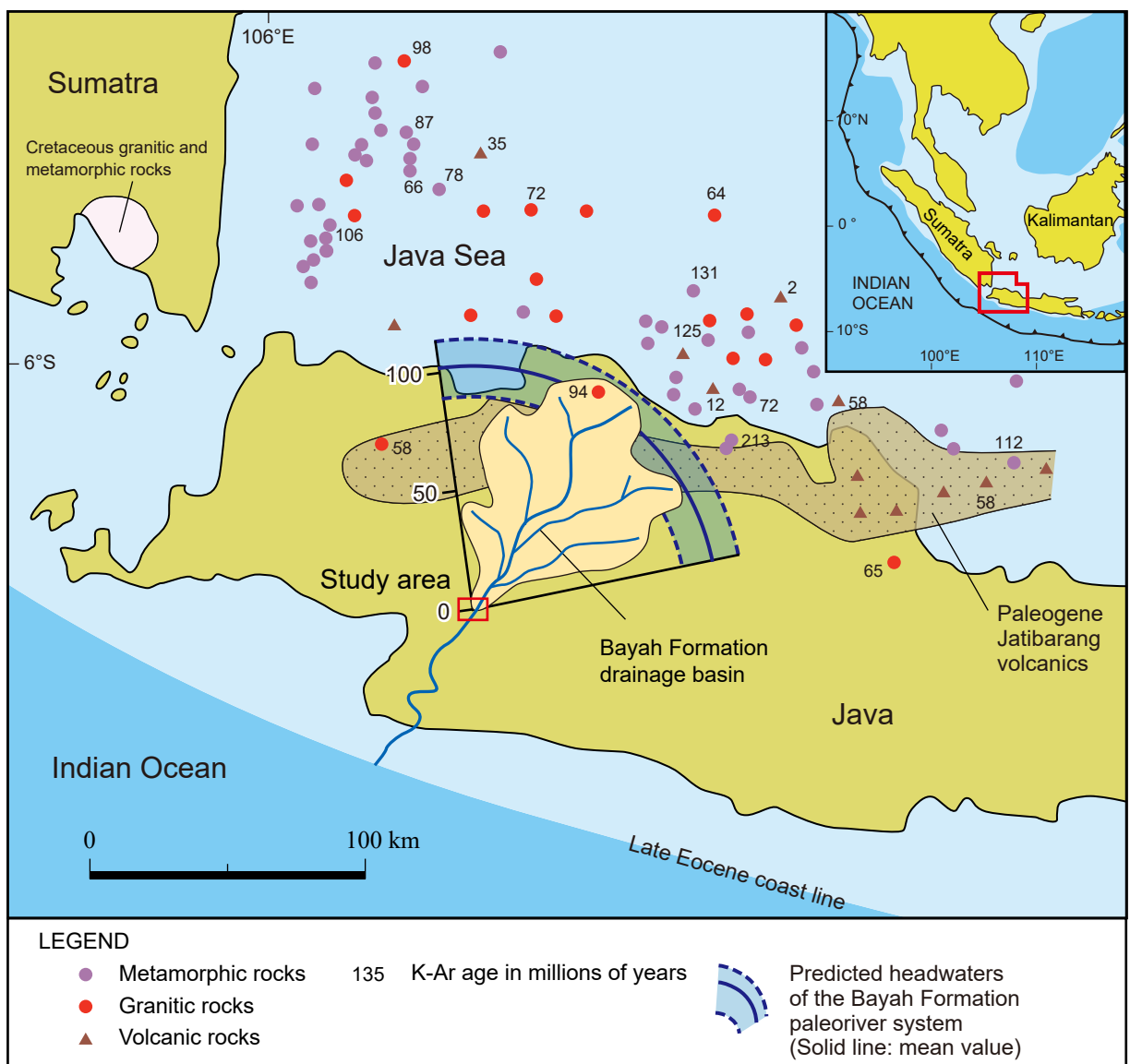


Fig. 37. A: Results of geomorphological and hydrological analyses of the Bayah Formation fluvial system. IV: Interval, N: number of measurements for bar deposit thickness. B: Predicted headwaters and drainage basin of the Bayah Formation paleoriver system based on the estimated maximum values of drainage basin area and length for each interval. Distribution of basement rocks and their K-Ar ages are based on Hamilton (1979) and Isotopic Ages Database by Southeast Asia Research Group, Royal Holloway University of London (<http://searg.rhul.ac.uk/current-research/isotopic-ages/>). Location of the Paleogene Jatibarang volcanics, and a late Eocene coastal line are after Soeria-Atmadja and Noeradi (2005) and Hall (2012), respectively.

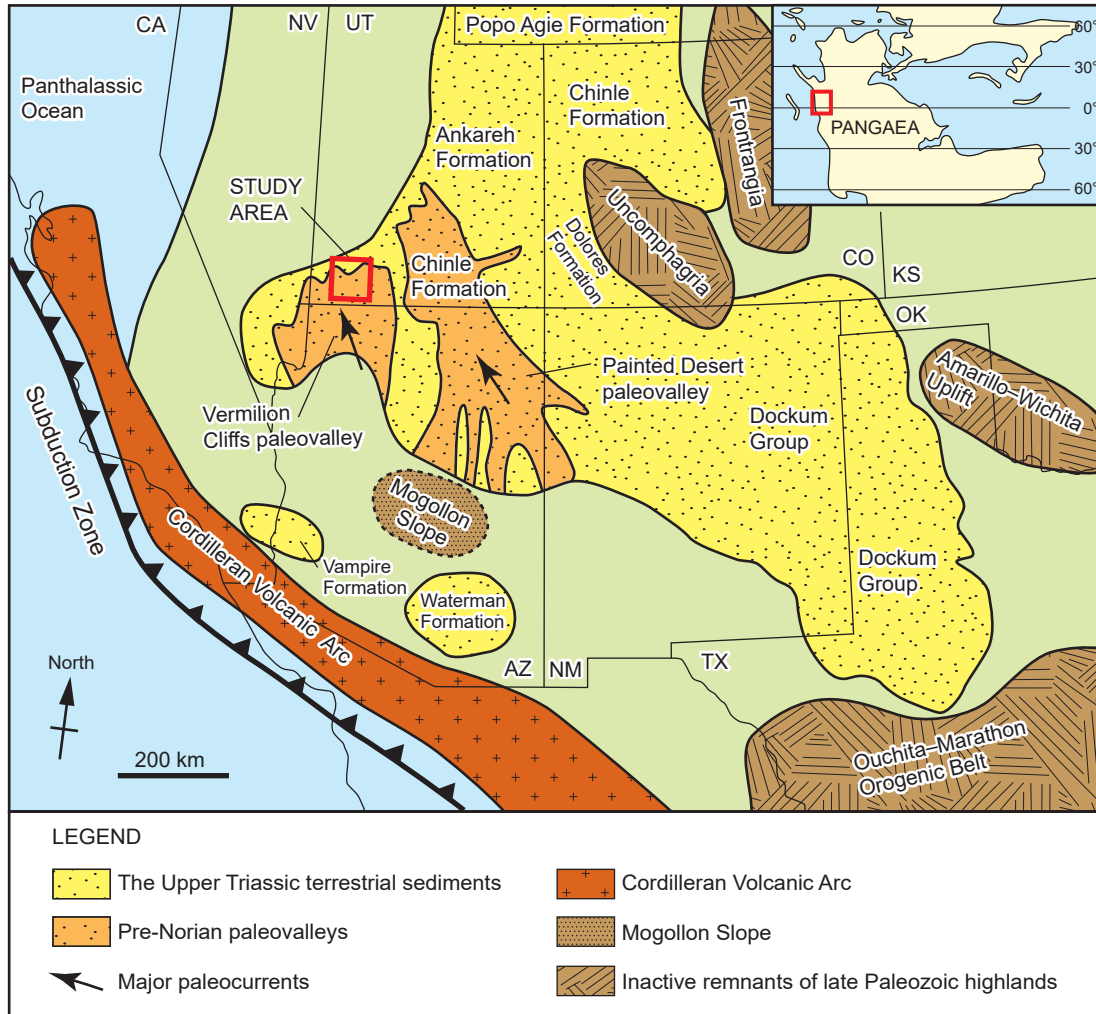


Fig. 38. Late Triassic paleogeography of the southwestern United States and distribution of the Upper Triassic terrestrial strata (modified from Martz et al., 2017). Inset map in the upper right indicates the distribution of the Pangaea during Triassic (modified from Trendell et al., 2012).

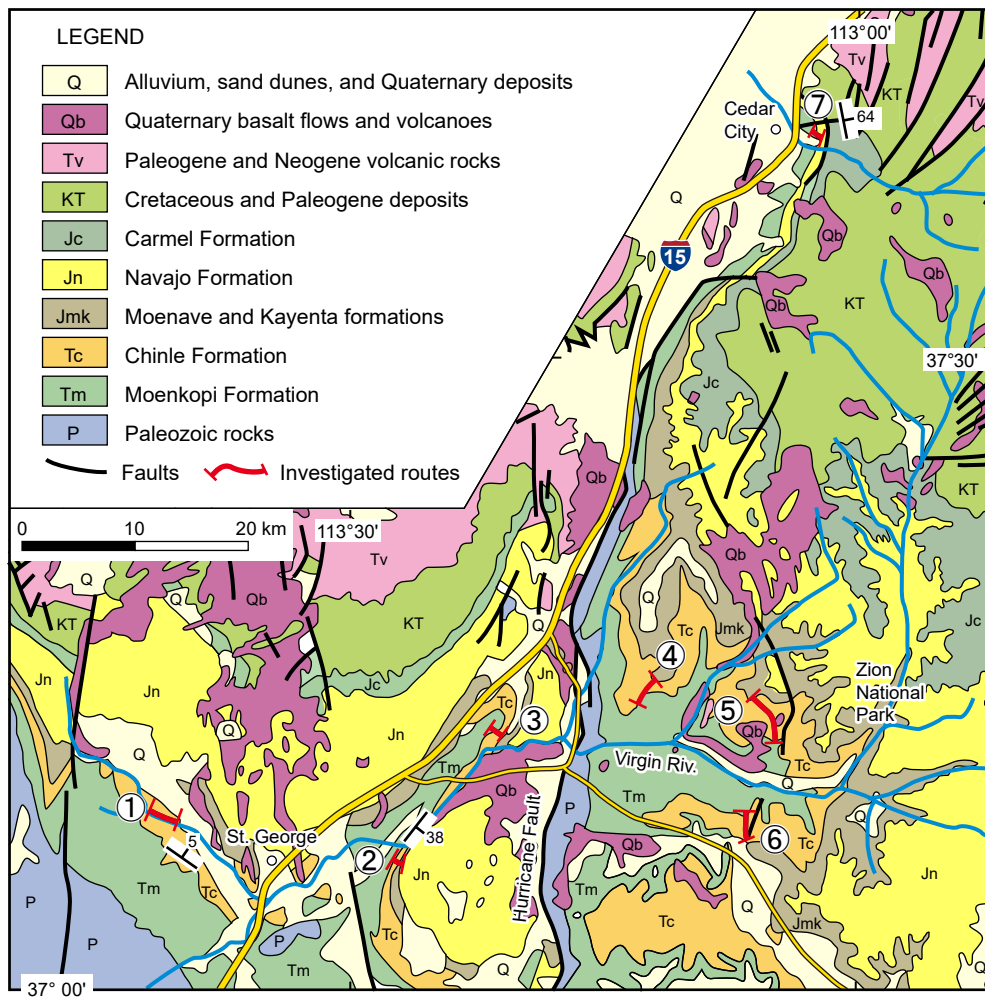


Fig. 39. Geologic map of the study area (simplified from Hintze, 1997). Circled numbers indicate the investigated routes; 1: Anasazi Trail, 2: Long Valley Recreation Area, 3: East Reef, 4: Hurricane Mesa, 5: Rockville, 6: Smithsonian Butte, 7: Cedar City.

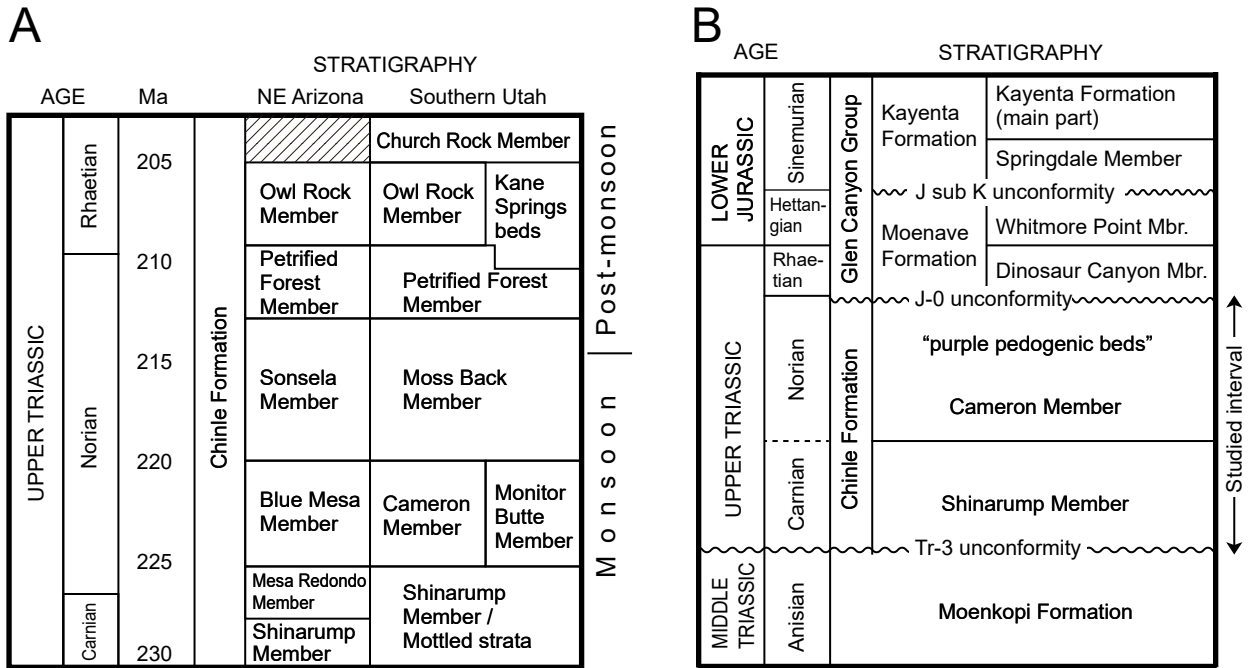


Fig. 40. A: Stratigraphy of the Upper Triassic in northeastern Arizona and southern Utah with an interpretation of climatic change. Data from Nordt et al. (2015) and Martz et al. (2017). B: Stratigraphy of the Middle Triassic–Lower Jurassic strata in southwestern Utah indicating the studied interval. Modified from Lucas and Tanner (2007) and Martz et al. (2017).

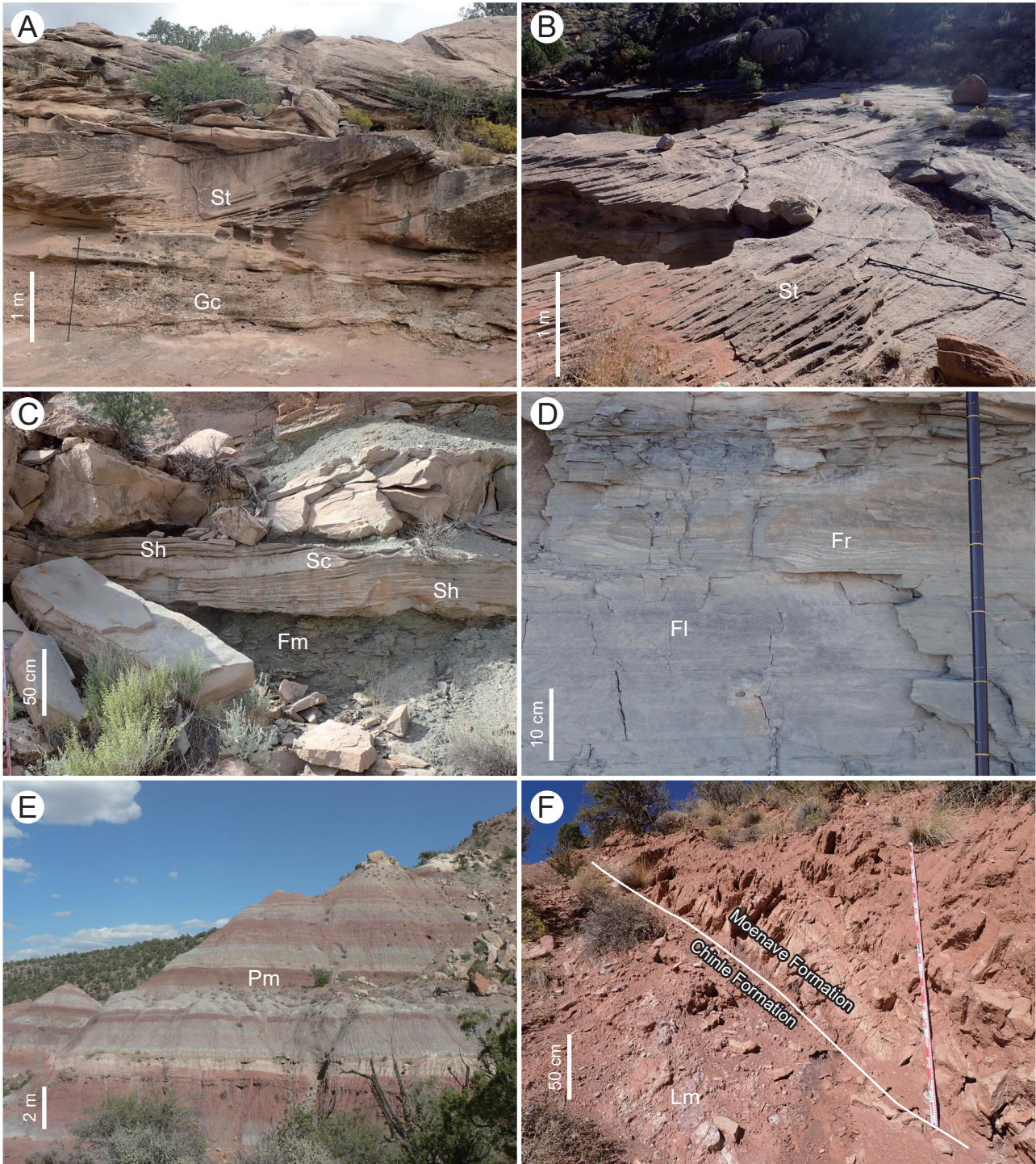


Fig. 41. Lithofacies types of the Chinle Formation. A: Clast-supported conglomerates (Gc) and trough cross-stratified sandstones (St) in the Shinarump Member at Route 5 (37°09'53.3"N, 113°01'33.5"W). B: Surface view of trough cross-stratified sandstones (St) in the Shinarump Member at Route 5 (37°10'25.4"N, 113°02'10.7"W). C: Horizontally stratified sandstones (Sh), sandstones with convoluted laminations (Sc), and massive mudstones (Fm) in the Shinarump Member at Route 4 (37°14'20.8"N, 113°12'30.1"W). D: Current ripple cross-laminated (Fr), and horizontally laminated (Fl), very fine-grained sandstones in the Shinarump Member at Route 4 (37°14'18.3"N, 113°12'30.1"W). E: Multi-colored massive mudstones (Pm) in the Cameron Member at Route 6 (37°07'34.0"N, 113°06'28.4"W). F: Massive limestone (Lm) in the "purple pedogenic beds" at Route 7 (37°40'27.3"N, 113°02'31.3"W). See Table 13 for descriptions and interpretations of the lithofacies types. See Fig. 39 for the investigated routes.

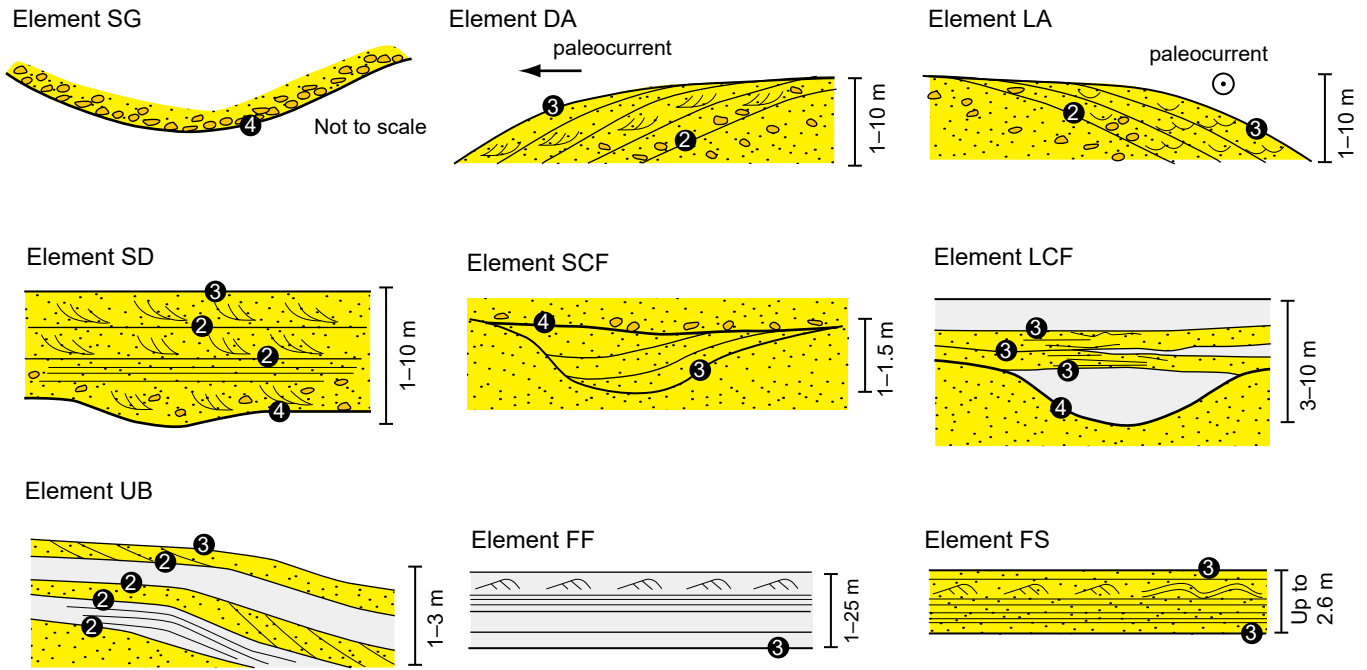


Fig. 42. Schematic illustration of architectural element types. Element SG: Scoured surface with gravel lags. Element DA: Downstream accreting, cross-stratified sandstones. Element LA: Laterally accreting, cross-stratified sandstones. Element SD: Sandy bedforms. Element SCF: Small-scale channel-fill deposits. Element LCF: Large-scale channel-fill deposits. Element UB: Upper bar deposits. Element FF: Floodplain muddy deposits. Element FS: Floodplain sandy deposits. Circled numbers indicate hierarchy of bounding-surface (BS) types. See Table 14 for descriptions and interpretations of architectural element types.

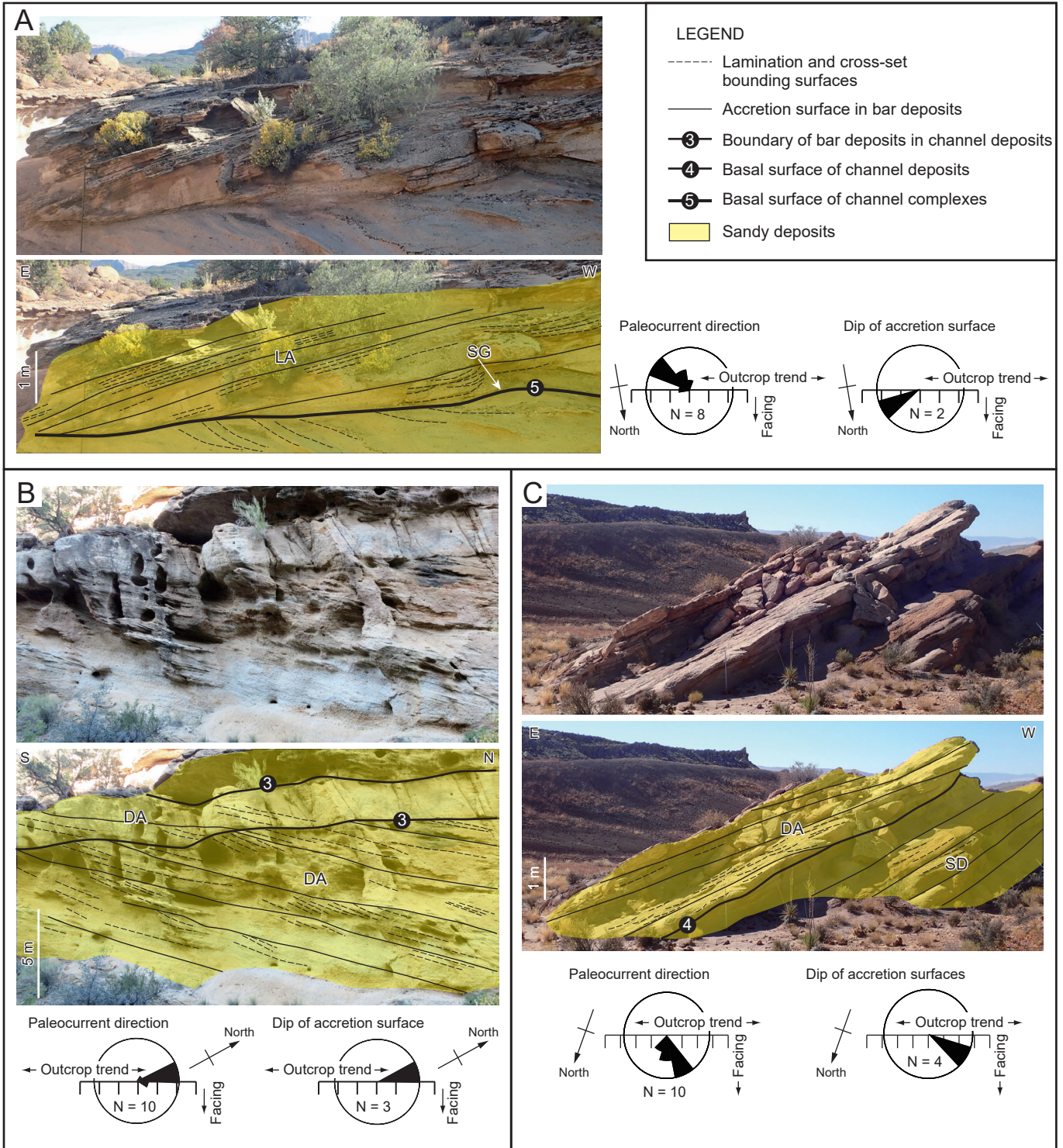


Fig. 43. A: Scoured surface with clast-supported gravel lags (SG) and laterally accreting, cross-stratified sandstones (LA) in the Shinarump Member at Route 5 (37°10'18.0"N, 113°02'00.6"W). B: Downstream accreting, cross-stratified sandstones (DA) in the Shinarump Member at Route 6 (37°08'06.8"N, 113°06'12.2"W). C: DA and sandy bedforms (SD) in the Cameron Member at Route 3 (37°12'07.6"N, 113°21'14.8"W). N in rose diagrams indicates the number of measurements. See Fig. 39 for the investigated routes.

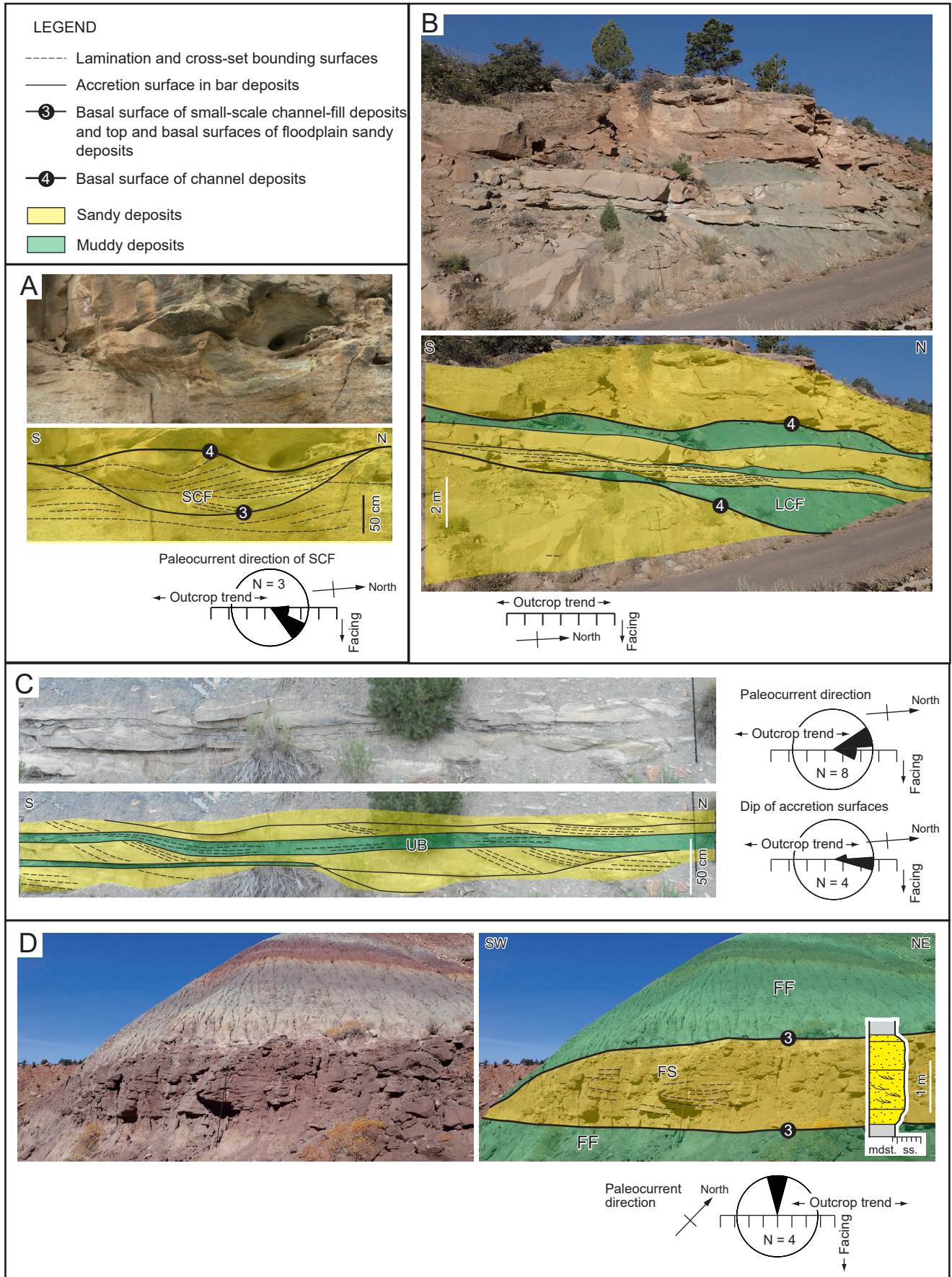


Fig. 44. A: Small-scale channel-fill deposits (SCF) in the Shinarump Member at Route 4 (37°14'19.9"N, 113°12'29.8"W). B: Large-scale channel-fill deposits (LCF) in the Shinarump Member at Route 4 (37°14'20.8"N, 113°12'30.1"W). C: Upper bar deposits (UB) in the Shinarump Member at Route 4 (37°14'17.0"N, 113°12'30.3"W). D: Floodplain muddy deposits (FF) and floodplain sandy deposits (FS) in the Cameron Member at Route 4 (37°14'33.6"N, 113°11'44.2"W). N in rose diagrams indicates the number of measurements. See Fig. 39 for the investigated routes.

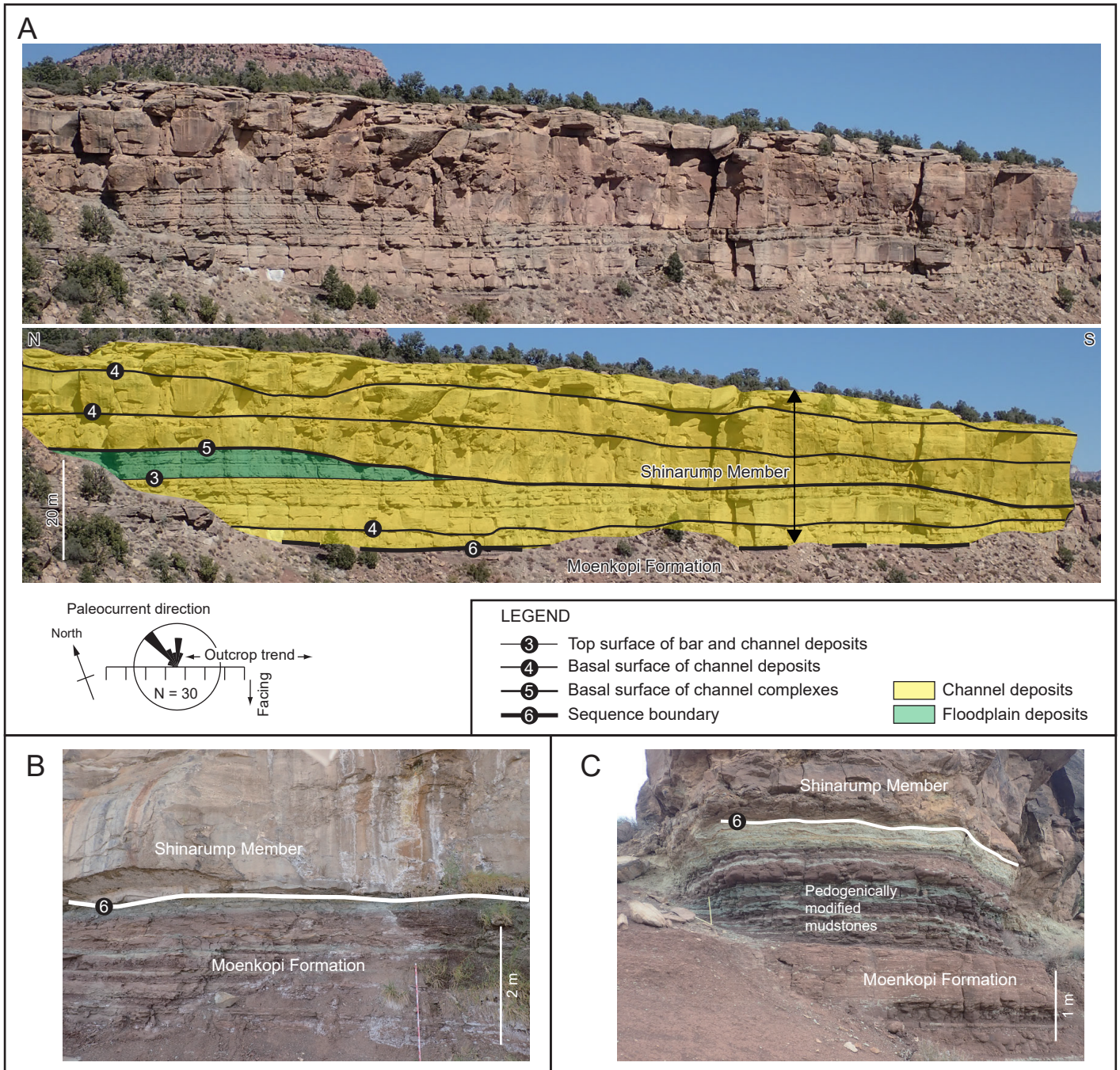


Fig. 45. A: Panorama photograph of the Shinarump Member at Route 4 ($37^{\circ}14'17.1''\text{N}$, $113^{\circ}12'18.7''\text{W}$). N in rose diagram indicates the number of measurements. B: Basal unconformity of the Chinle Formation on which a channel complex of the Shinarump Member overlies unsoiled sandstones and mudstones of the Moenkopi Formation. Route 4 ($37^{\circ}14'11.9''\text{N}$, $113^{\circ}12'31.0''\text{W}$). C: Basal unconformity of the Chinle Formation on the pedogenically modified mudstones of the uppermost part of the Moenkopi Formation. Route 5 ($37^{\circ}09'48.9''\text{N}$, $113^{\circ}01'29.3''\text{W}$). See Fig. 39 for the investigated routes.

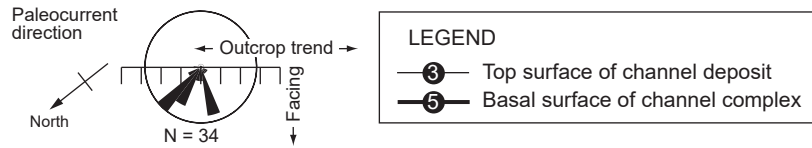
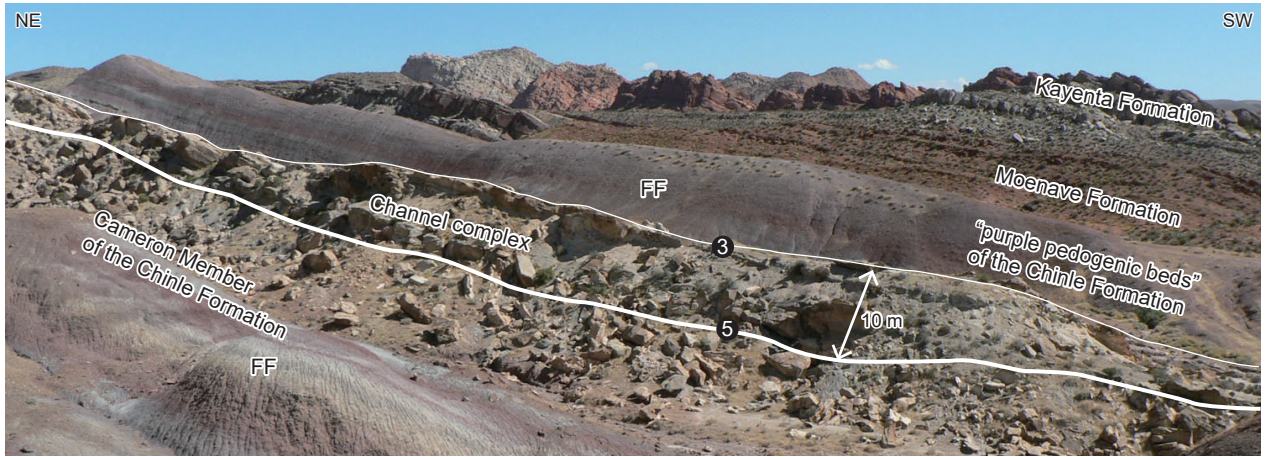


Fig. 46. Panorama photograph of the Cameron Member and "purple pedogenic beds" at Route 3 (37°12'11.5"N, 113°21'13.4"W). FF indicates floodplain muddy deposits. N in rose diagram indicates the number of measurements. See Fig. 39 for the investigated route.

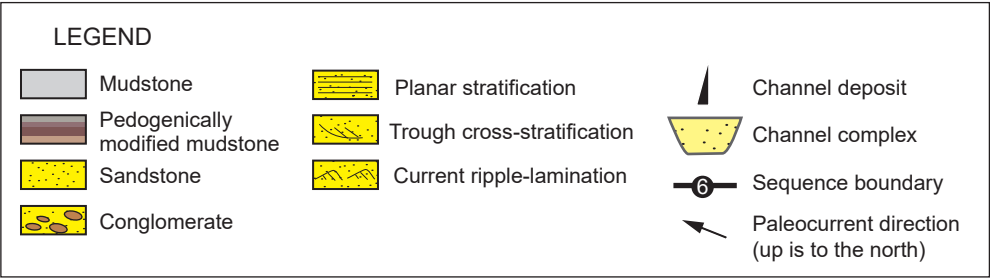
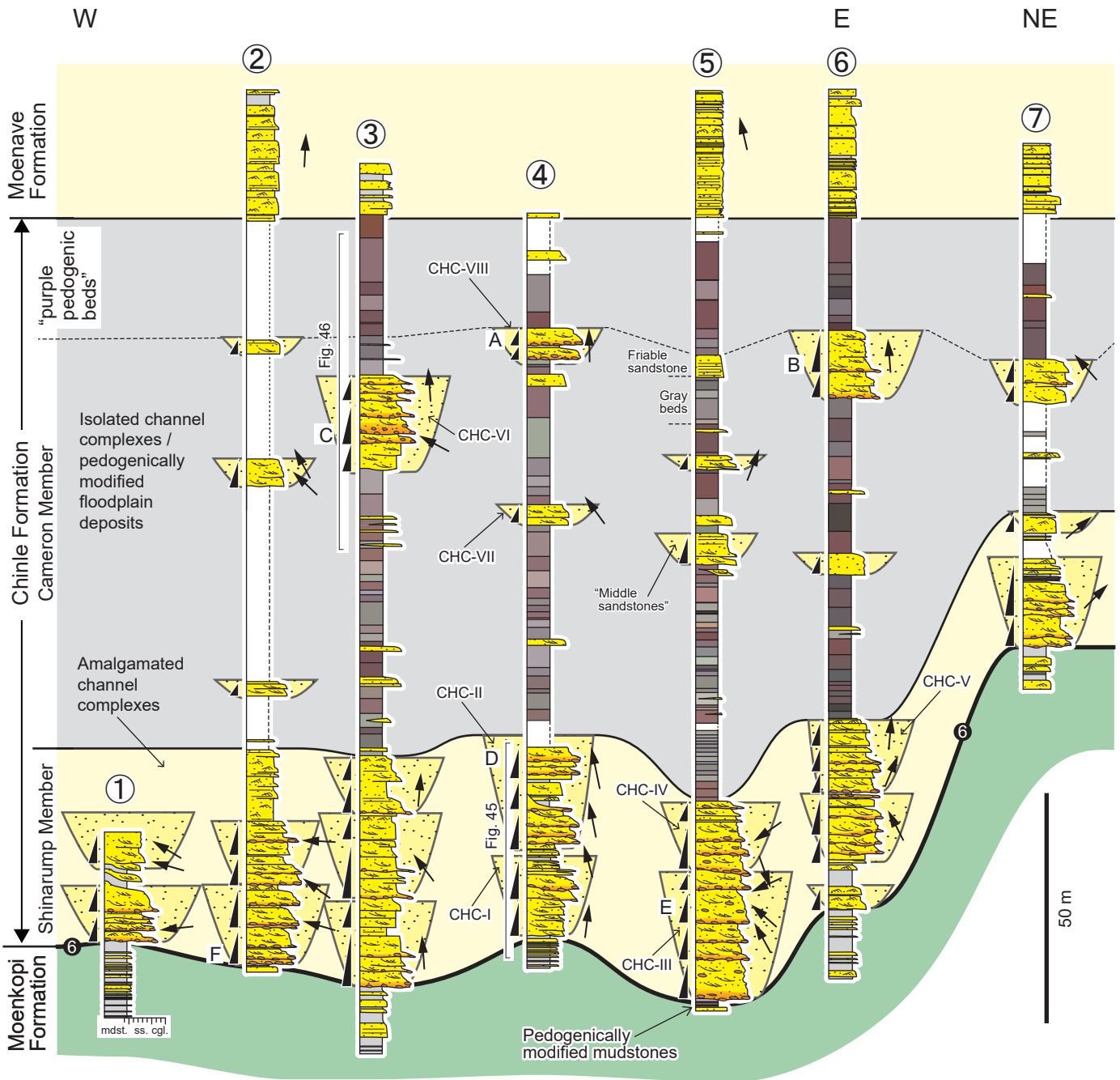


Fig. 47. Stratigraphic cross-section of the Chinle Formation. Circled numbers indicate the investigated routes shown in Fig. 39. Paleocurrent directions are averages of 5–10 measurements. CHC I–VIII indicates channel complexes in which paleohydrological analyses were conducted. See Fig. 48 for the results. A–F indicates sampling horizons for clast composition (Fig. 50). Friable sandstone, gray beds, and ‘middle sandstones’ in Route 5 are after Martz et al. (2017).

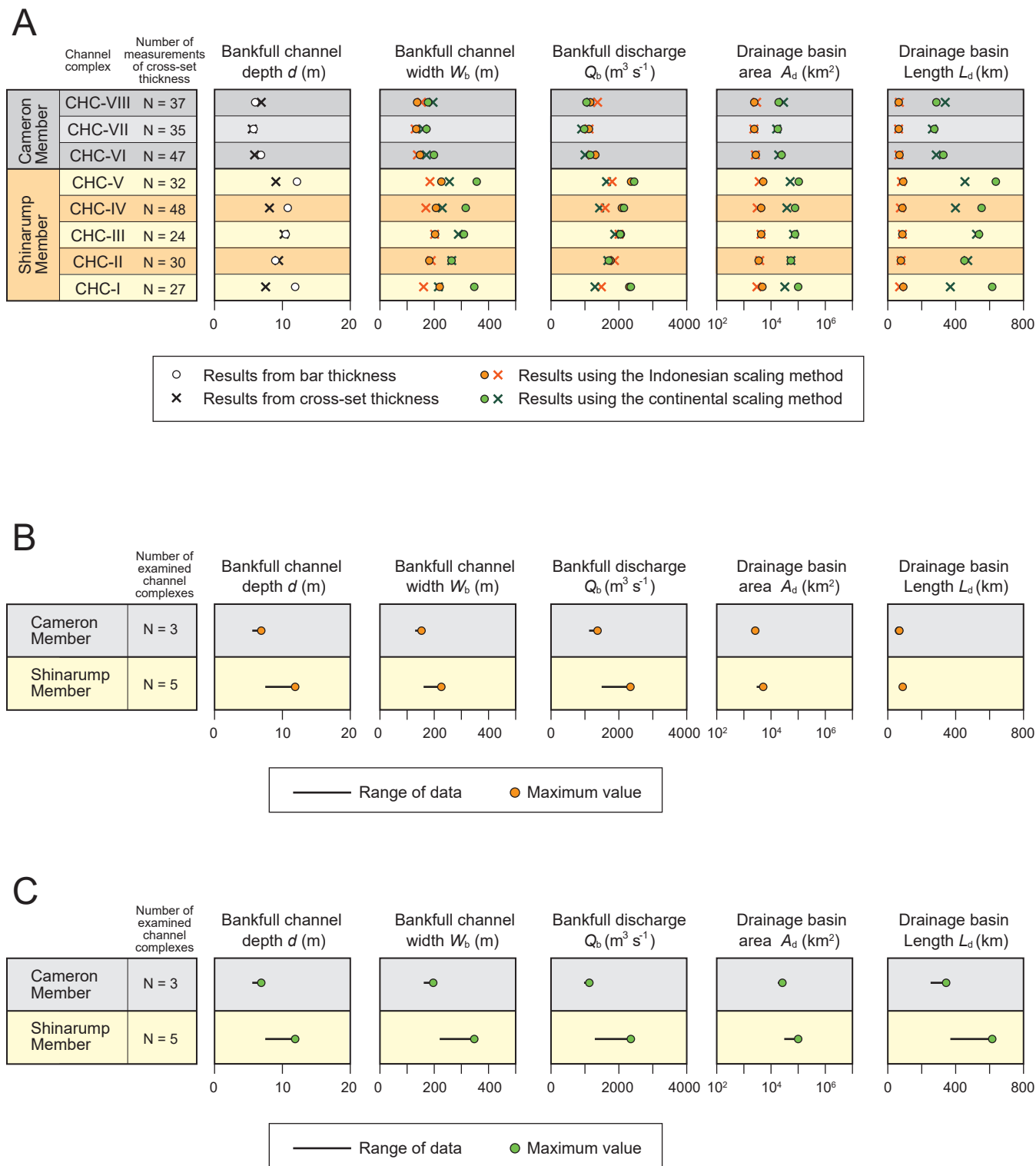


Fig. 48. Results of geomorphological and hydrological analyses of the Chinle Formation fluvial system. A: Estimated values for each examined channel complex. B: Estimated values for the Shinarump and Cameron members fluvial channels by the Indonesian scaling method. C: Estimated values for the Shinarump and Cameron members fluvial channels by the continental scaling method.

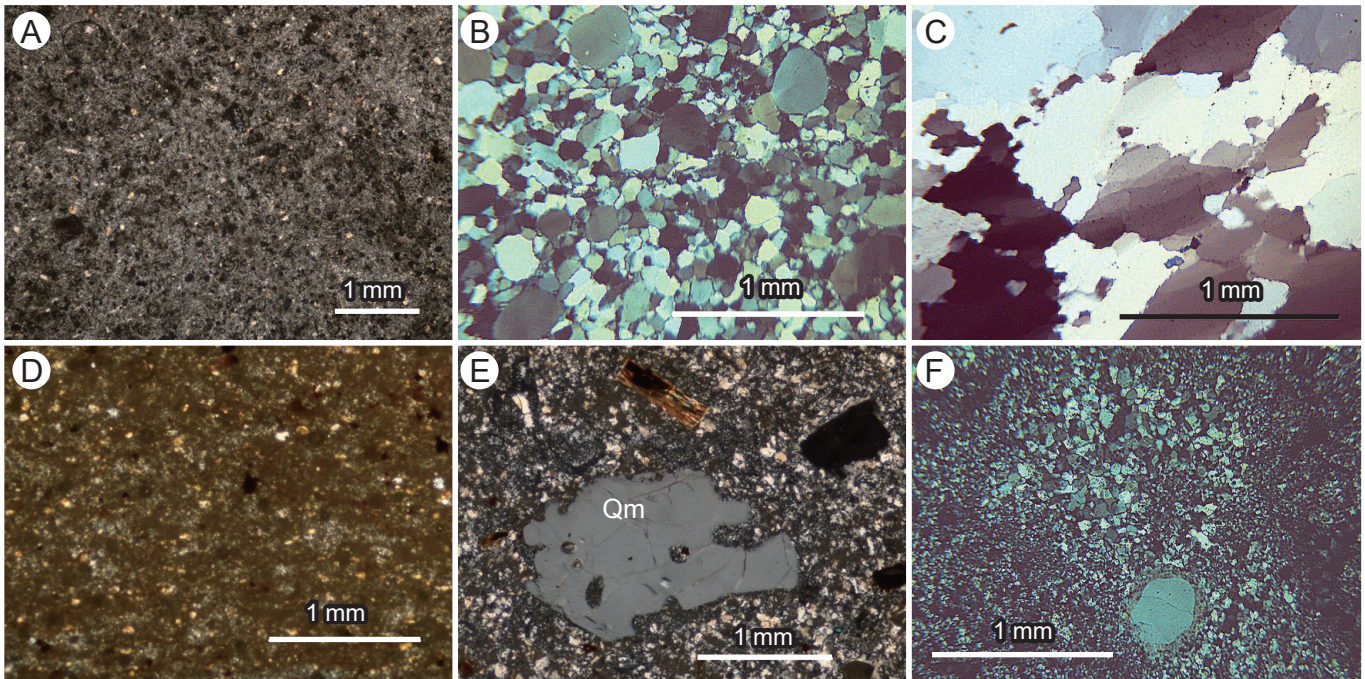


Fig. 49. Cross-polarized microscopic photographs of thin sections of conglomerate clasts from the Chinle Formation. A: Chert from the Cameron Member at Route 3. B: Quartzite from the Shinarump Member at Route 4. C: Polycrystalline quartz from the Shinarump Member at Route 4. D: Mudstone from the Cameron Member at Route 3. E: Acidic (rhyolitic) volcanic rock fragment showing felsitic texture including embayed monocrystalline quartz (Qm) from the Cameron Member at Route 3. F: Acidic vitric tuff with clots of quartz and/or feldspar (devitrification feature) from the Shinarump Member at Route 4. See Fig. 39 for the investigated routes.

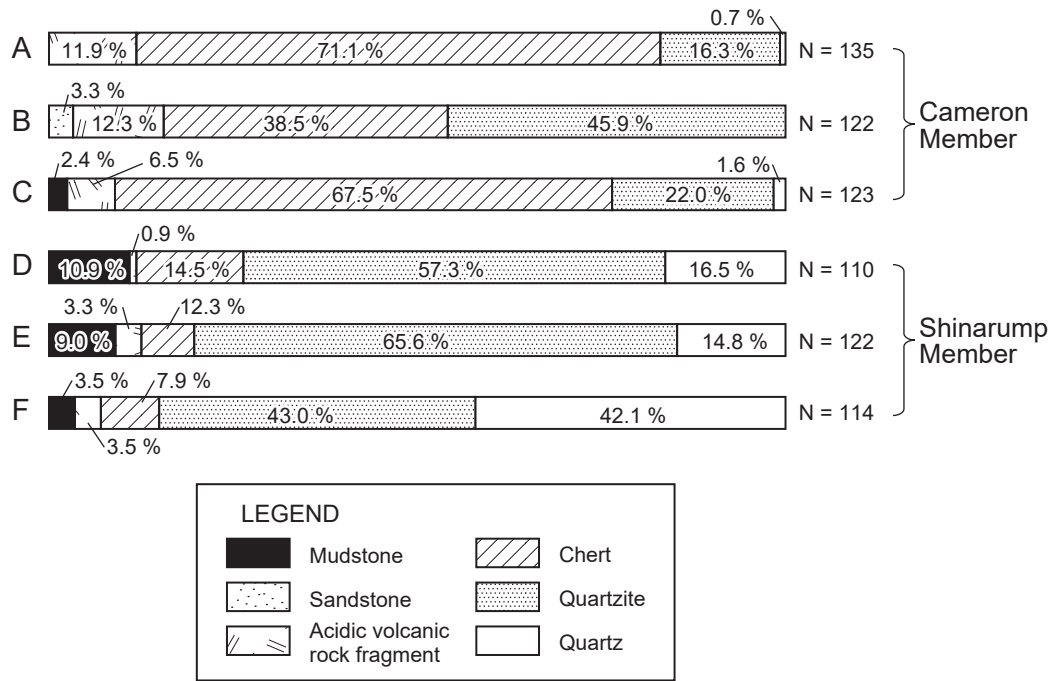


Fig. 50. Clast composition of conglomerates in the Chinle Formation. See Fig. 47 for the sampling locations and horizons.

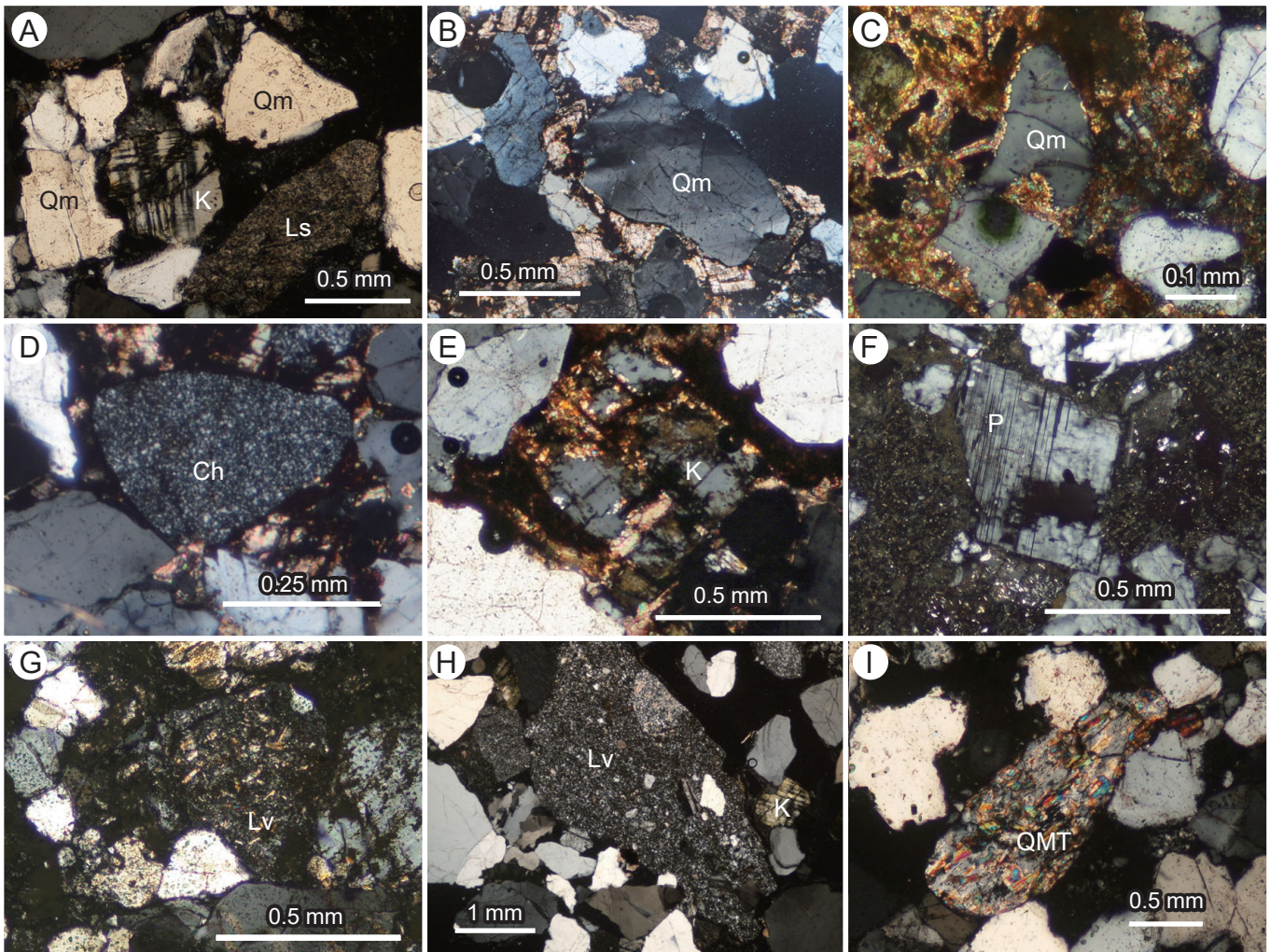


Fig. 51. Cross-polarized microscopic photographs of thin-sections of sandstone samples from the Chinle Formation. A: Monocrystalline quartz (Qm), K-feldspar (K), and sedimentary lithic fragment (Ls), the Cameron Member at Route 3, ER-Cs13. B: Qm with undulose extinction, the Shinarump Member at Route 6, SB-Ss16. C: Embayed Qm with rounded outline, the Cameron Member at Route 6, SB-Cs01. D: Chert (Ch), the Shinarump Member at Route 6, SB-Ss16. E: Partially dissolved K surrounded and replaced by authigenic clay minerals, the Shinarump Member at Route 6, SB-Ss12. F: Plagioclase feldspar (P), the Cameron Member at Route 3, ER-Cs05. G: Intersertal (felted) volcanic lithic fragment (Lv) with dull appearance, the Cameron Member at Route 3, ER-Cs05. H: Lv with felsitic texture, the Cameron Member at Route 3, ER-Cs13. I: Quartz-mica tectonite (QMT), the Shinarump Member at Route 6, SB-Ss06. See Fig. 39 for the investigated routes.

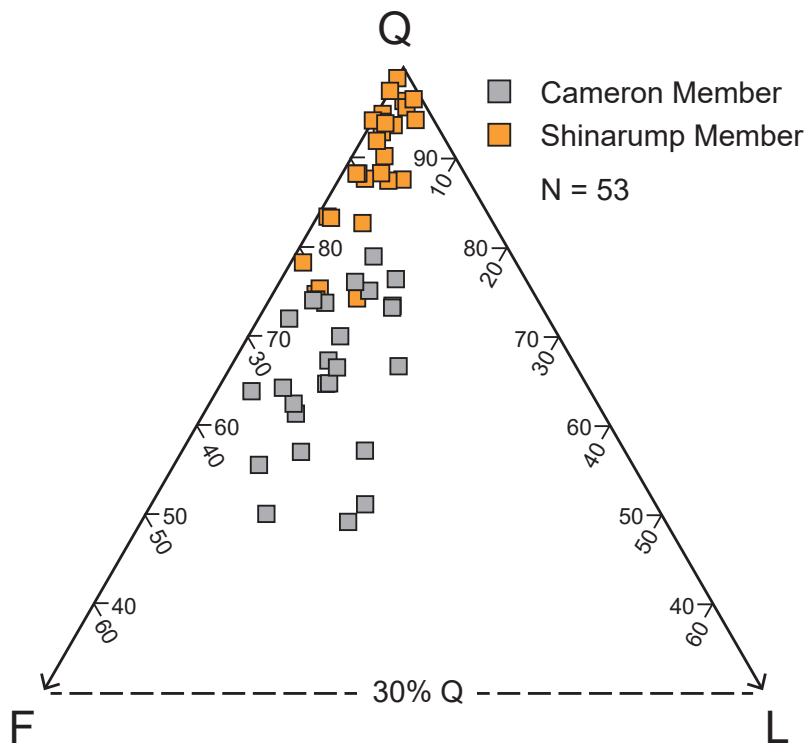


Fig. 52. Triangular QFL plot of the Chinle Formation sandstones. Q is total quartzose grains including monocrystalline quartz (Qm), polycrystalline quartz (Qp) (sub-grains < 0.063 mm), tectonic quartz (QT) (sub-grains < 0.063 mm), and sedimentary chert (Ch). F is total feldspar grains including plagioclase (P) and K-feldspar (K). L is total unstable lithic fragments including volcanic lithic fragment (Lv), sedimentary lithic fragment (Ls), and quartz-mica tectonite (QMT).

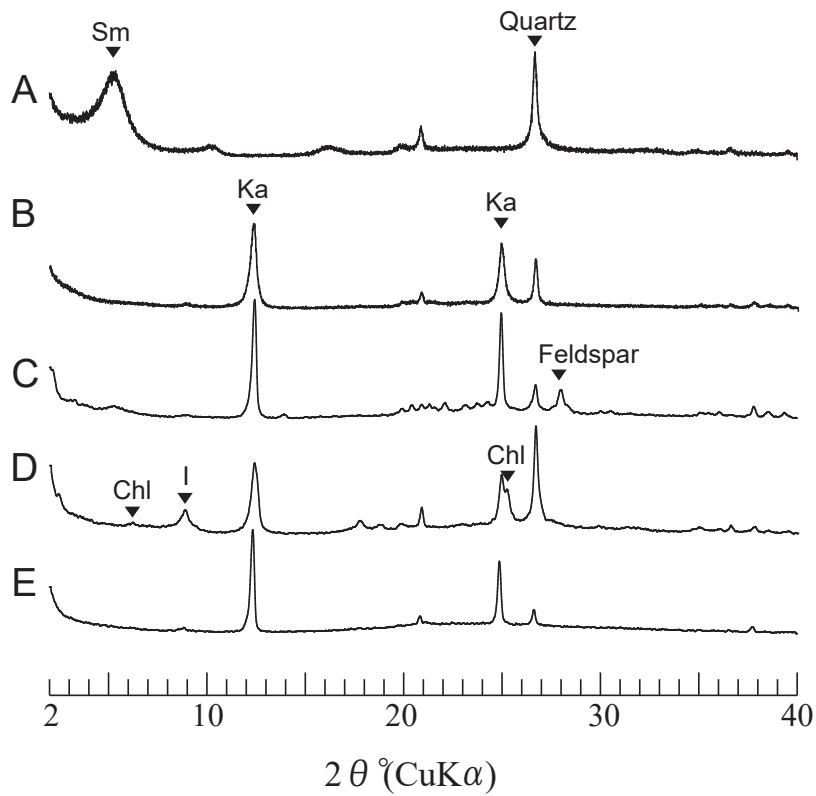


Fig. 53. Representative X-ray diffraction patterns (ethyleneglycol solvated) of sandstone and mudstone samples from the Chinle Formation. A: Mudstone sample from the "purple pedogenic beds" at Route 3, ER-Cm29. B: Mudstone sample from the Cameron Member at Route 3, ER-Cm04. C: Sandstone sample from the Cameron Member at Route 3, ER-Cs06. D: Mudstone sample from the Shinarump Member at Route 4, HM-Sm04. E: Sandstone sample from the Shinarump Member at Route 6, SB-Ss10. Ka: kaolinite, Chl: chlorite, I: illite, and Sm: smectite. See Fig. 39 for the investigated routes.

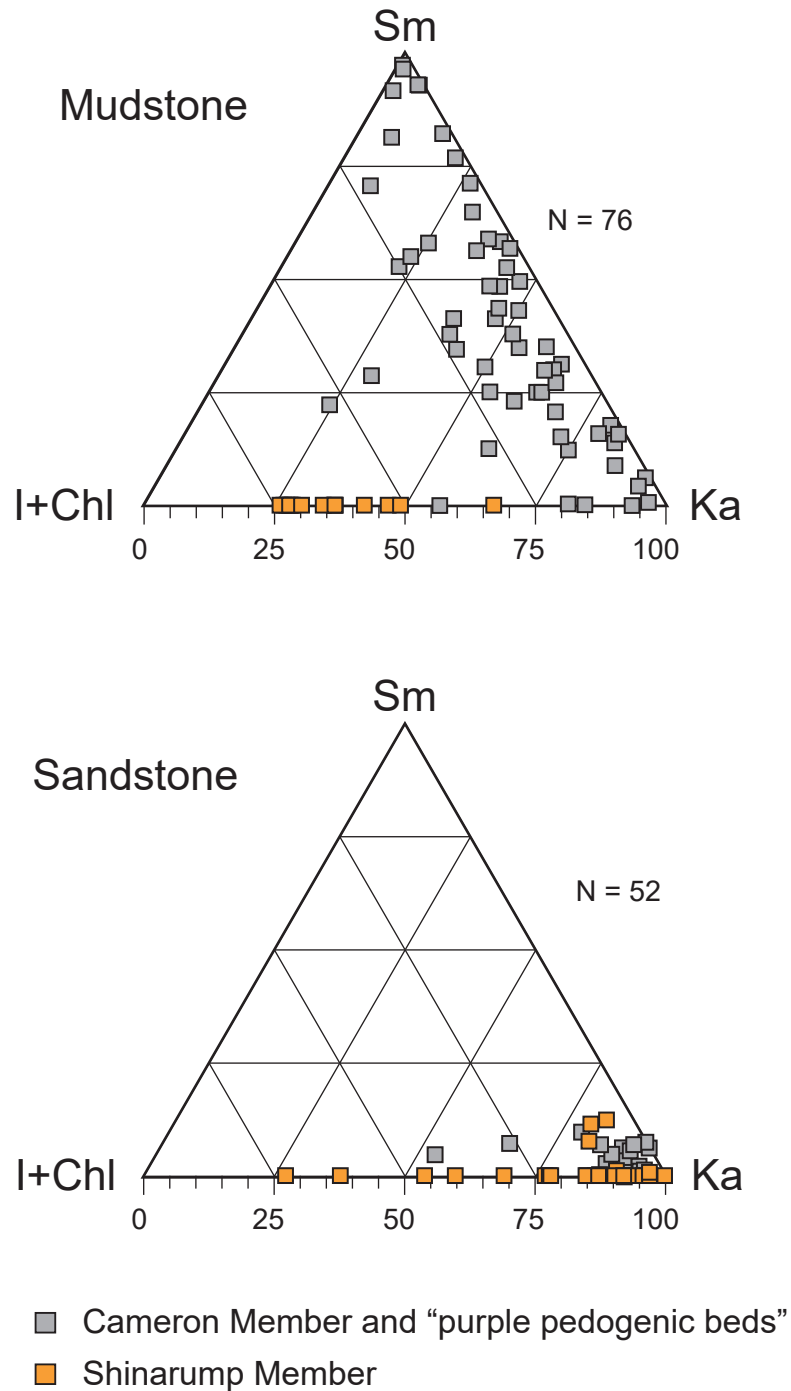


Fig. 54. Clay mineral composition of mudstone and sandstone samples of the Chinle Formation. Relative abundance of four major clay minerals was calculated following the method of Biscaye (1965). N indicates the number of data. Ka: Kaolinite, I: Illite, Chl: Chlorite, Sm: Smectite.

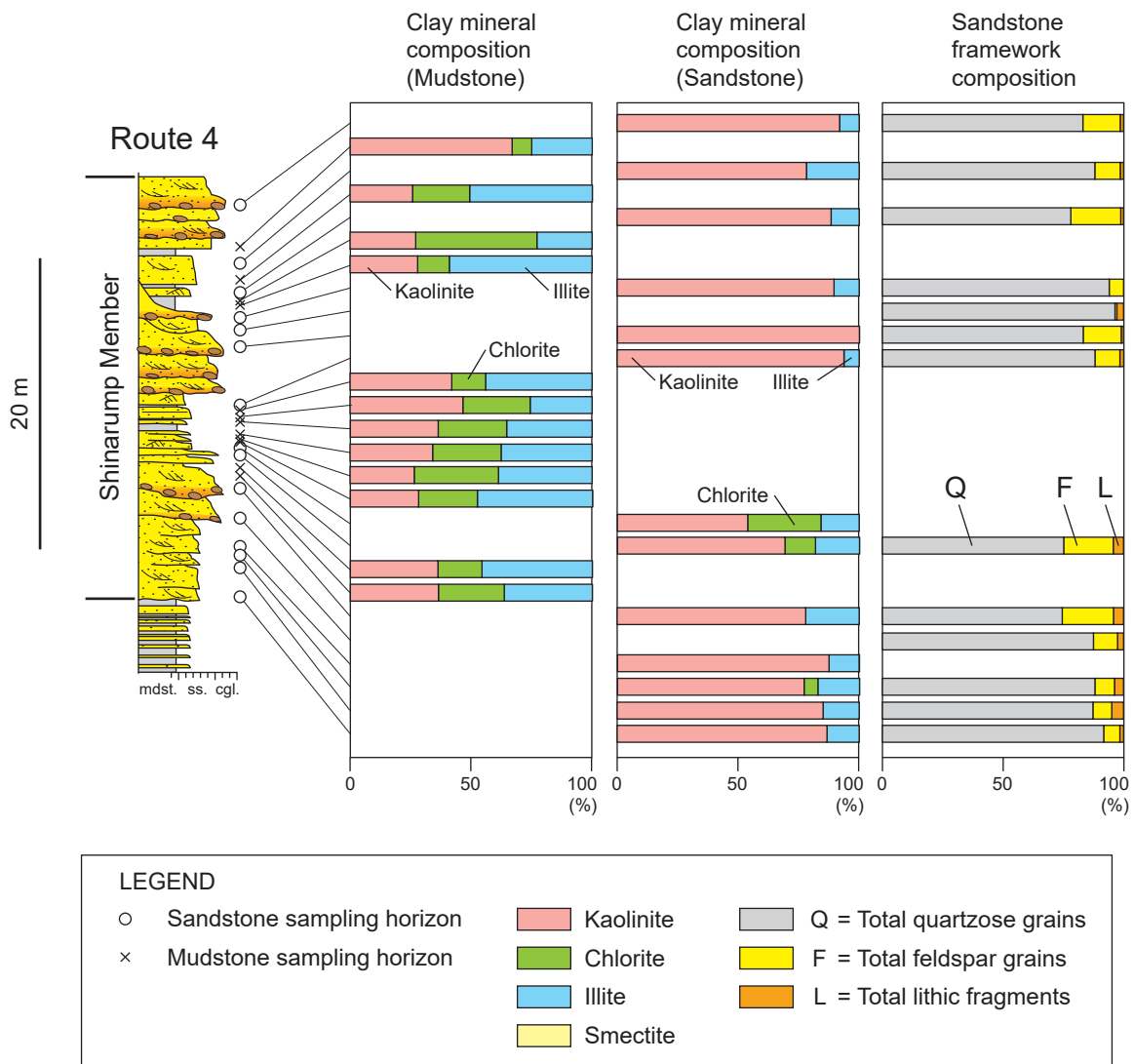


Fig. 55. Stratigraphic variations in clay mineral composition and sandstone framework composition of the Chinle Formation at Route 4 in Fig. 39. Relative abundance of four major clay minerals was calculated following the method of Biscaye (1965). See Fig. 47 for legend of section and Fig. 52 for Q, F, and L categories of framework grain types of sandstones.

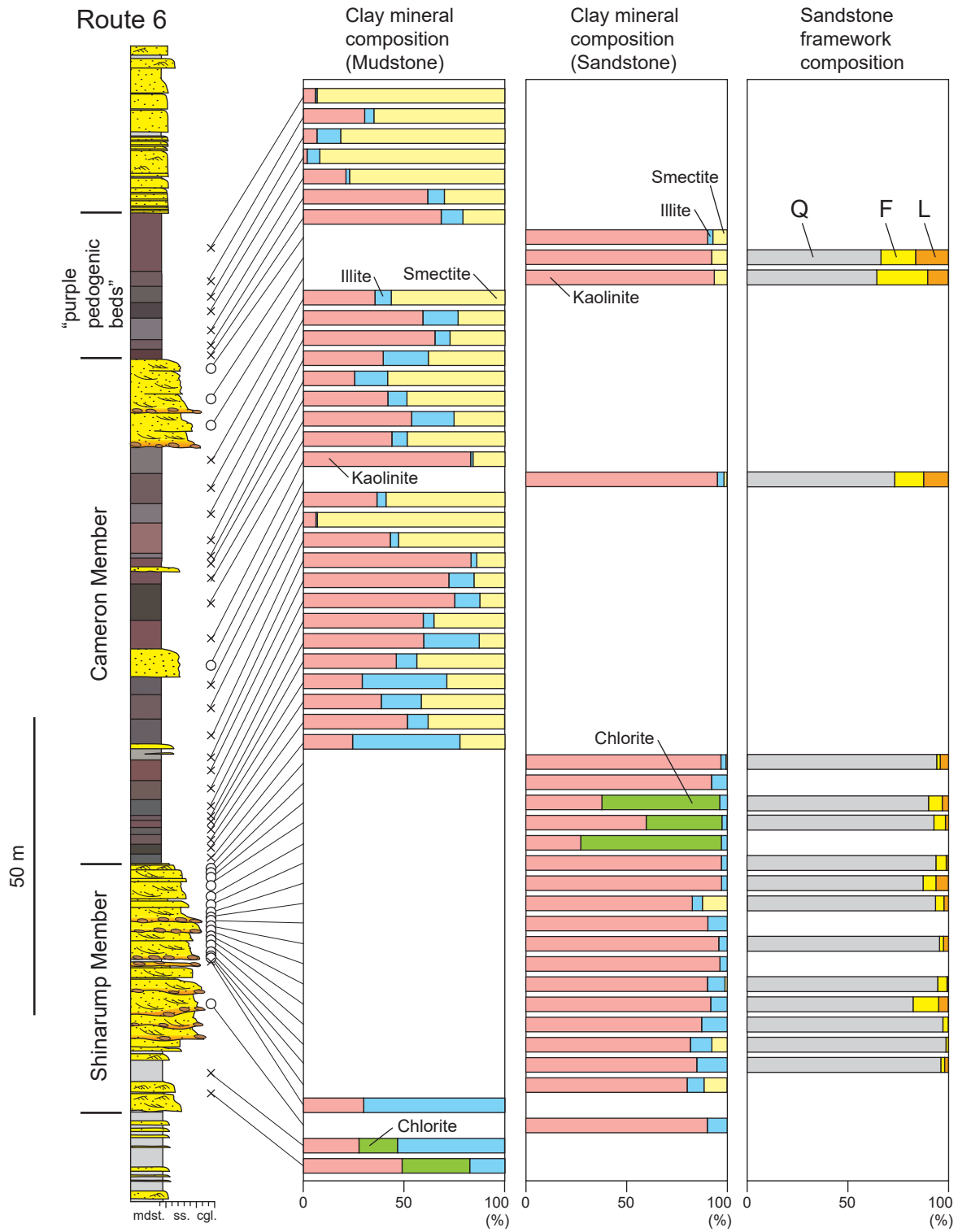


Fig. 56. Stratigraphic variations in clay mineral composition and sandstone framework composition of the Chinle Formation at Route 6 in Fig. 39. See Fig. 55 for legend of clay mineral composition and of framework grain types of sandstones, Fig. 47 for legend of section, and Fig. 52 for Q, F, and L categories of framework grain types of sandstones.

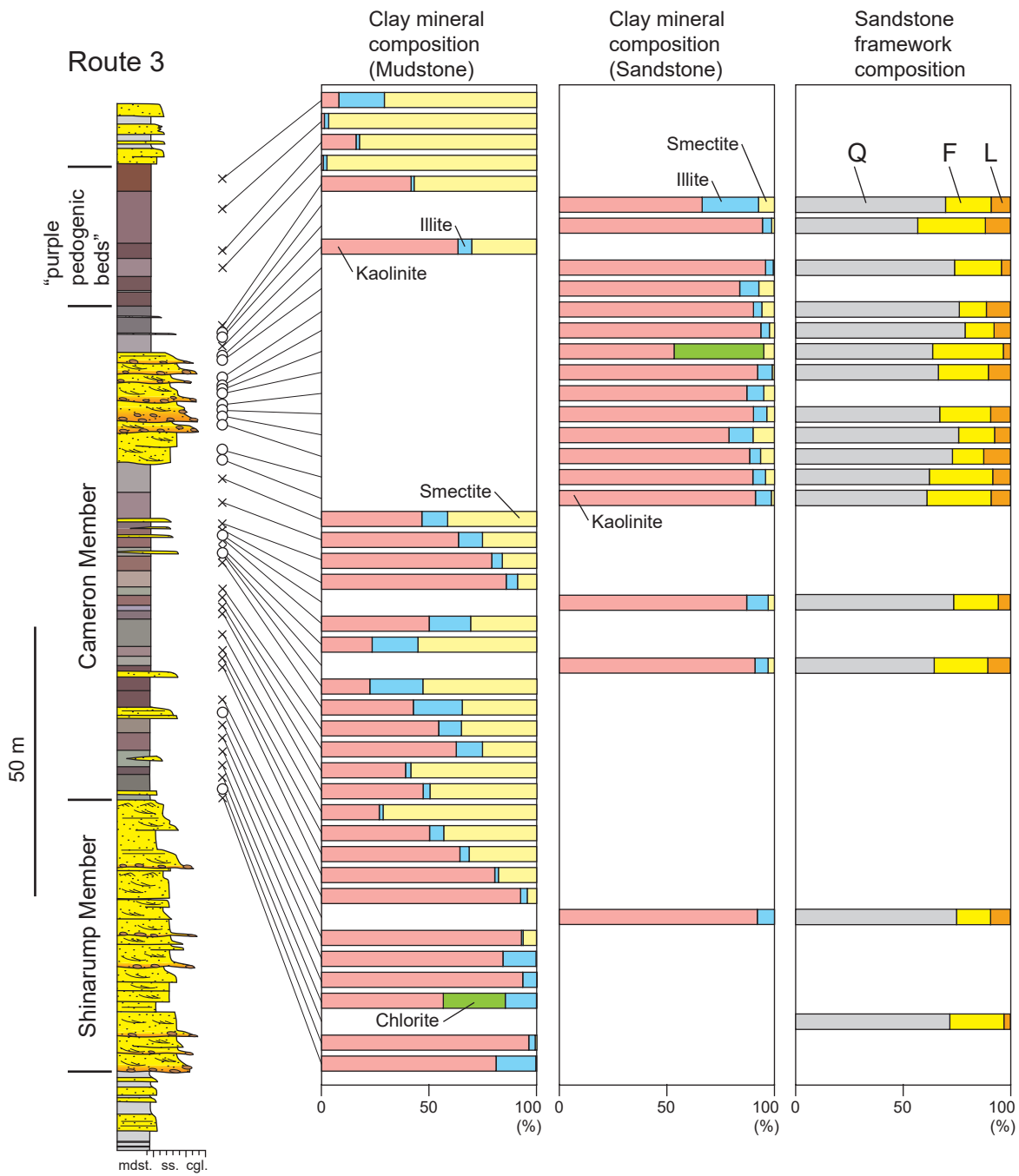


Fig. 57. Stratigraphic variations in clay mineral composition and sandstone framework composition of the Chinle Formation at Route 3 in Fig. 39. See Fig. 55 for legend of clay mineral composition and of framework grain types of sandstones, Fig. 47 for legend of section, and Fig. 52 for Q, F, and L categories of framework grain types of sandstones.

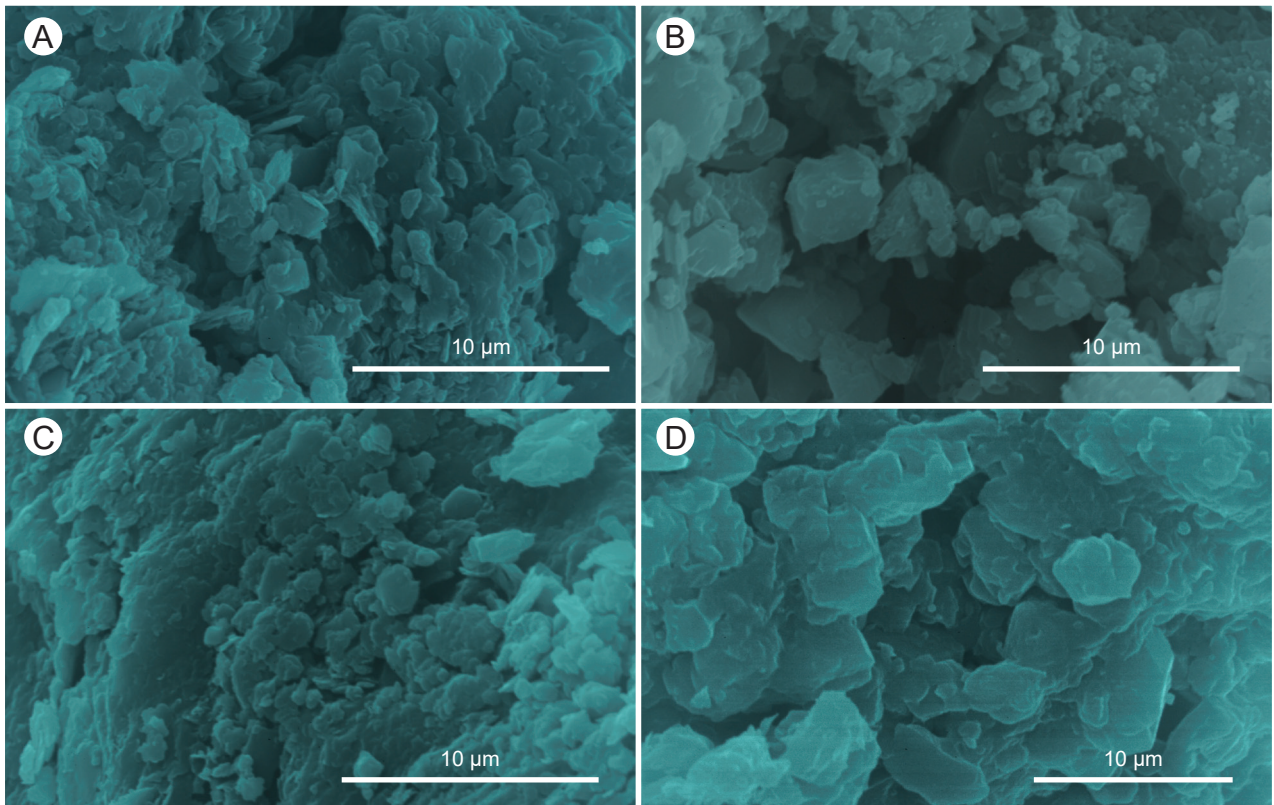


Fig. 58. Scanning electron microscopy (SEM) images of sandstone and mudstone samples from the Chinle Formation. A: Mudstone from the Shinarump Member at Route 4, HM-Sm09. B: Kaolinite-rich sandstone from the Cameron Member at Route 3, ER-Cs06. C: Kaolinite-rich mudstone from the Cameron Member at Route 3, ER-Cm04. D: Smectite-rich mudstone from the "purple pedogenic beds" at Route 3, ER-Cm29. See Fig. 38 for the investigated routes.

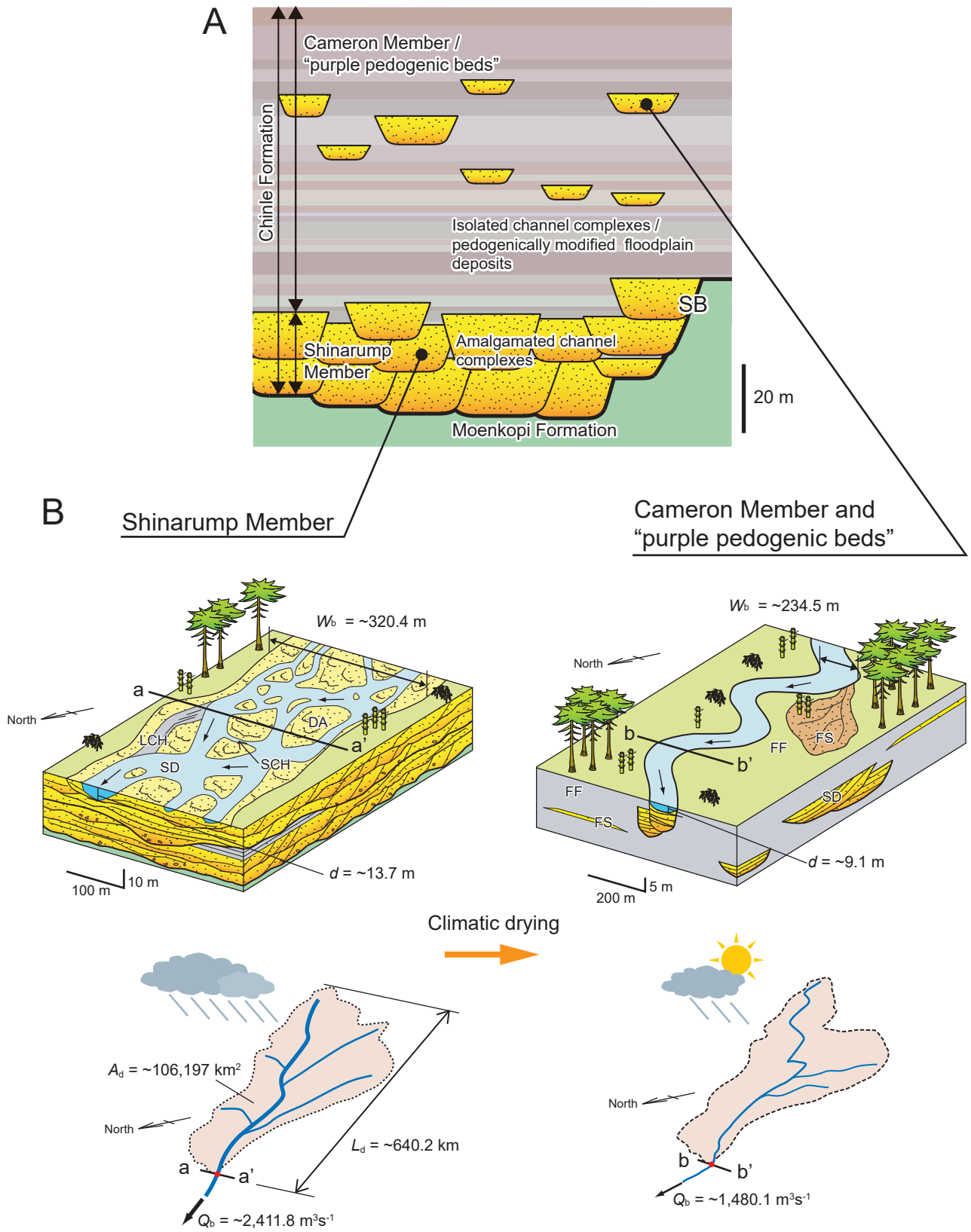


Fig. 59. A: Schematic illustration of stacking pattern of the Chinle Formation. B: Schematic illustrations of fluvial systems of the Shinarump Member, and the Cameron Member and “purple pedogenic beds” with paleohydrological parameters estimated by the continental scaling method.

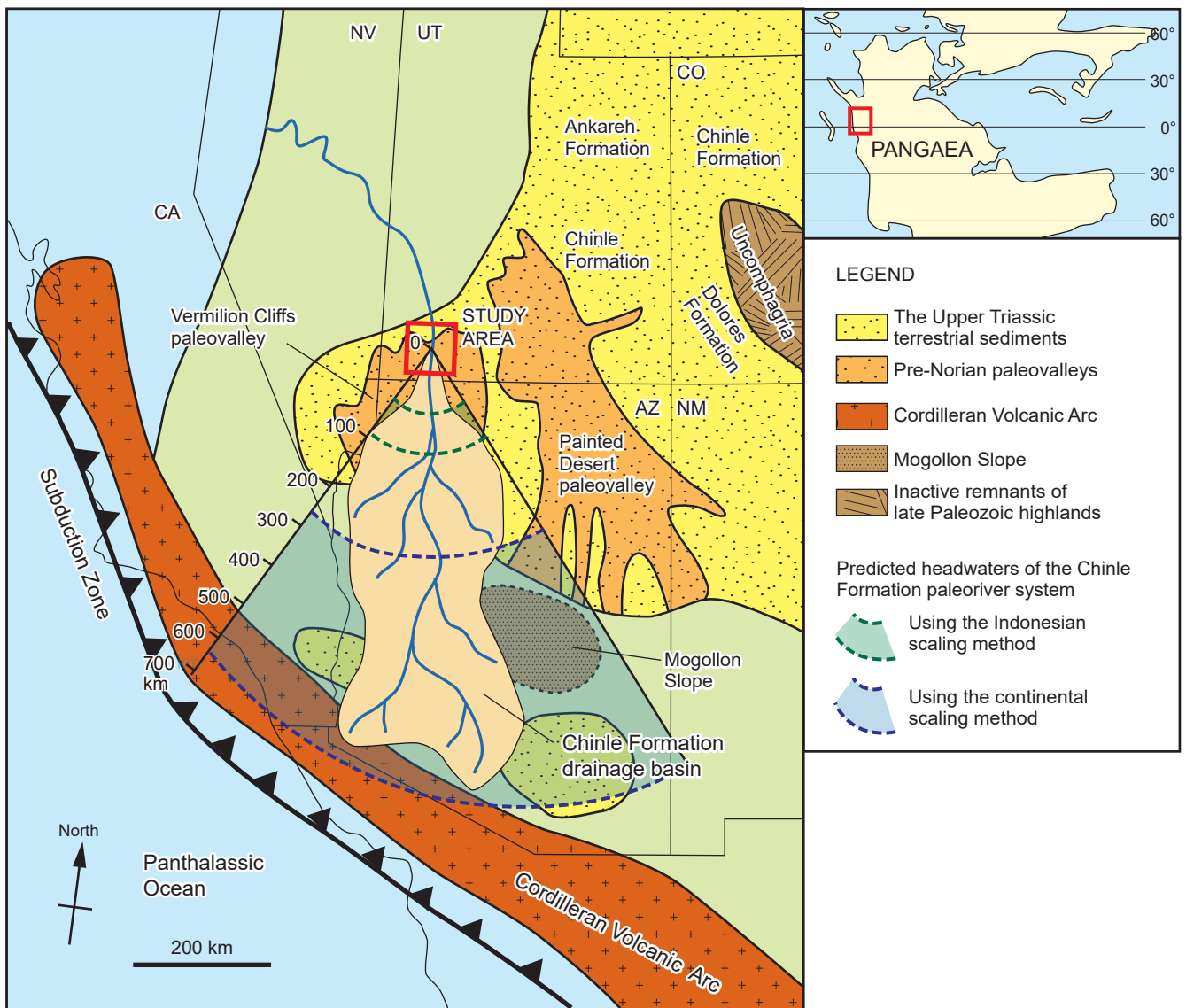


Fig. 60. Chinle Formation drainage basin based on the estimated maximum values of drainage basin area and length for each channel complex. Predicted headwaters from both the Indonesian scaling method and the continental scaling method were shown (see text). Paleogeographic map is modified from Martz et al. (2017). Inset map of the Pangaea is modified from Trendell et al. (2012).

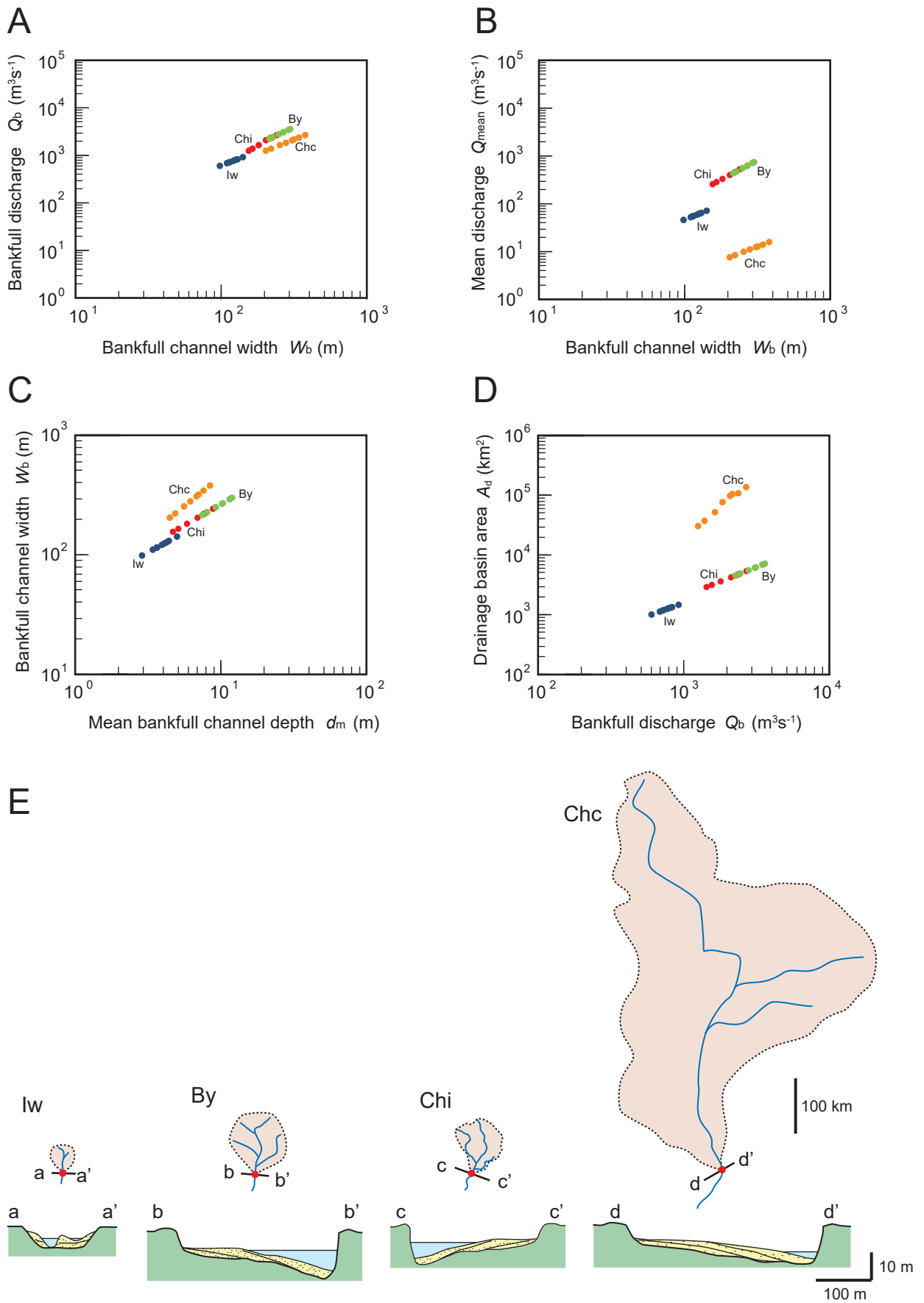


Fig. 61. Comparisons between reconstructed parameters of paleoriver systems. Iw: Iwaki Formation, By: Bayah Formation, Chi: Chinle Formation (Indonesian scaling method), and Chc: Chinle Formation (continental scaling method). A: Relationship between bankfull channel width (W_b) and bankfull discharge (Q_b). B: Relationship between W_b and mean discharge (Q_{mean}). C: Relationship between mean bankfull channel depth (d_m) and W_b . D: Relationship between Q_b and drainage basin area (A_d). E: Schematic illustrations of the paleoriver systems.

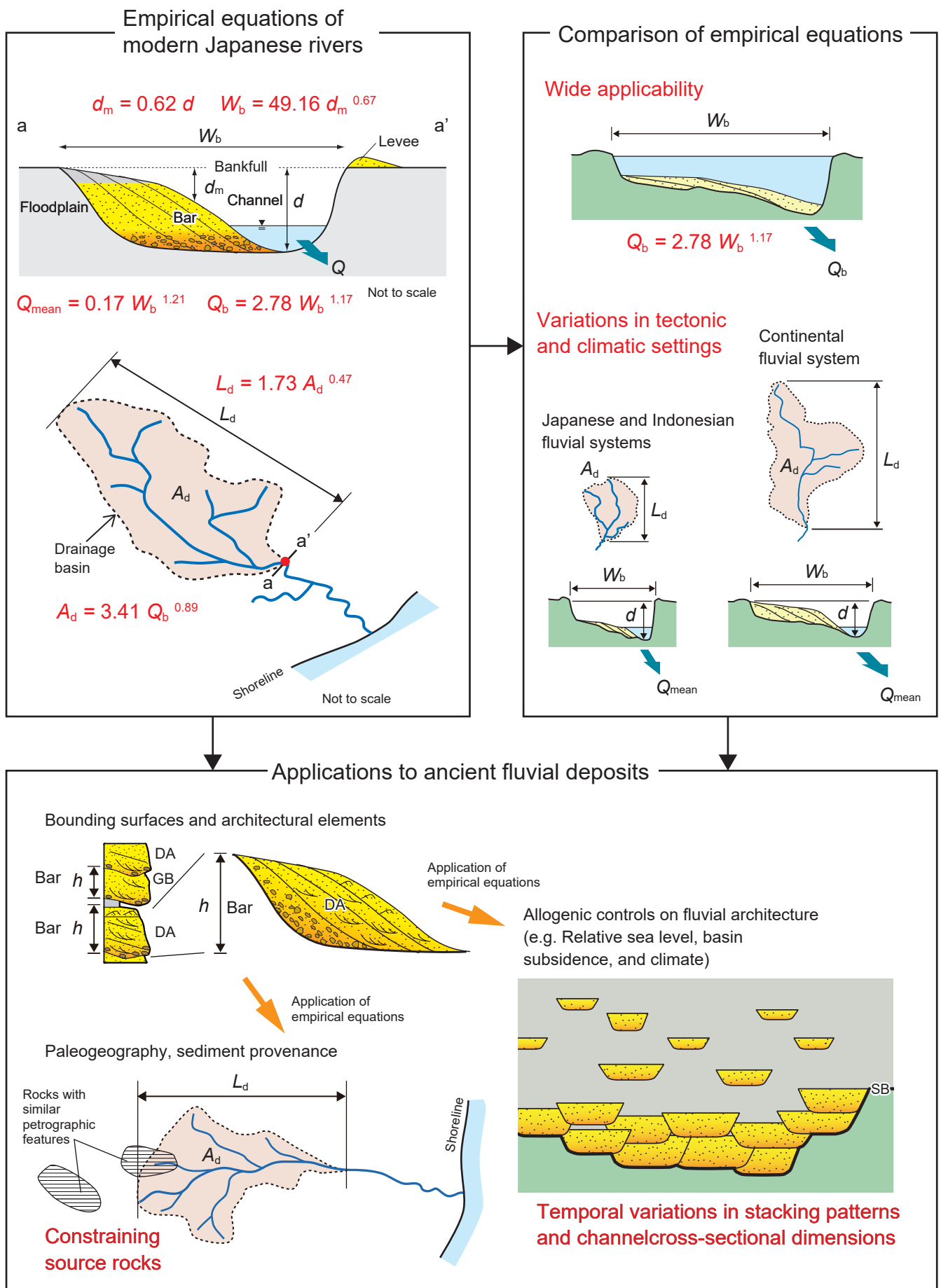


Fig. 62. Graphical summary of the present study. See Table 2 for the definitions of symbols.

Table 1. Hydrological and geomorphological data for the modern fluvial system in the Japanese Archipelago. The number represents the site number in Figs. 4, 5, and 6. See Table 2 for symbols.

No.	River system	River	Measurement site	W_b (m)	Q_{mean} ($m^3 s^{-1}$)	Q_b ($m^3 s^{-1}$)	Q_{max} ($m^3 s^{-1}$)	A_d (km^2)	L_d (km)	Observed year of Q_{mean} and Q_{max}
1	Teshio	Teshio	Tsukumobashi	39.7	25.74	182.74	802.7	716.7	44.3	1968 - 2004
2	Teshio	Teshio	Nayoroohashi	75.0	81.31	730.40	1889.36	1719.2	59.3	1953 - 2004
3	Teshio	Teshio	Bifukabashi	121.8	133.73	1317.55	2718.54	2899.2	70.9	1967 - 2004
4	Teshio	Teshio	Ponpira	106.3	190.64	1764.54	3360.95	4029.1	118	1953 - 2004
5	Teshio	Nayoro	Makunbetsu	55.4	26.87	430.41	1130.18	695.2	-	1958 - 2004
6	Teshio	Teshio	Teshioohashi	182.3	225.05	-	3384.88	4839.2	143.6	1962 - 2004
7	Rumoi	Rumoi	Owada	16.7	11.72	141.75	700.02	234.1	-	1962 - 2004
8	Ishikari	Ishikari	Nakaaiibetsu	88.0	49.42	285.84	899.8	1082.5	32.5	1957 - 2004
9	Ishikari	Ishikari	Asahibashi	96.0	73.75	503.67	1804.83	1917.2	54.2	1957 - 2004
10	Ishikari	Ishikari	Ino	162.3	132.62	1040.77	4025.32	3378.6	60.9	1953 - 2004
11	Ishikari	Chubetsu	Akatsukibashi	42.3	14.84	86.00	821.66	263.4	-	1964 - 2004
12	Ishikari	Biei	Nishikagura	42.5	23.25	188.12	1291.27	645	-	1957 - 2004
13	Ishikari	Ishikari	Osamunai	109.8	144.69	952.07	4505.16	3558	72.5	1958 - 2004
14	Ishikari	Ishikari	Hashimotocho	156.9	229.41	2031.87	5730.26	5711	-	1951 - 2004
15	Ishikari	Uryu	Tadoshi	60.1	46.16	548.62	1553.68	996	-	1952 - 2004
16	Ishikari	Sorachi	Akabira	82.0	91.75	890.59	3914.96	2531	-	1958 - 2004
17	Ishikari	Ishikari	Tsukigata	172.3	347.2	2819.55	8833.57	9306	119.6	1970 - 2004
18	Ishikari	Ishikari	Ishikariohashi	450.0	469.68	3543.32	11330	12697	141.4	1962 - 2004
19	Ishikari	Yubari	Maruyama	33.4	32.24	885.91	2037.71	792	-	1959 - 2004
20	Ishikari	Yubari	Kiyohorobashi	30.1	37.15	493.49	2029.65	1116	-	1962 - 2004
21	Ishikari	Chitose	Nishikoshi	31.9	18.82	31.47	99.33	367	-	1954 - 2004
22	Ishikari	Yoyohira	Ishiyama	39.3	13.1	183.31	1259.54	550	-	1973 - 2004
23	Ishikari	Yoyohira	Kariki	49.1	27.61	285.46	2435.2	651	-	1956 - 2004
24	Ishikari	Ikusyunbetsu	Nishikawamukai	14.4	12.3	-	638.38	324.7	-	1974 - 2004
25	Shiribetsu	Shiribetsu	Nakoma	81.6	67.82	332.10	1493.3	1402.2	-	1965 - 2004
26	Shiribeshi-Toshibetsu	Shiribeshi-Toshibetsu	Imakane	45.6	23.6	147.68	1100.8	361.4	25.4	1956 - 2004
27	Mu	Mu	Mukawa	139.5	38.6	1140.53	2991	1228	81.2	1974 - 2004
28	Saru	Saru	Hiratori	80.3	48.22	1174.10	5120.73	1253	67.2	1964 - 2004
29	Tokachi	Tokachi	Kyoeibashi	183.6	45.46	172.47	300.44	803.8	44	1988 - 2004
30	Tokachi	Tokachi	Obihiro	139.9	84.92	1139.96	4750.02	2677.8	67.1	1955 - 2004
31	Tokachi	Tokachi	Moiwa	212.1	220.82	4487.78	10479.1	8276.9	95.6	1954 - 2004
32	Tokachi	Otofuke	Otofuke	83.0	7.74	150.00	725.46	707.9	-	1967 - 2004
33	Tokachi	Satsunai	Nantaibashi	126.3	29.75	517.95	1014.27	608.1	-	1965 - 2004
34	Tokachi	Toshibetsu	Toshibetsu	97.2	64.61	1281.14	2005.7	2715.2	-	1959 - 2004
35	Tokachi	Otofuke	Shihoro	183.1	5.63	-	522.25	540	-	1975 - 2004
36	Tokachi	Satsunai	Dainiokawabash	196.8	27.05	-	1495.67	580	-	1966 - 2004
37	Tokachi	Toshibetsu	Azumabashi	112.0	58.54	-	1606.77	2365.3	-	1974 - 2004
38	Kushiro	Kushiro	Teshikaga	31.7	11.98	36.59	92.31	459	-	1967 - 2004
39	Kushiro	Kushiro	Shibechea	58.9	26.34	174.98	778	894.6	-	1956 - 2004
40	Kushiro	Shinkushiro	Hirosato	55.7	61.95	214.73	310.9	2172.1	-	1977 - 2004
41	Abashiri	Abashiri	Bihoro	22.2	14.32	300.62	872.19	824.4	-	1955 - 2004
42	Abashiri	Abashiri	Hongo	56.5	20.1	321.18	745.37	1120.4	-	1956 - 2004
43	Tokoro	Tokoro	Oketo	21.3	8.18	106.21	368.75	421.7	-	1970 - 2004
44	Tokoro	Tokoro	Kitami	66.3	22.57	424.90	931.97	1394.2	-	1954 - 2004
45	Yubetsu	Yubetsu	Kaisei	120.3	31.25	350.12	1291.38	1334.8	-	1954 - 2004
46	Syokotsu	Syokotsu	Kamisuyokotsu	61.0	29.07	420.57	1501.01	1050.6	-	1955 - 2004
47	Iwaki	Iwaki	Kamiiwakibashi	30.0	24.27	211.71	1780.48	409.8	-	1960 - 2004
48	Iwaki	Iwaki	Goshogawara	79.4	75.14	573.24	1692.4	1740.3	-	1953 - 2004
49	Yoneshiro	Yoneshiro	Junisho	53.1	57.25	245.88	2463.91	1167.4	-	1962 - 2004
50	Yoneshiro	Yoneshiro	Takanosu	114.2	101.21	578.90	2978.61	2109	-	1957 - 2004
51	Yoneshiro	Ani	Yonaizawa	83.9	51.35	328.02	1631.43	683.6	-	1959 - 2004
52	Yoneshiro	Yoneshiro	Futatsui	174.2	207.37	1073.35	6800	3750.4	-	1954 - 2004
53	Omono	Yakunai	Kawai	26.4	10.79	80.74	376.48	145	-	1982 - 2004
54	Omono	Omono	Yanagidabashi	72.4	27.67	229.61	1297.19	475.6	-	1982 - 2004
55	Omono	Naruse	Anyoji	33.2	19.99	159.58	1073.16	255	-	1982 - 2004
56	Omono	Omono	Omonogawabash	193.8	71.14	562.90	2426.38	1240	-	1982 - 2004
57	Omono	Omono	Omagaribashi	178.4	110.1	793.18	2236.55	1882.1	-	1982 - 2004
58	Omono	Tama	Nagano	75.8	75.72	695.74	2177.6	1088	-	1978 - 2004
59	Omono	Omono	Jinguji	139.3	216.56	1499.09	4344.51	3336.5	-	1982 - 2004
60	Omono	Omono	Tsubakigawa	209.3	258.52	1573.04	3519.41	4034.9	-	1938 - 2004
61	Koyoshi	Koyoshi	Todorokibashi	74.9	61.38	460.71	1939.4	937	-	1972 - 2004
62	Mogami	Mogami	Nukanome	25.2	13.96	180.89	913.91	359.1	27.7	1975 - 2004
63	Mogami	Mogami	Nishiotuka	45.2	45.36	459.21	1817.52	1017.9	36.9	1960 - 2004
64	Mogami	Mogami	Koide	115.4	74.13	597.45	2595.77	1350.1	42.3	1953 - 2004
65	Mogami	Mogami	Miyajuku	67.9	107.55	769.48	2936.28	1816.8	63.6	1964 - 2004

Table 1. (continued)

No.	River system	River	Measurement site	W_b (m)	Q_{mean} ($\text{m}^3 \text{s}^{-1}$)	Q_b ($\text{m}^3 \text{s}^{-1}$)	Q_{max} ($\text{m}^3 \text{s}^{-1}$)	A_d (km^2)	L_d (km)	Observed year of Q_{mean} and Q_{max}
66	Mogami	Mogami	Nakago	88.1	112.72	800.35	3215.66	2100.4	71	1955 - 2004
67	Mogami	Mogami	Nagasaki	105.7	118.68	1117.34	2551.42	2146.9	-	1977 - 2004
68	Mogami	Su	Sushiarai	23.7	15.12	176.33	666.55	421.7	-	1960 - 2004
69	Mogami	Mogami	Nishine	112.3	39.73	205.52	1480.65	478.4	-	1965 - 2004
70	Mogami	Mogami	Shimono	120.7	189.4	1568.67	3806.79	3534.3	78.1	1964 - 2004
71	Mogami	Mogami	Inashita	100.6	207.62	1555.54	4133.36	3769.5	85.3	1955 - 2004
72	Mogami	Mogami	Oishida	106.2	209.89	1378.92	3556.49	3963	97.2	1957 - 2004
73	Mogami	Mogami	Horinouchi	127.5	223.97	1535.31	3385.78	4515.6	104	1957 - 2004
74	Mogami	Sake	Maki	75.4	50.37	457.31	3079.64	617.6	-	1942 - 2004
75	Mogami	Mogami	Takaya	178.7	369.93	2194.70	6060.75	6270.9	113.8	1959 - 2004
76	Mogami	Mogami	Sagoshi	199.2	400.15	2301.78	6326.68	6497.2	128.5	1967 - 2004
77	Aka	Aka	Kumaide	101.1	64.98	411.43	2067.8	551.5	-	1966 - 2004
78	Aka	Aka	Hamanaka	98.1	74.85	462.53	1830.17	695.1	-	1959 - 2004
79	Takase	Takase	Uwano	32.5	15.07	176.69	382.77	344.2	-	1980 - 2004
80	Mabechi	Mabechi	Kenyoshi	47.6	47.73	498.55	1419.8	1751.1	-	1963 - 2004
81	Kitakami	Kitakami	Mejibashi	94.3	89.77	706.46	2040.21	2184.9	44.7	1951 - 2004
82	Kitakami	Kitakami	Shiwabashi	111.8	109.8	989.32	2470.34	2579.8	60.2	1961 - 2004
83	Kitakami	Sarugaishi	Yasuno	32.8	16.67	214.28	888.33	956.9	-	1964 - 2004
84	Kitakami	Kitakami	Asahibashi	156.3	154.43	1454.83	3315.35	4228.6	78.4	1955 - 2004
85	Kitakami	Kitakami	Otokoyama	172.5	217.46	2098.44	4824.62	5458.7	92.4	1951 - 2004
86	Kitakami	Kitakami	Sakuragibashi	157.9	270.66	2548.69	7159.2	6006	102.7	1963 - 2004
87	Kitakami	Kitakami	Omagaribashi	237.3	257.59	2506.57	5263.67	6398.9	114.3	1961 - 2004
88	Kitakami	Kitakami	Kozenji	136.2	301.97	2449.52	5412.31	7065.6	126.8	1951 - 2004
89	Kitakami	Kitakami	Oizumi	154.5	327.11	3350.11	5896.48	7800	148.1	1959 - 2004
90	Kitakami	Kitakami	Maiya	201.7	314.32	2961.85	4711.72	7862.5	155	1964 - 2004
91	Kitakami	Kitakami	Tome	262.4	323.88	3327.18	5455.28	7869.4	156	1953 - 2004
92	Kitakami	Kyukitakami	Kurazone	147.8	117.4	466.98	885.83	7962.6	-	1962 - 2004
93	Kitakami	Eai	Arao	68.2	18.21	230.80	824.6	405	-	1956 - 2004
94	Kitakami	Eai	Wakuya	27.8	22.37	243.13	561.63	471	-	1958 - 2004
95	Kitakami	Kyukitakami	Wabuchi	201.5	188.49	1072.77	2049.39	9804.5	-	1960 - 2004
96	Naruse	Naruse	Sanbongibashi	72.8	26.45	386.84	1637.38	550.8	-	1951 - 2004
97	Naruse	Naruse	Nodabashi	103.8	33.65	605.78	2973.14	707	-	1951 - 2004
98	Naruse	Yoshida	Ochiai	30.1	6.26	195.17	724.22	197.2	-	1951 - 2004
99	Naruse	Yoshida	Hatayamabashi	28.3	10.74	400.76	1074.04	335	-	1978 - 2004
100	Natori	Natori	Yokata	49.6	17.52	417.85	1706.46	424.3	-	1963 - 2004
101	Natori	Natori	Natoribashi	120.0	15.89	450.78	1876	431.3	-	1969 - 2004
102	Natori	Hirose	Hirosebashi	44.3	10.62	354.84	1613.12	309.3	-	1963 - 2004
103	Abukuma	Abukuma	Shirakawa	37.7	6.44	89.83	588	172.4	-	1960 - 2004
104	Abukuma	Abukuma	Sukagawa	60.6	23.58	425.76	1485.66	910.2	-	1940 - 2004
105	Abukuma	Abukuma	Akutsu	90.7	52.27	993.02	2761.22	1865.2	-	1951 - 2004
106	Abukuma	Abukuma	Motomiya	98.2	60.98	1245.18	3607	2283.5	-	1939 - 2004
107	Abukuma	Abukuma	Fukushima	116.8	82.75	1615.02	4138.67	3171.9	-	1951 - 2004
108	Abukuma	Abukuma	Fushiguro	136.4	101.35	1913.37	5409.3	3663.4	-	1951 - 2004
109	Abukuma	Abukuma	Tateyama	157.5	118.79	2307.21	6399.11	4132.5	-	1966 - 2004
110	Abukuma	Shiroishi	Funaokaohashi	87.8	27.17	473.50	1314.19	796.4	-	1968 - 2004
111	Kuji	Kuji	Sakakibashi	81.5	15.55	666.24	1928.58	1422	62.7	1979 - 2004
112	Kuji	Kuji	Tomioka	67.0	25.48	-	2554.4	950.8	54.5	1979 - 2004
113	Kuji	Kuji	Yamagata	95.2	25.71	431.58	1662.21	897.8	45.3	1979 - 2004
114	Naka	Naka	Noguchi	154.8	79.28	1487.08	3960.62	2181	-	1958 - 2004
115	Naka	Naka	Kurobane	80.8	29.8	488.53	1600.5	648.5	-	1979 - 2004
116	Tone	Tone	Fukawa	184.7	372.05	4712.44	7812.74	12458	169.4	1938 - 2004
117	Tone	Tone	Toride	173.9	314.74	4377.10	7780.53	11340	160.9	1970 - 2004
118	Tone	Tone	Mefukibashi	201.2	143.44	3677.88	8476.4	8849	143.2	1979 - 2004
119	Tone	Tone	Kitasekiyado	238.9	136.77	4204.17	7880.29	8771.2	129.7	1960 - 2004
120	Tone	Tone	Tonesekiyado	310.6	225.58	5387.97	11086.8	8564.3	126.9	1961 - 2004
121	Tone	Tone	Kurihashi	254.0	237.62	5194.27	10577.2	8588	120.5	1979 - 2004
122	Tone	Tone	Kawamata	271.2	148.2	3343.38	11403.1	6018	102.4	1979 - 2004
123	Tone	Tone	Futto	268.0	207.89	3369.01	10401.2	5986	90.1	1979 - 2004
124	Tone	Tone	Yattajima	391.6	175.02	2950.49	9222.35	5150	73.7	1979 - 2004
125	Tone	Tone	Kamifukushima	107.9	130.16	1268.85	5603.06	3661	65.1	1979 - 2004
126	Tone	Tone	Maebashi	135.7	132.6	1638.35	5650.99	3266.4	57.6	1973 - 2004
127	Tone	Tone	Iwamoto	88.5	90.23	914.59	2850.33	1691.9	-	1953 - 2004
128	Tone	Katashina	Kamikuya	39.4	7.67	491.19	1721.87	633	-	1953 - 2004
129	Tone	Agatsuma	Murakami	64.0	24.22	606.89	2354.06	1239	44.6	1958 - 2004
130	Tone	Tone	Yakatabara	32.0	43.46	354.26	1322.14	980.9	-	1954 - 2004
131	Tone	Karasu	Iwahana	125.8	28.47	923.23	4456.1	1220.8	-	1969 - 2004

Table 1. (continued)

No.	River system	River	Measurement site	W_b (m)	Q_{mean} ($m^3 s^{-1}$)	Q_b ($m^3 s^{-1}$)	Q_{max} ($m^3 s^{-1}$)	A_d (km^2)	L_d (km)	Observed year of Q_{mean} and Q_{max}
132	Tone	Karasu	Takamatsu	69.5	13.79	384.71	2999.37	536.3	-	1969 - 2004
133	Tone	Karasu	Kamisatomi	29.2	6.74	119.46	973.25	156	-	1963 - 2004
134	Tone	Usui	Annaka	28.9	4.25	160.51	813.07	121.1	-	1969 - 2004
135	Tone	Kabura	Iwai	149.7	11.65	463.99	2608.74	555.2	-	1969 - 2004
136	Tone	Okai	Kuroko	44.2	21.97	393.22	1119.11	580	-	1960 - 2004
137	Tone	Okai	Miya	21.9	6.24	111.47	540.39	222.7	-	1960 - 2004
138	Tone	Kinu	Kinugawa-Mitsu	114.9	58.04	1612.72	3927.3	1740.1	-	1960 - 2004
139	Tone	Kinu	Hirakata	71.4	54.85	1691.05	3089.39	1626.4	-	1963 - 2004
140	Tone	Edo	Nishisekiyado	70.9	109.89	1153.60	2166.51	8664.3	-	1938 - 2004
141	Tone	Edo	Noda	101.4	109.37	1140.21	3698	8687.9	-	1953 - 2004
142	Tone	Edo	Nagareyama	151.5	no data	1101.37	3123	8705.3	-	1954 - 2004
143	Tone	Watarase	Fujioka	61.2	38.21	1250.60	1914.56	1209.5	-	1980 - 2004
144	Tone	Watarase	Sakawadakami	91.1	22.12	1066.99	1848.15	748.4	-	1979 - 2004
145	Tone	Watarase	Ashikaga	119.9	20.72	-	3888	691.8	-	1964 - 2004
146	Tone	Watarase	Takatsudo	57.7	18.46	946.93	3511.3	472.4	-	1961 - 2004
147	Tone	Uzuma	Nakazato	23.2	7.1	157.86	420.89	205.4	-	1979 - 2004
148	Tone	Omoi	Otome	70.9	33.22	1238.21	3131.71	760	-	1979 - 2004
149	Ara	Ara	Oashibashi	47.1	24.5	1379.21	5586.65	1019	-	1967 - 2004
150	Ara	Iruma	Sugama	43.9	20.11	913.40	2503.08	712.5	-	1967 - 2004
151	Ara	Ara	Yorii	87.2	28.11	1330.29	5512.04	905	-	1952 - 2004
152	Tama	Tama	Ishihara	181.4	41.46	1163.69	2862.33	1040	-	2000 - 2004
153	Tama	Tama	Chofubashi	52.6	19.06	460.05	1610.08	433	-	2000 - 2004
154	Tsurumi	Tsurumi	Kamenokobashi	25.0	10.79	165.91	520.36	134	-	2000 - 2004
155	Fuji	Fuji	Kitamatsuno	169.3	72.99	2847.36	12395.8	3539.8	84.6	1970 - 2004
156	Fuji	Fuji	Shimizubata	116.5	59.67	1176.01	5711.5	2179.1	46.1	1978 - 2004
157	Fuji	Fuji	Funayamabashi	133.0	14.8	133.17	743.63	481.5	28.4	1959 - 2004
158	Fuji	Fuefuki	Torinkyo	74.0	24.56	447.46	2631.6	916.3	-	1976 - 2004
159	Fuji	Fuefuki	Isawa	58.8	14.13	-	1335.42	504.1	-	1991 - 2004
160	Agano	Aga	Oya	227.3	36.45	633.23	2562.86	868	-	1966 - 2004
161	Agano	Nippashi	Minamiohashi	132.2	38.46	163.75	585.03	1033.4	-	1967 - 2004
162	Agano	Aga	Yamashina	109.0	115.44	1146.20	3343.18	2741.9	-	1974 - 2004
163	Agano	Agano	Maoroshi	170.8	402.48	2521.89	8927.78	6997	-	1979 - 2004
164	Shinano	Chikuma	Kuisege	99.2	61.7	850.73	4130.9	2595.9	-	1977 - 2004
165	Shinano	Sai	Rikugo	106.6	102.71	695.82	3171.51	2335	64.6	1965 - 2004
166	Shinano	Sai	Koichi	124.5	124.44	682.71	3849.32	2773	94.2	1977 - 2004
167	Shinano	Chikuma	Tategahana	124.1	232.87	1493.82	7440.46	6442.3	110.5	1979 - 2004
168	Shinano	Chikuma	Ikuta	101.8	56.03	761.37	3625.14	2036.4	-	1955 - 2004
169	Shinano	Shinano-chuuryu	Iwasawa	190.3	131.62	2231.86	7335.5	8126	182.1	1962 - 2004
170	Shinano	Uono	Horinouchi	104.0	157.68	651.20	3657.35	1408	-	1978 - 2004
171	Shinano	Shinano-chuuryu	Ojya	283.0	503.11	2652.20	9638.26	9719	187.5	1976 - 2004
172	Shinano	Nakanokuchi	Itai	76.6	115.89	213.17	595.27	390.4	-	1957 - 2004
173	Shinano	Shinano-karyu	Aramachi	101.3	223.66	486.39	2388.35	768.6	-	1958 - 2004
174	Seki	Seki	Takada	107.2	50.24	309.47	2504.47	703	-	1960 - 2004
175	Hime	Hime	Yamamoto	172.8	44.39	509.40	2355.14	697.7	-	1955 - 2004
176	Kurobe	Kurobe	Unazuki	75.7	36.53	436.13	2158.3	637	47.9	1959 - 2004
177	Jyogajji	Jyogajji	Kameiwa	90.8	16.51	198.58	2764.02	344	-	1968 - 2004
178	Jintsu	Jintsu	Osawanoohashi	115.4	84.02	818.76	6007.16	2065	63.5	1968 - 2004
179	Jintsu	Ida	Sugiharabashi	46.7	24.45	99.51	899.9	250.1	-	1966 - 2004
180	Jintsu	Jintsu	Jintsuohashi	155.7	184.36	949.37	6412.72	2688	75.3	1972 - 2004
181	Sho	Sho	Komaki	50.5	99.32	364.84	2544.9	1090	71.3	1967 - 2004
182	Sho	Sho	Daimon	103.3	47.12	311.14	2645.76	1120	90.9	1974 - 2004
183	Oyabe	Oyabe	Tsuzawa	62.5	28.03	165.52	1187.5	280	-	1974 - 2004
184	Oyabe	Oyabe	Nagae	64.6	58.31	304.71	1594.24	569	-	1977 - 2004
185	Tedori	Tedori	Nakajima	237.6	77.75	453.32	2878.25	732	42	1962 - 2004
186	Ara	Ara	Tsuzurayama	121.0	119.21	876.62	4074.02	1127	-	1958 - 2004
187	Kakehashi	Kakehashi	Haneda	28.1	17.92	90.15	674.17	167.3	27.6	1958 - 2004
188	Kano	Kano	Ohito	100.8	21.68	569.75	4069.16	322	-	1956 - 2004
189	Kano	Kano	Chitosebashi	61.4	25.38	575.59	2784.46	390	-	1965 - 2004
190	Kano	Kano	Tokura	60.2	39.7	643.35	1873.6	568	-	1950 - 2004
191	Kano	Kise	Honjuku	37.5	7.54	125.46	1047.49	259	-	1968 - 2004
192	Abe	Abe	Tegoshi	393.6	41.44	1097.82	4861.74	537	41	1977 - 2004
193	Abe	Abe	Ushizuma	331.3	117.93	723.18	3096.56	287.6	28.7	1986 - 2004
194	Abe	Warashina	Narama	47.0	10.23	294.72	1314.27	112.2	-	1959 - 2004
195	Oi	Oi	Kanza	446.8	76.51	1814.67	5832.55	1160	87.1	1969 - 2004
196	Kiku	Kiku	Kamo	20.2	2.23	62.30	597.18	34.2	-	1955 - 2004
197	Tenryu	Tenryu	Inatomi	50.2	20.58	177.75	490.32	730.8	23.5	1952 - 2004

Table 1. (continued)

No.	River system	River	Measurement site	W_b (m)	Q_{mean} ($\text{m}^3 \text{s}^{-1}$)	Q_b ($\text{m}^3 \text{s}^{-1}$)	Q_{max} ($\text{m}^3 \text{s}^{-1}$)	A_d (km^2)	L_d (km)	Observed year of Q_{mean} and Q_{max}
198	Tenryu	Tenryu	Ina	52.1	37.55	248.11	836.37	968.4	27.4	1969 - 2004
199	Tenryu	Tenryu	Miyagase	136.2	84.57	689.37	3416.99	2224.3	64.3	1956 - 2004
200	Tenryu	Tenryu	Kashima	242.2	241.44	2620.38	10014.3	4880	147.6	1943 - 2004
201	Tenryu	Keta	Inui	108.3	21.37	469.44	1800	317	-	1962 - 2004
202	Toyo	Toyo	Furi	63.1	16.06	349.89	2130.69	248.8	-	1946 - 2004
203	Toyo	Toyo	Ishida	74.6	28.47	822.54	4568.84	545	-	1946 - 2004
204	Toyo	Toyo	Togo	74.3	32.02	997.37	3856.05	634	-	1971 - 2004
205	Yahagi	Yahagi	Iwazu	71.8	44.49	815.40	4227.47	1355.9	-	1939 - 2004
206	Yahagi	Yahagi	Yonezu	162.1	48.03	794.69	3943.28	1656.7	-	1938 - 2004
207	Shonai	Toki	Tajimi	61.1	14.17	170.48	1835.87	367	-	1980 - 2004
208	Shonai	Shonai	Biwajima	121.3	26.48	303.39	3519.59	705	-	1957 - 2004
209	Kiso	Kiso	Inuyama	213.4	292.33	2371.27	14098.6	4683.8	106.3	1951 - 2004
210	Kiso	Ibi	Okajima	74.6	54.06	634.44	2324.56	606.4	39.5	1964 - 2004
211	Kiso	Ibi	Mangoku	87.4	85.84	1528.50	4490.6	1195.8	54.2	1961 - 2004
212	Kiso	Neo	Yamaguchi	121.4	36.49	644.91	2755.21	397	-	1963 - 2004
213	Kiso	Makita	Hirosebashi	152.1	8.73	225.22	1331.72	182.8	-	1977 - 2004
214	Kiso	Kuise	Takabuchi	23.1	13.19	-	442.1	174	-	1979 - 2004
215	Kiso	Nagara	Mino	121.4	89.55	1199.71	7132.35	1076	-	1966 - 2004
216	Kiso	Nagara	Chusetsu	170.7	115.4	1338.44	7666.87	1606.8	-	1954 - 2004
217	Kiso	Nagara	Sunomata	170.7	130.4	1460.87	7957.61	1914	-	1939 - 2004
218	Kiso	Ijira	Furukawabashi	25.3	7.07	71.89	448.95	121	-	1982 - 2004
219	Suzuka	Suzuka	Takaoka	110.2	10.33	282.97	1907.1	268.6	-	1974 - 2004
220	Suzuka	Utsube	Kawarada	21.9	2.17	69.76	2037.55	50.7	-	1970 - 2004
221	Kumozu	Kumozu	Onogi	58.9	14.44	369.33	3956.3	304.2	-	1961 - 2004
222	Kushida	Kushida	Ryogun	78.4	20.83	671.82	3749.55	388.9	-	1963 - 2004
223	Miya	Miya	Iwade	177.2	47.24	1823.24	7198.02	780	-	1975 - 2004
224	Singu	Kumano	Oga	236.0	166.31	5438.90	18000	2251	-	1951 - 2004
225	Kino	Kino	Imose	84.3	23.83	758.00	6783.03	463.7	19.5	1976 - 2004
226	Kino	Kino	Suda	58.5	33.36	582.45	5505.12	802.8	39.6	1943 - 2004
227	Kino	Kino	Hashimoto	163.7	39.89	875.78	7650	835.2	43.9	1954 - 2004
228	Kino	Kino	Mitani	201.9	36.56	960.21	6301.49	1048.9	52.3	1973 - 2004
229	Kino	Kishi	Kishi	63.7	8.09	285.95	1216.23	260	-	1960 - 2004
230	Kino	Kino	Funatodaini	215.6	59.25	1356.59	7800	1558	72.4	1952 - 2004
231	Yamato	Yamato	Itahigashi	33.5	12.43	75.74	656.45	250.4	-	1973 - 2004
232	Yamato	Yamato	Oji	57.2	19.41	168.12	1690.07	655.2	-	1954 - 2004
233	Yamato	Ishi	Domyoji	54.8	5.23	77.57	1192.89	215.2	-	1954 - 2004
234	Yamato	Yamato	Kashiwara	96.9	24.29	342.45	2497	962	-	1955 - 2004
235	Yodo	Yasu	Mikumoto	87.5	12.53	-	2500	296.2	23.3	1964 - 2004
236	Yodo	Yasu	Yasu	148.7	11.9	337.56	2236.61	387	36	1975 - 2004
237	Yodo	Seta	Toriigawa	160.2	136.44	604.37	984.3	3846.2	70.5	1952 - 2004
238	Yodo	Daido	Kurozu	69.6	6.19	72.20	733.26	193	-	1969 - 2004
239	Yodo	Uji	Uji	92.3	176.63	848.41	1979.52	4354	84.5	1955 - 2004
240	Yodo	Kizu	Shimagahara	59.8	17.78	388.06	2570	524.9	-	1962 - 2004
241	Yodo	Nabari	Nabari	89.2	14.3	261.10	4030	428.6	-	1955 - 2004
242	Yodo	Kizu	Kamo	111.4	45.12	897.18	6200	1456	-	1938 - 2004
243	Yodo	Kizu	Inooka	186.6	47.67	1115.15	6410	1559	-	1952 - 2004
244	Yodo	Kizu	Yawata	128.7	50.56	897.65	4744	1596	-	1955 - 2004
245	Yodo	Katsura	Shinmachi	94.2	17.73	-	1704.4	540	-	1956 - 2004
246	Yodo	Katsura	Hozukyo	32.3	26.41	242.62	2357.23	741	-	1956 - 2004
247	Yodo	Katsura	Katsura	132.3	27.71	246.17	2276.74	887	-	1938 - 2004
248	Yodo	Kamo	Fukakusa	46.4	7.67	43.08	473.6	156	-	1958 - 2004
249	Yodo	Katsura	Noso	68.7	46.05	240.21	3133.9	1100	-	1955 - 2004
250	Yodo	Yodo	Hirakata	237.7	267.33	1751.87	7970	7281	95.5	1952 - 2004
251	Yodo	Ina	Musyu	23.5	6.83	61.78	1037.12	235.2	-	1970 - 2004
252	Yodo	Ina	Gunkobashi	71.6	8.21	99.86	1571.7	322.8	-	1970 - 2004
253	Kako	Kako	Itaba	91.7	35.03	410.85	2802.58	893.2	-	1969 - 2004
254	Kako	Kako	Kunikane	222.4	46.6	625.30	4029.54	1656	-	1951 - 2004
255	Ibo	Ibo	Yamazakidaini	75.7	23.99	196.30	3045.19	485.9	33.8	1938 - 2004
256	Ibo	Ibo	Tatsuno	135.4	29.04	-	2403.67	622.4	48.2	1951 - 2004
257	Ibo	Ibo	Kamigawara	113.4	26.59	305.89	3647.48	795.5	55.3	1973 - 2004
258	Kuzuryu	Kuzuryu	Nakatsuno	123.8	108.71	715.94	4532.4	1239.6	-	1952 - 2004
259	Kuzuryu	Hino	Miono	50.4	50.52	312.57	3384.87	688	-	1966 - 2004
260	Kuzuryu	Hino	Fukatani	164.9	76.42	602.51	2452.6	1281	-	1958 - 2004
261	Kita	Kita	Takatsuka	78.1	11.76	142.04	897.44	201.6	-	1972 - 2004
262	Yura	Yura	Ayabe	113.6	36.21	316.18	3623.13	755.2	-	1970 - 2004
263	Yura	Yura	Fukuchiyama	124.2	52.47	400.47	6500	1344.3	-	1953 - 2004

Table 1. (continued)

No.	River system	River	Measurement site	W_b (m)	Q_{mean} ($m^3 s^{-1}$)	Q_b ($m^3 s^{-1}$)	Q_{max} ($m^3 s^{-1}$)	A_d (km^2)	L_d (km)	Observed year of Q_{mean} and Q_{max}
264	Yura	Haze	Osada	83.8	12.83	153.09	1287.24	379.5	-	1992 - 2004
265	Maruyama	Maruyama	Kamioda	131.2	29.21	246.41	5011.32	700	26.4	1962 - 2004
266	Maruyama	Maruyama	Fuichiba	114.4	37.92	330.01	3263.15	837	33.5	1971 - 2004
267	Maruyama	Izushi	Hirohara	27.6	8.63	38.06	1198.43	194.7	-	1971 - 2004
268	Sendai	Hatto	Wakasa	27.3	9.58	63.54	581.84	152.8	-	1964 - 2004
269	Sendai	Sendai	Gyotoku	110.7	60.94	263.91	4265.79	1053.7	-	1956 - 2004
270	Sendai	Sendai	Fukurogawara	126.2	50.03	250.86	3441.5	871.4	-	1976 - 2004
271	Tenjin	Tenjin	Koda	89.8	24.01	149.81	1770.65	464	-	1965 - 2004
272	Hino	Hino	Mizoguchi	80.6	21.74	169.58	1561.1	660	-	1963 - 2004
273	Hino	Hino	Kuzumo	145.5	33.98	245.64	1800.6	860	-	1962 - 2004
274	Gono	Gono	Yoshida	59.1	11.42	224.71	1512.22	400.3	-	1952 - 2004
275	Gono	Basen	Minamihatashiki	70.7	17.29	241.49	2348.76	679.5	24.1	1952 - 2004
276	Gono	Saijyo	Miyoshi	57.4	35.93	368.68	3003.98	630.8	-	1952 - 2004
277	Gono	Gono	Ozekiyama	111.6	75.12	830.59	6739.34	1981	25.7	1956 - 2004
278	Gono	Gono	Tsuga	115.6	108.41	1197.09	8477.1	2890	48	1952 - 2004
279	Gono	Gono	Kawahira	111.9	151.49	1725.38	9197.37	3807	69.2	1969 - 2004
280	Gono	Gono	Awaya2	50.6	19.63	295.87	2910.66	670.7	-	1958 - 2004
281	Takatsu	Takatsu	Takatsuno	80.0	51.98	529.38	5200	1076	42.7	1969 - 2004
282	Saba	Saba	Shinbashi	53.2	18.84	279.54	1406.93	423.1	-	1962 - 2004
283	Saba	Shimaji	Shimaji	22.5	7	85.40	526.59	127.6	-	1970 - 2004
284	Oze	Oze	Ryogokubashi	41.0	12.19	207.05	746.98	330	-	1970 - 2004
285	Ota	Ota	Take	42.5	13.86	249.23	4414.18	635	-	1953 - 2004
286	Ota	Ota	Imuro	73.0	30.1	539.89	6136.8	1082	-	1969 - 2004
287	Ota	Misasa	Nakafukawa	44.4	9.55	162.79	926.91	271	-	1960 - 2004
288	Ota	Ota	Yaguchi 1	144.0	79.5	739.89	7004.52	1527	-	1970 - 2004
289	Ota	Ota	Nakano	140.3	32.36	568.87	4291.24	1143	-	1976 - 2004
290	Ashida	Ashida	Fuchu	88.6	12.6	150.95	1395.6	488.9	-	1962 - 2004
291	Ashida	Ashida	Yamate	148.3	13.12	170.22	1606.75	817.1	-	1966 - 2004
292	Ashida	Ashida	Gobun	126.1	10.17	240.31	1667.76	648.4	-	1978 - 2004
293	Ashida	Takaya	Miyuki	19.6	2.83	37.92	245.95	146	-	1977 - 2004
294	Takahashi	Takahashi	Hiwa	121.4	62.13	1002.82	7040.02	1985.8	-	1963 - 2004
295	Asahi	Asahi	Makiyama	69.4	57.51	620.31	4650.15	1586.6	-	1965 - 2004
296	Yoshii	Yoshii	Hisagi	62.8	41.16	227.43	3842.46	978.8	-	1959 - 2004
297	Yoshii	Yoshino	Yunogo	59.9	18.92	292.48	2906.4	490.1	-	1960 - 2004
298	Yoshii	Yoshii	Tsuse	85.6	63.29	709.33	6987.25	1675.1	-	1986 - 2004
299	Yoshii	Yoshii	Miyasu	238.0	61.9	889.22	7265.34	1996.1	-	1966 - 2004
300	Shigenobu	Shigenobu	Yamanouchi	18.7	2.3	76.60	413.04	55.3	-	1963 - 2004
301	Shigenobu	Shigenobu	Omotegawa	42.1	2.37	69.41	724.93	67.1	-	1967 - 2004
302	Shigenobu	Ishite	Yuwatari	16.2	1.95	47.29	370.75	105.4	-	1956 - 2004
303	Shigenobu	Shigenobu	Deai	132.7	10.11	322.74	2278.16	445	-	1956 - 2004
304	Hiji	Oda	Boyashiki	50.0	13.24	184.93	1901.89	371.5	-	1980 - 2004
305	Hiji	Hiji	Ozu	119.4	38.1	353.43	3196.93	984	-	1956 - 2004
306	Hiji	Yauchi	Niiya	42.8	2.08	28.44	282.24	56.7	-	1959 - 2004
307	Watari	Shimanto	Taisyō	45.9	54.56	1575.60	9095.56	942	-	1960 - 2004
308	Watari	Ushiro	Akita	53.7	7.98	221.33	1735.58	145.7	-	1979 - 2004
309	Watari	Nakasuji	Isonokawa	39.0	6.39	176.32	980.32	93.9	-	1953 - 2004
310	Niyodo	Niyodo	Kawaguchi	42.9	41.05	1455.52	8016.74	944.6	-	1961 - 2004
311	Niyodo	Niyodo	Ino	332.4	102.57	1910.48	13513.7	1462.7	-	1957 - 2004
312	Monobe	Monobe	Fukabuchi	211.8	31.38	508.24	4396.24	468.3	-	1961 - 2004
313	Naka	Naka	Wajiku	104.6	69.55	1575.99	7225.97	690	-	1963 - 2004
314	Naka	Naka	Furusyo	248.7	65.17	1968.77	7604.61	765	-	1956 - 2004
315	Yoshino	Yoshino	Toyonaga	78.7	67.11	1222.20	9080.8	933.2	54.1	1958 - 2004
316	Yoshino	Yoshino	Ikeda	179.9	109.9	2311.92	14047.5	2073.8	70	1954 - 2004
317	Yoshino	Yoshino	Iwazu	446.8	142.56	3099.78	16426.5	2810	101.1	1953 - 2004
318	Yoshino	Yoshino	Cyuobashi	541.4	136.53	2502.57	16305.8	3044	115.2	1955 - 2004
319	Yoshino	Kyuyoshino	Kyuyohinogawa	31.6	44.75	53.22	282.9	0	-	1963 - 2004
320	Doki	Doki	Goyobashi	23.8	1.33	86.50	891.23	72.1	-	1974 - 2004
321	Doki	Doki	Tsunekanebashi	13.7	1.88	102.61	1017.82	90	-	1974 - 2004
322	Onga	Onga	Kawashima	80.3	12.22	337.53	1790.79	292	-	1960 - 2004
323	Onga	Onga	Hinodebashi	106.6	31.58	799.70	2656.11	695	-	1951 - 2004
324	Onga	Hikosan	Nakajima	50.7	13.47	370.32	1347.9	326	-	1954 - 2004
325	Onga	Inunaki	Miyatabashi	29.7	4.83	123.34	713.51	123	-	1957 - 2004
326	Matuura	Matsuura	Mutabe	40.5	12.48	287.65	1791.66	275	22.5	1963 - 2004
327	Honmyo	Honmyo	Urayama	21.3	2.1	36.87	721.8	35.8	-	1959 - 2004
328	Rokkaku	Ushizu	Myokenbashi	26.6	4.35	104.86	1094.46	95	-	1958 - 2004
329	Chikugo	Chikugo	Ohira	36.2	13.44	539.17	2256.4	532.8	28.1	1958 - 2004

Table 1. (continued)

No.	River system	River	Measurement site	W_b (m)	Q_{mean} ($m^3 s^{-1}$)	Q_b ($m^3 s^{-1}$)	Q_{max} ($m^3 s^{-1}$)	A_d (km^2)	L_d (km)	Observed year of Q_{mean} and Q_{max}
330	Chikugo	Chikugo	Kobuchi	140.8	56.16	908.12	3873.9	1125	34.8	1955 - 2004
331	Chikugo	Chikugo	Arase	84.4	75.79	1133.43	4528.87	1443	44.8	1968 - 2004
332	Chikugo	Chikugo	Esonoshuku	191.1	76.13	1164.00	5358.97	1566	51.6	1956 - 2004
333	Chikugo	Chikugo	Katanose	127.3	82.21	1235.83	5785.31	1812	59.8	1956 - 2004
334	Chikugo	Chikugo	Senoshita	212.1	98.3	1485.21	6070	2295	69.2	1965 - 2004
335	Chikugo	Kusu	Ogase	49.3	17.39	495.74	2053.6	540.5	-	1956 - 2004
336	Yabe	Yabe	Funagoya	53.6	21.53	478.88	2752.46	460.0	-	1974 - 2004
337	Kikuchi	Kikuchi	Bunda	72.7	27.24	401.53	2976.36	554.0	-	1972 - 2004
338	Kikuchi	Kikuchi	Tamana	105.7	39.55	604.36	4274.35	906.0	-	1952 - 2004
339	Shira	Shira	Jinnai	57.7	23.52	374.37	1703.5	425.0	-	1956 - 2004
340	Shira	Shira	Yotsugibashi	65.7	25.41	414.74	1760.54	477.0	-	1957 - 2004
341	Midori	Midori	Chukobashi	67.6	35.42	424.91	1962.1	519.0	-	1962 - 2004
342	Midori	Midori	Jonan	108.1	36.31	432.48	2686.05	681.0	-	1960 - 2004
343	Midori	Mifune	Mifune	31.1	6.97	89.26	1396.35	120.0	-	1974 - 2004
344	Midori	Kase	Dairokubashi	78.9	19.75	141.77	840.96	220.0	-	1974 - 2004
345	Kuma	Kuma	Hitoyoshi	99.1	77.42	1060.61	5317.83	1137.0	-	1950 - 2004
346	Kuma	Kuma	Yokoishi	142.4	120.74	1723.19	6953.39	1868.0	-	1968 - 2004
347	Kuma	Kuma	Yanase	74.5	34.8	341.60	3049.18	521.0	-	1952 - 2004
348	Sendai	Sendai	Yoshimatsu	52.3	21.33	355.40	1270.04	284.0	24.6	1960 - 2004
349	Sendai	Sendai	Arata	69.8	31.21	418.42	1178.18	428.0	33.8	1979 - 2004
350	Sendai	Sendai	Onobuchi	118.6	90.78	1313.00	3598.66	1348.0	65.7	1956 - 2004
351	Kimotsuki	Kimotsuki	Takarabashi	51.2	15.7	171.65	1048.7	244.0	-	1978 - 2004
352	Kimotsuki	Kimotsuki	Matase	98.7	31.85	295.86	1727.27	450.0	-	1978 - 2004
353	Oyodo	Oyodo	Hiwatashi	86.8	61.12	863.91	3424.53	861.0	-	1963 - 2004
354	Oyodo	Oyodo	Takaoka	111.8	107.67	1505.47	6166.9	1564.0	-	1954 - 2004
355	Oyodo	Oyodo	Kashiwada	208.4	144.86	2467.76	7136.39	2126.0	-	1965 - 2004
356	Oyodo	Honjo	Arashida	65.0	29.88	615.42	2365.41	381.0	-	1955 - 2004
357	Omaru	Omaru	Takajo	97.2	33.26	1113.40	4060.91	396.3	-	1955 - 2004
358	Gokase	Gokase	Miwa	122.7	62.15	1373.31	9179.6	1044.1	-	1953 - 2004
359	Gokase	Gokase	Kumata	138.0	33.24	745.36	5500	519.0	-	1953 - 2004
360	Bansho	Bansho	Banshobashi	100.0	12.54	479.50	2922.57	278.0	-	1954 - 2004
361	Ono	Ono	Inukai	96.1	62.36	1439.86	9373.17	1239.0	-	1956 - 2004
362	Ono	Ono	Shiratakibashi	163.9	61.82	1547.95	9330.56	1381.0	-	1950 - 2004
363	Oita	Oita	Dojiri	47.5	20.71	316.22	2228.04	412.0	-	1972 - 2004
364	Oita	Oita	Akegawarabashi	66.0	22.33	368.81	3570	494.0	-	1950 - 2004
365	Oita	Oita	Funaiohashi	91.1	27.84	506.08	3825.91	601.0	-	1969 - 2004
366	Oita	Nanase	Gomazuru	17.5	5.2	119.90	1208.33	93.0	-	1966 - 2004
367	Yamakuni	Yamakuni	Shimotobaru	99.1	21.03	646.26	3131.48	483.0	-	1954 - 2004
368	Kase	Kase	Kawakami	44.1	14.12	148.14	1039.23	225.5	-	1973 - 2004

Table 2. List of symbols used in this study.

h	Thickness of bar deposit (m)
S_{mean}	Mean cross-set thickness (cm)
H_{mean}	Mean dune height (cm)
d	Bankfull channel depth (m)
d_{m}	Mean bankfull channel depth (m)
W	Channel width (m)
W_{b}	Bankfull channel width (m)
C	Bankfull cross-sectional area (m ²)
P_{w}	Wetted perimeter (m)
Q_{mean}	Mean discharge (m ³ s ⁻¹)
Q_{b}	Bankfull discharge (m ³ s ⁻¹)
Q_{max}	Maximum discharge (m ³ s ⁻¹)
Q_2	2-year flood discharge (m ³ s ⁻¹)
A_{d}	Drainage basin area (km ²)
L_{d}	Drainage basin length (km)
D_{50}	Median grain size (mm)
S	Slope
L_{b}	Backwater length (km)
N	Number of data
r	Correlation coefficient
R^2	Coefficient of determination
p	Level of significance

Table 3. Cross-sectional data of river channels in the Kanto region. The numbers correspond to the site number in Figure 7. See Table 2 for the definitions of symbols.

No.	River system	River	Site name	W_b (m)	d (m)	C (m^2)	P_w (m)	d_m (m)
1	Kuji	Kuji	Sakakibashi	148.5	7.2	873.6	157.3	5.6
2	Kuji	Kuji	Tomioka	106.5	5.6	466.9	113.6	4.1
3	Kuji	Kuji	Yamagata	98.0	2.9	155.6	94.8	1.6
4	Naka	Naka	Noguchi	168.0	6.4	697.5	173.5	4.0
5	Naka	Naka	Kurobane	91.5	3.3	97.7	93.8	1.0
6	Tone	Tone	Futto	485.0	7.2	2,384.7	499.8	4.8
7	Tone	Tone	Yattajima	404.0	5.8	1,630.4	417.5	3.9
8	Tone	Tone	Kamifukushima	115.0	8.4	480.7	120.3	4.0
9	Tone	Tone	Maebashi	162.0	8.1	552.4	169.4	3.3
10	Tone	Agatsuma	Murakami	65.0	5.2	232.4	67.7	3.4
11	Tone	Karasu	Iwahana	162.0	6.1	689.3	171.8	4.0
12	Tone	Karasu	Takamatsu	85.0	3.9	311.6	89.9	3.5
13	Tone	Karasu	Kamisatomi	34.2	3.5	64.1	37.5	1.7
14	Tone	Usui	Annaka	52.6	6.6	233.1	60.1	3.9
15	Tone	Kabura	Iwai	39.5	3.7	97.3	43.4	2.2
16	Tone	Watarase	Sakawadakami	144.0	6.8	675.6	152.5	4.4
17	Tone	Watarase	Ashikaga	185.0	3.9	341.1	188.4	1.8
18	Tone	Uzuma	Nakazato	32.0	2.3	33.3	34.0	1.0
19	Tone	Omoi	Otome	60.0	6.5	256.8	64.9	4.0
20	Ara	Ara	Oashibashi	156.0	8.7	886.1	166.1	5.3
21	Ara	Iruma	Sugama	96.0	9.4	752.2	112.0	6.7
22	Ara	Ara	Yorii	80.5	4.2	162.5	87.0	1.9
23	Tama	Tama	Ishihara	180.0	6.6	517.8	188.1	2.8
24	Tsurumi	Tsurumi	Kamenokobashi	31.0	3.9	75.7	32.6	2.3

Table 4. Relationships between the bankfull channel width, discharges, drainage basin area, and drainage basin length for fluvial system in the Japanese Archipelago. See Table 2 for the definitions of symbols.

Relationships between bankfull channel width and mean discharge					
Region	Equation	N	r	R^2	p
Hokkaido	$Q_{\text{mean}} = 0.70 W_b^{0.95}$	46	0.67	0.45	2.9×10^{-7}
Northeast Japan	$Q_{\text{mean}} = 0.12 W_b^{1.37}$	124	0.79	0.63	6.8×10^{-28}
Chubu region	$Q_{\text{mean}} = 0.53 W_b^{0.93}$	28	0.67	0.45	8.8×10^{-5}
Southwest Japan	$Q_{\text{mean}} = 0.14 W_b^{1.18}$	169	0.75	0.57	3.5×10^{-32}
Japan (average)	$Q_{\text{mean}} = 0.17 W_b^{1.21}$	367	0.73	0.53	6.5×10^{-62}

Relationships between bankfull channel width and bankfull discharge					
Region	Equation	N	r	R^2	p
Hokkaido	$Q_b = 2.89 W_b^{1.17}$	41	0.72	0.51	1.3×10^{-7}
Northeast Japan	$Q_b = 4.18 W_b^{1.15}$	123	0.79	0.62	1.6×10^{-27}
Chubu region	$Q_b = 4.47 W_b^{1.01}$	27	0.77	0.59	6.5×10^{-7}
Southwest Japan	$Q_b = 2.33 W_b^{1.17}$	165	0.75	0.56	1.1×10^{-30}
Japan (average)	$Q_b = 2.78 W_b^{1.17}$	356	0.75	0.56	7.1×10^{-65}

Relationships between bankfull channel width and maximum discharge					
Region	Equation	N	r	R^2	p
Hokkaido	$Q_{\text{max}} = 43.44 W_b^{0.81}$	46	0.58	0.33	2.7×10^{-5}
Northeast Japan	$Q_{\text{max}} = 36.14 W_b^{0.94}$	125	0.79	0.63	4.7×10^{-28}
Chubu region	$Q_{\text{max}} = 52.33 W_b^{0.84}$	28	0.72	0.52	5.5×10^{-6}
Southwest Japan	$Q_{\text{max}} = 39.22 W_b^{0.96}$	169	0.73	0.54	1.0×10^{-29}
Japan (average)	$Q_{\text{max}} = 39.47 W_b^{0.93}$	368	0.71	0.51	3.4×10^{-58}

Relationships between bankfull discharge and drainage basin area					
Region	Equation	N	r	R^2	p
Hokkaido	$A_d = 15.86 Q_b^{0.72}$	41	0.87	0.75	2.3×10^{-13}
Northeast Japan	$A_d = 1.20 Q_b^{1.07}$	118	0.91	0.83	3.6×10^{-47}
Chubu region	$A_d = 4.10 Q_b^{0.83}$	27	0.74	0.54	3.2×10^{-6}
Southwest Japan	$A_d = 5.58 Q_b^{0.78}$	164	0.82	0.68	5.5×10^{-42}
Japan (average)	$A_d = 3.41 Q_b^{0.89}$	350	0.85	0.71	9.2×10^{-97}

Relationships between drainage basin area and drainage basin length					
Region	Equation	N	r	R^2	p
Hokkaido	$L_d = 2.26 A_d^{0.44}$	17	0.87	0.76	5.1×10^{-6}
Northeast Japan	$L_d = 1.13 A_b^{0.52}$	36	0.94	0.88	1.6×10^{-17}
Chubu region	$L_d = 1.48 A_b^{0.51}$	14	0.75	0.56	0.002
Southwest Japan	$L_d = 2.16 A_d^{0.44}$	39	0.82	0.68	3.1×10^{-11}
Japan (average)	$L_d = 1.73 A_b^{0.47}$	106	0.89	0.79	2.5×10^{-37}

Table 5. Relationships between the cross-sectional parameters of river channels in the Kanto region. See Table 2 for the definitions of symbols.

Equation	r	R^2	p	N
$d_m = 0.62 d$	0.87	0.76	3.3×10^{-8}	24
$W_b = 49.16 d_m^{0.67}$	0.47	0.22	0.02	24

Table 6. Empirical equations linking the channel width (W or W_b) and the mean (Q_{mean}) and bankfull (Q_b) discharges from modern fluvial systems in the Japanese Archipelago and the Eurasian, North American, and Australian continents, and Indonesian Archipelago.

Equation	Reference	Applicable range	Remarks
Channel width–mean discharge relations			
$Q_{\text{mean}} = 0.17 W_b^{1.21}$	Present study	$13.7 \leq W_b \leq 541.4$ m	Rivers in the Japanese Archipelago. Data are from 367 sites along various Japanese rivers.
$Q_{\text{mean}} = 0.0055 W^{2.17}$ ($W = 10.99 Q_{\text{mean}}^{0.46}$)	Carlston (1965)	–	Meandering rivers mostly from central U.S.A. W is channel width. Revised by Bridge (2003).
$Q_{\text{mean}} = 0.027 W_b^{1.17}$	Osterkamp and Hedman (1982)	$0.8 \leq W_b \leq 430$ m	Missouri river basin, U.S.A. Width data were described as the active channel width, but Williams (1984b) regarded them as the bankfull channel width.
$Q_{\text{mean}} = 0.06 W_b^{1.66}$	Williams (1984a)	$1.8 \leq W_b \leq 67$ m	Meandering rivers in Sweden.
$Q_{\text{mean}} = 0.06 W_b^{1.65}$	Adhiperdana (2018)	$4 \leq W_b \leq 466$ m	Rivers in Java, Sumatra, and Kalimantan islands, Indonesia.
Channel width–bankfull discharge relations			
$Q_b = 2.78 W_b^{1.17}$	Present study	$13.7 \leq W_b \leq 541.4$ m	Rivers in the Japanese Archipelago. Q_b is the mean annual flood discharge. Data are from 356 sites along various Japanese rivers.
$Q_b = 0.126 W_b^{1.84}$ ($W_b = 3.0825 Q_b^{0.543}$)	Dury (1976)	$12 \leq Q_b \leq 290,000$ m ³ s ⁻¹	Unbraided rivers in U.S.A., U.K., European mainland, U.S.S.R., Australia, China, and India. Width data were originally defined as the bed width, but some data have been regarded as the bankfull channel width by Williams (1984b). Q_b is 1.58-year flood discharge.
$Q_2 = 1.9 W_b^{1.22}$	Osterkamp and Hedman (1982)	$0.8 \leq W_b \leq 430$ m	Missouri river basin, U.S.A. Width data were originally described as the active channel width. Q_2 is the 2-year flood discharge.
$Q_b = 1.0 W_b^{1.3}$	Williams (1984a)	$1.8 \leq W_b \leq 67$ m	Meandering rivers in Sweden. Q_b is the average annual peak discharge.
$Q_b = 0.05 W_b^{2.04}$ ($W_b = 4.33 Q_b^{0.49}$)	Mackey (1993)	–	Cited by Bridge (2003).
$Q_b = 1.09 W_b^{1.42}$	Adhiperdana et al. (2018)	$4 \leq W_b \leq 466$ m	Rivers in Java, Sumatra, and Kalimantan islands, Indonesia.

Table 7. Data of bankfull discharge (Q_b), drainage basin area (A_d), and drainage basin length (L_d) for the modern fluvial system in the Indonesian Archipelago. Data of Q_b and A_d are based on Adhiperdana et al. (2018) and the Center for Water Resources Development and Research (2011).

No.	Islands	River system	River	Measurement site	Q_b ($m^3 s^{-1}$)	A_d (km^2)	L_d (km)
1	Java	Ciliman	Ciliman	Leuwikopo	84.68	105.8	-
2	Java	Ciliman	Ciliman	Munjul	118.95	318.5	-
3	Java	Cibungur	Cisata	Pasir sereh	47.60	60	-
4	Java	Cibungur	Cilemer	Cipadung	28.56	153.6	-
5	Java	Cibungur	Cimoyan	Pasir Gadung	54.83	74.2	-
6	Java	Cibungur	Cikadueun	Cibogo	91.08	32.2	-
7	Java	Cidano	Cidano	Peusar	44.57	212.75	-
8	Java	Cibama	Cibama	Kalumpang	62.12	46.8	-
9	Java	Cidano	Cidanghiang	Cibitung	2.36	8.9	-
10	Java	Cidano	Cibojong	Tambakan	11.45	18.7	-
11	Java	Cidano	Cikalumpang	Panggilingan	4.30	28	-
12	Java	Cibanten	Cibanten	Pabuaran	20.05	49.8	-
13	Java	Ciujung	Ciberang	Sabagi	211.65	301.2	-
14	Java	Ciujung	Ciberang	Jembatan Keong	349.81	612.5	-
15	Java	Ciujung	Cisimet	Leuwidamar	132.57	395	-
16	Java	Ciujung	Ciujung	Kragilan	818.88	1562.7	-
17	Java	Ciujung	Ciujung	Rangkasbitung	728.81	1063.8	-
18	Java	Ciujung	Ciujung	Cileuleus (Cilandak)	138.44	217	-
19	Java	Ciujung	Ciujung hulu	Bojongmanik	44.55	90.6	-
20	Java	Ciujung	Ciujung	Kedung Cinde	462.00	16	-
21	Java	Cidurian	Cidurian	Kopomaja	190.74	296.4	-
22	Java	Cidurian	Cidurian	Parigi	250.26	602.2	-
23	Java	Ciujung	Cibeureum	Neglasari	62.20	127.4	-
24	Java	Cidurian	Cidurian	Ranca Sumur	85.17	319.4	-
25	Java	Cisadane	Cisadane	Genteng	85.29	185	-
26	Java	Cisadane	Cisadane	Babakan	273.82	1146	-
27	Java	Kali Angke	Kali Grogol	Pal Merah	5.68	10.6	-
28	Java	Kali Angke	Kali Angke	Rawabuaya	18.64	260.6	-
29	Java	Kali Angke	Kali Pasanggaraha	Sawangan	27.85	56.3	-
30	Java	Kali Angke	Kali Pasanggaraha	Kebon Jeruk	38.10	123	-
31	Java	Ciliwung	Ciliwung	Katulampa	317.71	151.76	-
32	Java	Ciliwung	Ciesek	Palumbon (Paseban)	8.40	3.7	-
33	Java	Ciliwung	Ciliwung	Ratujaya	230.39	231	-
34	Java	Ciliwung	Ciliwung	Kampung Kelapa	223.17	158	-
35	Java	Ciliwung	Ciliwung	Sugutamu	150.56	266.6	-
36	Java	Ciliwung	Kali Krukut	Bendungan Hilir	48.83	63.8	-
37	Java	Kali Sunter	Kali Sunter	Cipinang Muara	22.17	137.7	-
38	Java	Cisadane	Cisadane	Batubeulah	696.23	819.6	-
39	Java	Cisadane	Cisadane	Legokmuncang	144.25	196	-
40	Java	Citarum	Cikeruh	Cikuda	42.94	54.2	-
41	Java	Citarum	Cibodas	Jatisari	20.46	18.8	-
42	Java	Citarum	Cijalupang	Peundeuy	19.43	20.7	-
43	Java	Citarum	Cikeruh	Babakan Bandung	30.90	48	-
44	Java	Citarum	Cirasea	Cengkrong	29.09	64	-
45	Java	Citarum	Cirasea	Andir	29.94	68.3	-
46	Java	Citarum	Cipanjal	Kepuh	27.10	15.7	-
47	Java	Citarum	Citarum	Cibangoak	40.30	86.8	11.20
48	Java	Citarum	Cisangkuy	Kamasan	139.21	205.7	-
49	Java	Citarum	Ciwidey	Cukanggenteng	59.50	175.3	-
50	Java	Citarum	Cisangkuy	Pataruman	58.22	92.7	-
51	Java	Citarum	Citarum	Tanjungpura	941.80	6063.3	115.20
52	Java	Citarum	Citarum	Nanjung	397.43	1718	31.50
53	Java	Citarum	Cikapundung	Maribaya	68.65	98.8	-
54	Java	Citarum	Cikapundung	Pasirluyu (bypass)	67.82	76	-
55	Java	Citarum	Cigulung	Maribaya	82.97	36.8	-
56	Java	Citarum	Cikapundung	Gandok	70.36	90.4	-
57	Java	Citarum	Citarum	Dayeuhkolot	322.45	1035.8	26.7
58	Java	Citarum	Cidurian	Sukapada	12.12	17.9	-
59	Java	Citarum	Citarik	Rancakemit	72.78	263.8	-
60	Java	Citarum	Citarum	Mahmud	230.90	1667.5	-
61	Java	Citarum	Citarik	Bendung Cangkuang	20.64	35.8	-
62	Java	Citarum	Citarum	Majalaya	133.28	176.5	12.30
63	Java	Citarum	Cimahi	Cicakung	7.26	26.8	-
64	Java	Citarum	Cibereum	Cihideung	1.29	26.7	-

Table 7. (continued)

No.	Islands	River system	River	Measurement site	Q_b ($m^3 s^{-1}$)	A_d (km^2)	L_d (km)
65	Java	Citarum	Cilalawi	Cilalawi	86.09	125.3	-
66	Java	Citarum	Cimeta	Bepak	64.75	132.5	-
67	Java	Citarum	Cisokan	Mangled	245.43	623	-
68	Java	Citarum	Cibalagung	Leuwigarut	79.34	45.1	-
69	Java	Cilamaya	Cilamaya	Cipeundeuy	215.96	265	-
70	Java	Ciasem	Ciasem	Curug ageung	34.93	169	-
71	Java	Cimanuk	Cimanuk	Bojongloa	80.66	286	-
72	Java	Cimanuk	Cimanuk	Leuwidaun	193.15	456.6	-
73	Java	Cimanuk	Cimanuk	Leuwigoong	209.79	759.6	-
74	Java	Cimanuk	Cimanuk	Wado	308.45	1263	-
75	Java	Cimanuk	Cimanuk	Tomo	486.70	1966.3	-
76	Java	Cimanuk	Cipeles	Warung Peti	141.47	436.7	-
77	Java	Cimanuk	Cipeles	Sukatali	326.40	286	-
78	Java	Cimanuk	Cilutung	Dam Kamun	592.34	620.5	-
79	Java	Cimanuk	Cilutung	Bantar Merak	690.35	340	-
80	Java	Cimanuk	Cimanuk	Jatibarang	709.00	3321.8	-
81	Java	Cimanuk	Cimanuk	Monjot	821.59	2788	-
82	Java	Cimanuk	Cikeruh	Jatiwangi	842.71	103	-
83	Java	Cimanuk	Cimanuk	Kertasemaya	1146.64	3305	-
84	Java	Cisanggarung	Cisanggarung	Baok	468.65	815	-
85	Java	Cisanggarung	Cisanggarung	Jembatan Losari	1139.96	834.9	-
86	Java	Cisanggarung	Cisanggarung	Cibinuang	60.14	675	-
87	Java	Cisanggarung	Cisanggarung	Pasuruan	406.10	826	-
88	Java	Pemali	Pemali	Notog	241.79	855.9	-
89	Java	Cisanggarung	Cijangkelok	Cibendung	126.40	127.5	-
90	Java	Kabuyutan	Kali Kabuyutan	Kertasari	23.01	97.3	-
91	Java	Pemali	Pemali	Kedung Tukang	324.68	851.2	-
92	Java	Pemali	Pemali	Bantar Kawung	576.15	339.3	-
93	Java	Pemali	Pemali	Rengas Pendawa	497.33	1111	-
94	Java	Pemali	Pemali	Brebes	910.67	863.2	-
95	Java	Kali Gung	Kali Gung	Pesayangan	316.91	139.9	-
96	Java	Kali Rambut	Kali Rambut	Cipero	29.28	127	-
97	Java	Kali Waluh	Waluh	Sungapan	69.60	136.9	-
98	Java	Comal	Comal	Kecepit	80.18	126.8	-
99	Java	Comal	Genteng	Kaliwadas	147.13	173.9	-
100	Java	Comal	Comal	Sukowati	560.60	359.41	-
101	Java	Comal	Comal	Jatijero	567.63	739.4	-
102	Java	Comal	Lumeneng	Watukumpul	79.88	72.5	-
103	Java	Kupang	Kupang	Pagarukir	87.18	34.7	-
104	Java	Kupang	Kali Pekalongan	Kuripan Kidul	168.44	138	-
105	Java	Sambong	Sambong	Kedungdowo	105.91	97.5	-
106	Java	Glagah	Glagah	Kedung Sari	62.08	20.5	-
107	Java	Bodri	Bodri	Juwero	535.52	522.3	-
108	Java	Belukar	Belukar	Sejomerto	119.65	105.1	-
109	Java	Blorong	Blorong	Kedung Pucung	193.22	157.9	-
110	Java	Garang	Garang	Pajangan	341.72	189.8	-
111	Java	Garang	Kreo	Kalipancur	192.93	66.6	-
112	Java	Serang	Serang	Muncar	84.90	97.7	-
113	Java	Serang	Serang	Guwo	419.00	266.2	-
114	Java	Serang	Serang	Tongpait	556.36	2531.6	-
115	Java	Serang	Laban	Jengglong	235.89	72.8	-
116	Java	Serang	Giren	Giren	7.16	12.1	-
117	Java	Lusi	Lusi	Menduran	331.30	1997.3	-
118	Java	Serang	Lusi	Kunduran	208.25	734.5	-
119	Java	Serang	Lusi	Banjarrejo	220.95	402.6	-
120	Java	Serang	Lusi	Tawangharjo	719.70	1642	-
121	Java	Juana	Logung	Kedung Mojo	44.59	49.8	-
122	Java	Sulang	Sulang	Sulang	67.64	45.8	-
123	Java	Sulang	Besek	Tlogo	10.88	12.7	-
124	Java	Bengawan Solo	Bengawan Solo	Kedung Areng	376.33	937	28.70
125	Java	Bengawan Solo	Gondang	Stren (Bojonegoro)	37.86	67	-
126	Java	Bengawan Solo	Tirtomoyo	Sulingi	476.81	163.8	-
127	Java	Bengawan Solo	Bengawan Solo	Jurang Gempal	762.72	1216	34.00
128	Java	Bengawan Solo	Dengkeng	Paseban	192.39	213.4	-
129	Java	Bengawan Solo	Bengawan Solo	Jurug	554.91	3206.7	56.60
130	Java	Bengawan Solo	Goseng	Ngunut	35.00	5.96	-

Table 7. (continued)

No.	Islands	River system	River	Measurement site	Q_b ($m^3 s^{-1}$)	A_d (km^2)	L_d (km)
131	Java	Bengawan Solo	Plawatan	Donorejo	37.66	2.6	-
132	Java	Bengawan Solo	Wungu	Pakisbaru	7.89	2.03	-
133	Java	Bengawan Solo	Ngunut II	Kuwon	31.57	1.86	-
134	Java	Bengawan Solo	Padas	Grasak	60.25	34.85	-
135	Java	Bengawan Solo	Tapan	Tapan	9.24	1.84	-
136	Java	Bengawan Solo	Temon	Duwet Lor	200.91	42.5	-
137	Java	Bengawan Solo	Alang	Kedungpadas	121.98	54.4	-
138	Java	Bengawan Solo	Keduang	Ngadipiro	119.88	359.9	-
139	Java	Bengawan Solo	Wuryantoro	Tiken	166.04	17.9	-
140	Java	Bengawan Solo	Cemoro	Ngrukun	225.26	199.7	-
141	Java	Kali Klero	Klero	Genaharjo	13.96	43	-
142	Java	Bengawan Solo	Cawak	Kedung Lerep (Bojonegoro)	47.26	64.97	-
143	Java	Bengawan Solo	Kerjo	Pejok	152.18	50.8	-
144	Java	Bengawan Solo	Kali Gandong	Setren (Bojonegoro)	43.02	67	-
145	Java	Kali Lamong	Lamong	Simoanggrok	76.00	209	-
146	Java	Bengawan Solo	Pacal	Senganten	46.00	13.53	-
147	Java	Kali Gembul	Gembul	Merakurak	39.74	67.5	-
148	Java	Bengawan Solo	Bengawan Solo	Napel	1965.70	95	-
149	Java	Bengawan Solo	Bengawan Solo	Kauman	1185.40	5195.6	89.50
150	Java	Bengawan Solo	Kali Madiun	Ngawi	813.61	4202	-
151	Java	Bengawan Solo	Kali Keang	Ponorogo	45.65	115	-
152	Java	Bengawan Solo	Kali Madiun	Nambangan	481.40	2126	-
153	Java	Bengawan Solo	Bengawan Solo	Cepu	1906.95	1125	-
154	Java	Bengawan Solo	Bengawan Solo	Bojonegoro	1945.21	3956.5	-
155	Java	Bengawan Solo	Bengawan Solo	Babat	1656.71	16286.2	183
156	Java	Bengawan Solo	Bengawan Solo	Karang Geneng	1272.39	6872	-
157	Java	Bengawan Solo	Bengawan Solo	Karang Binangun	1248.48	16997	218.70
158	Java	Bengawan Solo	Kali Kening	Selogabus	313.72	6286.2	-
159	Java	Bengawan Solo	Bengawan Solo	Sembayat	2307.43	17416	222.4
160	Java	Kali Brantas	Kali Brantas	Kertosono	994.16	7112	97.70
161	Java	Kali Brantas	Kali Brantas	Ploso	1008.03	10045	95.3
162	Java	Kali Brantas	Kali Sumberampel	Baros	124.98	5.3	-
163	Java	Kali Brantas	Kali Brantas	Pundensari	635.33	4093	93.1
164	Java	Kali Brantas	Kali Bangsal	Kedung Uneng	5.78	54.7	-
165	Java	Kali Brantas	Kali Bagong	Temon	108.11	41.6	-
166	Java	Kali Brantas	Kali Keser	Keser	74.42	42.8	-
167	Java	Kali Brantas	Kali Duren	Trenggalek	13.78	15	-
168	Java	Kali Brantas	Kali Lahar	Bacem	12.24	37.3	-
169	Java	Kali Brantas	Kali Brantas	Mojooroto (Kediri)	588.68	6361.8	108.00
170	Java	Kali Brantas	Kali Sayang	Jabon	22.65	11.3	-
171	Java	Kali Brantas	Kali Brantas	Kertosono	934.28	7112	98.00
172	Java	Bengawan Solo	Kali Gangseng	Sugiharas	89.03	70.4	-
173	Java	Kali Welang	Kali Welang	Purwodadi	54.22	145.7	-
174	Java	Kali Welang	Kali Welang	Pohjethek	145.25	467	-
175	Java	Kali Rejoso	Kali Rejoso	Winongan (Pasuruan)	75.22	201.7	-
176	Java	Kali Gembong	Kali Gembong	Warung Dowo	214.45	70.79	-
177	Java	Kali Kramat	Kali Kramat	Probolinggo	91.68	191.9	-
178	Java	Kali Pekalen	Kali Pekalen	Condong	55.32	162.6	-
179	Java	Kali Pekalen	Kali Rondoningo	Jurang Jero	15.85	82.3	-
180	Java	Kali Deluwang	Kali Deluwang	Demung (Besuki)	145.39	85	-
181	Java	Kali Sampean	Kali Sampean	Masabit	216.51	612.3	-
182	Java	Kali Bajumati	Kali Bajumati	Bajumati	27.34	198	-
183	Java	Kali Madiun	Kali Slahung	Sumoroto	165.70	779	-
184	Java	Cisanggarung	Cisanggarung	Cilengkrang	293.40	644.35	-
185	Java	Cibuni	Cibuni	Cibungur	682.66	1080.75	-
186	Java	Cibuni	Cibuni	Palatar	163.00	283	-
187	Java	Cikaso	Cikaso	Parungseah	647.70	487.2	-
188	Java	Cimandiri	Citarik	Pajagan	98.04	233.8	-
189	Java	Citanduy	Citanduy	Cirahong	389.32	622	-
190	Java	Citanduy	Citanduy	Leuwitonjong	190.32	444.8	-
191	Java	Citanduy	Citanduy	Pataruman	853.52	1416.2	-
192	Java	Citanduy	Ciloseh	Sukaratu	121.14	36	-
193	Java	Citanduy	Cimuntur	Banaruka	110.75	250.43	-
194	Java	Citanduy	Ciseel	Cilisung	185.14	190.2	-
195	Java	Citanduy	Ciseel	Binangun	232.10	327.2	-
196	Java	Citanduy	Cimeneng	Stinggil	132.39	20.7	-

Table 7. (continued)

No.	Islands	River system	River	Measurement site	Q_b ($m^3 s^{-1}$)	A_d (km^2)	L_d (km)
197	Java	Citanduy	Ciseel	Ciawitali	229.87	596.6	-
198	Java	Citanduy	Cimuntur	Cibeka	60.50	602	-
199	Java	Citanduy	Barokeh	Sawangan	174.51	30.8	-
200	Java	Citanduy	Cijolang	Bebedahan	367.79	473.15	-
201	Java	Citanduy	Cijolang	Cibali	9.00	9.6	-
202	Java	Citanduy	Citanduy	Karangsari	704.57	2682	-
203	Java	Ciwulan	Ciwulan	Sukaraja	726.01	524.4	-
204	Java	Cilangla	Cilangla	Leuwineukteuk	482.74	176.7	-
205	Java	Cilangla	Cijalu	Ciawitali	231.26	91.6	-
206	Java	Cibuni	Cibuni	Cibungur	509.28	1080.75	-
207	Java	Cibuni	Cibuni	Palatar	320.15	283	-
208	Java	Cikaso	Cikaso	Parungseah	845.30	487.2	-
209	Java	Cimandiri	Cimandiri	Tegaldatar	193.78	520.6	-
210	Java	Cimandiri	Cimandiri	Leuwilung	189.95	87.6	-
211	Java	Cimandiri	Citarik	Pajagan	83.01	233.8	-
212	Java	Progo	Tangsi	Susukan	176.41	119.1	-
213	Java	Progo	Elo	Mendut	251.03	444.2	-
214	Java	Progo	Progo	Borobudur	688.29	948	50.90
215	Java	Progo	Progo	Kranggan II	281.00	423.4	28.20
216	Java	Progo	Progo	Badran	148.59	591.95	33.40
217	Java	Bogowonto	Bogowonto	Pungangan	153.73	346.9	-
218	Java	Kali Jali	Kali Jali	Winong	269.59	144.3	-
219	Java	Padegolan	Padegolan	Pajengkolan	412.14	212.6	-
220	Java	Lokulo	Lokulo	Kali Gending	279.37	270	-
221	Java	Serayu	Serayu	Banjarnegara	629.70	704.3	-
222	Java	Serayu	Begaluh	Krasak	131.85	233	-
223	Java	Serayu	Merawu	Clangap	202.38	218.6	-
224	Java	Serayu	Klawing	Dagan	43.89	31.3	-
225	Java	Serayu	Klawing	Slinga	836.85	586.8	-
226	Java	Serayu	Serayu	Banyumas	1197.91	2631.3	-
227	Java	Serayu	Serayu	Rawalo	1395.37	2826.5	-
228	Java	Serayu	Tajum	Tipar Kidul	331.50	247.5	-
229	Java	Serayu	Banjaran	Kober	207.62	44.5	-
230	Java	Serayu	Tambra	Karang Tengah	185.50	55.9	-
231	Java	Citanduy	Cikawung	Cimei	169.33	526	-
232	Java	Citanduy	Cikondang	Cibungur	18.75	21.5	-
233	Java	Citanduy	Cikuya	Surusunda	8.08	16.5	-
234	Java	Kali Progo	Progo	Duwet	469.17	1712.3	61.70
235	Java	Kali Oyo	Oyo	Bunder	141.02	505.5	-
236	Java	Kali Opak	Kedung Keris	Kedung Keris	4.67	12	-
237	Java	Kali Opak	Winongo	Padokan	47.78	48.85	-
238	Java	Kali Opak	Opak	Karangsemut	147.31	431.8	-
239	Java	Kali Opak	Oyo	Dogongan	333.32	1017	-
240	Java	Kali Opak	Oyo	Kedungmiri	205.86	957.5	-
241	Java	Kali Opak	Code	Pogung	14.23	30.4	-
242	Java	Kali Opak	Opak	Pulo	8.59	12.8	-
243	Java	Kali Opak	Tambakbayan	Seturan	2.91	12.6	-
244	Java	Kali Opak	Gajahwong	Papringan	12.34	10.25	-
245	Java	Kali Opak	Code	Kaloran	29.04	41.1	-
246	Java	Kali Progo	Progo	Kali Bawang	342.73	1676	59.3
247	Java	Kali Progo	Progo	Bantar	685.80	2008	-
248	Java	Kali Serang	Progo	Sapon	286.50	1520	84.50
249	Java	Kali Serang	Serang	Durungan	264.01	107	-
250	Java	Kali Serang	Serang	Bendungan	146.34	125.3	-
251	Java	Kali Serang	Serang	Pengasih	109.80	84.6	-
252	Java	Kali Serang	Ngrancah	Sermo	7.80	17.6	-
253	Java	Kali Brantas	Kali Ngasinan	Parit raya Bendo	186.58	137.4	-
254	Java	Kali Tambong	Kali Tambong	Pakistaji	76.87	119.5	-
255	Java	Kali Baru	Kali Baru	Karangdoro	279.91	372.4	-
256	Java	Kali Mayang	Kali Sanen	Sanenrejo (Jember)	187.07	272.7	-
257	Java	Kali Bedadaung	Kali Bedadung	Rawatamtu	597.59	695.9	-
258	Java	Kali Asem	Kali Asem	Sentul	57.26	182.8	-
259	Java	Kali Bondoyudo	Kali Bondoyudo	Wonorejo	203.61	276.3	-
260	Java	Kali Bomo	Kali Bomo Bawah	Rogojampi	123.46	94.2	-
261	Java	Kali Bomo	Kali Bomo Atas	Parijati (Srono)	100.84	80	-
262	Java	Kali Lorok	Kali Lorok	Wonodadi	87.57	210.2	-

Table 7. (continued)

No.	Islands	River system	River	Measurement site	Q_b ($m^3 s^{-1}$)	A_d (km^2)	L_d (km)
263	Java	Kali Grindulu	Kali Grindulu	Gunung Sari	490.32	249.1	-
264	Java	Kali Mayang	Kali Mayang	Pakusari	11.55	217.5	-
265	Sumatra	Kr. Baro	Kr. Baro	Klibeut	121.06	265.6	-
266	Sumatra	Kr. Baro	Kr. Baro	Kemala dalam	141.20	232.4	-
267	Sumatra	Kr. Baro	Kr. Baro	Kp. Geuni Puni	72.96	121.0	-
268	Sumatra	Kr. Peudada	Kr. Peudada	Menasang Lawang	178.95	458.0	-
269	Sumatra	Kr. Peusangan	Kr. Peusangan	Beukah	406.75	2006.5	-
270	Sumatra	Kr. Peusangan	Kr. Peusangan	Simp. Jaya	556.36	2077.0	-
271	Sumatra	Kr. Peusangan	Kr. Sempo	Sempo	74.68	2378.0	-
272	Sumatra	Kr. Mane	Kr. Mane	Lhok Kuyun	112.62	448.8	-
273	Sumatra	Kr. Mane	Kr. Tuan	Lhok Joek	66.78	96.9	-
274	Sumatra	Kr. Jambo Aye	Kr. Jambo Aye	Lhok Nibong	816.16	4418.9	-
275	Sumatra	Kr. Jambo Aye	Kr. Jambo Aye	Rampah	749.84	4097.0	-
276	Sumatra	Kr. Tamiang	Kr. Tamiang	Kuala Simpang	1158.67	4094.0	-
277	Sumatra	Kr. Seumayam	Kr. Seumayam	Seumayam	42.26	110.6	-
278	Sumatra	S. Langkat	S. Wampu	Stabat	950.58	1621.3	-
279	Sumatra	S. Bingai	S. Bingei	Kp Pahlawan	263.80	970.0	-
280	Sumatra	S. Wampu	S. Mencirim	Binjai	348.23	120.0	-
281	Sumatra	S. Belawan	S. Belawan	Asam Kumbang	214.55	201.3	-
282	Sumatra	S. Belawan	S. Belawan	Kp. Lalang	98.70	245.6	-
283	Sumatra	S. Deli	S. Deli	Helvetia	79.44	161.3	-
284	Sumatra	S. Deli	S. Deli	Simeme	69.64	133.8	-
285	Sumatra	S. Percut	S. Percut	Tembung	64.37	166.3	-
286	Sumatra	S. Blumai	S. Blumai	Tanjung Morawa	172.75	250.0	-
287	Sumatra	S. Ular	S. Ular	Pulau Tagor	214.73	1012.5	-
288	Sumatra	A. Blutu	S. Blutu	Pekan Selasa	12.94	930.0	-
289	Sumatra	A. Padang	S. Padang	Tebing Tinggi	153.81	934.4	-
290	Sumatra	Bah Bolon	Bah Bolon	Batu Gajah	130.41	593.1	-
291	Sumatra	Bah Bolon	Bah Bolon	Nagori Bandar	202.93	679.5	-
292	Sumatra	Bah Bolon	Bah Tongguran	Tembaan	344.59	758.0	-
293	Sumatra	S. Serdang	S. Serdang	Serdang	229.98	703.0	-
294	Sumatra	S. Asahan	S. Asahan	Porsea	142.40	3568.0	-
295	Sumatra	S. Asahan	S. Asahan	Siruar	165.73	3782.0	-
296	Sumatra	S. Asahan	S. Asahan	Simorea	190.07	3850.0	-
297	Sumatra	S. Asahan	S. Silau	Buntupane	109.58	482.5	-
298	Sumatra	S. Asahan	S. Silau	Kisaran Naga	283.39	1011.9	-
299	Sumatra	S. Asahan	S. Asahan	Pulau Raja	361.79	500.0	-
300	Sumatra	S. Kualu	S. Kualuh	Pulau Dogom	365	545.6	-
301	Sumatra	S. Kualu	A. Natas	Bdr. Durian	205.51	525.6	-
302	Sumatra	S. Bilah	A. Merbau	Merbau/ simpang empat	155.77	298.0	-
303	Sumatra	S. Barumun	Bt. Pane	Lubuk Sipelanduk	192.92	828.0	-
304	Sumatra	S. Barumun	Bt. Pane	Gunung Tua	383.24	850.0	-
305	Sumatra	S. Barumun	S. Barumun	Binanga	610.23	3128.8	-
306	Sumatra	S. Barumun	Bt. Barumun	Kuta Pinang	645.03	6781.0	-
307	Sumatra	Bt. Rokan	Bt. Sumpur	Batu Bertindih	163.876	268.0	-
308	Sumatra	Bt. Rokan	Bt. Sontang	Ulu Sontang	113.5	52.7	-
309	Sumatra	Batang Kampar	Batang Mahat	Pangkalan Kotobaru	259.9	686.2	-
310	Sumatra	Bt. Rokan	Bt. Lampasi	Batu Hampar	48.45	45.6	-
311	Sumatra	Bt. Kuantan	Bt. Ombilin	Tanjung Ampalu	381.82	1150.0	-
312	Sumatra	Bt. Kuantan	Bt. Sinamar	Taram	371.29	1437.5	-
313	Sumatra	Bt. Kuantan	Bt. Agam	Padang Tarab	111.45	272.5	-
314	Sumatra	Bt. Kuantan	Bt. Selo	Saruaso	57.76	323.9	-
315	Sumatra	Bt. Kuantan	Bt. Sukam	Muara Batu	1343.19	545.6	-
316	Sumatra	Batang Kuantan	Bt. Pelangki	Dusun Tuo	248.62	611.3	-
317	Sumatra	Bt. Kuantan	Bt. Sumpu Malalo	Sumpu Malalo	37.12	169.9	-
318	Sumatra	Bt. Hari	Bt. Hari	Sungai Dareh	1644.95	4952.3	-
319	Sumatra	Bt. Hari	Bt. Sangkir	Sampu	294.51	845.2	-
320	Sumatra	Bt. Hari	Bt. Siat	Koto Baru	171.01	475.0	-
321	Sumatra	Bt. Hari	Bt. Suliti	Sungai Ipuh	29.69	250.0	-
322	Sumatra	S. Rokan	Bt. Lubuk	Pasar Tangun	378.66	613.8	-
323	Sumatra	S. Rokan	Bt. Rokan Kiri	L. Bendahara	752.48	4848.0	-
324	Sumatra	S. Rokan	Bt. Lubuk	Ujung Gurap	71.09	1243.0	-
325	Sumatra	S. Rokan	Bt. Sosa	Dalu Dalu	292.82	1123.0	-
326	Sumatra	S. Rokan	Bt. Kumu	Tj Medan	160.11	3799.0	-
327	Sumatra	S. Rokan	Bt. Kumu	Kotabangun	111.08	556.3	-
328	Sumatra	S. Siak	Bt. Tapungkiri	Pantai Cermin	192.39	1716.0	-

Table 7. (continued)

No.	Islands	River system	River	Measurement site	Q_b ($m^3 s^{-1}$)	A_d (km^2)	L_d (km)
329	Sumatra	S. Siak	S. Tandun	Tandun	453.6	197.5	-
330	Sumatra	S. Kampar	S. Kampar Kanan	D. Bingkuang	1546.15	4000.0	-
331	Sumatra	S. Kampar	Bt. Kampar kiri	Lipat Kain	915.01	3431.0	-
332	Sumatra	S. Kampar	Bt. Lipai	Kebun Durian	172.2	556.9	-
333	Sumatra	S. Kampar	Bt. Kampar Kanan	Muara Mahat	1344.08	3174.0	-
334	Sumatra	S. Kampar	Kampar Kanan	Muara Takus	899.9	1675.0	-
335	Sumatra	Bt. Kuantan	Bt. Kuantan	Lb. Ambacang	1253.93	7350.0	-
336	Sumatra	Bt. Kuantan	Bt. Kuantan	Bandar Alai	1024.4	193.3	-
337	Sumatra	Bt. Kuantan	Bt. Kuantan	Batu Gajah	1073	11960.0	-
338	Sumatra	Bt. Kuantan	Bt. Kuantan	P. Berhala	1280.54	1167.5	-
339	Sumatra	Bt. Kuantan	S. Cinahu	Pejangki	255.65	1009.0	-
340	Sumatra	Batanghari	Bt Hari	Sei Dareh	1732.53	4952.3	-
341	Sumatra	Batanghari	Batang Sangir	Sampu	252.48	845.2	-
342	Sumatra	Batanghari	Bt. Tabir	M. Jernih	335.51	910.0	-
343	Sumatra	Batanghari	Bt. Tembesi	Muara Inum	994.6	1455.0	-
344	Sumatra	Batanghari	Bt. Ule	Lb. Tapus	258.2	344.4	-
345	Sumatra	Batanghari	Batang Hari	Muara Kilis	3068.52	17824.0	174
346	Sumatra	Batanghari	Batang Hari	Muara Tembesi	4385.64	36135.0	232.1
347	Sumatra	Batanghari	Bt. Tebo	Air Gemuruh	496.38	1831.6	-
348	Sumatra	Batanghari	Bt. Kumpeh	Pematang Bidaro	117.89	375.0	-
349	Sumatra	Batanghari	Bt. Hari	Duren	6393.62	38704.0	-
350	Sumatra	Batanghari	Sei Ulak	Ulakderas	137.39	187.5	-
351	Sumatra	Batanghari	Bt. Merao	Debai	75.67	591.5	-
352	Sumatra	Batanghari	Bt. Sangkir	Tanah Kampung	46.61	131.0	-
353	Sumatra	Batanghari	Bt. Asai	Dusun Benso	741.11	1258.0	-
354	Sumatra	Batanghari	Bt. Bungo	Rantau Pandan	116.29	410.6	-
355	Sumatra	Batanghari	Bt. Singkut	Rantau Tenang	73.67	327.5	-
356	Sumatra	Batanghari	Bt. Merangin	Bangko	1851.87	3645.0	-
357	Sumatra	Batanghari	Bt. Tabir	Rantau Panjang	560.32	1046.0	-
358	Sumatra	Batanghari	Bt. Pelepat	Rantau Kelayang	201.05	412.5	-
359	Sumatra	Batanghari	Bt Alai	Tirtakencana	56.91	655.0	-
360	Sumatra	Batanghari	Bt. Mesumai	Sei Manau	73.97	396.8	-
361	Sumatra	Batanghari	Bt. Merangin	Pulau Rengas	1346.33	2916.0	-
362	Sumatra	A. Musi	S. Lematang	S. Rotan	758.14	6890.0	-
363	Sumatra	A. Musi	S. Klingi	Lubuk Rumbai	565.67	1828.0	-
364	Sumatra	A. Musi	A. Megang	Megang Sakti	44.42	292.0	-
365	Sumatra	A. Musi	A. Enim	Dusun Lingga	597.33	1178.0	-
366	Sumatra	A. Musi	A. Komerling	Minanga	949.33	500.0	-
367	Sumatra	A. Musi	A. Belitang	Tirtanadi	48.91	77.0	-
368	Sumatra	A. Musi	A. Lengkayap	Bt. Putih	848.92	970.0	-
369	Sumatra	A. Musi	A. Malus	Tj Raya	69.72	75.0	-
370	Sumatra	A. Musi	A. Rawas	Muara Rupit	1271.59	3138.0	-
371	Sumatra	A. Musi	A. Temelat	Ciptodadi	22.52	86.3	-
372	Sumatra	A. Musi	A. Perigi	Darmabakti	24.21	73.8	-
373	Sumatra	A. Musi	A. Lematang	Lebakbudi	626.29	2040.0	-
374	Sumatra	A. Musi	A. Baal	Terawas	239.21	332.0	-
375	Sumatra	A. Musi	A. Rawas	Pulau Kidak	905.38	1325.0	-
376	Sumatra	A. Musi	A. Kungku	Ciptodadi	50.9	227.0	-
377	Sumatra	A. Musi	W. Selabung	Kt. Agung	88.66	409.0	-
378	Sumatra	A. Musi	A. Lematang	Pinang belarik	894.25	3676.0	-
379	Sumatra	A. Musi	A. Kelingi	Ulak Surung	404.16	332.0	-
380	Sumatra	A. Musi	A. Ogan	Tj Raja	902.94	6314.0	144.7
381	Sumatra	A. Musi	A. Komerling	Martapura	442.01	4267.0	-
382	Sumatra	A. Musi	S. Komerling	Mangunjaya	150.67	1500.0	-
383	Sumatra	W. Mesuji	W. Mesuji	Labuan Batin	244.55	285.0	-
384	Sumatra	W. T. Bawang	W. Umpu Kanan	Pakuan Ratu	571.73	3427.0	-
385	Sumatra	W. T. Bawang	W. Umpu	Rantau Temiang	57.96	205.0	-
386	Sumatra	W. T. Bawang	W. Abung	Ogan Enam	89.61	170.0	-
387	Sumatra	W. T. Bawang	W. Rarem	Propal/ Kotabumi	272.81	913.0	-
388	Sumatra	W. T. Bawang	W. Tahmi	Tanjung Agung	238.75	509.0	-
389	Sumatra	W. T. Bawang	W. Umpu	Negeri Batin	240.24	559.0	-
390	Sumatra	W. T. Bawang	W. Girham	Rantau Jangkung	149.01	525.0	-
391	Sumatra	W. T. Bawang	W. Besay	Banjarmasin	131.79	604.0	-
392	Sumatra	W. T. Bawang	W. Besay	Petay (Sumberjaya)	91.13	329.0	-
393	Sumatra	W. T. Bawang	W. Umpu Kiri	Gunung Katun	194.83	3043.0	-
394	Sumatra	W. T. Bawang	W. Besay	Sukajaya	92.86	268.0	-

Table 7. (continued)

No.	Islands	River system	River	Measurement site	Q_b ($m^3 s^{-1}$)	A_d (km^2)	L_d (km)
395	Sumatra	W. T. Bawang	W. Giham	Filla Masin	64.31	367.0	-
396	Sumatra	W. T. Bawang	W. Giham	Air Ringkih	60.03	356.7	-
397	Sumatra	W. T. Bawang	W. Pedada	Banjar Agung	229.08	203.0	-
398	Sumatra	W. Seputih	W. Tatayan	Sindang Asri	18.4	111.5	-
399	Sumatra	W. Seputih	W. Waya	Banyuwangi	17.2	309.0	-
400	Sumatra	W. Seputih	W. Pangabuan	Terbanggi Besar	163.81	650.0	-
401	Sumatra	W. Seputih	W. Terusan	Gunung Batin	82.65	3043.0	-
402	Sumatra	W. Seputih	W. Seputih	Buyut Udik	182.99	1648.0	-
403	Sumatra	W. Seputih	W. Seputih	Segala Mider	23.55	240.0	-
404	Sumatra	W. Seputih	W. Pengabuan	Blambangan Pagar	101.28	170.0	-
405	Sumatra	W. Seputih	W. Raman	Raman Endra	51.32	226.0	-
406	Sumatra	W. Seputih	W. Pengabuan	Gedung Hatta	151.04	113.0	-
407	Sumatra	W. Seputih	Bt. Hari	Raman Fajar	51.55	208.0	-
408	Sumatra	W. Sekampung	W. Sekampung	Pujorahayu	341.18	1743.0	-
409	Sumatra	W. Sekampung	W. Sekampung	Jurak	266.42	682.0	-
410	Sumatra	W. Sekampung	W. Sekampung	Kunzir	146.61	719.0	-
411	Sumatra	W. Sekampung	W. Bulak	Dam Gatel (Weir)	119.75	790.0	-
412	Sumatra	W. Sekampung	W. Bulok	Bulokerto	168.56	850.0	-
413	Sumatra	W. Sekampung	W. Ketibung	Sidomulyo	28.41	341.0	-
414	Sumatra	W. Sekampung	W. Kandis	Tegal Lega / Trikora	44.36	254.0	-
415	Sumatra	W. Sekampung	W. Sekampung	Krisnowidodo	470.52	1707.0	-
416	Sumatra	Kr. Aceh	Kr. Aceh	Kp. Seulimeun	166.25	471.6	-
417	Sumatra	Kr. Aceh	Kr. Aceh	Kp. Darang	245.23	1291.0	-
418	Sumatra	Kr. Aceh	Kr. Keumireun	Siron	105.85	208.0	-
419	Sumatra	Kr. Aceh	Kr. Aceh	Pasi	275.55	1578.0	-
420	Sumatra	Kr. Aceh	Kr. Aceh	Lampisang Tunong	129.58	667.0	-
421	Sumatra	Kr. Boga	Kr. Boga	Kp Boga	156.89	216.18	-
422	Sumatra	Kr. Aceh	Kr. Jreue	Kp. Jreue	49.55	174.85	-
423	Sumatra	Kr. Lambesoi	Kr. Lambesoi	Sango	492.65	412.5	-
424	Sumatra	Kr. Bulan	Lawe Bulan	Kutacane	35.63	17.2	-
425	Sumatra	Kr. Gimpang	Lawe Alas	Gempang	151.83	656	-
426	Sumatra	Kr. Alas	Lawe Alas	Suka Rimbun	260.73	2615.3	-
427	Sumatra	Kr. Kluet	Kr. Kluet	Gn. Puding	483.33	1275	-
428	Sumatra	Kr. Susoh	Kr. Susoh	Kota Tinggi	87.89	193.8	-
429	Sumatra	Kr. Bah Barot	Kr. Bah Barot	Kp. P. Cermin	326.72	2378	-
430	Sumatra	Kr. Tripa	Kr. Tripa	G. Kong	492.13	3054.05	-
431	Sumatra	Kr. Seunagan	Kr. Seunagan	Driengguru	202.67	596	-
432	Sumatra	Kr. Seunagan	Kr. Seunagan	Py. Udeng/ Kulu	234.68	909.5	-
433	Sumatra	Kr. Meureubo	Kr. Meureubo	Meunasah Rayek	704.54	1688	-
434	Sumatra	Kr. Woyla U/S	Kr. Woyla U/S	M. Tutut	543.42	2327	-
435	Sumatra	Kr. Woyla	Kr. Woyla D/S	Kuala Bhee	734.36	1244.19	-
436	Sumatra	Kr. Teunom	Kr. Teunom	Tui Kareng	919.25	2236	-
437	Sumatra	Kr. Sabe	Kr. Sabe	Panggong	285.68	298.9	-
438	Sumatra	Bt. Natal	Bt. Natal	Rantau Sore	219.66	676.3	-
439	Sumatra	Bt. Gadis	Bt. Gadis	Perbangunan	367	841.65	-
440	Sumatra	Bt. Gadis	Bt. Angkola	Air Libung	141.1	633.8	-
441	Sumatra	Bt. Toru	Aek Sigeon	Pasar Sironggit	112.25	350.6	-
442	Sumatra	Bt. Toru	Batang Toru	Hapesong Baru	456.71	2773	-
443	Sumatra	A. Kolang	A. Kolang	Kp. Kolang	332.16	464.4	-
444	Sumatra	A. Sibundong	A. Sibundong	Dolok Sanggul	38.85	58	-
445	Sumatra	A. Silang	A. Silang	Marade	52.6	163.8	-
446	Sumatra	Bt. Kuantan	Bt. Sumani	Bandar Padung	217.59	837.5	-
447	Sumatra	Bt. Kuantan	Bt. Lembang	Kt Baru/ B. Kudo	87.54	152.5	-
448	Sumatra	Bt. Tapan	Bt. Indrapura	Air Batu	263.49	328.5	-
449	Sumatra	Bt. Tapan	Bt Tapan	Lubuk Begalung	304.83	450.4	-
450	Sumatra	Bt. Tapan	Bt Lunang	Lunang	689.83	143.8	-
451	Sumatra	Bt. Air Haji	Bt. Air Haji	Danau	307.06	370	-
452	Sumatra	Air Gadang	Bt. Pelepah	Tj Masjid	139.21	345.1	-
453	Sumatra	Bt. Kambang	Bt. Lengayang	Koto Baru	245.65	141.3	-
454	Sumatra	Bt. Suratih	Bt. Suratih	Ganting	122.01	249.5	-
455	Sumatra	Bt. Tarusan	Bt. Tarusan	Kayu Gadang	265.03	388.7	-
456	Sumatra	Bt. Arau	Bt Arau	Lubuk Sari	119.72	47.5	-
457	Sumatra	Bt. Air Dingin	Bt. Air Dingin	L. Minturun	225.96	116.5	-
458	Sumatra	Bt. Anai	Bt. Anai	Kandang Ampat	34.81	71.9	-
459	Sumatra	Bt. Tapakis	Bt. Tapakis	Kota Gadis	39	28	-
460	Sumatra	Bt. Mangau	Bt Mangau	Kurai Taji	213.89	214.4	-

Table 7. (continued)

No.	Islands	River system	River	Measurement site	Q_b ($m^3 s^{-1}$)	A_d (km^2)	L_d (km)
461	Sumatra	Bt Pariaman	Bt Pariaman	Jati Mudik	73.73	54.2	-
462	Sumatra	Bt. Atokan	A. Naras	Durian Dangka	127.54	51.8	-
463	Sumatra	Bt. Atokan	Bt. Kalulukutan	Batu Ampa	110.65	57.8	-
464	Sumatra	Bt Simamar	Bt. Antokan	Siguhung	96.6	295	-
465	Sumatra	Bt. Masang	Bt. Masang	Sipisang	122.91	458	-
466	Sumatra	Bt. Masang	Bt Patimah	Kapundung	439.6	363	-
467	Sumatra	Bt. Pasaman	Bt. Pasaman	A Gadang	919.21	1338.8	-
468	Sumatra	Bt. Pasaman	Bt. Tongar	Lb. Panjang	121.31	50.75	-
469	Sumatra	Bt. Pasaman	Bt. Kenaikan	Muara Kiawai	92.17	278	-
470	Sumatra	Bt. Sikabau	Bt Sikabau	Ujung gading	255.66	382	-
471	Sumatra	Bt. Pasaman	Bt. Tongar	Lb. Toreh	182.06	266	-
472	Sumatra	Bt. Sikilang	Bt. Sikilang	Sei Aur	340.39	156	-
473	Sumatra	Batang Gadis	Bt. Batahan	Silaping	242.14	310	-
474	Sumatra	A. Musi Kejalo	A. Musi Kejalo	Cawang Lama	9.35	40	-
475	Sumatra	A. P.Guci	A. Padang Guci	Bungin Tambun	79.23	158.8	-
476	Sumatra	A. Kedurang	A. Kedurang	Batu Ampar	105.34	42.5	-
477	Sumatra	A. Nipis	A. Bangkenang	Sukarami	112.05	128.2	-
478	Sumatra	A. Manas	A. Mana	Bandar Agung	292.48	587.5	-
479	Sumatra	A. Maras	A. Maras	Maras Hulu	57.2	20.2	-
480	Sumatra	A. Alas	A. Alas	Rantau Panjang	517.42	431.3	-
481	Sumatra	A. Nelas	A. Nelas	Lubuk Puding	192.57	85.6	-
482	Sumatra	A. Bengkulu	A. Bengkulu	Kancing	51.28	376.3	-
483	Sumatra	A. Lemau	A. Lemau	Paku Haji	59.6	170.6	-
484	Sumatra	A. Lais	A. Lais	Kuro Tidur	24.22	143.2	-
485	Sumatra	A. Bintunan	A. Bintunan	Lubuk Banyau	93.63	293.8	-
486	Sumatra	A. Urai	A. Urai	Urai Hulu / Ketahun	65.92	228	-
487	Sumatra	A. Ketahun	A. Ketahun	Tunggang	284.18	966	-
488	Sumatra	A. Lelangi	A. Lelangi	Lubuk Mindai	114.32	285.26	-
489	Sumatra	A. Rami	A. Rami	Pulau	136.94	170	-
490	Sumatra	A. Ipuh	A. Ipuh	Sibak Muko (Muko)	511.41	696.3	-
491	Sumatra	A. Teramang	A. Bantal	Pondok Baru	355.39	390.6	-
492	Sumatra	A. Teramang	A. Teramang	Trunggang	313.91	331.3	-
493	Sumatra	A. Dikit	A. Dikit	Saribulan	346.54	1012.19	-
494	Sumatra	A. Selagan	A. Selagan	Tras. Trujam	196.81	453	-
495	Sumatra	A. Majunto	A. Majunto	Lalang Luas	125.78	443.8	-
496	Sumatra	A. Majunto	A. Majunto Hilir	Lubuk Pinang	370.2	621.5	-
497	Sumatra	W. Semangka	W. Semangka	Liwa	48.55	243	-
498	Sumatra	W. Semangka	W. Semangka	Srikuncoro	235.6	1413	-
499	Kalimantan	S. Pesaguan	S. Pesaguan	Tumbangtiti	103.88	549	-
500	Kalimantan	S. Kapuas	S. Sekadau	Nanga Taman	236.1	1410	-
501	Kalimantan	S. Kapuas	S. Sengarit	Binjai	149.72	315	-
502	Kalimantan	S. Kapuas	S. Landak	Serimbu	84.75	650	-
503	Kalimantan	S. Kapuas	S. Sekayam	Balai Karangan	251.58	907	-
504	Kalimantan	S. Kapuas	S. Mengkiyang	Balai Sebut	138.51	945	-
505	Kalimantan	S. Kapuas	S. Mengkiyang	Balai Jeropet	302.52	1410	-
506	Kalimantan	S. Kapuas	S. Sekayam	Kembayan	1254.95	2290	-
507	Kalimantan	S. Kapuas	S. Tayan	Sosok	123.42	431	-
508	Kalimantan	S. Sekayam	S. Ensabai	Beruak	57.02	115	-
509	Kalimantan	S. Sekayam	S. Sekayam	Mentunai	962.24	2760	-
510	Kalimantan	S. Sekayam	S. Pinoh	Kota baru	723.15	2710	-
511	Kalimantan	S. Mempawah	S. Menpawah	Karangan	145.34	907	-
512	Kalimantan	S. Landak	S. Menyuke	Darit	186.24	329	-
513	Kalimantan	S. Kapuas	S. Sengah	KerANJI Paidang	36.11	89.1	-
514	Kalimantan	S. Selakau	S. Selakau	Seboteng	69.76	108	-
515	Kalimantan	S. Landak	S. Landak	Monggo	1206.93	3710	-
516	Kalimantan	S.Sambas	S. Sebalau	Bengkayang	13.55	55.8	-
517	Kalimantan	S. Sambas Besar	S. Seluas	Tadan	209.1	312	-
518	Kalimantan	S. Sambas	S. Sambas Kecil	Ledo	202.58	1380	-
519	Kalimantan	S. Sambas	S. Kumba	Seluas	269.36	64	-
520	Kalimantan	S. Barito	S. Barito	Muara Teweh	4670.62	48375	228.7
521	Kalimantan	S. Barito	S. Paku	Tampa	30.26	562.5	-
522	Kalimantan	S. Barito	S. Karau	Ampah	86.06	1531	-
523	Kalimantan	S. Barito	S. Montallat	Kandui	71.82	676	-
524	Kalimantan	S. Kahayan	S. Manuhing	Tumbang Talaken	204.39	313	-
525	Kalimantan	S. Kapus	S. Kapuas	Pujon	1159.46	18028	-
526	Kalimantan	S. Kahayan	S. Rungan	Tumbang Jutuh	361.11	370	-

Table 7. (continued)

No.	Islands	River system	River	Measurement site	Q_b ($m^3 s^{-1}$)	A_d (km^2)	L_d (km)
527	Kalimantan	S. Kahayan	S. Katingan	Kasongan	3507.82	12525	-
528	Kalimantan	S. Mentaya	S. Mentaya	Kuala Kuayan	848.75	4539	-
529	Kalimantan	S. Lamandau	S. Arut	Pangkut	278.96	4968	-
530	Kalimantan	S. Lamandau	S. Lamandau	Nanga Bulik	1471.64	500	-
531	Kalimantan	S. Karau	S. Awang	Hayaping	13.16	62	-
532	Kalimantan	S. Barito	S. Tabanio	Bajuin	39.06	425	-
533	Kalimantan	S. Barito	S. Negara	Amuntai	388.15	5770	-
534	Kalimantan	S. Barito	S. Tabalong	Tanjung	661.25	1834	-
535	Kalimantan	S. Barito	S. Tapin	Linuh	126.9	168	-
536	Kalimantan	S. Barito	S. Batu Alai	Batu Tangga	138.63	344	-
537	Kalimantan	S. Barito	S. Tapin	Kuranji	75.44	284	-
538	Kalimantan	S. Barito	S. Barabai	Kasarangan	53.29	250	-
539	Kalimantan	S. Barito	S. Uya	Teratau	30.95	109	-
540	Kalimantan	S. Barito	S. Barabai	Baruhbatung	62.04	153	-
541	Kalimantan	S. Barito	S. Hanyar	Dusun Hanyar	228.82	196	-
542	Kalimantan	S. Barito	S. Pitap	Bihara	26.79	275	-
543	Kalimantan	S. Barito	S. Balangan	Lampihong	264.9	1542	-
544	Kalimantan	S. Barito	S. Tabalong Kiri	Mahe	310.6	2431	-
545	Kalimantan	S. Barito	S. Tabalong	Panaan	392.39	647	-
546	Kalimantan	S. Barito	S. Tabalong	Batupulut	149.93	694	-
547	Kalimantan	S. Barito	S. Ayu	Pasar Batulicin	187.8	351	-
548	Kalimantan	S. Mahakam	S. Telen	Keham	1170.4	7600	-
549	Kalimantan	S. Mahakam	S. Mahakam	K. Bangun	3117.28	56600	314.2
550	Kalimantan	S. Mahakam	S. Melak	Melak	3185.52	2658	-
551	Kalimantan	S. Mahakam	S. Kedang Kepala	Ancalong	1176.01	14400	-
552	Kalimantan	S. Mahakam	S. Klinjau	Longnah	564.12	4400	-
553	Kalimantan	S. Mahakam	S. Belayan	Tambang	1666.57	5600	-

Table 8. Data of drainage basin area (A_d) and drainage basin length (L_d) for the modern fluvial system in the contiguous United States. Data of A_d are based on Takahashi (2013).

No.	River system	A_d (km ²)	L_d (km)
1	Arkansas	415,000	1,483
2	Apalachicola	50,688	573
3	Yellowstone	180,000	686
4	Illinois	75,136	538
5	Wisconsin	30,000	383
6	Willamette	29,730	248
7	Ohio	528,200	1,156
8	Altamaha	37,600	436
9	Canadian	122,000	947
10	Kanawha	31,691	315
11	Kansas	155,698	797
12	Cumberland	46,830	497
13	Grand (MO)	20,390	175
14	Green	116,200	565
15	Cape Fear	24,150	330
16	Connecticut	29,100	453
17	Colorado (to the Gulf of Mexico)	103,341	931
18	Columbia	668,000	1,058
19	Savannah	25,511	391
20	Sacramento	71,432	419
21	Susquehanna	71,432	357
22	Sabine	25,268	384
23	Salmon (ID)	36,260	279
24	San Antonio	26,213	288
25	Santee	39,500	403
26	San Joaquin	83,409	262
27	San Juan	64,000	364
28	James	27,019	409
29	Susitna	51,800	335
30	Snake	278,000	768
31	Spokane	17,300	275
32	Suwannee	24,967	328
33	St. Johns	22,539	357
34	Tennessee	105,870	675
35	Delaware	36,568	402
36	Trinity (TX)	40,380	572
37	Neches	25,929	338
38	Niobrara	32,600	538
39	Neuces	43,512	354
40	Neosho	29,873	357
41	Noatak	29,873	335
42	Hudson	36,260	372
43	Pearl	21,999	338
44	Peace	3,540	109
45	Gila	149,800	624
46	Brazos	116,000	976
47	Platte	230,000	1,063
48	Humboldt	42,994	355
49	Pecos	113,960	800
50	Penobscot	22,300	216
51	Potomac	38,020	304
52	White (MO, AR)	72,189	405
53	White (SD)	26,418	373
54	Mississippi	3,250,000	3,135
55	Missouri	1,371,000	2,288
56	Milk	57,839	526
57	Yakima	16,000	200
58	Licking	9,310	213
59	Red	169,890	1,213
60	Roanoke	25,326	338
61	Ouachita	64,454	414
62	Washita	20,230	413
63	Wabash	85,340	461
64	Colorado	630,000	1,349

Table 9. Empirical equations stating relationship between bankfull channel depth (d) and mean bankfull channel depth (d_m), and between d_m and bankfull channel width (W_b) derived from the gravelly fluvial channels in the Kanto region and from previous studies as well.

Equation	Reference	Applicable range	Remarks
d_m-d relationships			
$d_m = 0.62 d$	Present study	$2.3 \leq d \leq 9.4$ m	Gravelly rivers in the Kanto region, central Japan. Data are from 24 sites.
$d_m = 0.57 d$	Bridge and Mackey (1993)	–	Combined equation (Leeder, 1973; Bridge and Mackey, 1993).
$d_m = 0.5819 d$	Moody et al. (2003)	$0.2 \leq d \leq 2.6$ m	Gravelly and sandy ephemeral and perennial streams of eastern Arizona and New Mexico.
$d_m = 0.65 d$	Adhiperdana et al. (2018)		Indonesian rivers. Data are from 86 sites.
W_b-d_m relationships			
$W_b = 49.16 d_m^{0.66}$	Present study	$1.0 \leq d_m \leq 6.7$ m	Gravelly rivers in the Kanto region, central Japan. Data are from 24 sites.
$W_b = 21.30 d_m^{1.45}$	Williams (1986)	$0.03 \leq d_m \leq 18$ m	Meandering rives of various climatic and tectonic settings (e.g. U.S.A., Canada, U.S.S.R., Australia, Sweden).
$W_b = 8.8 d_m^{1.82}$	Bridge and Mackey (1993)	–	Widely used equation for paleochannel reconstructions (e.g. Bridge, et al., 2000; McLaurin and Steel, 2007).
$W_b = 19.46 d_m^{1.58}$	Castro and Jackson (2001)	$0.3 \leq d_m \leq 5.1$ m	Streams of the Pacific Northwest, U.S.A. Combined equation by the present study.
$W_b = 30.23 d_m^{1.18}$	Moody et al. (2003)	$0.1 \leq d_m \leq 1.4$ m	Gravelly and sandy ephemeral and perennial streams of eastern Arizona and New Mexico. Combined equation by the present study.
$W_b = 242.4 d_m^{2.19}$	Xu (2004)	$0.4 < d_m < 3$ m	Gravelly braided rivers in various tectonic and climatic settings including rivers in New Zealand. Combined equation by the present study.
$W_b = 20.27 d_m^{1.40}$	Xu (2004)	$0.3 < d_m < 7$ m	Gravelly meandering rivers in various tectonic and climatic settings. Combined equation by the present study.
$W_b = 340.4 d_m^{1.04}$	Xu (2004)	$1.5 < d_m < 15$ m	Sandy braided rivers in various tectonic and climatic settings. Combined equation by the present study.
$W_b = 2.36 d_m^{2.53}$	Xu (2004)	$0.7 < d_m < 15$ m	Sandy meandering rivers in various tectonic and climatic settings. Combined equation by the present study.
$W_b = 36.18 d_m^{1.54}$	Modrick and Georgakakos (2014)	$0.06 \leq d_m \leq 5.7$ m	Southern California mountain streams, U.S.A. Combined equation by the present study.
$W_b = 52.88 d_m^{0.70}$	Adhiperdana et al. (2018)	$0.21 \leq d_m \leq 14.13$ m	Indonesian rivers. Data are from 86 sites.

Table 10. Definitions of bounding-surface (BS) types, and descriptions and interpretations of depositional-unit (DU) types in the Iwaki Formation fluvial deposits.

Order	Definition of bounding surface (BS)	Description of depositional unit (DU)	Interpretation of DU
1st	BS that defines individual cross-bedded sets within 2nd-order DU (reactivation surface).	Small-scale, gently inclined or tabular unit up to 50 cm in height; composed of fine- to very coarse-grained sandstones to pebble- to cobble-sized conglomerates.	DU formed by dune and ripple migrations (Miall, 1985, 1988; Bridge, 1993)
2nd	BS that partitions cross-stratification within 3rd-order DU (reactivation and/or accretion surface).	Large-scale, gently inclined or horizontal unit from a few centimeters to 6 m in height; composed of fine- to very coarse-grained sandstones to pebble- to cobble-sized conglomerates.	DU formed by bar migrations (Miall, 1985, 1988; Bridge, 1993)
3rd	BS that separates different lithofacies within 4th-order DU.	Tabular or gently inclined unit up to 6 m in height and tens of meters in width; composed of mudstones, sandstones, and conglomerates.	Mud drape, bar edge sand, small-scale channel-fill deposit, and main part of bar deposit
4th	Upper surfaces of thin sandy or muddy deposits including coal seams that laterally extend several meters to a few tens of meters, and laterally change into erosional surfaces.	Tabular unit up to 6 m in height and tens of meters in width; composed of mudstones, sandstones, and conglomerates; typically showing fining-upward trends.	Bar deposit (Miall, 1985, 1988; Bridge, 1993; Holbrook, 2001)
5th	Upper surfaces of tens of centimeters to several meters thick sandy or muddy deposits including coal seams that extend laterally up to hundreds of meters, and the base of muddy deposits (overbank-fine deposits), that laterally extend more than a few kilometers.	Tabular, occasionally lenticular unit up to 24 m in height; composed of any combination of component depositional units of 1st- to 4th-order; sandy and muddy deposits (up to several meters) develop in the uppermost part.	Channel (CH) deposit (Miall, 1985, 1988; Bridge, 1993; Gibling, 2006)
6th	Upper surfaces of thick (several meters to tens of meters) sandy or muddy deposits including coal seams that extend laterally more than a few kilometers.	Tabular unit up to 60 m in height and several kilometers in width; composed of any combination of component depositional units of 1st- to 5th-order; thick sandy and muddy deposits (up to tens of meters) develop in the uppermost part.	Channel complex (CHC) (Holbrook, 2001)

Table 11. Reconstructed parameters of the Iwaki Formation fluvial system. CHC: Channel complexes, CH: channel deposits. See the list of symbols in Table 2.

	N		h (m)	d (m)	d_m (m)	W_b (m)	Q_{mean} ($\text{m}^3 \text{s}^{-1}$)	Q_b ($\text{m}^3 \text{s}^{-1}$)	A_d (km^2)	L_d (km)	
CHC-I	CH-A	17	Max.	6.6	8.1	5.1	143.2	69.0	925.6	1489.0	53.6
		Min.	2.2	2.7	1.7	69.3	28.7	396.3	699.8	37.6	
		Mean	4.1	5.0	3.1	102.9	46.5	631.1	1056.6	45.6	
	CH-B	5	Max.	5.8	7.2	4.4	131.5	62.3	837.7	1362.4	51.4
		Min.	4.3	4.0	2.4	88.8	38.7	529.2	905.3	42.4	
		Mean	3.2	5.4	3.3	107.9	49.2	666.6	1110.0	46.7	
	CH-C	4	Max.	3.8	4.7	2.9	99.5	44.4	604.4	1018.8	44.9
		Min.	2.6	3.2	2.5	77.4	32.8	450.8	784.9	39.7	
		Mean	3.2	4.0	2.0	89.0	38.9	531.5	908.2	42.5	
	CH-D	5	Max.	5.4	6.7	4.1	125.4	58.8	792.8	1297.1	50.3
		Min.	2.4	3.0	3.3	73.4	30.8	423.8	742.9	38.7	
		Mean	4.4	5.4	1.8	108.1	49.3	668.0	1111.5	46.7	
CHC-II	CH-E	7	Max.	4.8	5.9	3.7	116.0	53.5	723.8	1196.3	48.4
		Min.	2.6	3.2	2.0	77.4	32.8	450.8	784.9	39.7	
		Mean	3.7	4.6	2.8	96.9	43.2	587.6	992.2	44.3	
	CH-F	7	Max.	5.6	6.9	4.3	128.5	60.5	815.3	1330.0	50.8
		Min.	2.5	3.1	1.7	75.4	31.8	437.4	764.1	39.2	
		Mean	3.6	4.5	1.9	95.8	42.6	580.0	980.5	44.1	
	CH-G	3	Max.	4.5	5.6	3.4	111.2	50.8	688.6	1,144.4	47.4
		Min.	2.2	2.7	1.7	94.5	28.7	396.3	699.8	37.6	
		Mean	3.6	4.4	2.7	69.3	41.9	571.2	966.5	43.8	
	CH-H	3	Max.	5.2	6.4	4.0	122.3	57.1	770.0	1,263.9	49.6
		Min.	3.2	4.0	2.4	88.8	38.7	529.2	905.3	42.4	
		Mean	4.4	5.4	3.4	109.1	49.8	674.4	1,121.8	46.9	
CHC-III	CH-I	7	Max.	4.8	5.9	3.7	116.0	53.5	723.8	1,196.3	48.4
		Min.	2.9	3.6	2.2	83.2	35.8	595.9	846.1	41.1	
		Mean	3.7	4.6	2.9	98.2	43.8	490.5	1,005.3	44.6	
	CH-J	4	Max.	4.8	5.9	3.7	116.0	53.5	723.8	1,196.3	48.4
		Min.	3.5	4.3	2.7	94.2	41.6	567.2	962.9	43.7	
		Mean	4.2	5.2	3.2	106.5	48.3	655.1	1,094.1	46.4	

		D_{50} (mm)	S	L_b (km)
CHC-I	CH-A	34.0	1/2,549	20.8
	CH-B	19.0	1/4,009	28.7
	CH-C	15.5	1/3,220	15.1
	CH-D	6.5	1/10,911	72.7
CHC-II	CH-E	19.0	1/3,318	19.7
	CH-F	21.5	1/3,421	23.7
	CH-G	19.0	1/3,111	17.3
	CH-H	18.0	1/3,794	24.4
CHC-III	CH-I	16.0	1/3,940	23.3
	CH-J	14.0	1/4,503	26.7

Table 12. Reconstructed parameters of the Bayah Formation fluvial system. IV: Intervals. See the list of symbols in Table 2. Values of d , d_m , W_b , Q_{mean} , and Q_b are from Adhiperdana (2018).

	N		d (m)	d_m (m)	W_b (m)	Q_{mean} ($\text{m}^3 \text{s}^{-1}$)	Q_b ($\text{m}^3 \text{s}^{-1}$)	A_d (km^2)	L_d (km)
IV1	48	Max.	15.8	10.3	270.0	599.4	3090.0	6209.7	103.4
		Min.	1.7	1.1	57.0	46.4	337.0	707.9	32.7
		Mean	5.7	3.7	132.0	184.7	1122.0	2300.9	61.1
IV2	53	Max.	17.8	11.6	294.0	689.6	3474.0	6965.1	109.9
		Min.	2.0	1.3	64.0	56.1	396.0	829.2	35.6
		Mean	7.5	4.9	160.0	253.5	1473.0	3004.4	70.4
IV3	24	Max.	16.0	10.4	272.0	606.8	3129.0	6286.5	104.1
		Min.	3.8	2.5	100.0	117.0	750.0	1550.5	49.6
		Mean	9.4	6.1	188.0	330.5	1844.0	3744.2	79.1
IV4	17	Max.	18.5	12.0	302.0	720.7	3615.0	7242.0	112.2
		Min.	2.1	1.4	65.0	57.6	412.0	862.0	36.3
		Mean	11.0	7.2	210.0	396.5	2156.0	4364.0	85.8
IV5	30	Max.	14.3	9.3	252.0	535.1	2799.0	5636.1	98.3
		Min.	2.3	1.5	71.0	66.6	463.0	966.5	38.6
		Mean	8.2	5.3	171.0	282.8	1610.0	3277.9	73.7
IV6	10	Max.	12.5	8.1	229.0	457.2	2444.0	4934.6	91.6
		Min.	4.9	3.2	120.0	157.9	973.0	2001.1	56.8
		Mean	9.2	6.0	185.0	321.8	1805.0	3666.6	78.2
IV7	25	Max.	11.6	7.5	217.0	418.4	2273.0	4596.0	88.2
		Min.	1.7	1.1	57.0	46.4	337.0	707.9	32.7
		Mean	5.6	3.6	131.0	182.4	1102.0	2260.7	60.5

Table 13. Lithofacies classification of the Chinle Formation.

Lithofacies	Description	Interpretation
Gc	Clast-supported, pebble-sized conglomerates with coarse-grained sandstone matrix.	Bedload deposition and/or lag gravel.
Gt / Gp	Trough or planar cross-stratified, pebble-sized conglomerates with coarse-grained sandstone matrix.	Migration of sinuous- or straight-crested gravel dunes.
St / Sp	Dull yellow orange-colored, trough or planar cross-stratified, very coarse- to fine-grained sandstones locally including pebble.	Migration of sinuous- or straight-crested sandy dunes.
Sh	Dull yellow orange-colored, horizontally stratified or laminated, fine- to very coarse-grained sandstones locally including pebble.	Migration and aggradation of plane beds.
Sr	Dull yellow orange-colored, current-ripple cross-laminated fine-grained sandstones.	Migration of current ripples.
Sc	Dull yellow orange-colored, medium- to fine-grained sandstones with convoluted lamination.	Secondary deformation after deposition.
Sg / Sig	Normally or inversely graded, very fine- to fine-grained structureless sandstones.	Accumulation from suspended loads with changes in temporal flow accelerating or decelerating.
Fm	Gray or light gray-colored, massive very fine-grained sandstones and mudstones.	Accumulation from suspended loads.
Fl	Gray or light gray-colored horizontally laminated very fine-grained sandstones and mudstones.	Alternating deposition of sandy and muddy suspended loads.
Fr	Gray or light gray-colored, ripple cross-laminated very fine-grained sandstones. Locally including climbing ripple cross-lamination.	Migration of current ripples.
Pm	Multi-colored mottled (gray, brownish gray, grayish red, reddish brown, and purplish gray) massive mudstones. Distinct slickenside and cross-cutting structure are common.	Pedogenetic modification after accumulation from suspended loads.
Lm	Light gray-colored massive or brecciated limestones.	Chemical precipitation of calcareous materials.

Table 14. Architectural element types of the Chinle Formation.

Element	Description	Interpretation
Element SG: Scoured surface with gravel lags	Erosional surfaces overlain by discontinuous Gc.	Lag deposits on channel bases (Jo, 2003; Hampson et al., 2013)
Element DA: Downstream accreting, cross-stratified sandstones	Gt, Gp, St and Sp with cross-set boundaries dip in the same direction as foresets of the constituent cross-sets. Commonly represents upward-fining trend up to 10 m.	Bar and channel-fill sandstone with downstream accretion surfaces (Thomas et al., 1987; Miall, 1988)
Element LA: Laterally accreting, cross-stratified sandstones	Gt, Gp, St and Sp with cross-set boundaries dip orthogonal to foresets of the constituent cross-sets. Commonly represents upward-fining trend up to 10 m.	Bar and channel-fill sandstone with lateral accretion surfaces (Miall, 1985, 1988; Thomas et al., 1987)
Element UB: Upper bar deposits	Alternating beds of sandstones (St, Sp) and mudstones (Fm, Fl, Fr) with boundaries dip in the same directions as foresets of the constituent cross-sets, or dip orthogonal to the foresets. Commonly occurring on DA or LA, and superimposed by FF.	Upper bar deposit (Bridge et al., 2000; Bridge, 2003; Xu et al., 2017)
Element SD: Sandy bedforms	Sheet like element comprising St, Sp, and Sh, locally including Gt and Gp. Cross-set boundaries are horizontal or dip slightly. Basal surface is horizontal or erosional.	Aggradation of dunes on low-relief bars (Miall, 1985)
Element LCF: Large-scale channel-fill deposits	Large-scale channelized geometry up to 8 m thick and 40 m wide filled with Fm, Fl, Fr, St, Sp, Sh, and Sr.	Filling of abandoned channels (Miall, 1985, 1996; Bridge, 1993)
Element SCF: Small-scale channel-fill deposits	St with erosionally based, small-scale lenticular geometry up to 1.5 m thick and 6 m wide.	Filling of minor and/or cross-bar channels (Allen, 1983; Jo, 2003; Lunt et al., 2004)
Element FF: Floodplain muddy deposits	Stacked element of Fm, Fl, Fr, and Pm. Locally including Lm.	Floodplain deposits formed in low energy environments (Miall, 1985, 1988)
Element FS: Floodplain sandy deposits	Horizontally based element composed of St, Sr, Sh, Sc, and Sg / Sig up to 2.6 m thick intercalated by FF.	Crevasse splay deposits (Hampson et al., 2013; Burns et al., 2017).

Table 15. Hierarchy of bounding-surface (BS) types of the Chinle Formation.

Hierarchy	Depositional unit (DU) types	Bounding-surface (BS) types	Interpretation of BS	Comparison of BS
1st-order	Cross-set	Cross-set bounding surfaces	Migration and change in migration conditions of dunes and ripples	1st- and 2nd-order bounding surfaces (Miall, 1988, 1996)
2nd-order	Bar growth unit	Cross-set bounding surfaces that truncate underlying strata and commonly dip 5–20°	Accretion of bar deposits	3rd-order bounding surface (Miall, 1988, 1996)
3rd-order	Bar and crevasse splay deposits	Top surfaces of bar and channel deposits; surface bounding different bar deposits in a channel deposit; top and basal surfaces of floodplain sandy deposits;	Abandonment of channels; change in depositional conditions in channels; deposition of floodplain sandy deposits	4th-order bounding surface (Miall, 1988, 1996); Nested channel cut (Holbrook, 2001)
4th-order	Channel deposit	Erosional surfaces commonly lined by discontinuous sheets of pebble-sized conglomerate	Migration and avulsion of individual channels and channel belts	5th- and 6th-order bounding surfaces (Miall, 1988, 1996); Channel-fill and channel-belt boundaries (Holbrook, 2001)
5th-order	Channel complex	Compound erosional surfaces composed of multiple 4th-order BS type, and commonly eroding underlying muddy deposits	Large scale erosion in fluvial valleys in response to autogenic and/or allogenic processes	Nested-valley boundary (Holbrook, 2001)
6th-order	Depositional sequence	Sequence boundary that consists of diachronous composite scour surfaces of channel complexes	Repeated erosion in response to allogenic events such as relative sea level fall, tectonic process, and climatic change	7th- and 8th-order bounding surfaces (Miall, 1988, 1996); Sequence boundary (Holbrook, 2001)

Table 16. Reconstructed parameters of the Chinle Formation fluvial system. Data of bar deposit thickness are from well-preserved, untruncated bar deposits. CHC: Channel complex. See the list of symbols in Table 2.

Estimations from bar deposit thicknesses using the Indonesian scaling method

		N		h (m)	d (m)	d_m (m)	W_b (m)	Q_{mean} (m ³ s ⁻¹)	Q_b (m ³ s ⁻¹)	A_d (km ²)	L_d (km)
Shinarump Member	CHC-I	1		9.6	11.9	7.7	220.8	430.5	2,339.1	4,727.0	89.5
	CHC-II	2	Max.	7.2	8.9	5.8	180.5	309.1	1,757.4	3,571.8	77.2
			Min.	7.1	8.8	5.7	178.8	304.2	1,733.1	3,523.4	76.6
	CHC-III	2	Max.	8.5	10.5	6.8	202.8	374.2	2,072.6	4,198.6	84.1
			Min.	7.4	9.1	5.9	184.0	319.0	1,805.9	3,668.4	78.3
	CHC-IV	2	Max.	8.7	10.7	7.0	206.1	384.4	2,121.1	4,294.8	85.1
			Min.	7.0	8.6	5.6	177.0	299.3	1,708.9	3,475.1	76.0
	CHC-V	2	Max.	9.9	12.2	7.9	225.6	446.1	2,411.8	4,870.8	90.9
			Min.	6.0	7.4	4.8	158.9	250.6	1,466.1	2,990.5	70.2
	Cameron Member	CHC-VI	1		5.4	6.7	4.3	147.6	222.0	1,320.3	2,698.8
CHC-VII		1		4.6	5.7	3.7	131.9	184.5	1,125.8	2,308.6	61.2
CHC-VIII		1		4.8	5.9	3.9	135.9	193.8	1,174.4	2,406.3	62.6

Estimations from bar deposit thicknesses using the continental scaling method

		N		h (m)	d (m)	d_m (m)	W_b (m)	Q_{mean} (m ³ s ⁻¹)	Q_b (m ³ s ⁻¹)	A_d (km ²)	L_d (km)
Shinarump Member	CHC-I	1		9.6	11.9	6.9	310.9	12.1	2,087.8	98,709.2	618.6
	CHC-II	2	Max.	7.2	8.9	5.2	234.5	8.7	1,480.2	49,830.0	448.6
			Min.	7.1	8.8	5.1	231.3	8.5	1,455.6	48,201.2	441.7
	CHC-III	2	Max.	8.5	10.5	6.1	275.9	10.5	1,805.1	73,922.3	540.0
			Min.	7.4	9.1	5.3	240.9	8.9	1,529.5	53,182.0	462.5
	CHC-IV	2	Max.	8.7	10.7	6.2	282.3	10.8	1,856.0	78,122.2	554.2
			Min.	7.0	8.6	5.0	228.1	8.4	1,431.1	46,603.7	434.7
	CHC-V	2	Max.	9.9	12.2	7.1	320.4	12.5	2,166.0	106,196.9	640.2
			Min.	6.0	7.4	4.3	196.1	7.0	1,190.3	32,310.8	366.0
	Cameron Member	CHC-VI	1		5.4	6.7	3.9	176.9	6.2	1,049.4	25,155.0
CHC-VII		1		4.6	5.7	3.3	151.2	5.2	866.3	17,185.5	272.0
CHC-VIII		1		4.8	5.9	3.4	157.6	5.4	911.5	19,014.3	285.2

Estimations from cross-set thicknesses using the Indonesian scaling method

		N	S_{mean} (cm)	H_{mean} (cm)	d (m)	d_m (m)	W_b (m)	Q_{mean} (m ³ s ⁻¹)	Q_b (m ³ s ⁻¹)	A_d (km ²)	L_d (km)
Shinarump Member	CHC-I	27	42.1	124.1	7.4	4.8	159.5	252.1	1,473.7	3,005.8	70.4
	CHC-II	30	52.6	154.8	9.3	6.0	186.1	325.1	1,835.6	3,727.4	78.9
	CHC-III	24	58.2	171.3	10.3	6.7	199.8	365.3	2,029.9	4,113.7	83.2
	CHC-IV	48	45.3	133.3	8.0	5.2	167.7	273.7	1,582.2	3,222.5	73.1
	CHC-V	32	51.4	151.3	9.1	5.9	183.2	316.6	1,794.2	3,645.1	78.0
Cameron Member	CHC-VI	47	33.6	99.0	5.9	3.9	136.1	194.3	1,177.0	2,411.5	62.7
	CHC-VII	35	30.9	90.9	5.5	3.5	128.3	176.2	1,081.9	2,220.4	60.0
	CHC-VIII	37	38.6	113.7	6.8	4.4	150.0	228.0	1,351.1	2,760.5	67.3

Estimations from cross-set thicknesses using the continental scaling method

		N	S_{mean} (cm)	H_{mean} (cm)	d (m)	d_m (m)	W_b (m)	Q_{mean} (m ³ s ⁻¹)	Q_b (m ³ s ⁻¹)	A_d (km ²)	L_d (km)
Shinarump Member	CHC-I	27	42.1	124.1	7.4	4.3	197.1	7.1	1,197.7	32,714.1	368.1
	CHC-II	30	52.6	154.8	9.3	5.4	244.8	9.1	1,559.7	55,294.0	471.1
	CHC-III	24	58.2	171.3	10.3	6.0	270.3	10.2	1,760.4	70,330.0	527.5
	CHC-IV	48	45.3	133.3	8.0	4.6	211.4	7.7	1,304.6	38,769.4	398.7
	CHC-V	32	51.4	151.3	9.1	5.3	239.3	8.9	1,517.5	52,361.9	459.2
Cameron Member	CHC-VI	47	33.6	99.0	5.9	3.4	157.9	5.5	913.9	19,114.2	285.9
	CHC-VII	35	30.9	90.9	5.5	3.2	145.4	5.0	825.9	15,628.3	260.1
	CHC-VIII	37	38.6	113.7	6.8	4.0	181.0	6.4	1,078.9	26,580.7	333.9

Table 17. Geomorphological and hydrological features of some modern fluvial channels in the contiguous United States. W_b : Bankfull channel width (m). Q_b : Bankfull discharge (m^3s^{-1}).

	W_b	Q_b	Reference
North Fork Virgin River near Springdale, Utah, U.S.A.	18 * ¹	60.0 * ²	Berwick (1962)
Virgin River near St. George, Utah, U.S.A.	30 * ¹	–	
Green River at Green River, Utah, U.S.A.	130 * ¹	640.0 * ³	Berwick (1962)
Colorado River at Hite, Utah, U.S.A.	160 * ¹	610.0 * ³	Berwick (1962)
Yellowstone River near Miles City, Montana, U.S.A.	219	1,544 * ⁴	Osterkamp and Hedman (1982)
Missouri River near Nebraska City, Nebraska, U.S.A.	270	2,554 * ⁴	Osterkamp and Hedman (1982)
Thompson River at Trenton, Missouri, U.S.A.	82.3	640 * ⁴	Osterkamp and Hedman (1982)

*¹ Measured from Google Maps (<https://www.google.co.jp/maps>)

*² $Q_{2.33}$

*³ $Q_{2.33}$ calculated using data of Berwick (1962)

*⁴ Q_2

Table 18. Framework composition of sandstones from the Chinle Formation. See Fig. 52 for the framework grain types of sandstones.

Sample	Location	Member	Quartz				Feldspar			Lithic rock fragment				Q	F	L
			Qm	Qp	QT	Ch	P	K	Lv	Ls	QMT	Point counted				
SB-Ss 02	Smithsonian Butte	Shinarump	473	22	18	0	0	10	5	2	3	533	513	10	10	
SB-Ss 04	Smithsonian Butte	Shinarump	445	24	17	13	0	6	0	0	0	505	499	6	0	
SB-Ss 05	Smithsonian Butte	Shinarump	506	6	5	4	0	14	0	0	0	535	521	14	0	
SB-Ss 06	Smithsonian Butte	Shinarump	416	17	2	0	5	62	8	4	13	527	435	67	25	
SB-Ss 07	Smithsonian Butte	Shinarump	460	15	2	14	0	24	0	3	0	518	491	24	3	
SB-Ss 09	Smithsonian Butte	Shinarump	467	13	4	9	0	10	5	8	0	516	493	10	13	
SB-Ss 11	Smithsonian Butte	Shinarump	460	21	9	2	0	22	4	8	0	526	492	22	12	
SB-Ss 12	Smithsonian Butte	Shinarump	449	13	0	4	2	32	22	11	0	533	466	34	33	
SB-Ss 13	Smithsonian Butte	Shinarump	456	17	4	1	9	17	0	3	2	509	478	26	5	
SB-Ss 15	Smithsonian Butte	Shinarump	458	18	2	8	11	19	3	5	0	524	486	30	8	
SB-Ss 16	Smithsonian Butte	Shinarump	433	17	1	11	6	29	3	10	3	513	462	35	16	
SB-Ss 18	Smithsonian Butte	Shinarump	443	17	3	17	2	7	0	11	10	510	480	9	21	
SB-Cs 01	Smithsonian Butte	Cameron	327	37	8	9	17	58	27	22	15	520	381	75	64	
SB-Cs 02	Smithsonian Butte	Cameron	346	13	0	19	32	116	58	0	2	586	378	148	60	
SB-Cs 03	Smithsonian Butte	Cameron	290	40	0	21	22	69	83	2	1	528	351	91	86	
ER-Cs 01	East Reef	Cameron	303	39	9	11	39	88	11	4	0	504	362	127	15	
ER-Cs 02	East Reef	Cameron	316	41	0	26	2	79	18	21	8	511	383	81	47	
ER-Cs 03	East Reef	Cameron	258	52	11	5	3	123	5	7	41	505	326	126	53	
ER-Cs 04	East Reef	Cameron	305	40	10	13	10	94	2	1	25	500	368	104	28	
ER-Cs 05	East Reef	Cameron	261	29	2	15	18	132	23	19	3	502	307	150	45	
ER-Cs 06	East Reef	Cameron	250	45	5	12	31	117	14	12	15	501	312	148	41	
ER-Cs 07	East Reef	Cameron	259	45	15	47	12	61	31	27	4	501	366	73	62	
ER-Cs 08	East Reef	Cameron	307	58	5	34	25	64	12	24	3	532	404	89	39	
ER-Cs 09	East Reef	Cameron	315	18	7	5	72	50	20	22	5	514	345	122	47	
ER-Cs 11	East Reef	Cameron	256	35	4	44	16	103	31	22	0	511	339	119	53	
ER-Cs 12	East Reef	Cameron	289	17	7	6	70	95	3	1	13	501	319	165	17	
ER-Cs 13	East Reef	Cameron	395	16	1	8	11	61	20	21	0	533	420	72	41	
ER-Cs 14	East Reef	Cameron	371	19	11	10	18	50	11	20	29	539	411	68	60	
ER-Cs 16	East Reef	Cameron	343	14	4	18	15	97	5	7	10	513	379	112	22	
ER-Cs 17	East Reef	Cameron	205	50	12	27	22	141	29	28	3	517	294	163	60	
ER-Cs 18	East Reef	Cameron	312	21	0	19	26	81	43	1	1	504	352	107	45	
HM-Ss 01	Hurricane Mesa	Shinarump	433	25	12	10	4	31	0	3	5	523	480	35	8	
HM-Ss 03	Hurricane Mesa	Shinarump	432	6	6	3	5	35	2	17	6	512	447	40	25	
HM-Ss 04	Hurricane Mesa	Shinarump	424	20	2	0	0	41	0	19	0	506	446	41	19	
HM-Ss 06	Hurricane Mesa	Shinarump	407	41	0	8	12	40	4	0	9	521	456	52	13	
HM-Ss 07	Hurricane Mesa	Shinarump	374	12	7	0	13	99	2	17	3	527	393	112	22	
HM-Ss 08	Hurricane Mesa	Shinarump	350	17	15	6	26	80	5	11	6	516	388	106	22	
HM-Ss 09	Hurricane Mesa	Shinarump	410	22	6	14	2	51	0	2	6	513	452	53	8	
HM-Ss 11	Hurricane Mesa	Shinarump	397	23	3	0	6	74	1	4	0	508	423	80	5	
HM-Ss 12	Hurricane Mesa	Shinarump	476	11	1	0	2	2	1	7	6	506	488	4	14	
HM-Ss 13	Hurricane Mesa	Shinarump	437	26	0	12	4	26	0	0	0	505	475	30	0	
HM-Ss 14	Hurricane Mesa	Shinarump	356	32	2	10	18	88	2	4	0	512	400	106	6	
HM-Ss 15	Hurricane Mesa	Shinarump	400	37	7	0	9	44	0	3	4	504	444	53	7	
HM-Ss 16	Hurricane Mesa	Shinarump	368	35	11	5	7	71	0	5	2	504	419	78	7	
LV-Cs 01	Long Valley	Cameron	267	12	4	6	21	107	76	7	7	507	289	128	90	
CC-Ss 01	Cedar City	Shinarump	339	27	7	2	22	87	8	6	9	507	375	109	23	
CC-Ss 02	Cedar City	Shinarump	358	15	3	10	11	80	23	15	6	521	386	91	44	
CC-Ss 03	Cedar City	Shinarump	447	27	5	0	0	25	3	4	0	511	479	25	7	
CC-Cs 01	Cedar City	Cameron	284	26	0	18	25	127	19	13	0	512	328	152	32	

Table 19. Clay mineral composition of sandstone and mudstone samples from the Chinle Formation. Ka: kaolinite, Chl: chlorite, I: illite, Sm: smectite, Sds: sandstone sample, Mds: mudstone sample.

Sample	Sds / Mds	Location	Member	Ka	Chl	I	Sm
SB-Ss 01	Sds	Smithsonian Butte	Shinarump	90.1	0.0	9.9	0.0
SB-Ss 02	Sds	Smithsonian Butte	Shinarump	80.1	0.0	8.4	11.4
SB-Ss 03	Sds	Smithsonian Butte	Shinarump	84.9	0.0	15.1	0.0
SB-Ss 04	Sds	Smithsonian Butte	Shinarump	81.7	0.0	10.7	7.6
SB-Ss 05	Sds	Smithsonian Butte	Shinarump	87.3	0.0	12.7	0.0
SB-Ss 06	Sds	Smithsonian Butte	Shinarump	91.8	0.0	8.2	0.0
SB-Ss 07	Sds	Smithsonian Butte	Shinarump	90.2	0.0	8.7	1.1
SB-Ss 08	Sds	Smithsonian Butte	Shinarump	96.4	0.0	3.6	0.0
SB-Ss 09	Sds	Smithsonian Butte	Shinarump	95.8	0.0	4.2	0.0
SB-Ss 10	Sds	Smithsonian Butte	Shinarump	90.4	0.0	9.6	0.0
SB-Ss 11	Sds	Smithsonian Butte	Shinarump	82.7	0.0	5.0	12.3
SB-Ss 12	Sds	Smithsonian Butte	Shinarump	97.2	0.0	2.8	0.0
SB-Ss 13	Sds	Smithsonian Butte	Shinarump	97.1	0.0	2.9	0.0
SB-Ss 14	Sds	Smithsonian Butte	Shinarump	27.3	69.8	2.9	0.0
SB-Ss 15	Sds	Smithsonian Butte	Shinarump	59.8	37.6	2.5	0.0
SB-Ss 16	Sds	Smithsonian Butte	Shinarump	37.8	58.5	3.8	0.0
SB-Ss 17	Sds	Smithsonian Butte	Shinarump	92.2	0.0	7.8	0.0
SB-Ss 18	Sds	Smithsonian Butte	Shinarump	96.7	0.0	2.5	0.7
SB-Sm 01	Mds	Smithsonian Butte	Shinarump	49.0	33.6	17.4	0.0
SB-Sm 02	Mds	Smithsonian Butte	Shinarump	27.6	19.1	53.2	0.0
SB-Sm 03	Mds	Smithsonian Butte	Shinarump	29.9	0.0	70.1	0.0
SB-Cs 01	Sds	Smithsonian Butte	Cameron	95.1	0.0	3.3	1.5
SB-Cs 02	Sds	Smithsonian Butte	Cameron	93.6	0.0	0.0	6.4
SB-Cs 03	Sds	Smithsonian Butte	Cameron	92.3	0.0	0.0	7.7
SB-Cs 04	Sds	Smithsonian Butte	Cameron	90.3	0.0	2.6	7.1
SB-Cm 01	Mds	Smithsonian Butte	Cameron	24.4	0.0	53.3	22.4
SB-Cm 02	Mds	Smithsonian Butte	Cameron	51.6	0.0	10.3	38.0
SB-Cm 03	Mds	Smithsonian Butte	Cameron	38.6	0.0	19.9	41.5
SB-Cm 04	Mds	Smithsonian Butte	Cameron	29.2	0.0	42.0	28.8
SB-Cm 05	Mds	Smithsonian Butte	Cameron	46.1	0.0	10.2	43.7
SB-Cm 06	Mds	Smithsonian Butte	Cameron	59.7	0.0	27.6	12.7
SB-Cm 07	Mds	Smithsonian Butte	Cameron	59.5	0.0	5.3	35.2
SB-Cm 08	Mds	Smithsonian Butte	Cameron	75.1	0.0	12.5	12.4
SB-Cm 09	Mds	Smithsonian Butte	Cameron	72.2	0.0	12.5	15.3
SB-Cm 10	Mds	Smithsonian Butte	Cameron	83.2	0.0	2.9	14.0
SB-Cm 11	Mds	Smithsonian Butte	Cameron	43.1	0.0	4.1	52.7
SB-Cm 12	Mds	Smithsonian Butte	Cameron	6.2	0.0	0.7	93.1
SB-Cm 13	Mds	Smithsonian Butte	Cameron	36.5	0.0	4.5	59.1
SB-Cm 14	Mds	Smithsonian Butte	Cameron	83.0	0.0	1.2	15.9
SB-Cm 15	Mds	Smithsonian Butte	Cameron	43.9	0.0	7.6	48.6
SB-Cm 16	Mds	Smithsonian Butte	Cameron	53.7	0.0	21.1	25.2
SB-Cm 17	Mds	Smithsonian Butte	Cameron	41.9	0.0	9.5	48.6
SB-Cm 18	Mds	Smithsonian Butte	Cameron	25.4	0.0	16.4	58.2
SB-Cm 19	Mds	Smithsonian Butte	Cameron	39.6	0.0	22.4	38.0
SB-Cm 20	Mds	Smithsonian Butte	Cameron	65.3	0.0	7.5	27.3
SB-Cm 21	Mds	Smithsonian Butte	Cameron	59.3	0.0	17.5	23.2
SB-Cm 22	Mds	Smithsonian Butte	Cameron	35.5	0.0	8.1	56.5
SB-Cm 23	Mds	Smithsonian Butte	"purple pedogenic beds"	68.4	0.0	10.8	20.8
SB-Cm 24	Mds	Smithsonian Butte	"purple pedogenic beds"	61.7	0.0	8.3	30.0
SB-Cm 25	Mds	Smithsonian Butte	"purple pedogenic beds"	21.1	0.0	1.8	77.0
SB-Cm 26	Mds	Smithsonian Butte	"purple pedogenic beds"	1.8	0.0	6.3	91.9
SB-Cm 27	Mds	Smithsonian Butte	"purple pedogenic beds"	6.7	0.0	11.8	81.6
SB-Cm 28	Mds	Smithsonian Butte	"purple pedogenic beds"	30.4	0.0	4.6	65.0
SB-Cm 29	Mds	Smithsonian Butte	"purple pedogenic beds"	5.9	0.0	0.9	93.2
ER-Cs 02	Sds	East Reef	Cameron	92.0	0.0	8.0	0.0
ER-Cs 03	Sds	East Reef	Cameron	90.9	0.0	6.1	2.9
ER-Cs 04	Sds	East Reef	Cameron	87.1	0.0	10.0	2.9
ER-Cs 05	Sds	East Reef	Cameron	91.2	0.0	7.4	1.4
ER-Cs 06	Sds	East Reef	Cameron	90.0	0.0	5.9	4.2
ER-Cs 07	Sds	East Reef	Cameron	88.5	0.0	5.1	6.4
ER-Cs 08	Sds	East Reef	Cameron	78.9	0.0	11.2	9.9
ER-Cs 09	Sds	East Reef	Cameron	90.3	0.0	6.2	3.6
ER-Cs 10	Sds	East Reef	Cameron	87.2	0.0	7.9	5.0
ER-Cs 11	Sds	East Reef	Cameron	92.2	0.0	6.8	1.0
ER-Cs 12	Sds	East Reef	Cameron	53.4	41.7	0.0	4.9
ER-Cs 13	Sds	East Reef	Cameron	93.7	0.0	4.0	2.4

Table 19. (continued)

Sample	Sds / Mds	Location	Member	Ka	Chl	I	Sm
ER-Cs 14	Sds	East Reef	Cameron	90.3	0.0	3.9	5.8
ER-Cs 15	Sds	East Reef	Cameron	83.9	0.0	8.9	7.1
ER-Cs 16	Sds	East Reef	Cameron	95.9	0.0	3.6	0.5
ER-Cs 17	Sds	East Reef	Cameron	94.4	0.0	4.3	1.3
ER-Cs 18	Sds	East Reef	Cameron	66.4	0.0	26.2	7.4
ER-Cm 01	Mds	East Reef	Cameron	81.1	0.0	18.5	0.4
ER-Cm 02	Mds	East Reef	Cameron	96.3	0.0	3.0	0.8
ER-Cm 03	Mds	East Reef	Cameron	56.6	28.8	14.5	0.1
ER-Cm 04	Mds	East Reef	Cameron	93.5	0.0	6.5	0.1
ER-Cm 05	Mds	East Reef	Cameron	84.3	0.0	15.4	0.2
ER-Cm 06	Mds	East Reef	Cameron	92.9	0.0	0.8	6.2
ER-Cm 07	Mds	East Reef	Cameron	92.5	0.0	3.1	4.4
ER-Cm 08	Mds	East Reef	Cameron	80.5	0.0	1.7	17.8
ER-Cm 09	Mds	East Reef	Cameron	64.3	0.0	4.3	31.4
ER-Cm 10	Mds	East Reef	Cameron	50.2	0.0	6.6	43.2
ER-Cm 11	Mds	East Reef	Cameron	26.8	0.0	1.8	71.4
ER-Cm 12	Mds	East Reef	Cameron	47.2	0.0	3.2	49.7
ER-Cm 13	Mds	East Reef	Cameron	39.0	0.0	2.5	58.5
ER-Cm 14	Mds	East Reef	Cameron	62.6	0.0	12.2	25.1
ER-Cm 15	Mds	East Reef	Cameron	54.4	0.0	10.6	35.0
ER-Cm 17	Mds	East Reef	Cameron	42.6	0.0	22.8	34.6
ER-Cm 18	Mds	East Reef	Cameron	22.4	0.0	24.7	53.0
ER-Cm 19	Mds	East Reef	Cameron	23.5	0.0	21.3	55.2
ER-Cm 20	Mds	East Reef	Cameron	50.0	0.0	19.3	30.7
ER-Cm 21	Mds	East Reef	Cameron	85.8	0.0	5.3	8.9
ER-Cm 22	Mds	East Reef	Cameron	79.1	0.0	4.9	16.0
ER-Cm 23	Mds	East Reef	Cameron	63.6	0.0	11.2	25.1
ER-Cm 24	Mds	East Reef	Cameron	46.6	0.0	12.0	41.4
ER-Cm 26	Mds	East Reef	Cameron	63.4	0.0	6.4	30.1
ER-Cm 27	Mds	East Reef	Cameron	41.6	0.0	1.4	57.0
ER-Cm 29	Mds	East Reef	"purple pedogenic beds"	0.8	0.0	1.7	97.5
ER-Cm 30	Mds	East Reef	"purple pedogenic beds"	16.0	0.0	1.6	82.4
ER-Cm 31	Mds	East Reef	"purple pedogenic beds"	1.3	0.0	2.0	96.7
ER-Cm 32	Mds	East Reef	"purple pedogenic beds"	8.0	0.0	21.2	70.8
HM-Ss 01	Sds	Hurricane Mesa	Shinarump	86.7	0.0	13.3	0.0
HM-Ss 03	Sds	Hurricane Mesa	Shinarump	85.1	0.0	14.9	0.0
HM-Ss 05	Sds	Hurricane Mesa	Shinarump	77.1	5.7	17.2	0.0
HM-Ss 04	Sds	Hurricane Mesa	Shinarump	87.4	0.0	12.4	0.2
HM-Ss 07	Sds	Hurricane Mesa	Shinarump	77.9	0.0	22.1	0.0
HM-Ss 08	Sds	Hurricane Mesa	Shinarump	69.2	12.6	18.2	0.0
HM-Ss 09	Sds	Hurricane Mesa	Shinarump	93.7	0.0	6.3	0.0
HM-Ss 11	Sds	Hurricane Mesa	Shinarump	100.0	0.0	0.0	0.0
HM-Ss 13	Sds	Hurricane Mesa	Shinarump	89.6	0.0	10.4	0.0
HM-Ss 14	Sds	Hurricane Mesa	Shinarump	88.4	0.0	11.6	0.0
HM-Ss 15	Sds	Hurricane Mesa	Shinarump	78.2	0.0	21.8	0.0
HM-Ss 16	Sds	Hurricane Mesa	Shinarump	91.9	0.0	8.1	0.0
HM-Sm 01	Mds	Hurricane Mesa	Shinarump	36.4	27.2	36.4	0.0
HM-Sm 02	Mds	Hurricane Mesa	Shinarump	36.2	18.2	45.6	0.0
HM-Sm 03	Mds	Hurricane Mesa	Shinarump	53.9	30.3	15.8	0.0
HM-Sm 04	Mds	Hurricane Mesa	Shinarump	26.5	34.8	38.7	0.0
HM-Sm 05	Mds	Hurricane Mesa	Shinarump	28.2	24.3	47.6	0.0
HM-Sm 06	Mds	Hurricane Mesa	Shinarump	34.1	28.3	37.6	0.0
HM-Sm 07	Mds	Hurricane Mesa	Shinarump	36.3	28.3	35.3	0.0
HM-Sm 08	Mds	Hurricane Mesa	Shinarump	46.6	27.8	25.6	0.0
HM-Sm 09	Mds	Hurricane Mesa	Shinarump	42.0	14.0	44.0	0.0
HM-Sm 10	Mds	Hurricane Mesa	Shinarump	27.9	13.1	59.0	0.0
HM-Sm 11	Mds	Hurricane Mesa	Shinarump	27.1	50.1	22.8	0.0
HM-Sm 12	Mds	Hurricane Mesa	Shinarump	25.8	23.6	50.7	0.0
HM-Sm 13	Mds	Hurricane Mesa	Shinarump	66.9	8.1	25.0	0.0